

University of Technology Sydney

**Assisting Product Designers with Balancing Strength
and Surface Texture of Handheld Products Made from
3D Printed Polymers**

**by
Stefan Lie**

A thesis submitted in fulfilment for the degree of
Doctor of Philosophy

in the
School of Design
Faculty of Design Architecture and Building

July 2020

Certificate of original authorship

I, Stefan Lie, declare that this thesis is submitted in fulfilment of the requirements for the award of Doctor of Philosophy in the School of Design, Faculty of Design Architecture and Building at the University of Technology Sydney.

This thesis is wholly my own work unless otherwise referenced or acknowledged. In addition, I certify that all information sources and literature used are indicated in the thesis.

This document has not been submitted for qualifications at any other academic institution.

This research is supported by the Australian Government Research Training Program.

Production Note:

Signature: Signature removed prior to publication.

Date: 8 July 2020

Acknowledgments

I would like to thank my supervisor Associate Professor Bert Bongers for his continued assistance and positive reinforcement throughout the course of my PhD research.

Thanks to my co-supervisor Professor Dikai Liu for seeing me through both my Masters and my PhD research.

Thanks to Dr. Barry Liu for this support and guidance during my material testing experiments and trusting me with his equipment.

Thanks to our Head of School, Kate Sweetapple, for her patience and support while I completed my PhD.

Thanks to Professor Jennifer Loy for her expert advice on all things 3D printing.

Thanks to my colleagues in Roderick Walden, Anton Nemme and Berto Pandolfo for their support and understanding.

Thanks to the CCDP (Centre for Contemporary Design Practice) for funding the 3D printing costs.

Thanks to the Faculty of Design Architecture and Building for providing me with a full time scholarship.

Thanks to Dr Christina Houen for editing this thesis according to the guidelines of the university and of the Institute of Professional Editors.

Above all, I would like to thank my wife Nicola and my two sons Rolf and Tino for their patience and continued encouragement and for understanding how important my research is to me.

The world of organized artifice is transforming in ways that are poorly understood and little explored. There are two reasons why this is happening. First, new forms of design and manufacture are appearing that lack historical precedent, and are bound to create substantial novelty. Second, the production methods currently used are not sustainable. They are large in scale, have long histories, and have been extensively researched and developed, but they can't go on in their present form. The status quo uses archaic forms of energy and materials which are finite and toxic. They wreck the climate, poison the populace and foment resource wars.

They have no future.

— Bruce Sterling in *Shaping Things* (2005, p. 5)

Contents

Certificate of original Authorship	2
Acknowledgments	3
Preface	4
List of figures	8
List of tables	12
Glossary of terms and abbreviations	14
Abstract	16
Chapter 1. Introduction	17
1.1 Background and motivation	20
Chapter 2. Existing knowledge and related literature	25
2.1 3D printing	25
2.1.1 Types of 3D printing processes and available materials	27
2.1.2 Post-processing of 3D printed polymer parts	28
2.1.3 Discussion of 3D printing	33
2.2 The process of designing a product	35
2.2.1 Design for manufacturing (DFM)	37
2.2.2 Designing for 3D printing/additive manufacturing (DFAM)	38
2.2.3 Discussion of product design process	43
2.3 End-use products made from 3D printed polymers	44
2.3.1 Static mechanical properties of three 3D printed polymers	55
2.3.2 Benchmark studies of 3D printed polymers	60
2.3.3 AM polymer/process specific studies	61
Studies of Fused Deposition Modelling in ABS	61
Studies of Material Jetting in TPGDA	69
Studies of Selective Laser Sintering in PA	75
2.3.4 Discussion of end-use products made through 3D printing	80
2.4 Strategies to optimise part orientation	81
2.4.1 Discussion of methods to optimise part orientation	85
2.5 Interacting with products	86
2.5.1 Discussion of interacting with products	93
2.6 Discussion of existing knowledge and related literature	94
Chapter 3.0 Research questions and methodology	96
3.1 Research questions	98
3.2 Methodology	98
3.2.1 Methodology part 1	101

3.2.2 Methodology part 2	104
3.3 Limitations of scope	106
3.4 Research hypothesis	108
Chapter 4.0 Experiments	112
4.1 Experiments to determine the mechanical properties of the three 3D printed polymers at a 45 deg incline	112
4.1.1 Making the test specimens	114
4.1.2 Tensile testing	117
4.1.3 Izod impact testing (notched)	121
4.1.4 Flexural or 3-point bend testing	124
4.2 Experiment to determine clear visual representation of the surface of a 3D printed part prior to building	126
Chapter 5.0 Results	138
5.1 Mechanical property test results of the three 3D printed polymers	138
5.1.1 Results for tensile testing	139
5.1.2 Results for Izod impact testing	142
5.1.3 Results for 3 point bend testing	143
5.2 Results for a clear visual surface representation	144
Chapter 6.0 Analysis and communication of results	147
6.1 Analysis of the results in response to research question 1a	147
6.1.1 Variation of ABS properties based on build orientation	148
6.1.2 Variation of TPGDA properties based on build orientation	150
6.1.3 Variation of PA properties based on build orientation	151
6.2 Analysis of the results in response to research question 1b	152
6.3 Analysis of the results in response to research question 2	154
Chapter 7.0 Discussion	155
7.1 Selecting a surface appearance	156
Application to practice through design process	160
7.2 Selecting the most suitable polymer based on a mechanical property	161
7.2.1 Example of selecting a polymer based on max. tensile strength	161
Application to practice through design process	163
7.2.2 Example of selecting a polymer based on impact strength	164
Application to practice through design process	165
7.2.3 Example of selecting a polymer based on flexural strength	165
Application to practice through design process	167

7.3	Selecting the most suitable build orientation for each polymer	167
7.3.1	Scenario 1: Selecting a build orientation for ABS	168
7.3.2	Selecting a build orientation for TPGDA and PA	173
	Application to practice through design process	174
7.4	Balancing mechanical properties with surface appearance	175
7.4.1	Scenario 2: Visualisation of a polymer based on max tensile strength	175
	Application to practice through design process	184
7.4.2	Scenario 3: Redesign of a product to suit a specific polymer	185
	Application to practice through design process	200
7.5	The approach and tools in review	200
Chapter 8.0 Conclusion		202
8.1	Thesis recap	202
8.2	Contribution to knowledge	207
8.2.1	A new approach for product design	207
8.2.2	Material property data	210
8.2.3	Unanticipated discoveries	211
8.3	Wider reaching implications	212
Appendices		216
Appendix A		216
	ProJet general post processing wax removal process	
Appendix B		217
	Supplier material data sheets for ABS, TPGDA and PA	
Appendix C		220
	Load cell certification by Australian Calibration Services	
Appendix D		221
	Sample spreadsheet of recorded tensile specimen dimensions	
Appendix E		222
	Izod impact testing report by LMATS Pty Ltd	
Appendix F		234
	Sample spreadsheet 3-point bend specimen dimensions	
Appendix G		235
	Human ethics application with Nil/Neg risk to participants	
Appendix H		236
	ASTM standard: D638-14, D256 – 10 and D790 – 15	
Bibliography		285

List of figures

Figure 2.1:	General post-processing of an SLS part (courtesy of i.materialise).	29
Figure 2.2:	Teapot 3D printed in ABS by FDM with support material still in place.	29
Figure 2.3:	Stair-stepping effect of FDM in ABS, layer height 0.254mm.	30
Figure 2.4:	Stair-stepping and surface roughness of SLS in PA, layer height 0.1mm.	31
Figure 2.5:	3D printed surface textures (courtesy of Lehrmitt Design Studios).	32
Figure 2.6:	Schematic representation of the FDM process (courtesy of additively).	33
Figure 2.7:	Schematic representation of the MJ process (courtesy of additively).	34
Figure 2.8:	Schematic representation of the SLS process (courtesy of additively).	34
Figure 2.9:	Immortal-Mechanical-Paddles by Soludus on a PS4 controller.	40
Figure 2.10:	E-NABLE prosthetic limb (courtesy of E-NABLE Medellin).	45
Figure 2.11:	3D printed Limelight track lights (courtesy of Limelight).	46
Figure 2.12:	3D printed lug-nut starter tool (courtesy of Eckhart).	46
Figure 2.13:	Typical setup of the Sydney Harbour Bridge grit-blasting robot.	48
Figure 2.14:	A robot set up ready to blast a section of the Sydney Harbour Bridge.	48
Figure 2.15:	The interactive stepping tiles in use.	49
Figure 2.16:	The main tile.	50
Figure 2.17:	Warped main tile.	51
Figure 2.18:	Complete Visionsearch system set up and in use.	52
Figure 2.19:	How a Head Distancer is used.	53
Figure 2.20:	Visionsearch Head Distancer fully assembled.	53
Figure 2.21:	Orthogonal orientation notation (ASTM 2013b).	57
Figure 2.22:	Inclined build orientations do not have an ASTM notation.	57
Figure 2.23:	Schematic of FDM extrusion head (courtesy of MegaDepot).	62
Figure 2.24:	Detail of ABS tensile specimen built in the XYZ (HF) orientation.	62
Figure 2.25:	SEM cross section of ABS built in HF orientation.	64
Figure 2.26:	SEM cross section of ABS built in HoE orientation.	64
Figure 2.27:	HF orientation (perspective view).	65
Figure 2.28:	HoE (top view).	65
Figure 2.29:	Raster pattern experiments by Ziemian, Sharma and Ziemian.	66
Figure 2.30:	Schematic image of MJ process (Barclift & Williams 2012, p. 876).	70
Figure 2.31:	Orthogonal orientation notation according to ASTM (ASTM 2013b).	74
Figure 2.32:	Schematic of SLS process (courtesy of additively).	75

Figure 2.33:	Flow chart of Leutenecker-Twelsiek, Klahn, and Meboldt's method.	84
Figure 2.34:	Salt and Pepper Maracas by Naoto Fukasawa.	87
Figure 2.35:	3D printed nautilus shell jewellery piece showing build steps.	89
Figure 2.36:	3D printed jewellery pieces showing build steps.	90
Figure 2.37:	Toolpath visualisation through Stratasys Catalyst software.	91
Figure 2.38:	Effect of orientation upon surface roughness visualisation.	92
Figure 2.39:	Best surface quality on a selected area of a model.	93
Figure 3.1:	Diagram of the methodology.	100
Figure 3.2:	Orthogonal orientation notation (ASTM 2013b).	102
Figure 3.3:	Inclined build orientations do not have an ASTM notation.	103
Figure 3.4:	Diagram of Methodology Part 1.	104
Figure 3.5:	Diagram of Methodology Part 2.	105
Figure 3.6:	Diagram of the methodology.	110
Figure 4.1:	Tensile specimen build orientation and arrangement for ABS and TPGDA.	114
Figure 4.2:	Tensile specimen build orientation and arrangement for PA.	115
Figure 4.3:	Izod impact specimen build orientation for ABS, TPGDA and PA.	115
Figure 4.4:	Flexural specimen build orientation for ABS, TPGDA and PA.	116
Figure 4.5:	Dimensions of tensile test specimens (all dimensions in mm).	118
Figure 4.6:	Tensile specimen build orientations for ABS and TPGDA.	119
Figure 4.7:	Tensile specimen build orientations for SLS in PA.	119
Figure 4.8:	Tensile test set up on Shimadzu ASG-X.	120
Figure 4.9:	Dimensions of Izod test specimens (all dimensions in mm).	122
Figure 4.10:	Izod specimen build orientations for ABS, TPGDA and PA.	122
Figure 4.11:	Izod test set up at LMATS Pty Ltd.	123
Figure 4.12:	Dimensions of flexural test specimens (all dimensions in mm).	124
Figure 4.13:	Flexural test specimens for ABS, TPGDA and PA.	125
Figure 4.14:	Flexural test setup on Shimadzu ASG-X.	120
Figure 4.15:	Image of the real turning handle.	130
Figure 4.16:	Software: Slicer (for Fusion 360 V1.0.0 by Autodesk).	131
Figure 4.17:	Software: Slic3r V1.2.9.	131
Figure 4.18:	Software: Simplify3D V4.0.1.	132
Figure 4.19:	Software: CatalystEx V3.5 (by Stratasys).	132
Figure 4.20:	Software: Cura V3.0.4 (for Ultimaker).	133
Figure 4.21:	Software: Cubicreator3 V3.6 (by Cubicon).	133

Figure 4.22:	Survey Welcome page.	135
Figure 4.23:	Main survey page.	136
Figure 4.24:	Survey thank you page.	137
Figure 5.1:	Raw data of test on SLS in V as output by Trapezium X.	139
Figure 5.2:	Calculated data for SLS in V as presented in Excel.	139
Figure 5.3:	Results of survey in terms of preference and percentage.	145
Figure 5.4:	Number of participants who completed and submitted the survey.	145
Figure 5.5:	Sample of individual response Progress (time spent on survey).	146
Figure 6.1:	ABS build orientation chart.	148
Figure 6.2:	TPGDA build orientation chart.	150
Figure 6.3:	PA build orientation chart.	151
Figure 6.4:	Comparison of tensile strength between the three polymers.	153
Figure 6.5:	Comparison of impact strength between the three polymers.	153
Figure 6.6:	Comparison of flexural strength between the three polymers.	154
Figure 7.1:	3D printed Nautilus shell pendant showing spiralling build steps.	157
Figure 7.2:	Nautilus shell pendant in Cura as it was built.	158
Figure 7.3:	Nautilus shell pendant in Cura in a different orientation.	159
Figure 7.4:	Gold and silver broaches showing build steps (courtesy of sculpteo).	160
Figure 7.5:	Comparison of tensile strength between the three polymers.	163
Figure 7.6:	Comparison of impact strength between the three polymers.	165
Figure 7.7:	Flexing clip on the battery cover of a remote (courtesy of Epson).	166
Figure 7.8:	Comparison of flexural strength between the three polymers.	167
Figure 7.9:	ABS Build Orientation Chart.	168
Figure 7.10:	ABS Impact Chart and views of acceptable range.	170
Figure 7.11:	Aviator Frame shown in HF orientation.	170
Figure 7.12:	Aviator Frame shown in I 45 orientation.	171
Figure 7.13:	Aviator frame shown in V orientation.	171
Figure 7.14:	HF to I 45 acceptable range of orientation shown in blue.	172
Figure 7.15:	Four build orientations in relation to mechanical properties of TPGDA.	174
Figure 7.16:	Four build orientations in relation to mechanical properties of PA.	174
Figure 7.17:	Diagram of Scenario 2.	176
Figure 7.18:	Comparison of tensile strength between the three polymers.	177
Figure 7.19:	PA build orientation chart.	178
Figure 7.20:	The acceptable range, shown in blue, for max tensile in PA.	179

Figure7.21:	HF facing up and down.	180
Figure 7.22:	I 45 facing up and down.	180
Figure 7.23:	V option 1.	180
Figure 7.24:	V option 2.	180
Figure 7.25:	Horizontal build steps.	181
Figure 7.26:	Vertical build steps.	181
Figure 7.27:	I 45 options 1 and 2, both of which are asymmetrical.	182
Figure 7.28:	Frame with diagonal build steps.	182
Figure 7.29:	I 45 orientation.	183
Figure 7.30:	View of the section of the frame that will come in contact with the skin.	183
Figure 7.31:	Screen grab for print bureau operator.	184
Figure 7.32:	The Visionsearch Head Distancer.	185
Figure 7.33:	The Visionsearch Head Distancer in use.	186
Figure 7.34:	Outlined in red is the section of Head Distancer to be under tension.	187
Figure 7.35:	Outline shows where it was hollowed out to reduce material volume.	188
Figure 7.36:	Diagram of Scenario 3.	189
Figure 7.37:	Comparison charts of the three polymers.	190
Figure 7.38:	TPGDA build orientation chart.	191
Figure 7.39:	The three areas on the original design that will need to be redesigned.	192
Figure 7.40:	The redesigned Head Distancer.	193
Figure 7.41:	The changes to the three areas after redesigning the Head Distancer.	194
Figure 7.42:	Possible HF orientations.	196
Figure 7.43:	On its side could also be considered HF.	196
Figure 7.44:	The area of focus for selection of build orientation.	197
Figure 7.45:	Acceptable range for scenario 3.	197
Figure 7.46:	Final build orientation.	198
Figure 7.47:	Close-up showing surface detail.	199
Figure 7.48:	Screen grab for 3D print bureau operator.	199
Figure 8.1:	Methodology Diagram.	205

List of tables

Table 2.1:	Material data supplied by Stratasys for FDM in ABS	58
Table 2.2:	Material data supplied by 3D Systems for MJ in TPGDA	58
Table 2.3:	Material data supplied by EOS for SLS in PA	58
Table 2.4:	Build parameters used by Ahn et al (2002)	63
Table 2.5:	Chung Wang, Lin and Hu (2007), test results	63
Table 2.6:	Build parameters used by Chung Wang, Lin and Hu (2007)	66
Table 2.7:	Build parameters used by Ziemian, Sharma and Ziemian (2012)	67
Table 2.8:	Build parameters used by Rayegani and Onwubolu (2014)	68
Table 2.9:	Build parameters used by Pilipovic, Raos and Šercer (2009)	71
Table 2.10:	Build parameters used by Kęsy and Kotliński (2010)	71
Table 2.11:	Build parameters used by Barclift and Williams (2012)	72
Table 2.12:	Build parameters used by Cazon, Morer and Matey (2014)	73
Table 2.13:	Build parameters used by Mueller, Shea and Daraio (2015)	75
Table 2.14:	Build parameters used by Gibson and Shi (1997)	76
Table 2.15:	Build parameters used by Ajouk et al. (2006)	77
Table 2.16:	Build parameters used by Caulfield, McHugh and Lohfeld (2007)	78
Table 2.17:	Build parameters used by Starr, Gornet and Usher (2011)	78
Table 5.1:	ABS results for max. load, extension at max. load and max. strength	140
Table 5.2:	ABS results for load at fracture, extension at fracture, fracture strength	140
Table 5.3:	ABS results for Young's modulus	40
Table 5.4:	TPGDA results for max. load, extension at max. load and max. strength	141
Table 5.5:	TPGDA results for load at fracture, extension at fracture, fracture strength	141
Table 5.6:	TPGDA results for Young's modulus	141
Table 5.7:	PA results for max. load, extension at max. load and max. strength	141
Table 5.8:	PA results for Load at fracture, extension at fracture, fracture strength	142
Table 5.9:	PA results for Young's modulus	142
Table 5.10:	ABS results for Izod impact (notched) testing	142
Table 5.11:	TPGDA results for Izod impact (notched) testing	143
Table 5.12:	PA results for Izod impact (notched) testing	143
Table 5.13:	ABS results for max. load, stroke at max. load and flexural stress	143

Table 5.14:	TPGDA results for max. load, stroke at max. load and flexural stress	144
Table 5.15:	PA results for max. load, stroke at max. load and flexural stress	144
Table 5.16:	Breakdown of the results from the online survey	144
Table 6.1:	ABS build orientation variations of max. tensile strength	149
Table 6.2:	ABS build orientation variations of impact strength	149
Table 6.3:	ABS build orientation variations of max. flexural strength	149
Table 6.4:	TPGDA, build orientation variations of max. tensile strength	150
Table 6.5:	TPGDA build orientation variations of impact strength	151
Table 6.6:	TPGDA build orientation variations of max. flexural strength	151
Table 6.7:	PA build orientation variations of max. tensile strength	151
Table 6.8:	PA build orientation variations of impact strength	152
Table 6.9:	PA build orientation variations of max. flexural strength	152
Table 7.1:	ABS build orientation variations of impact strength	173
Table 7.2:	PA build orientation variations of max. tensile strength	178
Table 7.3:	TPGDA build orientation variations of max. tensile strength	195
Table 7.4:	TPGDA, build orientation variations of max. flexural strength	195

Glossary of terms and abbreviations

3D	Three dimensional.
3D printing	3 Dimensional printing.
ABS	Acrylonitrile Butadiene Styrene, a synthetic thermoplastic polymer used for AM in FDM machines.
Algorithm	A process or set of rules for followed in calculations or other problem-solving operations.
AM	Additive Manufacturing.
Anisotropic	Materials that have different physical properties when measured in different directions.
ASTM	American Society for Testing and Materials
Build orientation	The build orientation is the way parts are placed within the build volume.
Build volume	The specific x, y and z size of the 3D volume an AM machine is capable of building within, where x is width, y is depth and z is height, typically represented in mm. Parts to be built must fit within the build volume.
CAD	Computer Aided Design.
CNC	Computer Numerically Controlled.
DDM	Direct Digital Manufacturing.
DFM	Design For Manufacturing.
DFAM	Design For Additive Manufacturing.
DIN	Is German for Deutsches Institut für Normung (english: German Institute for Standardisation).
DIN EN ISO	The prefix to a test method, e.g. DIN EN ISO 180, that adheres to all three standards.
EN	Is German for Europa Norm (English: European Standard). Member states are required to adhere to EN standards.
End-use product	A product that has been manufactured for actual use, so must be usable, repeatedly if necessary, in the way that it is intended.
FDM	Fused Deposition Modelling.
Generic algorithm	A method for solving both constrained and unconstrained optimization problems based on a natural selection process that mimics biological evolution. The algorithm repeatedly modifies a population of individual solutions (mathworks.com).
Handheld product	A portable product that can be used while it is being held and carried by one or both hands, ranging from static products such as bottle openers to hair dryers and complex electronic devices such as digital cameras.
HCI	Human Computer Interaction.

HF	Horizontal Flat. In the context of this research HF stands for a test specimen or part built in the XYZ orientation.
HoE	Horizontal on Edge. In the context of this research HoE stands for a test specimen or part built in the XZY orientation.
HRI	Human Robot Interaction.
I 45	Inclined at 45 degrees. In the context of this research I 45 stands for a test specimen or part built in the XZY at a 45 degree incline along X orientation.
ID	Industrial Design.
ISO	International Standards Organisation.
Isotropic	Materials that have the same physical properties when measured in different directions.
MJ	Material Jetting.
PA	Polyamide, a synthetic thermoplastic polymer used for AM in SLS machines.
Photopolymer	A light activated synthetic thermoset polymer that hardens when exposed to ultraviolet light, used for AM in MJ machines.
Polymer	Commonly referred to as plastic or resin, is a substance which has a molecular structure built up chiefly or completely from a large number of similar units bonded together.
SEM	Scanning Electron Microscope.
SLS	Selective Laser Sintering.
STL file	Standard Triangulation Language, the most widely accepted file format for 3D printing.
Thermoplast	A polymer that is formed by heating it up and hardens while cooling down, can be repeatedly remoulded through reheating.
Thermoset	A polymer that hardens during setting, by means of a chemical reaction that requires heat, cannot be remoulded through reheating or any other means.
TPGDA	Tripropylene Glycol Diacrylate, a synthetic thermoset photopolymer resin used for AM in MJ machines.
UTS	Ultimate Tensile Strength.
V	Vertical. In the context of this research V stands for a test specimen or part built in the ZXY orientation.
Visualisation	The representation of an object, situation, or set of information as a chart or other image.

Abstract

This research provides product designers using 3D printing to manufacture handheld products for end-use with a new approach, which enables them to make knowledge-directed decisions with regard to build orientation in relation to part strength and surface appearance. Because 3D printing machines deposit material in horizontal layers, they become anisotropic, which means they display different physical properties in different directions. To ascertain how much these physical properties differ, test samples were 3D printed in three different polymers and in three different build orientations, which were horizontal at 0 deg, inclined at 45 deg, and vertical at 90 deg.

Product designers also consider how the product will feel and look when it is interacted with, which makes the surface texture a key consideration. The surface of parts made through 3D printing can display characteristics such as stair-stepping; therefore, it is essential to visualise the surface before printing. To address this, six 3D printing software applications were assessed for their ability to visually represent the surface texture of a part before printing. The data resulting from the mechanical property testing was translated into a set of tools that represent the data graphically. The tools enable comparisons to be made between the mechanical properties of the three polymers, namely ABS (Acrylonitrile Butadiene Styrene), TPGDA (Tripropylene Glycol Diacrylate) and PA (Polyamide). The assessment of the six 3D printing software applications showed that Cura provides the most adequate representation of a part's surface.

This research is significant, since to date, no data or tools such as the results presented here on the mechanical properties of the three polymers at a 45 deg incline have been published, nor is there any data that enables the direct comparison of the three polymers in relation to horizontal, inclined at 45 degrees, and vertical build orientations. The ability to visually represent surface texture in relation to build orientation through Cura before printing will assist product designers. Both in combination or individually, the results of this research will provide product designers with a new approach which will help them make knowledge-directed decisions when designing a part to be manufactured through 3D printing in the polymers ABS, TPGDA, or PA.

Chapter 1. Introduction

This research is about using 3D (three-dimensional) printing in polymer materials to manufacture handheld products for end-use. 3D printing is a digital manufacturing process through which parts can be manufactured from a digital 3D model that has been created using CAD (computer aided design) software. The 3D printing machine translates the digital 3D model into information that enables it to lay down material in horizontal layers, one on top of the previous, and in so doing, a part is built layer by layer. Due to this method of adding layers, the more technical term for this process is Additive Manufacturing (AM). However, 3D printing is the more generally accepted term, and will be the term used throughout this thesis. Until recently, 3D printing in polymers was predominantly used for prototyping and making models, but more and more product designers are using it to make end-use products. End-use products are products that have been manufactured for actual use, so must be usable, repeatedly if necessary, in the way that they are intended. This thesis is titled *Assisting Product Designers with Balancing Strength and Surface Texture of Handheld Products Made from 3D Printed Polymers*, reflecting the need for a new approach in this area. The research has been conducted *for* product designers *by* a product designer, who recognised the need to provide a new approach in situations where 3D printing in polymers is being considered as a method to make an end-use product or parts thereof. In essence, the research addresses two issues:

1. The strength of parts made from 3D printed polymers;
2. The surface texture on parts made from 3D printed polymers.

What those two things have in common is *build orientation*.

The build orientation (the exact details of which will be explained in Section 2.1: 3D printing) is referred to as the orientation in which a part is built by a 3D printing machine. It has an effect on both the strength of a part and its surface texture, depending on the way the part is oriented. Firstly, the build orientation has an effect on part strength, because 3D printing machines lay down the material in layers. This layering makes the material from which a 3D printed part is made anisotropic, which means that it will have different physical properties when measured in different directions, similar to wood. Knowing

how strong a part will be is important, because it is the way product designers ensure the part will be strong enough to withstand the forces exerted on it while people are using it. Product designers are responsible for the work they produce and must ensure their products are safe to use. Further, the surface texture is important because it affects how a part looks and how it feels when it is being touched and interacted with. In many situations, a build orientation of a part that is optimal for strength is not optimal for its surface texture, and vice versa. This means that product designers need an approach they can apply to their design process whereby they can be confident that a part will be strong enough and safe to use, while at the same time ensuring it looks and feels the way the designer wants it to. This thesis presents an approach that assists them with finding a balance between the strength and surface texture of a part.

The thesis title also refers to handheld products, which are portable products that can be used by hand or while being held and carried by one or both hands. Handheld products range from static products such as bottle openers to hair dryers, and complex interactive electronic devices such as digital cameras. Interaction with the products and the author's experience provide the context for focusing on the product typology of handheld products. As people go about their daily activities, they frequently use products in this size range, and thus have experience with using them. Because handheld products are used and interacted with by hand, they provide a logical connection to the importance of surface texture. The author has experience with designing and making end-use products designed to be used by hand using 3D printing, which is the inspiration for this research.

The author is an academic design practitioner and senior lecturer in product design, with over three decades of experience in designing and manufacturing products. He is a qualified toolmaker and worked in that profession for eight years, manufacturing injection moulding tools for polymer products. After completing his Bachelor of Industrial Design, he practised as a designer-maker, crafting his own products, and as a design consultant, directing his own company for ten years. The author then expanded on his existing design knowledge by completing a Masters by Research in Engineering (MEng) in Human-Computer Interaction (HCI) and Human Robot Interaction (HRI). While completing his MEng, he worked as part of a team on a robotic system

designed to sandblast rust and old paint off the Sydney Harbour Bridge (Lie, Liu & Bongers 2012); more will be said about his project in Section 2.3: End-use products made from 3D printed polymers. While working on this project, his task was the design, development and implementation of the Operator Control Unit designed to interact with and manipulate the robotic system, which became the core element of his Master's thesis (Lie 2012). The aspect that connects that project to the research presented in this thesis is that only two robots were made for low volume bespoke production, and 3D printing was used to manufacture end-use parts of the robotic system. There are many different types of 3D printing processes and materials, which are all explained in detail in section 2.1 3D: printing. As an industrial designer who was trained to design products for mass production, manufacturing only two units was unusual. Several traditional manufacturing methods, such as machining and welding of metal parts, were utilised to build many components of the robotic system, but 3D printing was deemed appropriate for several components. 3D printing was not new to the author; he had been using it for many years to produce models and prototypes of design projects he was working on. Although he had considered using it for end-use part production on several occasions, he never did so, because material specifications in relation to material properties were unreliable, and part costs were usually prohibitively high. But this project was well resourced, and when it was decided that the team would design and manufacture its own operator control unit customised to the needs of its users, 3D printing was chosen to manufacture its housing. In the process of getting the CAD files ready for 3D printing, the team could never be certain if their parts would be strong enough to withstand the harsh environment of grit-blasting in building and construction that they would be exposed to. To be certain that their parts would be strong enough, the author had several of them 3D-printed in various materials and build orientations, and destructively tested them to see how well they would perform. This was expensive, time consuming, and wasteful, and he frequently wished for an approach that would assist him with optimising the strength of the parts he was working on in terms of choice of materials, part orientation, and surface texture.

1.1 Background and motivation

To be able to consider designing a 3D product for end-use, the product designer must consider how it will be made, which can be done in a multitude of ways, ranging from handmade to large volume mass production. Humans have been making things with their hands since they stopped walking on all fours, and the resulting structural changes in the hand prepared our human ancestors for increased use of tools and for our own remarkable ability to design and manufacture them (Wilson 1998). When making something by hand, the quality of the resulting artefact depends on the skills and experience of the craftsman. Due to this, many craftspeople fine tune their skills over many years in one particular field (Sennett 2009). An example of such a profession is a surgical instrument maker who predominantly works with surgical grade stainless steel and designs, and makes surgical instruments specifically customised to the specialised needs of individual surgeons. Although this approach limits the craftsman to a particular field of specialisation, it allows them a very high degree of flexibility in customising the products they make to the needs of one specific individual.

At the other end of this spectrum sits large volume or mass-production, where products are produced in the thousands or hundreds of thousands or more. Mass-production and mass consumption have their roots in the years before 1800, but it was not until the beginning of the nineteenth century that the word 'mass' took on a real meaning (Sparke 1992). Ever since the industrial revolution, which started in 1760 and was driven forward by the American system of manufacture, first implemented around 1850, we have been mass-producing the majority of our products. Some early examples are the Singer Standard No. 1 sewing machine, invented in 1858 (Sparke 1992), and the Thonet Chair Type No. 14 (1859), of which 50 million had been manufactured by 1910 (Sembach, Leuthäuser & Gössel 1991). But it was Henry Ford who gave the term mass-production the meaning it carries today, when he invented the moving line system of the production line for chassis assembly of the T model Ford in 1914 (Sparke 1992). Indeed, to this day, the vast majority of our products are mass-produced, which means they become homogenised in their functions and appearance in order to satisfy large groups of users (Ball & Overhill 2012). The main reason for doing this is to keep costs low through standardisation of parts; making many of the same allows production to be

streamlined. As Ford stated, “The way to make automobiles is to make one automobile like another automobile, to make them all alike, to make them come from the factory all alike, just like one pin is like another when it comes from a pin factory” (Rae 1967, p. 59). Although this brings the price of products down, producing products in this way comes at a price of a different kind. Apart from homogenised functions and appearance, customising mass-produced products to the specific needs of people is almost impossible, yet highly desirable. Another issue is overproduction, where more is produced than can be sold/consumed, clearly demonstrating that we need to find other ways to manufacture our products. As Sterling states:

... the production methods currently used are not sustainable. They are large in scale, have long histories, and have been extensively researched and developed, but they can't go on in their present form. The status quo uses archaic forms of energy and materials which are finite and toxic. (2005, p. 5)

The low cost of consumer products also encourages over-consumption, which is not the fault of product designers, but rather, is something developed nations in particular are guilty of.

However, due to new manufacturing technologies such as 3D printing, a new possibility has emerged that offers, both in terms of cost and implementation, the manufacture of products in production numbers as low as one single unit (Campbell et al. 2003). To quote Sterling once more:

The world of organized artifice is transforming in ways that are poorly understood and little explored. There are two reasons why this is happening. First, new forms of design and manufacture are appearing that lack historical precedent, and are bound to create substantial novelty. (2005, p. 5)

It is likely that one of the new forms of manufacture that Sterling is speaking of is 3D printing, of which a detailed explanation can be found in Section 2.1: 3D printing. As mentioned earlier in this section, the author has used 3D printing as a method to manufacture products for end use on past projects. He repeatedly found himself becoming frustrated with the lack of information and data available to make knowledge-directed decisions about how best to make a product through 3D printing, specifically in polymers. This is not to say that

there is no information available, but it is rather insufficient and presented in abstract ways, which makes it challenging to apply in practice during the design process of a product or design project. In Section 2.3: End-use products made from 3D printing, several case studies are presented that discuss this in detail; however, some examples of insufficient information are:

1. Supplier test data on the Material Data Sheets (MDS) cannot be relied on as they frequently do not correlate with independent test results (this will be further discussed in Section 2.3.2: Benchmark studies of 3D printed polymers);
2. Two different standards are used, ASTM and ISO, and within each of those, different types of testing methods are applied; this makes cross referencing the data almost impossible. Where data is available, it is typically presented in abstract tables and charts that require additional steps of data interpretation and/or visualisation to make it useful to product design process.

If well-established manufacturing methods are used, design development is the stage in the design process during which a product, or parts thereof, are optimised so they can be made. Typically, following concept design, design development is the formative stage, which seeks to refine the chosen concept into a product that satisfies the requirements outlined in the product design specification (design brief) (Milton & Rodgers 2013). At this stage, it is common practice that a product designer (or design team) takes control of the project, although they don't do this in isolation, and if necessary, will continue to communicate with other relevant stakeholders, especially when decisions need to be made that affect the original concept in fundamental ways. During this stage, product designers will consider: first, how the product will be *handled* (interaction); second, what *form* it will take; and third, its *materiality*. Interaction defines and drives how a person will experience and make use of the product. Form relates to what physical form the product and its individual parts will be given and how it will feel. Materiality defines what the product will be made from, and is also related to how it will feel, as well as how it will be able to withstand the mechanical forces that will be exerted on it. Design development is a complex stage, because all three of those elements are interdependent, need to be considered almost simultaneously, and, as a result,

are constantly cross referenced against each other. To assist them during this process, product designers use existing knowledge such as reference material and expertise to guide decisions and resolve details. For interaction and form, the literature ranges from anthropometrics to user experience and affordances to cognitive object recognition (see Section 2.5: Interacting with products). In the case of materiality, there is also much reference material available if well-established manufacturing processes, such as injection moulding in polymers, are to be employed. However, if designers want to make parts using 3D printing, they need to consider and account for this earlier in the design process than the design development stage. This is because 3D printing offers more freedom to design parts with complex geometries that don't require dedicated tooling, as well as certain characteristics that 3D printing materials have, such as strength and surface texture, that need to be considered (more on this in Section 2.4: Strategies to optimise part orientation), and there is currently a lack of knowledge available to make knowledge-directed decisions, for instance, regarding part strength (see Section 2.3.1: Static and mechanical properties of the three 3D printed polymers). When 3D printing in polymers, there are different materials and methods to choose from, and because the material is deposited in horizontal layers, the orientation in which the part is built may have an effect on strength (see Section 2.3.3: Material/process specific studies). On handheld objects, the build orientation can have additional meaning if the build layers are visible or the surface texture is rough, because it will affect the way a person experiences the product's visual appearance and tactility when interacting with it. An analogy for this is a craftsman selecting a piece of wood to make a product from. If the wood grain is to be seen (not covered with an opaque paint finish) it will have an effect on the visual appearance of the product, and so will affect the way a person will experience it (see Section 2.5: Interacting with products). More pertinent to this research, however, is that the direction of the wood grain in relation to the part geometry or the way it is to be used can have an effect on strength, so the craftsman must take that into consideration as well. The build orientation in 3D printing affects a part's strength in similar ways that the grain direction does in wood, because the printers deposit the material in horizontal parallel layers. As mentioned earlier, and as the reviewed literature proves (see discussion in section 2.3.4: Discussion of end-use products made

through 3D printing), there is currently a lack of knowledge available to designers in relation to build orientation and part strength, specifically for parts to be built in polymers. If designers have more knowledge regarding build orientation in relation to strength, they will be able to design more efficiently, and create potentially stronger and more durable parts while using less material. Therefore, collecting and analysing data on material strength in relation to build orientation for 3D printed polymers from which end-use parts could be made will be of benefit to designers. To investigate this, Research Question 1a and 1b (see Section 3.1: Research questions) are posed, in answer to which, Methodology Part 1 was developed: three material testing methods were selected, all of which are in accordance with the standards of the American Society for Testing and Materials (ASTM). Test samples were then printed in three different materials/machine types, namely:

1. Fused Deposition Modelling (FDM) in Acrylonitrile Butadiene Styrene (ABS).
2. Material Jetting (MJ) in Tripropylene Glycol Diacrylate (TPGDA).
3. Selective Laser Sintering (SLS) in Polyamide (PA).

For each test method, the test samples were printed in several different orientations, at 0 deg (horizontal), at a 45 deg incline, and at 90 deg (vertical). The analysed data and the resulting approach will help designers wanting to utilise 3D printing in polymers for end-use production to design their parts more effectively (see Section 3.2.1: Methodology Part 1).

Because the feel and look on the surface of a product is a design consideration, product designers need to be able to visually check the appearance of a surface based on a specific build orientation. To assist designers with this, research question 2 was posed (see Section 3.1: Research questions) for which Methodology Part 2 was developed, where six software applications were analysed, the results of which offer an approach for clear surface representation prior to building the part (see Section 3.2.2: Methodology Part 2).

Chapter 2. Existing knowledge and related literature

This chapter is divided into six sections that each examines either existing knowledge or literature that is related to this research. The bulk of this chapter is in the form of a literature review, yet it has been titled “Existing knowledge and related literature”. This is because some things, such as 3D printing, simply need explaining so it is clear what areas are being looked at more closely than others. The framework of this chapter is set by the author’s experience as a practising designer, and the directions of investigation are specific to his needs. Each section ends with a discussion which, in combination, lead into Chapter 3.0: Research questions and methodology.

2.1 3D printing

Additive Manufacturing (AM) is the technically correct term for products that are made using processes where the material that the product is manufactured from is deposited in layers, each one added on top of the next. The other, more widely accepted, term is three-dimensional or 3D printing; therefore, this term will be used from this point on. 3D printing is done inside 3D printing machines where the process of depositing the material is referred to as building, and the area inside the machine where parts are built is called the build volume. The American Society for Testing and Materials (ASTM) defines 3D printing as processes of joining [adding] materials to make objects from virtual 3D model data, usually layer upon layer, as opposed to subtractive and formative manufacturing methodologies (ASTM 2015b). Subtractive manufacturing methods are methods where material is removed in the process, such as carving a form out of a solid block of material. Formative manufacturing methods are methods where the existing form of a material is re-shaped into a new one, such as folding a piece of paper to create a structure or object such as a paper plane. The 3D printing concept is based on solid freeform manufacturing technologies for the direct automated production of bespoke parts and products in small to medium-sized batches, without resorting to specific moulds and tools (Monzón et al. 2015). 3D printing was first commercialised in 1987 in the form of stereolithography (Wohlert 2016), and up until the early 2000s, was predominantly used for the production of prototypes, proof of concept models, verifying if parts fit

together with other parts, and checking part geometry before investing in tooling for mass-production.

According to Gibson, Rosen & Stucker (2010) a 3D printed part is created in eight steps:

- Step 1, CAD. All 3D printed parts must start from a virtual 3D software model that fully describes the external geometry.
- Step 2, conversion to STL. The CAD file is converted to STL (Standard Triangulation Language) which is the file format accepted by nearly every 3D printing machine. This file forms the external closed surfaces of the original CAD model and forms the basis for calculation of the slices.
- Step 3, transfer to 3D printing machine and STL file manipulation. The STL file must be transferred to the 3D printing machine. Here there may be some general manipulation of the file so that it is the correct size, position, and orientation for building.
- Step 4, machine setup. The 3D printing machine must be properly set up prior to the build process. Such settings would relate to the build parameters like the material constraints, energy source, layer thickness, timing, etc.
- Step 5, build. Building of the part is mainly an automated process and the machine can largely carry on without supervision. Only superficial monitoring of the machine needs to take place at this time, to ensure no errors have taken place, like running out of material, power, or software glitches, etc.
- Step 6, removal. Once the build is completed, the parts must be removed.
- Step 7, post processing. Once removed from the machine, parts may require an amount of additional cleaning up before they are ready for use (see also Section 2.1.2).
- Step 8, application. Parts are now ready to be used.

It is important to note that Gibson, Rosen and Stucker's eight steps are only about the manufacturing of a part, the process one has to take to make a part through 3D printing. This research aims to improve on the product design process for 3D printed parts, the process of which needs to start long before

the above Step 1. The author would therefore add an additional step before Step 1, which is the process of designing the part, without which none of the other steps can happen. This is the predominant reason why an entire section has been dedicated to product design process (see section 2.2: The process of designing a product), because a review of the product design process enables a clear argument for the stage in the process at which decisions need to be made in relation to material, build orientation, and surface texture.

2.1.1 Types of 3D printing processes and available materials

Although all 3D printing systems work on the same principal, they can be categorised into seven distinctly different processes (Wohlers 2016):

- *Material extrusion*- a 3D printing process in which material is selectively dispensed through a nozzle or orifice (aka Fused Deposition Modelling or FDM).
Materials: Thermoplastics, ceramics, composites, metal-filled clays, concrete, food, and living cells suspended in a hydrogel or other substance.
Requires support material.
- *Material jetting*- a 3D printing process in which droplets of build material are selectively deposited.
Materials: Photopolymers and wax-like materials.
Requires support material.
- *Binder jetting*- a 3D printing process in which a liquid bonding agent is selectively deposited to join powder materials.
Materials: Plaster-based and acrylate-based powders, sand, metal.
Does not require support material.
- *Sheet lamination*- a 3D printing process in which sheets of material are bonded to form a part.
Materials: Paper, metal foils.
Does not require support material.
- *Vat photopolymerisation*- a 3D printing process in which liquid photopolymer in a vat is selectively cured by light-activated polymerisation.
Materials: Liquid photopolymers.

Requires support material.

- *Powder bed fusion*- a 3D printing process in which thermal energy selectively fuses regions of a powder bed (aka Selective Laser Sintering or SLS).

Materials: Polymer and metal.

Polymers do not require support material, metals do.

- *Directed energy deposition*- a 3D printing process in which focused thermal energy is used to fuse materials by melting as they are being deposited. Most direct energy deposition systems use a 4- or 5-axis motion system or a robotic arm to position the deposition head, so the build process is not limited to successive horizontal layers on parallel planes.

Materials: Metal.

Does not require support material.

2.1.2 Post-processing of 3D printed polymer parts

Once manufactured, all 3D printed parts require some degree of post-processing. Post-processing means that after the 3D printing machine has completed building the part, some work needs to be done to it before it can be used. General post-processing is the work that must be done before a part is ready for use. General post-processing begins with the part being removed from the machine, which is done manually. With the exception of SLS, both FDM and MJ require their parts to be built on a build platform which the part is adhered to during the build, so the part may need to be removed from the build platform, which is also done manually. 3D printing processes that require support material then need to have that removed, which is also done by hand. With SLS, this is a straightforward process, because the support material is the leftover unsintered powder that surrounds the built parts. The parts are literally dug out of the powder and then cleaned up with a jet of compressed air or with a brush (see Figure 2.1).



Figure 2.1: General post-processing of an SLS part (courtesy of *i.materialise*).

For FDM, the process can be more time consuming, depending on how much support material was used and how complex the part geometry is. Figure 2.2 shows a teapot 3D printed in ABS with the support material still underneath and inside the part. There are methods to speed up the removal process, for example if water soluble support is used, and the part, including support material, can be placed in a tank containing hot water and detergent, which then dissolves the support material but not the part.



Figure 2.2: Teapot 3D printed in ABS by FDM with support material still in place.

MJ uses wax as support material, and once the part has been removed from its build platform, there are three more steps needed which require special equipment: 1. Bulk wax removal in a melting oven for approximately 30 min; 2. Fine wax removal in a heated oil bath; 3. Removing oil residue by washing the parts in warm soapy water (see data sheet in Appendix A).

With general post-processing complete, the part would theoretically be ready for use. However, additional post-processing may be desired, especially with respect to the surface texture and colour, depending on how the designer designed the part and what its intended use is. The surface texture is a particularly prominent characteristic of 3D printing because, as mentioned above, 3D printing machines deposit the material in horizontal parallel layers one on top of the next. This can lead to what is known as stair-stepping (see Figure 2.3) and depending on the layer thickness, the stepping can be prominent, in particular on FDM parts.

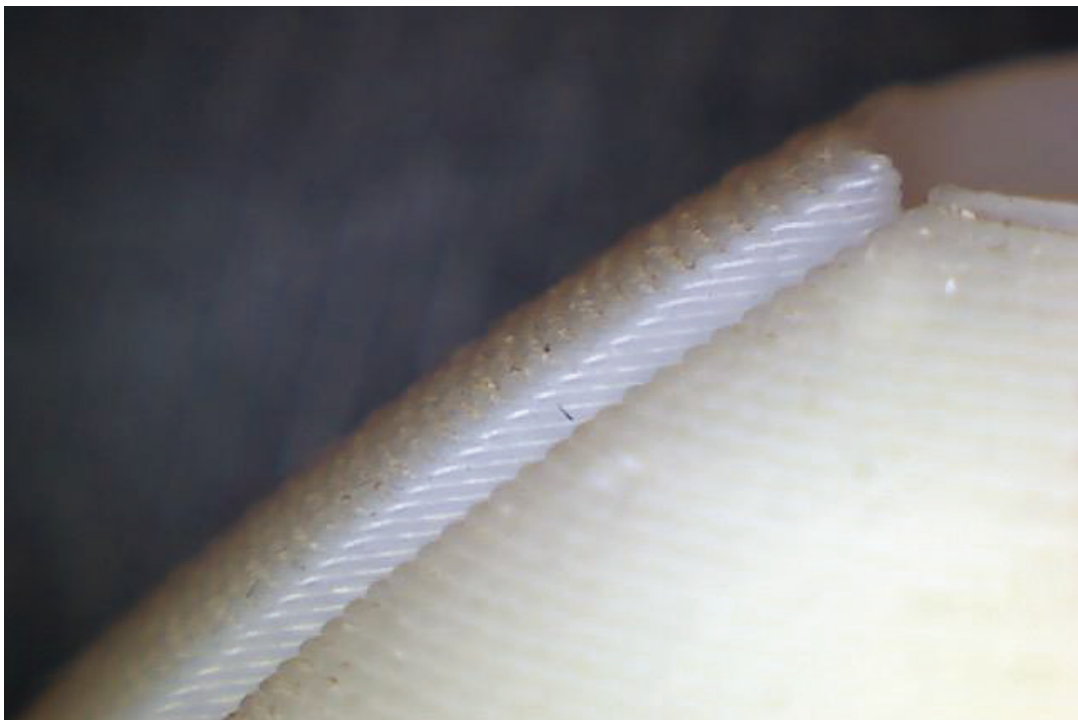


Figure 2.3: Stair-stepping effect of FDM in ABS, layer height 0.254mm.

Other processes, such as SLS, produce parts with a rough surface texture that visually resembles suede or flocking (see Figure 2.4), in addition to the stepping.

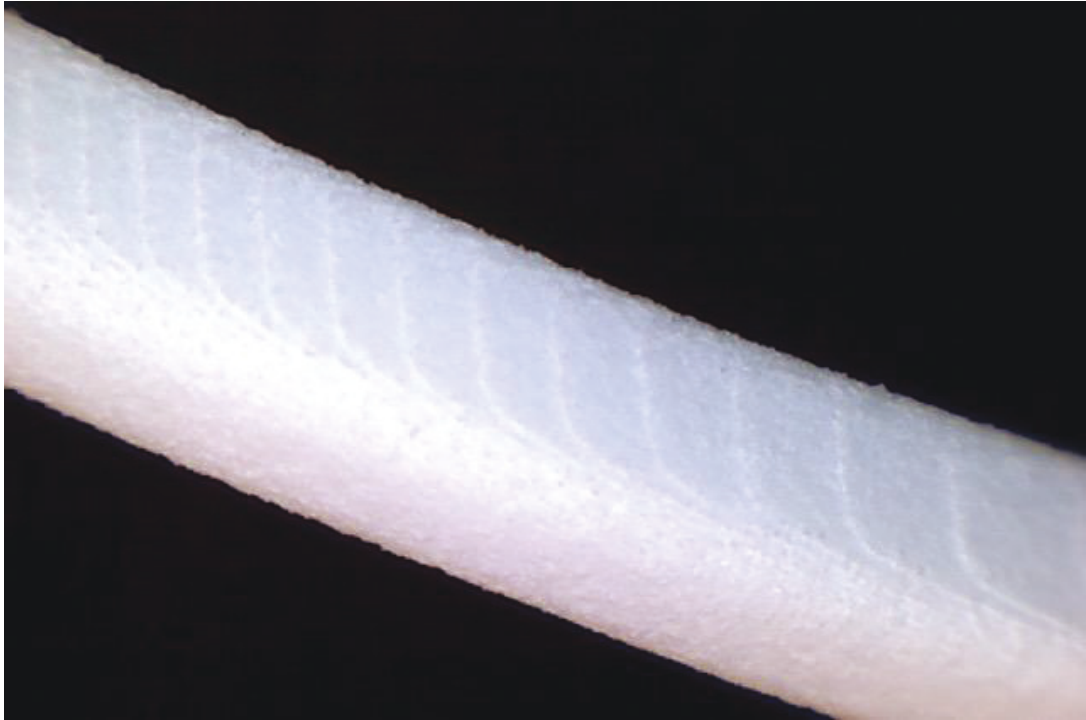


Figure 2.4: Stair-stepping and surface roughness of SLS in PA, layer height 0.1mm.

Both of these characteristics are typically cited as constraints or weaknesses of parts produced with 3D printing technology, because they are compared with parts manufactured in moulds which can produce any type of surface texture, even high gloss. To achieve surfaces on 3D printed parts comparable to those of moulded ones, considerable labour-intensive processes, such as sanding, filling/puttying, and polishing are required. Wohlers states that the primary advantages of 3D printing are design freedom and direct manufacturing from CAD data, which allow for on-demand manufacturing, a great amount of design variation, and short lead times - all at little additional cost (2016). When several post-processing steps are added to the manufacturing chain, the advantages of low inventories, short lead times, and on-demand manufacturing are partially lost (Wohlers 2016), which is the predominant argument to keep post-processing to a minimum. Some 3D printing service providers offer vibration grinding, a process that allows many parts to be made smooth at the same time. Vibration grinding is widely used, mainly to improve appearance (Wohlers 2016). The parts, together with grinding aggregates similar to pumice stones, are placed in large vats and agitated through vibration. The agitation causes the parts to rub up against the aggregate, which in turn grinds the surface of the parts smooth, and in some

cases can completely remove the surface characteristics from the 3D printing process (Wohlers 2016). It is a cost-effective method because it requires little hand finishing, but can affect the dimensional accuracy of a part, as it removes material from all surfaces and edges.

Rather than mechanically modifying the surface, as discussed above, it is possible to reduce or disguise roughness or the stair-stepping effect on the surface of a 3D printed part by applying a surface texture that is more pronounced than roughness or the stair-stepping. This has the effect of changing the way the surface reflects the light and in so doing detracts from roughness or the stair-stepping. Companies such as Lehrmitt Design Studios offer digital surface texture products that people can purchase and apply to their CAD models. Figure 2.5 shows some examples of the 3D printed surface textures that Lehrmitt Design Studios offer.

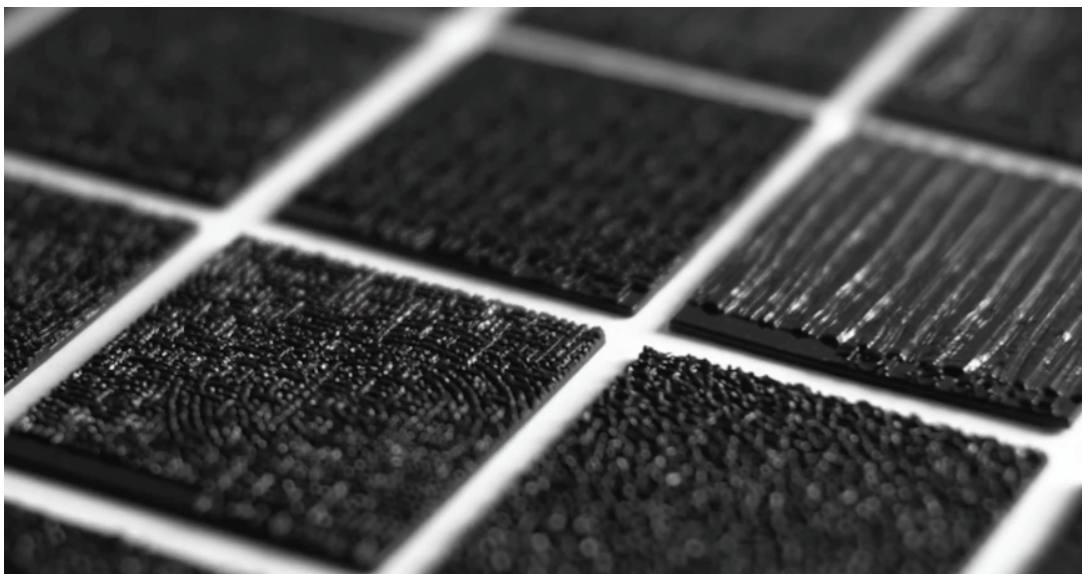


Figure 2.5: 3D printed surface textures (courtesy of *Lehrmitt Design Studios*).

Another challenge that 3D printed polymers face are the limitations of colour options during building. For both MJ and FDM there are a range of colours available, mainly limited to the primary and secondary colour spectrum; SLS polymers, on the other hand, are limited to white, dark grey, and black. Colouring parts post-build can be done through painting, either with a brush, spray painting or dipping, but this usually requires additional sanding in between coats. Dyeing is a popular method that can be used on all three materials but works best on SLS polymer parts. The dye from the process

penetrates deeply into the parts, resulting in rich, lasting colours without affecting the dimensions (Wohlers 2016). However, the current range of colours for dyeing offered by 3D printing service providers, such as iMaterialise and Shapeways, is also limited to primary and secondary colours.

2.1.3 Discussion of 3D printing

From this point forward, the research and discussions will be centred around, and in reference to, three polymers and their respective processes. The reasons for these limitations will be discussed in Section 2.3.1: Static mechanical properties of the three 3D printed polymers; here, they are summarised as follows:

- Ensuring the scope of the research is manageable.
- Covering the processes and materials suitable for end-use part production as recommended by the literature.
- Accessibility to 3D printing technology in the Sydney metro area.

Therefore, this research is limited to 3D printed parts made from these three polymers and their processes, which are:

1. *Material extrusion*, henceforth referred to as FDM (Fused Deposition Modelling) (see Figure 2.6), in the material ABS (Acrylonitrile Butadiene Styrene).

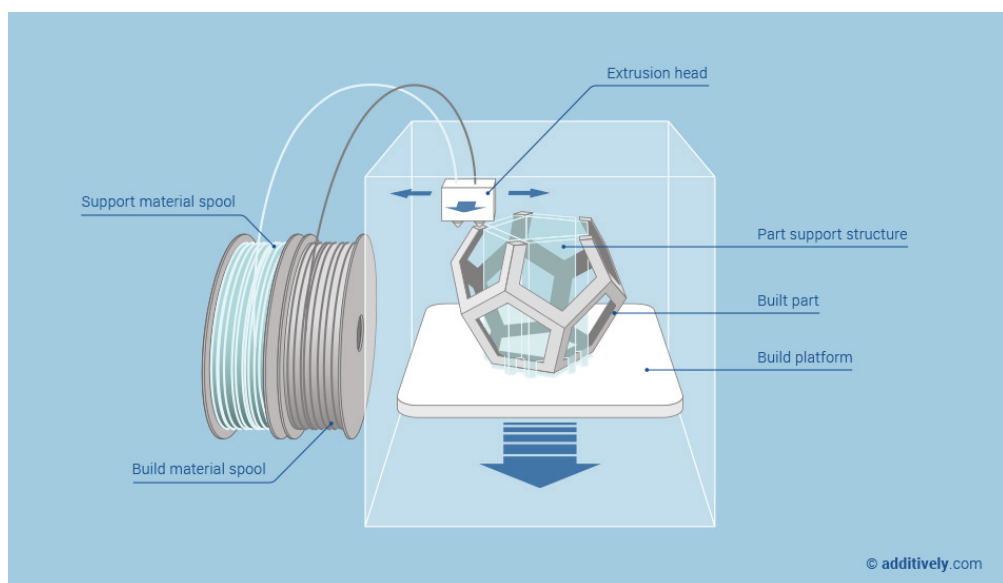


Figure 2.6: Schematic representation of the FDM process (courtesy of *additively*).

2. *Material jetting*, henceforth referred to MJ (see Figure 2.7), in the material TPGDA (Tripropylene Glycol Diacrylate).

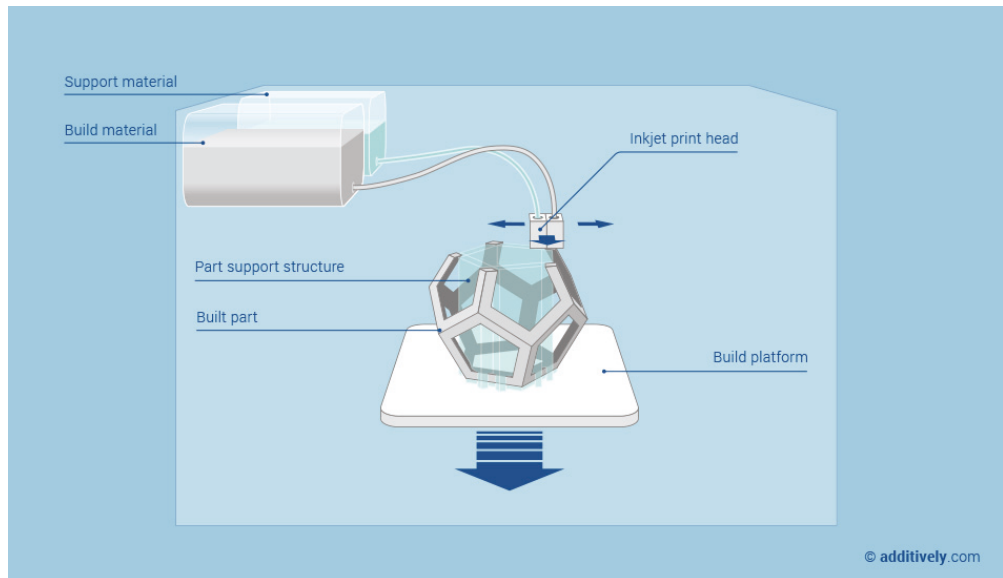


Figure 2.7: Schematic representation of the MJ process (courtesy of *additively*).

3. *Powder bed fusion*, henceforth referred to as SLS (Selective Laser Sintering) (see Figure 2.8), in the material PA (Polyamide).

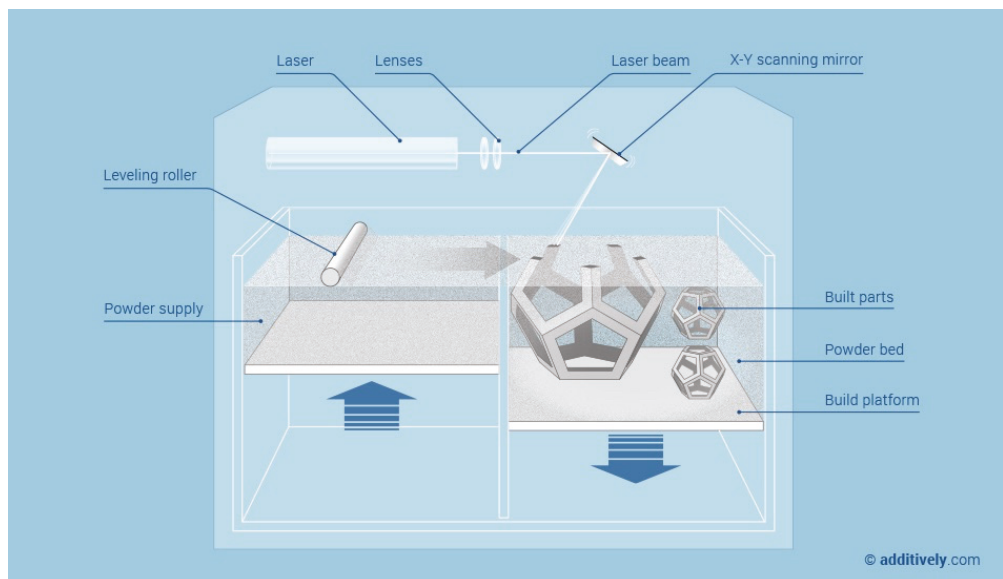


Figure 2.8: Schematic representation of the SLS process (courtesy of *additively*).

The general post-processing of 3D printed parts is taken as a given for this research, since it is typically done by the bureau or service provider and not by the person who has designed the part. Furthermore, general post-processing is typically done in the same way, albeit specific to a process and its material.

Additional post-processing, such as vibration grinding, manual sanding, dyeing and painting, will not be included as part of this research as it is a complex area in itself. This is because the way a part is post-processed can vary substantially, both in the way it is done and how the resulting part will look. For example, the same part made from PA through SLS could be finished by sanding it by hand or in a machine through vibration grinding, and it may be spray painted, painted with a brush, or dip dyed.

Reducing or disguising surface roughness or the stair-stepping effect on the surface of a 3D printed part by applying a surface texture will also not be included as part of this research. The reason for this is that the applied texture can influence the dimensional accuracy as well as the mechanical properties of a part.

2.2 The process of designing a product

It is important to understand when during the design process designers make key decisions about form, function, and materiality. What follows is an outline of the relevant stages of a typical product design process and how the stages relate to design for traditional manufacturing processes as well as design for 3D printing. It is understood that not all scholars and practitioners will agree with the titles and sequencing of the stages and that they may vary.

The process of designing a physical product is typically divided into several stages, which, according to Milton and Rodgers (2013, p. 14), are:

1. Opportunity identification
2. Research
3. The brief
4. Concept design
5. Design development
6. Detail design
7. Production.

Opportunity identification is the reason for a project to be initiated and can be defined as the point at which someone decides to commence it. This can be a

self-initiated project, where a single person has identified an opportunity and starts working on the project out of their own motivation; in other words, the initiator and the designer are the same person (Walden & Dorst 2013). The more typical way for a project to be initiated is where a person or corporation has identified an opportunity and engages a designer or design team to design the product for them. In this case, the initiator and the designer are usually not the same person or organisation, although many organisations have in-house design teams.

Research is the background and exploratory stage during which information is collected that will help to build a clear understanding of the problem space and to ascertain how uncovered issues could be best addressed. Once the problem space is clearly understood, more specific research needs to be conducted, for example into how the potential product will be interacted with and experienced. All physical artefacts are made to be interacted with by sentient animals, which means the artefact will be experienced both physically and psychologically. Other areas of research may include, but are not limited to, environmental sustainability of the product and how it will be made. For each area, there are a multitude of research methods available (see Kumar 2012; Milton & Rodgers 2013; Muratovski 2015) and it is up to the researcher/s to decide which ones will best suit the project they are working on. It is also not uncommon for certain research areas to be revisited and iterated as the project progresses through the later stages.

The brief is better understood as a document rather than a stage. It focuses on the construction and analysis of a design brief based on the research findings from the previous stage and identifies the customer's needs, and establishes a comprehensive product design specification (Milton & Rodgers 2013). The brief typically also functions as a form of contract that clearly frames the scope of the project and ensures both parties understand what their responsibilities are.

During *Concept design* the product begins to take shape conceptually. This can be in 2D form as drawings or sketches, in 3D form as mock ups, models or quick prototypes, or a combination of all. And often several concepts are being developed simultaneously. Because the concept is under development and is not fully constrained by limitations yet, it is important to explore as many

options as possible by iterating earlier concepts and developing them as far as possible.

Design development is the formative stage where all elements of the concept are brought together, the product is given its form and all functions are clearly defined. At this stage where interaction, form and materiality are paramount and need to be considered simultaneously, good design development is heavily dependent on the level of experience and expertise the designer has; the more experience and expertise, the more potential solutions the designer can consider (Cross 2006).

The *Detail design* stage covers the key steps of transforming the chosen concept design into a fully detailed design, with all the necessary dimensions and specifications of the product specified on a detailed drawing (Milton & Rodgers 2013).

Production is the final stage at which production of the product is implemented.

2.2.1 Design for manufacturing (DFM)

The above outlines the process a product or industrial designer would work through when designing a 3D product to be manufactured using traditional manufacturing methods, and is typically referred to as Design For Manufacture or DFM. Creating designs suitable for manufacturing has predominantly relied on designing for moulds as the basis of making multiple repeats (Loy 2015), so products can be mass-produced in factories at an industrial scale. The process of designing products for industries so they can be mass-produced is where the profession of industrial design derives its name. The two, design and industry, are so deeply connected, both pragmatically and historically, that designing in this way has become a school of thought or a philosophy, and it will take time to adapt and change this philosophy to suit different manufacturing technologies such as 3D printing. To begin with, product designers need to disconnect themselves from their reliance on traditional manufacturing technologies. Currently, the main concern of product designers is to design products in the most optimal way so they can be mass-produced. From the designer's perspective, mass-production is indirect manufacturing,

which means they are not directly involved in the manufacturing process itself. For example, the tools used for mass production are usually designed by design engineers, made by toolmakers, and the overall manufacturing process is then managed by production engineers. Product designers rely on those professionals to ensure that the manufacturing of the product is done correctly and runs smoothly. Loy states that 3D printing is now a viable direct manufacturing technology that has the potential to provide a paradigm shift for designers and will significantly change their role (2015). Direct manufacturing means that the product can be directly made with no in-between step, such as the need for dedicated tooling to manufacture the end product. This enables the designer to create products more specifically for function rather than having to compromise for the manufacturing process (Loy 2015). This brings with it the potential to bring the designer closer to the people they are designing for, and allows designers to make key decisions earlier in the process. For example, if the *design development* stage is the formative period in the design process of a product for traditional manufacturing methods, the previous *concept design* stage would be better suited as the formative stage for products made using 3D printing. It is also important to note that some stages may occur in a different sequence or may even be omitted altogether, as each product has its own unique set of requirements (Milton & Rodgers 2013). Furthermore, when using 3D printing for manufacturing, the *detail design* and *production* stages take on additional significance, because they allow for form, design details, the print orientation, and even the material of the product to be changed after production has commenced. This flexibility is nearly impossible to achieve using DFM manufacturing processes.

2.2.2 Design for 3D printing/additive manufacturing (DFAM)

As discussed in the previous section, the decisions relating to manufacturing in the stages of traditional DFM processes are not suitable for 3D printing and need to be rethought. The following section investigates methods aimed at optimising the design process for products to be manufactured using 3D printing, or simply put, designed for additive manufacturing (DFAM).

In the past two decades, there has been a lot of optimism in relation to the additional freedom that 3D printing can offer designers. This is due to the fact that when designing a product, or parts thereof for manufacture, using traditional DFM that requires a tool such as injection moulding, the part has to be designed in such a way that it can be demoulded and avoids non-uniform shrinkage. With moulding processes, the demoulding is addressed through draft and by avoiding undercuts, and non-uniform shrinkage is achieved by ensuring the part has a uniform wall thickness; as a result, product designers are taught to design relatively simple parts. However, the capabilities of 3D printing technologies provide an opportunity to rethink DFM to take advantage of the unique capabilities of these technologies (Gibson, Rosen & Stucker 2010). If a part is being made using 3D printing, none of these are a constraint any longer, hence the optimism. Indeed, one of the major benefits of 3D printing is that it is possible to make any complexity of geometry at no extra cost. This is virtually unheard of, as, in every conventional manufacturing technique, there is a direct link between the cost of a component and the complexity of its design (Hague, Mansour & Saleh 2003). This is a highly relevant observation and relates to Loy's earlier comment regarding the potential paradigm shift for designers, because the degree of complexity in relation to part geometry is likely to increase the more end-use products are manufactured using 3D printing. Diegel et al. state that 3D printing enables the creation of parts and products with complex features, which could not easily have been produced via subtractive or other traditional [DFM] manufacturing processes (2016). This is due to the fact that with DFM, the more complex the design, the more expensive the part becomes, and as a result, designers spend large amounts of time reducing this complexity to save cost during production. As Gibson, Rosen and Stucker put it, DFM is about the designer understanding the constraints imposed by manufacturing processes, then designing products to minimise the constraint violation (2010). Prior to 3D printing being considered for end-use production, this process of reducing complexity combined with the need for products to have broad market appeal has led to the products around us being simple and homogenous. As mentioned earlier, with 3D printing, complexity in relation to form no longer matters because almost any geometry can be made using 3D printing, so product designers will be able to save time formerly spent reducing part complexity. The Immortal-

Mechanical-Paddles for Playstation gaming, designed by Soludus, are an excellent example of such complexity (see Figure 2.9). These paddles, shown in red, are designed to reduce reaction time in computer console gaming and clamp onto a standard PS4 (PlayStation 4) controller, shown in black. The paddles are made with the 3D printing process SLS in the material PA and are built in one piece, with all moving parts assembled. The juxtaposition of the two devices contrasts DFM with DFAM very well, where the black PS4 controller was designed and made via DFM and the red Paddles through DFAM. And one does not have to understand computer gaming to appreciate the complexity of this device.



Figure 2.9: Immortal-Mechanical-Paddles by Soludus on a PS4 controller.

This is one area where product designers will need to adjust their design process when using 3D printing. However, despite the freedom 3D printing offers, as is the case with any manufacturing method, designers still need to consider some factors and will encounter some constraints when using 3D printing (Zhang et al. 2014) and therefore must have a clear understanding of the process and material characteristics of 3D printing before entering the design process (Leutenecker-Twelsiek, Klahn & Meboldt 2016).

Gibson, Rosen and Stucker believe that the objective of DFAM should be to maximise product performance through the synthesis of shapes, sizes, hierarchical structures, and realise this objective, designers should keep in mind several guidelines when designing products:

1. 3D printing enables the usage of complex geometry in achieving design goals without incurring time or cost penalties compared with simple geometry.
2. 3D printing enables the usage of customised geometry and parts by direct production from 3D data.
3. With 3D printing, it is often possible to consolidate parts, integrating features into more complex parts and avoiding assembly issues.
4. 3D printing allows designers to ignore all of the constraints imposed by conventional manufacturing processes (although 3D printing-specific constraints might be imposed). (Gibson, Rosen & Stucker 2010).

Two of the main challenges DFAM faces are the skills of the designer using CAD and the limitations of CAD software itself. Bodein, Rose and Caillaud state that courses offered by CAD training services or universities are generic because they have to prepare the learner to design new products, irrespective of the product development process (2013). This means that CAD skills for highly specific situations, such as DFAM, are only present if the designer has been trained for them. To assist designers with this shortfall Bodein, Rose and Caillaud suggest that additional coaching and support are necessary to enable an employee to be fully efficient (2013). The other challenge that DFAM faces is that the CAD tools used in product design, such as Solidworks, Rhinoceros, and SharkCAD Pro, were not developed with 3D printing in mind and do not accommodate or support the needs a designer might have when designing a product for 3D printing. For example, if geometric complexity no longer matters, CAD must be able to support models with tens and hundreds of thousands of features (Gibson, Rosen & Stucker 2010), and many CAD applications are not able to compute large numbers of features. This is connected to the computing power of the computers themselves, but until both the CAD applications and the computers can manage the calculations, this will remain a challenge. Gibson, Rosen and Stucker also state that the CAD applications need to represent the material in a physically based way, where

material composition and distribution must be represented and must be physically meaningful. They go on to say that the representations of properties also need to be physically represented, where desired distributions of physical and mechanical properties must be represented and tested for their physical basis (2010). In other words, a paradigm shift needs to take place: a change from fabrication-oriented construction to design-and-construction-oriented fabrication (Wendel et al. 2008) which shares similarities with the paradigm shift the designers themselves need to go through, as discussed earlier in Section 2.2.1: Design for manufacturing.

Chu, Graf and Rosen propose a formal framework for DFAM which is based upon the process-structure-property relationships from the materials science domain, where analysis of a material consists of examining the microstructure of the material after processing it, and determining its mechanical properties from the microstructure (2008). This approach is at odds with the process product designers typically work through, where the desired behaviour of the product guides the mechanical properties of the material. As we will see in Section 2.3.3: Material/process specific studies, much of the research into the mechanical properties of 3D printed polymers focuses on the microstructure by taking a materials science approach. It appears that the sorts of tools we need for DFAM are a combination of these two schools of thought, where the microstructure of the material and the desired behaviour of the product are automatically matched and updated, which at some point in the future could be achieved through generative modelling CAD applications.

To assist with DFAM, Zhang et al. propose a 2-level process that is brought into action after the design solution has been developed:

- Level 1: referred to as Macro Planning. Considerations: requirement analysing, design analysing and scenario selecting.
- Level 2: Micro planning. Considerations: data checking, orientation, packing planning, support generation, slicing. Tool-path planning and post-processing. (Zhang et al. 2014).

If the mechanical properties of a part are important, then some of the considerations need to be moved to different levels. For example, orientation would need to be a consideration even before level 1 is reached, because the

orientation can have considerable impact on part strength, as we will later see in Section 6.0: Analysis and communication of results.

Yang & Zhao critically reviewed 3D printing-enabled design theory and methodology and concluded that a generic design framework needs to be developed which initialises design from the perspective of achieving functionality; and that most of the current research work focuses on optimising the existing model designed by traditional design methods, which are largely limited by traditional manufacturing methods (2015). Considering the multitude of process parameters that need to be considered in DFAM, a generic framework will not suffice, but would rather have to be customisable. Nevertheless, as with earlier discussions, Yang & Zhao are advocating that new design methods are needed to improve DFAM.

Oropallo & Piegl are also of the view that to utilise the unique qualities of 3D printing, the design process must be rethought from the traditional approaches, and new tools must be created to accommodate this type of design; further, that the CAD software that is currently in use for 3D printing was not designed with 3D printing in mind (2016).

2.2.3 Discussion of product design process

In general, product designers who studied and practice design processes in the conventional sense of DFM need to shift to new and different ways that suit DFAM. This shift is multifaceted and encompasses an in-depth comprehension of the output capabilities of 3D printing technologies. On the pragmatic level, product designers need more tools to help with DFAM, mainly in the area of CAD. Until such time, optimising things such as part strength will need to be done manually, which, depending on the part geometry, can lead to inaccuracies, because it is based on the designer's knowledge of 3D-printed material strength. Furthermore, it will be time consuming and potentially expensive, because the parts will need to be built and tested every time the build orientation is changed.

3D printing offers the possibility of direct manufacturing, and if product designers accept ownership of the manufacturing processes of their products, they are directly accountable for all aspects of the product they have designed.

In Loy, Canning and Haskell's words, the idea of ownership determines a sense of responsibility both for the production of products and for their maintenance (2016).

2.3 End-use products made from 3D printed polymers

An end-use product is a product that has been manufactured for actual use, so must be usable, repeatedly if necessary, in the way that it is intended to be used. As mentioned earlier, 3D printing was commercialised in the late 1980s, and up until the year 2000, was predominantly used for rapid prototyping and for verifying part geometry before commencing mass production. It is estimated that the end-used part production segment of 3D printing accounts for 51.3% of the 3D printing market (Wohlers 2016). And although 3D printing is a long way from replacing traditional manufacturing methods for the production of most parts, some industries have started to rely on it quite heavily. For example, the hearing aid industry began transitioning to 3D printing around the year 2000, and over the past 16 years, an estimated 60 million devices have been produced with the help of 3D printing, according to Keith Guggenberger of Kg Consulting LLC, and former senior vice-president of operations at Starkey Hearing Technologies (Wohlers 2016). The abovementioned 51.3% market share includes all materials (plastics, composites and metals), and the majority of 3D printing end-use parts are likely to be made in metal. This is because 3D printed metal parts are well suited to production applications because they often offer similar or better material properties than parts made with conventional processes (Wohlers 2016). However, the production volume of 3D printed end-use parts made from polymers is steadily rising as well. For example, Boeing has installed tens of thousands of laser-sintered polymer parts on more than 16 different types of commercial and military aircraft (Wohlers 2016).

Below are further examples of end-use products made through 3D printing, followed by three projects presented here as case studies in which the author was directly involved in.

E-NABLE is a not-for-profit organisation made up of an online global community of volunteers referred to as "Digital Humanitarians" (E-NABLE

2019). These volunteers use their FDM 3D printers to manufacture prosthetic limbs for disadvantaged children and adults who ordinarily could not afford such a prosthetic limb (see Figure 2.10). Traditional prosthetic limbs are made by hand and are customised to the exact specifications of the person needing the limb. This requires highly skilled labour which makes limbs made in this way prohibitively expensive for disadvantaged people. All of E-NABLE digital files of their prosthetic limbs are open-source and customisable. 3D printing prosthetic limbs in the way E-NABLE volunteers do offers an alternative to the skilled labour option that allows for mass-customisation of limbs based on the needs of each individual.



Figure 2.10: E-NABLE prosthetic limb (courtesy of *E-NABLE Medellin*).

Paul Hearn of the lighting company Limelight Pty. Ltd. commissioned the Centre for Design Innovation at Swinburne University in Melbourne to design a series of 3D printed track and pendant lights for them (see Figure 2.11). Edgar states that Hearn could see the potential 3D printing could offer

to avoid massive investment in retooling, and zero risk of an expensive, unpopular design languishing on the shelf. With 3D printing you print to order (2016).



Figure 2.11: 3D printed Limelight track lights designed by Swinburne University (courtesy of *Limelight*).

Eckhart Pty. Ltd. develops specialised tools to make the assembly processes of their vehicles more efficient and safer for their workers (Eckhart 2018). Figure 2.12 shows a lug-nut starter tool that enables a worker to get all six lug-nuts on a car rim started all at the same time.



Figure 2.12: 3D printed lug-nut starter tool (courtesy of *Eckhart*).

However, even though the application of 3D printing for end-use part production is steadily rising, it does face challenges from manufacturing sectors that are sceptical about its viability. This has to do with the fact that the properties such as strength and surface texture of 3D printed plastics are frequently compared to those of their injection moulded or extruded counterparts. However, it should be noted that moulded materials have had over a century of development (Hopkinson & Dickens 2001), whereas layer manufactured materials have only had one-fifth of this time.

The products discussed in the case studies below are all products that originated through projects with real clients, where the clients engaged the author to design an end-use product for them. Since completing his Masters he has gravitated towards projects where 3D printing was used for end-use part production; three such projects are briefly outlined below. All projects were for real clients that had highly specific product requirements and all of the products are currently in everyday use. In all cases 3D printing in polymers was used to manufacture parts for end-use.

Case study 1: Sydney Harbour Bridge grit-blasting robot

This project, introduced earlier in Section 1.1: Background, was an industry partnership project between Roads and Maritime Services (RMS) and the Centre for Autonomous Systems (CAS) in the Faculty of Engineering and Information Technology (FEIT) at UTS. RMS is responsible for maintenance of the Harbour Bridge, and was investigating ways to reduce the exposure of their workers to hazardous substances while grit-blasting (Bibby 2010), as well as automating the grit-blasting process, but was unable to find any readily available solutions. CAS had already been conducting research in this area (Liu et al. 2008) and was confident it could deliver a solution tailored to the specific need RMS was trying to address (Paul et al. 2010). Figure 2.13 shows an overview of a typical setup of the robot.

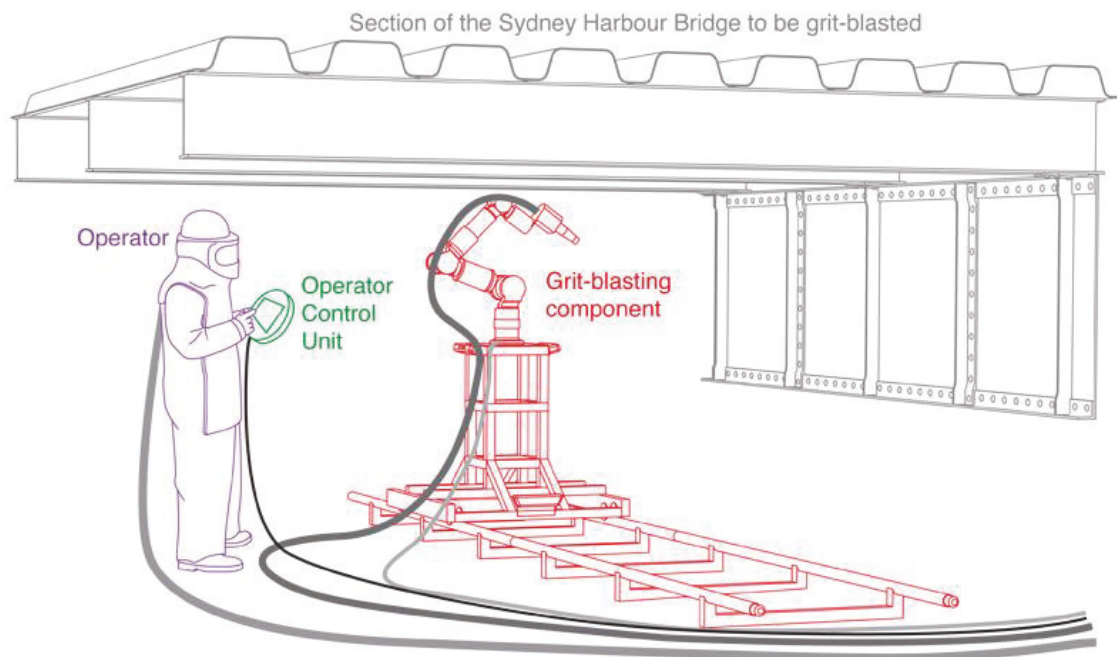


Figure 2.13: Typical setup of the Sydney Harbour Bridge grit-blasting robot.

RMS only needed two systems, so the challenge was to find ways that would make it possible to design and manufacture only two systems efficiently. Designing and building a customised robotic system is not unusual, but the operator control unit used to control the robotic system is typically purchased off the shelf. However, the team was unable to find a suitable operator control unit that would be robust enough to withstand the harsh conditions of a grit-blasting environment, so it was decided that they would design, manufacture and implement their own. This was achieved by taking a co-design approach both for concept and design development as well as manufacturing several key components, such as the housing through 3D printing.



Figure 2.14: A robot set up and ready to blast a section of the Sydney Harbour Bridge.

Figure 2.14 shows one of the robots set up and ready to blast a section of the Harbour Bridge. In the centre of the image, partly blue, is the robotic arm, and the yellow object to the right is our custom-made operator control unit. The project was a success, and there are currently two of these robotic systems operating on the Harbour Bridge.

Case study 2: Interactive stepping tiles

The interactive stepping tiles were developed to aid with the rehabilitation of people who have suffered a stroke. Figure 2.15 shows the tiles in use in one of many possible configurations.

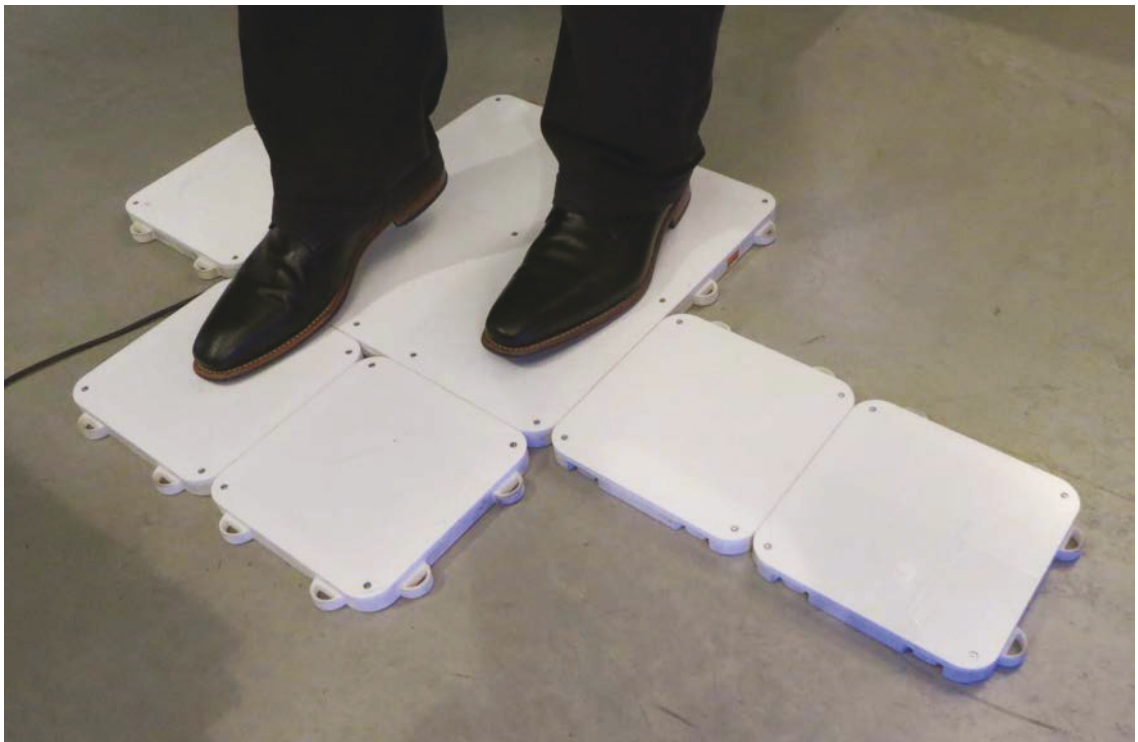


Figure 2.15: The interactive stepping tiles in use.

The tiles were designed and developed in the interactivation studio in the Faculty of DAB at UTS (Bongers, Smith, Donker & Pickrell 2014; Bongers et al. 2014). They are made to order by the interactivation studio, and there are currently five complete systems in use in hospitals and rehabilitation centres around Australia and Europe. Each system comprises a set of tiles (see Figure 2.15) and proprietary software developed by the interactivation studio. An early iteration of this project was presented at a UTS industrial design graduation

show in 2011, after which physiotherapists working in stroke rehabilitation enquired if there would ever be a robust version for purchase. It was unlikely that the tiles would be mass produced in the short to medium term, so the interactivation studio redesigned them to suit manufacturing on demand via computer aided manufacturing (CAM) processes such as 3D printing; in this case, selective laser sintering (SLS) in PA and laser cutting. Because the systems were manufactured on demand, the team was able to update and customise each version based on what they learnt from the previous one. To the clients, the changes were imperceptible, but for the team they were meaningful, in particular with regard to the 3D printed parts. Over time, they were able to reduce the volume of material used by a considerable amount, which reduced our resource consumption, build time and cost, as well as simplifying our assembly process. This project was, and continues to be, a good learning experience for working with 3D printing service providers, in this case Shapeways Pty Ltd, and the importance of being able to specify build orientations. The parts that were getting printed, such as the “main tile” shown in figure 2.16, are quite large at 450mm (length) x 450mm (width) x 18mm (height), as well as flat, which presented the team with some challenges.

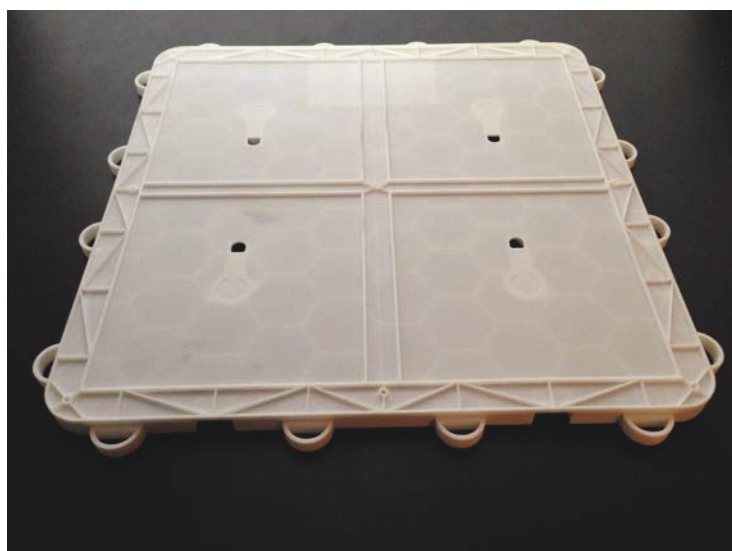


Figure 2.16: The main tile.

On some of these parts, there were problems with dimensional accuracy. This became a considerable problem, because the main tile is part of an assembly that consists of 3D printed and laser cut components. In some cases, the dimensional accuracy was out by several millimetres, which meant they

couldn't be assembled. In Figure 2.17, a gap can be seen between the edge of the white tile on the left and the yellow ruler to the right. Not only was the tile not dimensionally accurate, it was not straight, but rather curved along the edge, as can be seen in Figure 2.17.

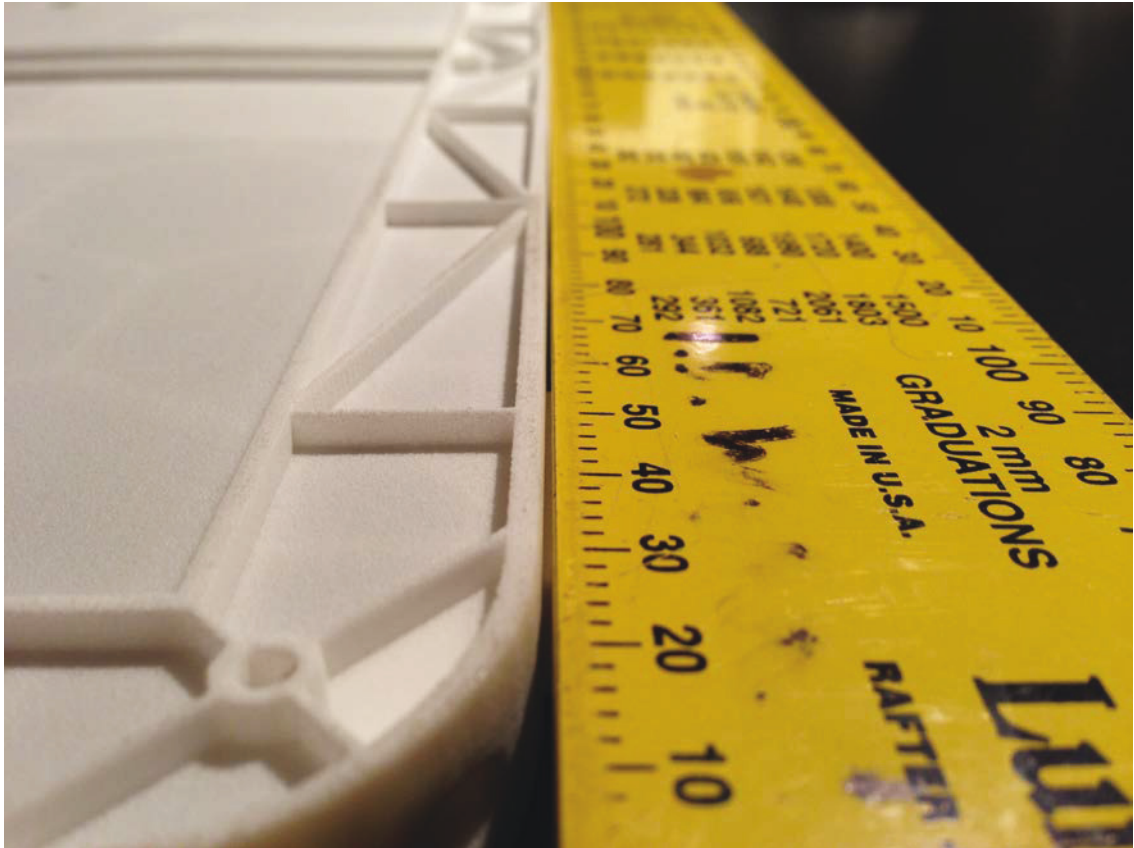


Figure 2.17: Warped main tile (please note the gap between the white tile and the yellow ruler.

This was discussed several times with the helpful technicians at Shapeways, who eventually realised that the warpage was occurring due to the way the parts were placed in the build volume. After further experimentation on the Shapeways side and modification of parts on the design team's side, it eventually became possible to get consistently accurate parts. This does highlight the importance of good working relationships with technicians at print bureaus to ensure reliable quality of 3D printed parts. Which also ties back to the notion of who bears the responsibility of a product once it is handed over to the people who will use it. If someone is the designer, manufacturer, seller, and distributor of a product, the majority of this responsibility lies with the designer, as discussed in Section 2.2.1: Design for manufacturing (DFM).

Case study 3: Visionsearch Head Distancer

Visionsearch Pty. Ltd. is the developer and sole distributor of a software and hardware system designed to assess patients suffering from a range of vision impairments and vision-impairing diseases. At the core of the Visionsearch system lies world-leading science developed by the Save Sight Institute at the University of Sydney. The Visionsearch system comprises a computer, the Visionsearch proprietary software, a screen, a handheld controller, a set of EMG (Electromyogram) electrodes placed on the patient's head, and the Head Distancer. Figure 2.18 shows a complete Visionsearch system setup and in use.

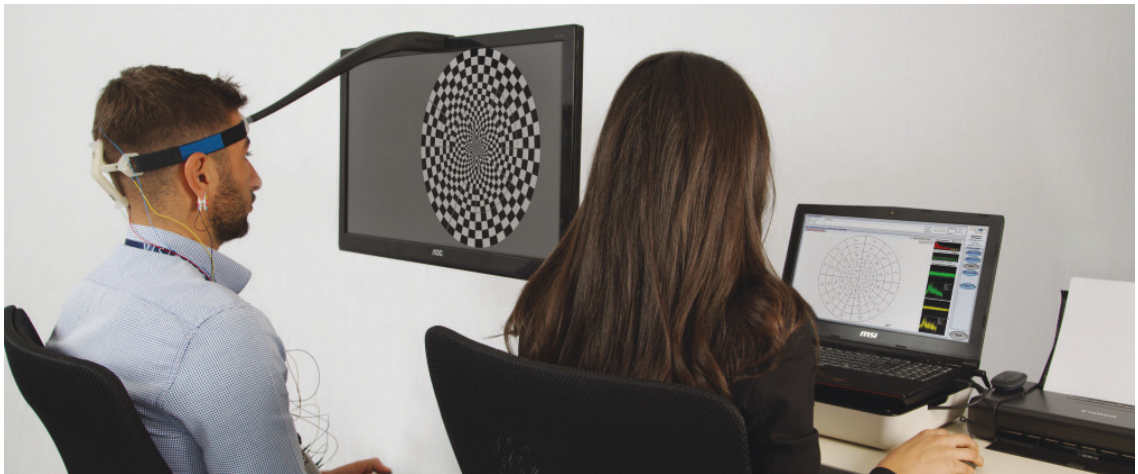


Figure 2.18: Complete Visionsearch system set up and in use.

Visionsearch distributes the system as a complete and integrated unit, including all aforementioned components. When a patient is utilising the system, they are required to watch a screen and react to cues on it. While doing so, they must maintain a given distance between their eyes and the screen as well as remaining level to and in the centre of the screen. To help patients, Visionsearch needed a distancing device that would allow patients to maintain the correct distance while not obstructing their field of view. Figure 2.19 shows how a head distancer is utilised and Figure 2.20 what it looks like fully assembled.

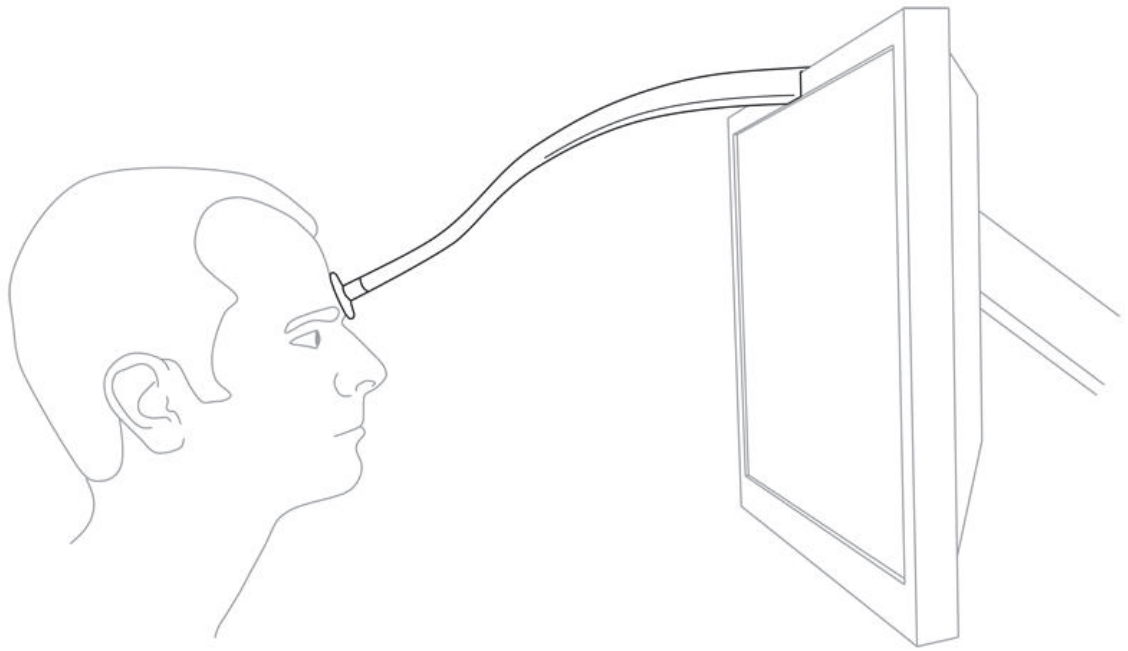


Figure 2.19: How a Head Distancer is used.



Figure 2.20: Visionsearch Head Distancer fully assembled.

Visionsearch installs 20-25 new systems per year, each system only requiring one head distancer; therefore, mass-producing the Head Distancers was out of the question. Due to the restraint on manufacturing and the highly specific

need this device needed to address, Visionsearch was referred to the author, who then conducted the project as an academic design practitioner. The main structural components of the head distancers are manufactured on demand via a 3D printing bureau as Visionsearch needs them.

Visionsearch purchases the screens annually in batches of 30 units, and as previous models are discontinued, the physical size, resolution, etc. changes. This means that approximately every two years, the Head Distancer needs to be customised to suit a new screen. As a result, it has been through three customisation cycles, with the most recent one designed in 2018.

In summary, 3D printing was used for these projects for two main reasons:

1. They all needed to be customisable to a specific need or application;
2. They all required low production numbers, ranging from 2 to 25 units.

However, because the team was using 3D printing to direct-manufacture the products, they were also directly responsible for the reliability and durability of the products. With traditional DFM, this responsibility is shared along the way, from design to point of sale, between the designers, toolmakers, production engineers etc. (see Section 2.2.1: Design for manufacturing (DFM)). As a result of this responsibility lying with the team, time and resources were spent to make sure their products would be up to their tasks. This was done by first building sections, individual components and entire parts from various materials and then testing them, often to the point at which they would fail, to learn how the products needed to be made so they would function reliably and be durable. This is not to say that with traditional DFM, product prototypes are not tested before production starts — they are. However, much more is known about polymers used in combination with traditional DFM, because designers have been working with them for almost a century (Hopkinson & Dickens 2001), which speeds up the prototyping/testing process. With 3D printed polymers, less is known about their properties, so more prototyping and testing needs to be conducted to ensure a product is fit for use. Naturally, all materials have many different properties, such as mechanical (static and dynamic), thermal, and chemical, and a designer of a product will be interested in all the properties a material might have if it is being considered for a product. Typically, the static mechanical properties are the first to be

considered; furthermore, testing for all properties was beyond the scope (both financially and temporally) of this research, and so has been limited to static mechanical properties. The following section investigates what is currently known about the static mechanical properties of the three 3D-printed polymers that can be used to produce end-use products and where the potential knowledge gaps are.

2.3.1 Static mechanical properties of the three 3D printed polymers

In Section 2.1.1: Types of 3D printing processes and available materials, it was stated that the focus of this research is limited to the three 3D-printed polymers ABS, TPGDA, and PA, and their respective accompanying processes FDM, MJ, and SLS. The reasons for this limitation are threefold:

1. Due to material cost, the scope of the research needed to be manageable in relation to how many different materials were to be tested, because several test samples would need to be built for each material. It was decided to focus solely on rigid 3D printed polymers, due to the fact that many handheld products are made from rigid polymers. 3D printed metals were briefly considered, but at the time their cost was prohibitively high.
2. Having decided on rigid polymers, they needed to be selected. The literature showed that SLS in PA and FDM in ABS are both tough and durable materials suitable for end-use part production (Wohlers 2016). MJ in TPGDA is widely used in 3D printing to build end-use parts in dentistry (Stansbury & Idacavage 2016) and hearing aids (Wohlers 2016). These three polymers were selected because of their suitability for end-use part production of handheld products, and it was decided not to add any more materials to the research due to the cost of building the test specimens.
3. The processes needed to be geographically accessible by the author, in the Sydney metropolitan area, so he could liaise directly with the bureaus that would build the samples and the technicians that operate the machines. This was because it needed to be ensured that the test samples were correctly oriented in the required build orientations, and

managing this face to face was deemed easier than via Skype, email or over the phone.

Each of the three polymers are proprietary materials supplied by the distributors of the 3D printing machines that use them. The distributors recommend that only the materials they supply be used with their machines, in order for them to be able to guarantee that the properties, mechanical and otherwise, of their materials are as stated on the material data sheets. Both bureaus (see Section 4.1.1: Making the test specimens) that were engaged to print the test samples confirmed that they only use proprietary materials supplied by the distributors. The data shown in Tables 2.1, 2.2, and 2.3, were taken from the material data sheets supplied the distributors Stratasys (for FDM in ABS), 3D Systems (for MJ in TPGDA), and EOS (for SLS in PA) respectively. Copies of the actual data sheets can be found in Appendix B.

3D printed parts are anisotropic, which means the physical properties of the material have different values when measured in different directions, similar to wood, which is stronger along the grain than across it. As with wood, 3D printed parts are therefore more likely to fail across the grain, which makes the build orientation an important consideration, because it directly influences the strength of a part. For this reason, the data set shown in Table 2.1 for ABS has two columns for values, one for XZY (horizontal on edge or HoE) (see Figures 2.21 and 2.22) build orientation, and one for ZXY (vertical or V) build orientation. In both of the other tables, 2.2 and 2.3, TPGDA and PA only contain one set of data per test, so there are no additional data in relation to build orientation. The ASTM standards use the coordinates X, Y, and Z to notate part orientations; see Figure 2.21. This can become confusing for people who are not accustomed to thinking in X, Y and Z coordinates. To help with this, the ASTM notations have been translated into acronyms that are easier to understand:

XYZ & YXZ = horizontal flat (HF)

XZY & YZX = horizontal on edge (HoE)

ZXY & ZYX = vertical (V)

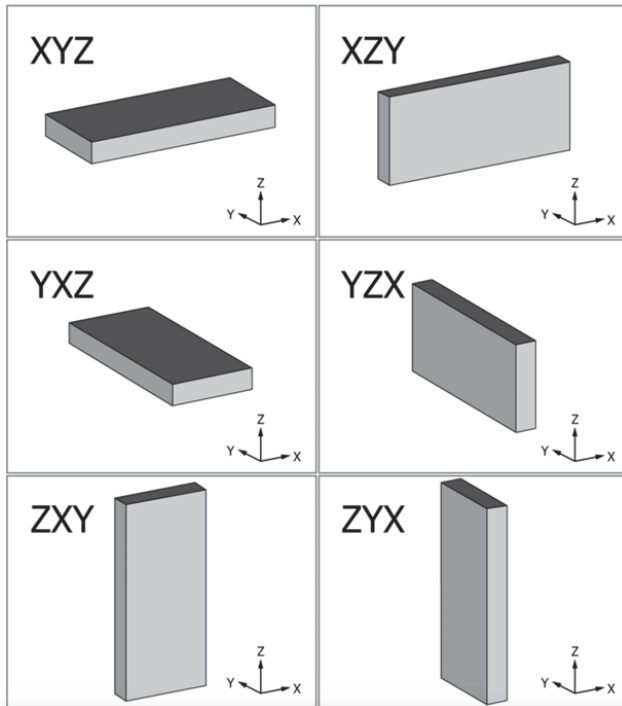


Figure 2.21: Orthogonal orientation notation (ASTM 2013b). The biggest dimension takes the 1st coordinate, the next biggest dimension the 2nd coordinate, and the smallest the 3rd coordinate.

At the time of writing, inclined build orientations did not have an ASTM notation, therefore one was created for this research:

Incline 45 (I 45), see Figure 2.22

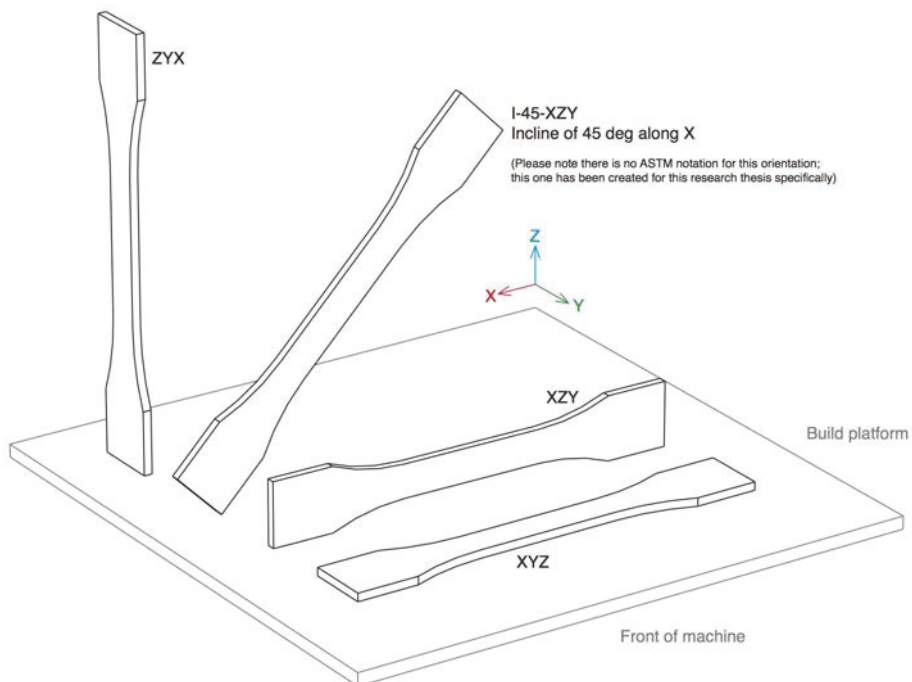


Figure 2.22: Inclined build orientations, such as I-45-XZY (I 45), do not have an ASTM notation, but because they will be discussed later, this notation has been created specifically for this research.

Table 2.1:

Material data supplied by Stratasy for FDM in ABS

Mechanical properties	Test method	Value XZY (HoE)	Value ZXY (V)
Tensile ultimate	ASTM D638	33 MPa	No data provided
Tensile yield	ASTM D638	31 MPa	No data provided
Tensile modulus	ASTM D638	2,200 MPa	No data provided
Tensile elongation at break	ASTM D638	6%	No data provided
Tensile elongation at yield	ASTM D638	4%	No data provided
Izod impact notched	ASTM D256	106 J/m	No data provided
Flexural strength	ASTM D790	58 MPa	35 Mpa (60% weaker than HoE)
Flexural modulus	ASTM D790	2,100 MPa	1,650 MPa
Flexural strain at break	ASTM D790	2 %	2 %

Table 2.2:

Material data supplied by 3D Systems for MJ in TPGDA

Mechanical properties	Test method	Value
Tensile strength	ASTM D638	42.4 MPa
Tensile modulus	ASTM D638	1,463 MPa
Tensile elongation at break	ASTM D638	6.83 %
Izod impact notched	-	No data provided
Flexural strength	ASTM D790	49 MPa

Table 2.3:

Material data supplied by EOS for SLS in PA

Mechanical properties	Test method	Value
Tensile strength	DIN EN ISO 527	1700 +-150 N/mm2 (MPa)
Tensile modulus	DIN EN ISO 527	45 +-3 N/mm2 (MPa)
Tensile elongation at break	DIN EN ISO 527	20 +-5 %
Izod impact notched	DIN EN ISO 180	4.4 +-0.4 kJ/m2
Flexural modulus	DIN EN ISO 178	1240 +-130 N/mm2 (MPa)

The data provided for both ABS and TPGDA is based on ASTM (American Society for Testing and Materials) test methods, and for PA on DIN EN ISO (Deutsches Institut für Normung, Europa Norm, International Standards Organization). In Australia, test methods and resulting values as recommended by the ASTM standards are used; however, the test methods and values provided by EOS are according to DIN EN ISO. Although the parameters between testing methods, e.g. for tensile testing ASTM D638 and DIN EN ISO 527, are similar, they are not the same. For example, the physical dimensions of the test specimens vary between the two standards, and although there are conversion formulas available, converting the data from one standard to the other mathematically is not recommended. For this reason, the data from the EOS data sheet for the material PA cannot be used for this research; however, what we can ascertain from all three data sheets are the types of tests that are recommended, namely tensile (strength, modulus and elongation), Izod impact (notched) and flexural strength (3-point bend), which are recommended as the three most useful tests for understanding the static mechanical properties of polymers (Gerdeen & Rorrer 2012).

Because all three of the chosen polymers have been in use for over five decades, their properties are well understood, so it is easy to predict how they may perform when they are used in conjunction with traditional manufacturing methods. ABS, for example, is the polymer most Lego parts are made from through injection moulding. However, because 3D printed materials become anisotropic, predicting how they may behave is challenging, even if they are made from a well understood polymer such as ABS. As mentioned in Section 2.3: End-use products made from 3D printed polymers, one of the first industries to utilise 3D printing to manufacture end-use products was the hearing aid industry, because it recognised the possibilities 3D printing offered to custom fit hearing aids to any person's ear canal. Due to the small size of these components, their mechanical properties were not much of a concern; however, other industries became interested in where the limits of 3D printed materials lie. Due to this, many studies have been conducted in relation to build orientation and strength (static mechanical properties) of 3D printed polymers. The majority of these studies are material and process specific, where the researchers have only concentrated on one material, e.g. ABS in FDM. However, there are several benchmark studies that provide an overview

or state of the art at a given point in time and that include all three polymers as well as other materials.

2.3.2 Benchmark studies of 3D printed polymers

In the following sections, reference will be made to several different testing standards, because not all researchers whose work was investigated used the same standards. This makes interpreting the results confusing, because they are not transferable from one standard to the next. To help clarify what the results mean, percentage values have been provided (wherever possible) at the end of each section to show how much stronger one build orientation is compared to another; e.g., the ultimate tensile strength of the HF (or XYZ) build was 45% higher than the V (or ZYX) build (see Figure 2.22 for clarification).

One of the earliest benchmark studies, conducted by Levy, Schindel & Kruth, investigated 3D printing from metals and polymers, as well as tooling made using 3D printing (2003). With regard to mechanical properties, they list test results that compare the tensile property of injection-moulded ABS to that of FDM ABS, but only for test samples built in the XYZ build orientation. They also provide tensile test data comparing SLS in PA with FDM in ABS, amongst others, but do not provide any information regarding build orientation. In both cases, Levy, Schindel & Kruth provide no information regarding the testing procedures.

In 2008, Kim and Oh published a comprehensive study that compared mechanical properties, such as tensile and compressive strengths, hardness, impact strength, and heat resistance, and surface roughness, geometric and dimensional accuracy, manufacturing speed, and material costs of several 3D printed polymers and polymer composite materials, including ABS and PA, but not TPGDA (2008). For tensile testing, the samples were built in horizontal and vertical orientations and tested according to ASTM D638. They found that FDM in ABS was 41% weaker in the vertical orientation and SLS in PA 15% weaker in the vertical orientation (Kim & Oh 2008). For impact testing, the samples were again built both in horizontal and vertical orientations and tested according to ASTM D256 (Charpy). Their results show that for SLS, the vertical orientation is 7% weaker than the horizontal, and for ABS, 96% weaker

in the horizontal than the vertical (Kim & Oh 2008). It is important to note that ASTM D256 includes impact testing procedures for both Izod and Charpy impact testing. Although both are impact tests, they are two different tests and the results are not comparable; since this research is only focussing on Izod results (see test methods listed above in Tables 2.1 and 2.3), the Charpy results are not that useful. Kim and Oh did not conduct any flexural testing.

At the time of writing, the most recent benchmark study, titled 'Mechanical properties of commercial rapid prototyping materials' was published in 2014 by Kotlinski (2014) and was conducted by first collecting accessible data from suppliers of 3D printing technology and then comparing the data. In relation to the three polymers chosen for this research, the test data in Kotlinski's study is the same as the information provided in the Material Data Sheets at the beginning of this section (see Tables 2.1, 2.2 and 2.3 above), which is not surprising, because the data is likely to come from the same source.

In summary, all three studies prove that parts oriented vertically are weaker than parts oriented horizontally, because they are anisotropic. It should be noted that all three benchmark studies only tested samples built horizontally and vertically, and there were no test samples built at an incline.

2.3.3 Material/process specific studies

Studies of Fused Deposition Modelling in ABS

To understand the intricacies of the following studies on FDM (fused deposition modelling) in ABS, it is necessary to understand how FDM parts are printed. The process can be described as follows: The ABS filament is led into the extrusion head, inside of which it is fed through a heating element where it melts. The melted filament is then forced through a nozzle with a smaller diameter (between 0.05mm and 0.3mm) than that of the filament and extruded onto the layer below it. Because the extruded ABS is molten, it fuses with the material that has already been deposited. As it extrudes, the extrusion head moves in the X-Y plane and deposits the material according to the part geometry of that layer. Once a layer is complete, the build platform to which the part is anchored drops vertically in the Z plane, after which the extrusion

head begins to deposit the next layer on top of the previous one as shown in Figure 2.23.

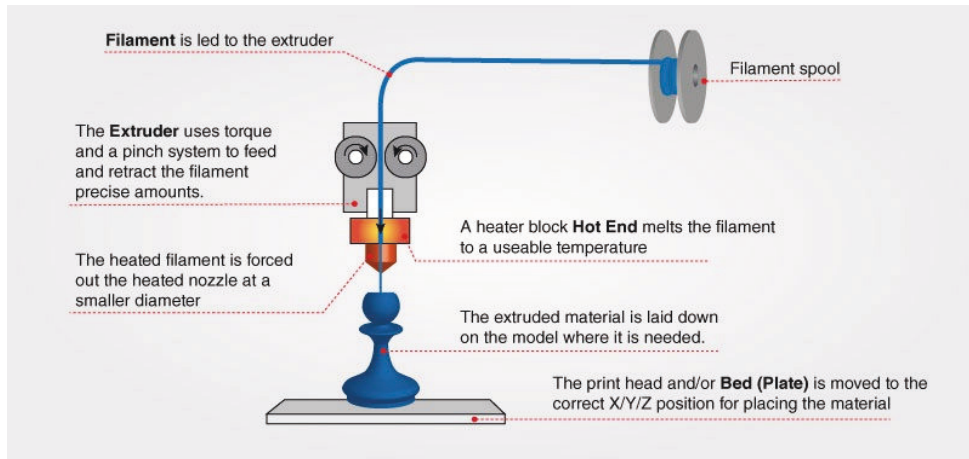


Figure 2.23: Schematic of FDM extrusion head (courtesy of *MegaDepot*).

As a result of this process the part is made up of many thin filaments of ABS (see Figure 2.24), that have been fused together as layers and make it anisotropic, similar to wood, as discussed earlier. This means the strength of an FDM ABS part can vary substantially depending on its build orientation, more so than with SLS or MJ parts.

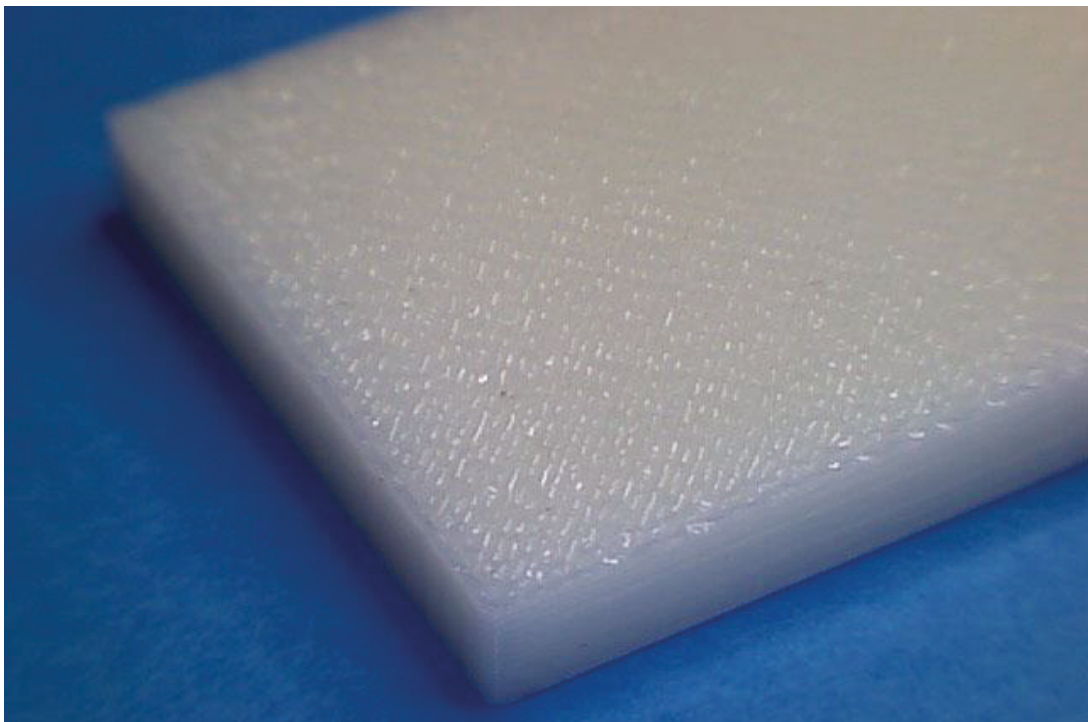


Figure 2.24: Detail of ABS tensile specimen built in the XYZ (HF) orientation. Each filament is 0.254 mm thick.

In 2002, Anh et al. tested FDM in ABS for tensile properties on samples that were built in the XYZ [HF] orientation, and generated a set of build rules based on their data. The most relevant build rule for the research presented in this thesis is build rule 1, which states: “build parts such that tensile loads will be carried axially along the fibres” (2002). They developed this build rule by altering the path or raster pattern in which the machine lays down the material. Although it makes sense that tensile loads should be carried axially along the fibres, the default pattern that FDM machines use is referred to as criss-cross, and it is not common practice for service providers to alter this pattern. So, making a part stronger using this method is not practical for the majority of people.

Table 2.4:
Build parameters used by Ahn et al (2002)

Build parameters	
Test method	ASTM D638
Machine	Stratasys FDM 1650
Material	Stratasys P400 ABS
Layer height	0.3mm

Five years later, in 2007, Chung Wang, Lin and Hu comparatively tested the ultimate tensile strength of ABS in HF, HoE and V orientations. Their data shows that the vertical orientation is the weakest (see Table 2.5).

Table 2.5:
Chung Wang, Lin and Hu (2007), test results

Mechanical properties	Test method	V	HF	HoE
Tensile ultimate	Not known	13 MPa	15 MPa	24 MPa

What is interesting, however, is that HoE is approximately 40% stronger than HF even though they are both built in the same plane. To investigate this, Chung Wang, Lin and Hu (2007) examined the fractured cross sections under a scanning electron microscope (SEM) and discovered that this is due to the fact

that there is over 50% more air present in the HF than the HoE, as Figures 2.25 and 2.26 clearly demonstrate.

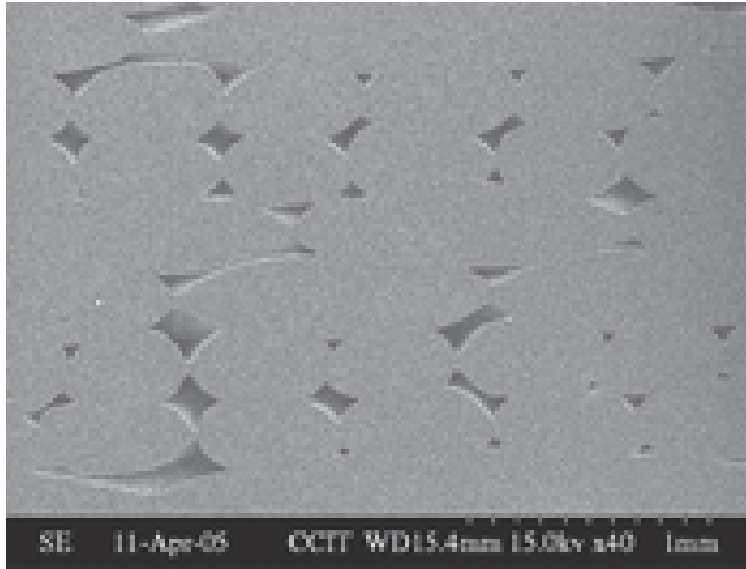


Figure 2.25: SEM cross section of ABS built in HF orientation; darker areas are air pockets (Chung Wang, Lin & Hu 2007, p. 312).

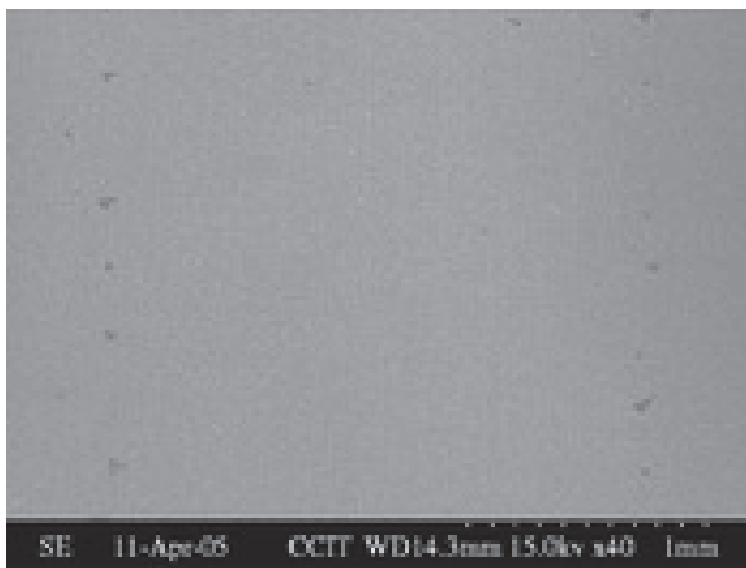


Figure 2. 26: SEM cross section of ABS built in HoE orientation; darker areas are air pockets (Chung Wang, Lin & Hu 2007, p. 312).

Because there is more air present in HF, it is not as dense as HoE and therefore not as strong. Chung Wang, Lin and Hu (2007) do not offer an explanation as to why there is more air present, but it is likely to have something to do with the way the extruder deposits the material over a longer or shorter travel distance. Figure 2.27 shows how the filament was deposited in HF (longer

travel distance), and in Figure 2.28, during HoE (shorter travel distance), one can see that there are wider gaps (more air) in HF.

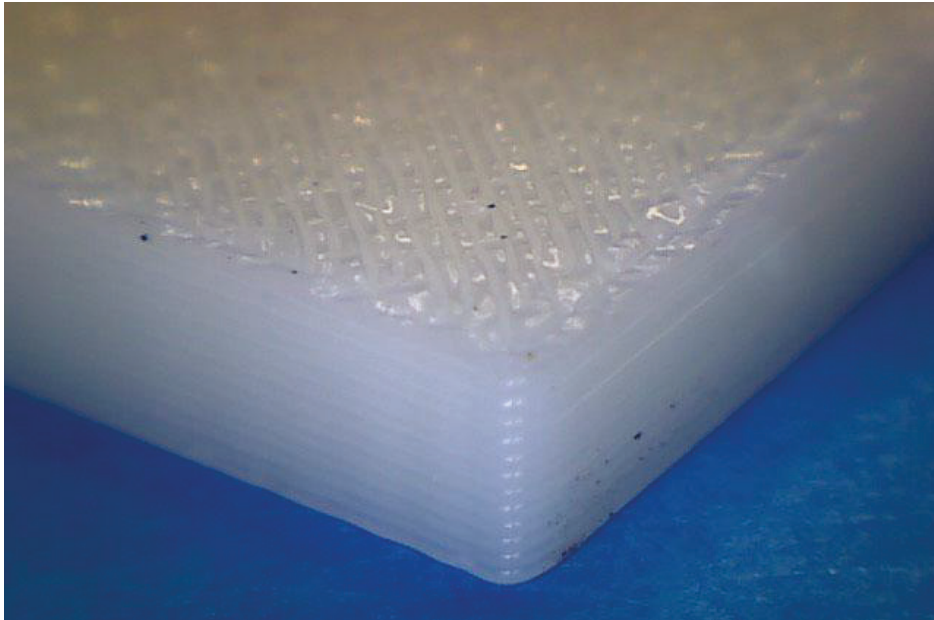


Figure 2.27: HF orientation (perspective view); longer travel distance clearly shows gaps between each filament (ABS filament thickness 0.254mm).

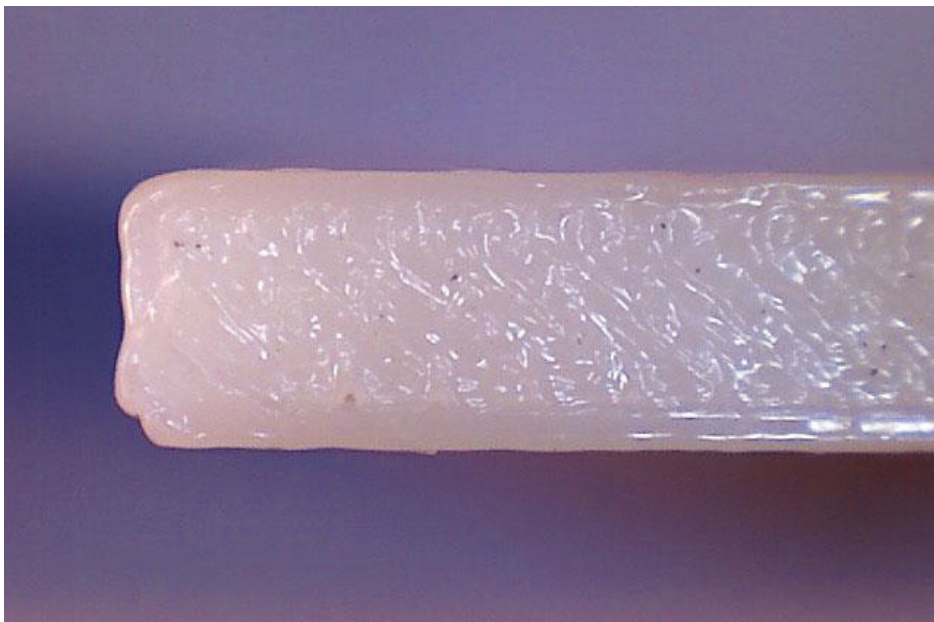


Figure 2.28: HoE (top view): shorter travel distance has less gaps and looks denser than the HF build in Figure 2.27 (ABS filament thickness 0.254mm).

Therefore, if the cross-section is larger, the extruder needs to travel further, which results in the filament being colder by the time the extruder returns with the next filament, and the lower temperature doesn't bond as well to the

previous one. On a smaller cross-section, the travel distance is shorter, so the temperature of the filament that has been deposited is higher, because it takes less time for the extruder to return with the next filament, which results in a better bonded and more dense build.

Table 2.6:

Build parameters used by Chung Wang, Lin and Hu (2007)

Build parameters	
Test method	ASTM D638-03
Machine	Stratasys Dimension BST
Material	Stratasys P400 ABS
Layer height	0.254mm

Expanding on Ahn et al.'s (2003) study discussed earlier, Ziemian, Sharma and Ziemian (2012) investigated the effects of FDM raster patterns on the strength of ABS test specimens built in XYZ orientation for tensile, impact and flexural properties, amongst others which are not relevant to this research. The raster patterns used are shown in Figure 2.29, where: (a) is longitudinal or 0 deg (i.e. raster aligned with long dimension of the specimen); (b) diagonal or 45 deg (i.e. rasters at 45 deg to the long dimension of the specimen); (c) transverse or 90 deg (i.e. rasters perpendicular to the long dimension of the specimen); and (d) default or +45/-45 deg criss-cross (representing the machine's default raster orientation) (Ziemian, Sharma & Ziemian 2012).

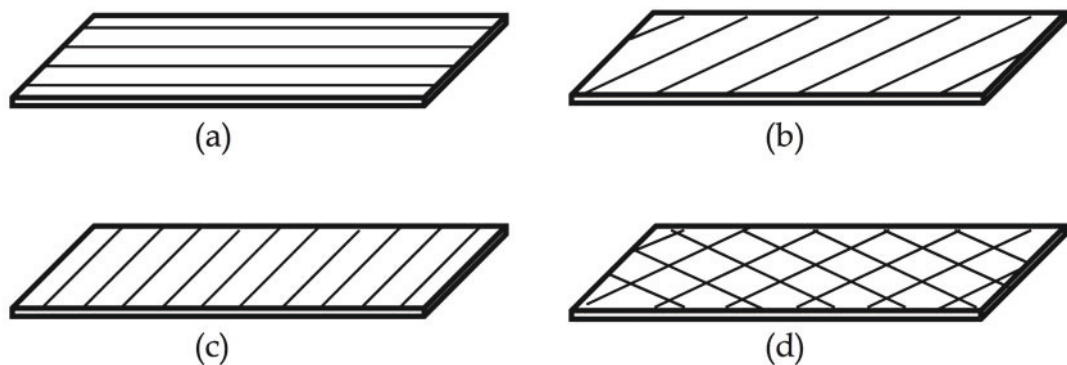


Figure 2.29: Raster pattern experiments by Ziemian, Sharma and Ziemian (2012, p. 163).

The test methods used by Ziemian et al. were ASTM D3039 for tensile, ASTM D790 for flexural, and ASTM D256 for impact (Izod pre-notched). According to ASTM 52910 Standard Guidelines for Design for Additive Manufacture, the actual test methods recommended for testing 3D printed polymers are ASTM D638 for tensile, ASTM D790 for flexural, and ASTM D256 for impact (more will be said about this in Section 4.0: Experiments). Both flexural and impact match, but ASTM D3039 is recommended for composite polymers, so it is unusual that Ziemian, Sharma & Ziemian chose this one for their tension tests; nevertheless, the results are interesting. The tensile mean ultimate strength is highest for the raster pattern: (a) 25.72 Mpa; (b) 16.22 MPa; (c) 14.56 MPa; and (d) 19.36 MPa. If we assume (a) is the strongest at 100%, this translates to (b) being 61.45%, (c) 56.23%, and (d) 74.09% (Ziemian, Sharma & Ziemian 2012). The values for mean ultimate strength of flexural testing are in the same order, with: (a) 38.1 MPa, (b) 25.7 MPa, (c) 23.3 MPa, and (d) 32.2 MPa. And for impact, the order is the same again, where for: (a) 2.991 J/cm; (b) 2.339 J/cm; (c) 1.599 J/cm; and (d) 2.514 J/cm (Ziemian, Sharma & Ziemian 2012). So, raster pattern (a) longitudinal is consistently the strongest, followed by (d) criss-cross. As mentioned earlier, criss-cross is the default raster pattern that FDM machines use to deposit the material, so to conduct their tests, Ziemian, Sharma & Ziemian had to alter the raster pattern in the software that maps the path the extruder travels. As discussed earlier, when using a bureau or service provider to have a part built, there is no option to alter standard parameters such as the raster pattern, which means controlling the strength of a parts in this way is pragmatically not achievable.

Table 2.7:

Build parameters used by Ziemian, Sharma and Ziemian (2012)

Build parameters	
Test method	ASTM D3039, ASTM D790, ASTM D256
Machine	Stratasys Vantage-i
Material	ABS (exact type is not specified)
Layer height	0.1778mm

Rayegani and Onwubolu also investigated tensile strength in relation to raster pattern angles and built test specimens in HF and V orientations. The

predominant focus of their research was to test the accuracy of the group method of data handling (GMDH) (Rayegani & Onwubolu 2014), which is an algorithm that can be used to predict the strength of a 3D-printed test specimen based on predefined build parameters. Their methodology was to first calculate how a test specimen may perform in theory using GMDH, and then compare this data with test data obtained from tests they conducted in practice on specimens physically built to the pre-defined parameters. The testing standards they used are in accordance with ISO R527:1966 (see Table 2.8) which, as with many of the other studies discussed earlier, is not the one recommended by ASTM. And although the research presented in this thesis does not focus on predicting strength through algorithms, the results from the physical tests they performed are relevant. Their results show that if the raster [filament] is 0.203mm in width, the ultimate tensile strength in HF orientation is 38.9 MPa and in V orientation 21.51 MPa (Rayegani & Onwubolu 2014), therefore V is approximately 45% weaker than HF.

Table 2.8:

Build parameters used by Rayegani and Onwubolu (2014)

Build parameters	
Test method	ISO R527:1966
Machine	Stratasys FDM Fortus 400mc
Material	ABS (exact type is not specified)
Layer height	0.2032mm

A study, conducted by Mohamed, Masood and Bohwmik in 2015 reviewed FDM process parameters and, after reviewing the published literature, concluded that it is clear that optimisation of process parameters of FMD 3D printing technology is one of the most critical design tasks in quality evaluation indicators for obtaining high quality parts, enhanced material response, and enhanced properties. They go on to say that to understand the mechanical properties and material behaviour of FDM parts, the effects of the process parameters on the quality characteristics of the parts must be studied more thoroughly (Mohamed, Masood & Bohwmik 2015). This is not a simple task, considering how many different types of machines are in use, each with its

own set of process parameters. For example, each of the above studies used a different machine, all made by Stratasys, but differing models. Furthermore, each team built their test specimens in a different layer thickness, and in some cases in different build orientations, which can have a substantial impact on strength, as Chung Wang, Lin and Hu proved (2007). In section 5 of their study, titled 'Research gap, problem and challenge', Mohamed, Masood and Bohwmik state that to improve the part quality and mechanical properties for FDM fabricated parts, it is necessary to understand the relationship between material properties and process parameters. They also comment that it remains a matter of concern that there are no absolute rules and guidelines designed to assist in their optimisation and evaluation method (2015). In view of these statements, there is a large degree of scope within which to move the research in this area forward for using FDM in ABS for end-use part production.

In addition to this, Gillespie states that, because the process makes parts in layers, the Z-axis properties will vary somewhat from the X-Y properties, and designers need to consider the possible effects of some stratification of properties of layers (Gillespie 2017); in other words, the properties may vary between layers. Although it is helpful to be aware of these effects that can have an effect on part strength, it is challenging for people who are not able to alter them to control them.

Studies of Material Jetting in TPGDA

Barclift and Williams state that in the process of MJ (material jetting), layers of an acrylic-based photopolymer are selectively jetted [squirted] onto a build tray via inkjet printing. The jetted photopolymer droplets are immediately cured with ultraviolet lamps that are mounted onto the print carriage (2012); See also Figure 2.30.

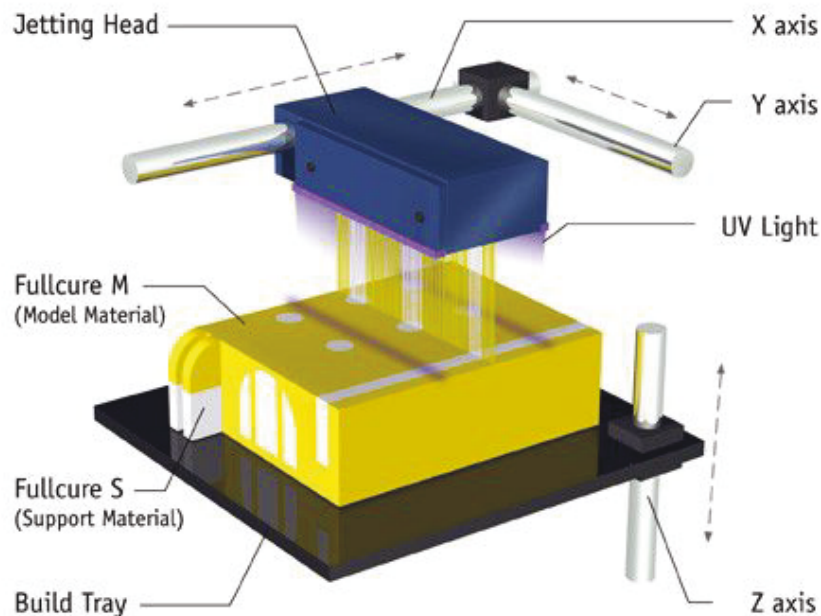


Figure 2.30: Schematic image of MJ process (Barclift & Williams 2012, p. 876).

In 2009, Pilipovic, Raos and Šercer conducted a comparative study into the tensile and flexural properties of the polyjet process [MJ] and 3D printing process [binder jetting] processes/materials (2009). They used ISO standards and don't provide any information regarding build orientation. The test results relevant to the research presented in this thesis are for polyjet or MJ using the Objet Eden 330 machine and the material FullCure 720. FullCure 720 is a transparent acryl photopolymer [TPGDA] suitable for rigid models, with a tensile strain at break of 20%; out of all the materials they tested the best mechanical properties belonging to the test specimens made of FullCure (Pilipović, Raos & Šercer 2009). Furthermore, they discovered that when comparing their data to the data on the MDS (material data sheets) supplied by the distributors, some of their values were lower than those stated on the MDS. This is an important insight, because it highlights how challenging it can be to ensure that every 3D printing machine produces parts according to specifications, in particular if one machine needed to guarantee a part will perform exactly as promised.

Table 2.9:

Build parameters used by Pilipovic, Raos and Šercer (2009)

Build parameters	
Test method	ISO 178:2001, ISO 527:1993
Machine	Objet Eden 330
Material	FullCure 720
Layer height	0.016mm

Kęsy and Kotliński comparatively tested the tensile properties in V, HoE, and HF (2010). They discovered that the difference between V and HoE is 3.6%, which suggests the anisotropic effects of the build layers are very low, too low to be taken into consideration. However, when they compared HoE with HF, they found that HoE was 29.6% stronger (Kęsy & Kotliński 2010). They concluded that this is due to the amount of UV light the parts are exposed to during build time; the more light a part receives, the higher its tensile strength (Kęsy & Kotliński 2010). In the next study, this effect will be explained in more detail.

Table 2.10:

Build parameters used by Kęsy and Kotliński (2010)

Build parameters	
Test method	ISO 527
Machine	Objet Eden 260
Material	FullCure 720
Layer height	Not specified

Barclift and Williams investigated what controllable factors cause variability in the tensile strength modulus of VeroWhite [TPGDA] parts manufactured through PolyJet [MJ] direct 3D printing (2012). They discovered that if parts are tightly grouped together, with 1mm gaps in between each part, their tensile strength is 17% higher than if the same parts are spaced far apart, for example in the XYZ build orientation. This is due what is referred to as “over-curing”, a side effect during which, as the UV light passes over tightly grouped parts, they are exposed to more UV light and therefore are cured more than

parts that are too far apart for the extra light to reach them (Barclift & Williams 2012). They also discovered that parts built in the XZY orientation have higher tensile strengths than XYZ, similar to FDM parts. In this case, the effect is due to what is referred to “curing print-through”, where in XZY, there is an increase in the number of layers in comparison to XYZ. This leads to the UV light passing over the same area more frequently and thus curing that material more. And if the parts in XZY are tightly grouped, their tensile strength increases yet again (Barclift & Williams 2012). So, the tensile strength of the same part can vary up to 31% depending on its orientation and whether it was built close to another part. Similar to Pilipovic, Raos and Sercer (2009), Barclift & Williams also found that there was a discrepancy of up to 54% of the tensile strength values on the suppliers’ MDS compared to their data (2012).

Table 2.11:

Build parameters used by Barclift and Williams (2012)

Build parameters	
Test method	ASTM D638
Machine	Objet Connex 350
Material	FullCure 830 VeroWhite
Layer height	Not specified

In 2014, Cazon, Morer and Matey determined whether specific build orientation parameters and post-process treatment had an effect on the mechanical strength and surface quality of polyjet [MJ] printed parts. Cazon, Morer and Matey built their test specimens taking into consideration the only two parameters that a regular user of the polyjet technology can modify: position and finish (2014). Although post-processing is not part of the scope of the research presented in this thesis, and Cazon, Morer and Matey used the ISO standard, the results regarding tensile strength in relation to build orientation are of interest. Most significantly, they found that, when comparing the ultimate tensile strength of XYZ [HF] with XZY [HoE], XYZ [HF] was 23% stronger than XZY [HoE] (2014). This contradicts Barclift & Williams's results, discussed earlier, who found HoE is stronger than HF. The reason for this may be that those two studies used different testing standards as well as different

machines and materials, albeit from the same supplier. Regardless of the reasons, this once again highlights that there are a large number of variables that need to be considered when using 3D printing for end-use part production.

Table 2.12:

Build parameters used by Cazon, Morer and Matey (2014)

Build parameters	
Test method	ISO 527-2:1996
Machine	Objet Eden 330
Material	FullCure 720
Layer height	0.016mm

The following year, Mueller, Shea and Daraio conducted a study with the aim of determining the mechanical properties [tensile] of parts fabricated with inkjet 3D printing [MJ] through efficient experimental design (2015). The determining factors they took into account were the placement of test specimens on the build platform, while paying attention to spacing them far enough apart to avoid over-curing. In addition to this, they used two batches with different expiry dates (one year apart, denoted as 2014 and 2015) of the same material examined, as well as building batches where the machine had different warm-up times; one batch of specimens is printed on the cold machine and compared to specimens printed on the warm machine (Mueller, Shea & Daraio 2015). The test specimens were built in all six orientations, as recommended by ASTM (see Figure 2.31).

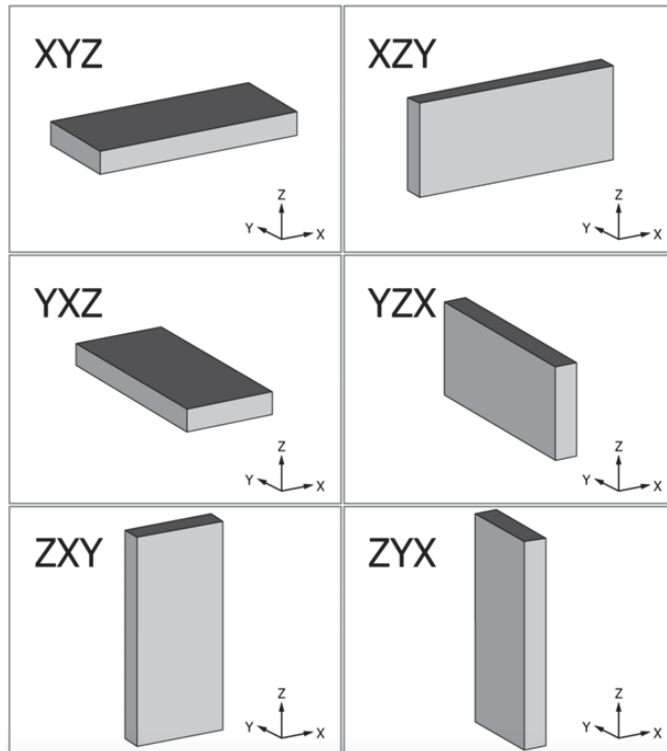


Figure 2.31: Orthogonal orientation notation according to ASTM (ASTM 2013b).

Unfortunately, Mueller, Shea and Daraio (2015) deemed their results for longitudinal orientation in Z invalid due to the multiple settings, which meant that a normal distribution could not be assumed. Nevertheless, they state that the higher number of layers means that printing in the vertical [Z] direction takes longer compared to other orientations, which leads to the highest UV exposure time of all the factors, and this should increase part strength. However, they go on to say that the high number of layers also leads to the highest number of intersections. And that as the mechanical properties of parts longitudinally aligned along Z are considerably lower than for the others, the weakening effect of more layers must be greater than the strengthening effect of the increased UV exposure (2015). This is both interesting and confusing at the same time, because unless one has complete control over all parameters, it is almost impossible to predict what the tensile strength of an MJ part is going to be. Furthermore, in previously published research, other 3D printer models were used, so the results cannot be compared directly (Mueller, Shea & Daraio 2015).

As with other studies discussed earlier, Mueller, Shea & Daraio found the suppliers' data listed on the MDS did not match. They state that the values found in this work are, on average, close to the upper boundary for the elastic

modulus, while the ultimate tensile strength exceeds the listed upper boundary by more than 8%. For the total strain at break, the experimental values are considerably lower than the lower boundary of the range (Mueller, Shea & Daraio 2015).

Table 2.13:

Build parameters used by Mueller, Shea and Daraio (2015)

Build parameters	
Test method	ASTM D638-10
Machine	Objet500 Connex3
Material	FullCure 835 VeroWhitePlus
Layer height	Not specified

In their general guidelines for MJ, Williams and Meisel state that parts are strongest in the X-axis and weakest in the Z-axis (2017).

Studies of Selective Laser Sintering in PA

As discussed in Section 2.1.1: Types of 3D printing process and available materials, SLS is a process during which defined sections of a polymer powder are fused together by the heat of a laser to form a solid part (see Figure 2.32).

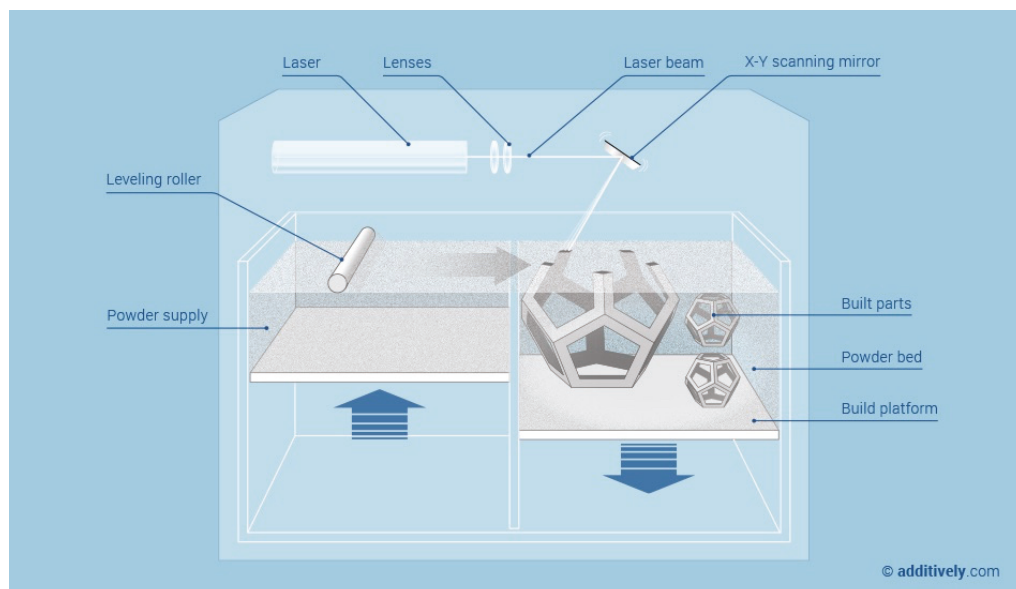


Figure 2.32: Schematic of SLS process (courtesy of *additively*).

Gibson and Shi investigated part orientation and found it to have an influence on mechanical [tensile] properties (1997). They built their specimens in HF, HoE, and V orientations, and found HF had the highest tensile strength, followed by HoE and V. The tensile strength in V is the worst because the applied force is in the layer direction (1997), which is due to anisotropy. They also discovered that the position a part is located in the build volume can influence its mechanical properties, but this is, once again, a parameter that a regular person engaging with a print bureau does not have control over.

Table 2.14:

Build parameters used by Gibson and Shi (1997)

Build parameters	
Test method	ASTM D638-D
Machine	Sinterstation 2000
Material	Fine nylon
Layer height	0.1mm

In 2006, Ajoku et al. investigated the end-of-vector (EOV) effect in laser sintered PA parts. Ajoku et al. state that all components built on an LS machine are affected by the EOV effect, and that this effect is caused by the degree of a laser beam exposure at the start of a sinter scan on a part (2006). Ajoku et al. describe the EOV effect as follows:

As the laser begins to scan a line of powder on the edge of a layer, there is always an initial burst of energy, which stabilises after a few milliseconds. These short bursts of energy at the edges result in components being much denser at the edges than at the centres, thus improving the mechanical properties in thin sections where the X dimension is small. It should be noted that this phenomenon only occurs at the start of each vector and not, as the name suggests, at the end of each vector (2006, p. 1080).

Using ISO standards, they tested the tensile, flexural and compressive properties of samples built in HF and V orientations, and discovered that for both tensile and compression, HF was strongest, followed V. The same applies to flexural, where HF was strongest, followed V; therefore, thin parts that are to

be subjected to flexural stress should be built in the HF orientation. Overall, the study showed that HF parts have better properties than V parts, which shows how vital it is to consider which mechanical properties are most important before building LS nylon-12 parts that will serve as an end-use product (Ajoku et al. 2006).

Table 2.15:

Build parameters used by Ajouk et al. (2006)

Build parameters	
Test method	ISO 527, ISO 178, ISO 604
Machine	3D Systems Vanguard SI
Material	DuraForm Polyamide (nylon 12)
Layer height	0.1mm

In 2006, Caulfield, McHugh and Lohfeld compared the tensile properties of PA parts built with 7 different laser power levels at 6, 9, 11, 13, 15, 18 and 21W (Watts), with 11W being the default level. The higher the laser power, the higher the temperature becomes at which the polymer powder is sintered (melted) together; this is referred to as the energy density level. They built their test specimens in HoE and V orientations, and although it was not documented in their study, it was observed that the HoE orientation showed higher strength and modulus relative to the V orientation (Caulfield, McHugh & Lohfeld 2007). They also discovered that when sintering at higher energy density levels, the bonds between the powder particles become stronger, which leads to a more ductile behaviour with large plastic regions in the stress-strain curves (2007). One effect of this was that when the laser was running at an 18W power level, the orientation no longer mattered — the yield strength of HoE and V were the same. However, due to the increase of power/heat, additional material around the parts was also melted, which made the parts larger and thus affected the dimensional accuracy of the parts. Unfortunately, the level of power is one of those parameters a regular person is not able to change when engaging with a print bureau or service provider.

Table 2.16:

Build parameters used by Caulfield, McHugh and Lohfeld (2007)

Build parameters	
Test method	ASTM D638-00
Machine	DMT Sinterstation 2500
Material	DuraForm Polyamide
Layer height	Not specified

In 2011, Starr, Gornet and Usher studied the effect of process conditions on mechanical [tensile] properties of PA through variation of process conditions, including laser power, laser speed, scan spacing, layer thickness, build orientation, and build position (2011). The only process condition of interest to this research is build orientation, because it is the only parameter one has control over as an everyday person using a service provider. With regard to build orientation, they found that at a power level of 14W (approximately default), HF had the highest yield stress, followed by HoE and V, which confirms Ajoku et al.'s 2006 results.

Table 2.17:

Build parameters used by Starr, Gornet and Usher (2011)

Build parameters	
Test method	ASTM (number not specified)
Machine	Sinterstation 2500 Plus
Material	DuraForm Polyamide (nylon 12)
Layer height	0.1 - 0.15mm

In their paper titled 'Performance limitations in polymer laser sintering', Bourell et al. reviewed the state of the art of commercial LS machines (2014). They state that one of the main problems for LS part properties is porosity in between layers in the Z plane. Powder that is deposited and coalesced in layers gives rise to normal anisotropic mechanical properties, where the ductility normal to the powder layer is different (worse) than the in-plane directions. This is because pores tend to be aligned in the plane of the powder layers. Irregular or flaky powders result in large isolated pores and cored spherulites,

while regular granular powders result in smaller aligned pores with less coring and better surface finish (2014). In other words, the more consistent powder granules are in shape and size, the better the part quality. Bourell et al. go on to say that this is further complicated by problems that arise as a result of inconsistent powder deposition and incomplete particle melting, and that incomplete melting is complicated by the fact that commercial LS machines often have uneven heating and cooling of the powder bed surface (2014). These are concerning factors that make it challenging to predict how a part may perform.

A study conducted in 2017 by Schimd et al. compared two polyamide 12 (PA12) powders used in industrial LS applications: duraform PA and orgasol IS. The PA 2200 powder used by EOS behaves in a similar way to duraform PA, and for this reason was not included in the study (2017). They built test specimens in all 6 orientations (see Figures 2.21 and 2.31) and after tensile and impact testing (using ISO standards) compared the two powders to each other, as well as the results of those published in the suppliers MDS's reports. Schimd et al. (2017, p. 14) concluded that:

- The HF orientation of the values of this work matches relatively well with the MDS values for Young's modulus and tensile strength.
- For elongation at break in HF direction, only about half of the published value was achieved.
- With regard to revealing the anisotropy of the parts, an analysis for the HF and V direction data leads to the following statements:
 - For tensile strength, duraform remains at nearly the same level, while orgasol drops to almost half the value.
 - For elongation at the break, the drop for duraform is 50%, whilst orgasol loses 85% of initial magnitude.

In summary, this means that orgasol-IS is much more affected by anisotropic mechanical properties than duraform PA (2017). As we can see, even though we should be able to expect two Polyamide 12 powders to have the same or at least very similar properties, this is not the case.

Seepersad states that interlayer porosity, which can result from incomplete melting and/or inconsistent powder spreading, can cause particularly diminished ductile properties in the Z-direction across build layers, relative to parts built with major axes parallel to the build plane (2017). Again, as Schmid et al. also discovered, this can be avoided if the powder is of acceptable quality.

2.3.4 Discussion of end use products made through 3D printing

The existing knowledge and ongoing research is good for further improving the mechanical properties of the materials themselves in specific ways and/or at the micro level, such as reducing air gaps during an FDM build, controlling UV exposure during an MJ build, and experimenting with laser power for SLS. From the point of view of applying existing knowledge to product design, the following statements can be made for:

FDM in ABS:

- Parts built in the V orientation are considerably weaker than in HF and HoE.
- If possible, orient parts such that tensile loads will be carried axially along the fibres.
- Parts with thin cross sections that are to be subjected to tensile and flexural forces are best built in HoE orientation.
- Tensile and flexural tests on horizontal ABS test specimens should be conducted in both HF and HoE orientations.

MJ in TPGDA:

- Parts built in the V orientation are weaker than in HF and HoE.
- There are a substantial number of variables that affect the mechanical properties of MJ parts, ranging from the distance between adjacent parts to the amount of UV exposure and age of the material; this makes predicting its mechanical properties very challenging.
- Parts with thin cross sections that are to be subjected to tensile and flexural forces are best built in HoE orientation.

- Tensile and flexural tests on MJ test specimens should be conducted in both HF and HoE orientations.

SLS in PA:

- Parts built in the V orientation are weaker than in HF and HoE.
- Flexural horizontal test specimens should be built in both HF and HoE orientations.
- If possible ensure that the material duraform PA is used rather than orgasol IS, as this will produce parts with more consistent mechanical properties.

For product designers using 3D printed polymers to produce end-use parts, the existing knowledge is difficult to interpret and/or apply to practice for these reasons:

- Supplier test data on the MDSs cannot be relied on.
- Test data is only available for horizontal and vertical orientations.
- Two different standards are used, ASTM and ISO, and within each of those, different types of testing methods are applied; this makes cross referencing the data almost impossible.
- Within each material, several different machine types are used, which means the results cannot be compared directly, as discussed earlier; see also Mueller, Shea and Daraio (2015).
- The majority of the literature reviewed focuses on investigating the mechanical properties by experimenting with the materials through altering process parameters on the 3D printing machines, which an everyday person does not have access to and therefore cannot do.

2.4 Strategies to optimise part orientation

The purpose of reviewing the following literature was to ascertain if anyone has developed a method to optimise the mechanical properties of a part based on build orientation. When using 3D printing to manufacture a part, there are many variables to consider, such as part strength, surface texture, build time, and cost. Determining the optimal build orientation of a part is an essential

task in RP [3D printing] process (Zaragoza-Siqueiros & Medellín-Castillo 2014). For example, support material can cost the same as the build material, so when people use 3D printing technologies, such as FDM and MJ that require support material, they try to reduce the amount of support material needed by orienting the part in such a way that the least amount of support material is needed. This also saves time, because the lesser the amount of material deposited, the sooner the part will be finished. That example is centred around the economic consideration of saving on build cost, and if part strength or surface texture is not of paramount importance, then minimising support material is a good strategy. In any case, as a part is being placed in a build volume, it is clear that its orientation is important, so to help with optimising the orientation process, researchers have been investigating methods ranging from simple step-by-step methods to coded algorithms.

The staircase effect on the surface of 3D printed parts can affect a part's accuracy both dimensionally and volumetrically. To determine the best part orientation in RP [3D printing] processes, Masood, Rattanawong and Lovenitti developed a generic algorithm to minimise VE (volumetric error) in a part due to the staircase effect (2003).

Thrimurthulu, Pandey and Venkata Reddy attempted to obtain an optimum part deposition orientation for FDM through enhancing part finish and reducing build time, by developing a real coded genetic algorithm to obtain the optimum solution (2004).

Byun & Lee used the simple additive weighting method, a widely used multi-criteria method for decision making (2006), by developing an algorithm. Among the criteria they revised were: average weighted surface roughness, which considers the stair-stepping effect; build time calculated by laser/knife/nozzle travel; and part cost calculated by build cost rate, labour cost rate, and material cost (Byun & Lee 2006).

Ahn, Kim and Lee looked at fabrication direction optimisation to minimise post-machining in layered manufacturing [3D printing], by applying a genetic algorithm to obtain a reliable solution for a complex geometry CAD model (2007).

A paper by Pandey, Venkata Reddy and Dhande described and compared various attempts made by others to determine part deposition orientation, and concluded that the determination of an optimal part deposition orientation is a difficult and time-consuming task, as one has to trade-off among various contradicting objectives like part surface finish and build time (2007).

Phatak and Pande also used a genetic algorithm-based strategy to obtain optimum orientation of parts, where the objective criteria for optimisation was considered to be a weighted average of the performance measures, such as minimising build time, staircase error, and the material used in the hollowed model (2012).

Verma and Rai presented a systematic approach to quantify additive manufacturing quote attributes, namely process build time and energy consumption (2014). The computational model they developed to do this is capable of doing this almost in real time, which means it could potentially help manufacturers (3D printing bureau/service providers) return online quotes for 3D printing in real time, as is now the case.

Guessasma et al. reviewed the challenges of 3D printing technologies from a topology optimisation perspective (2015). Topology optimisation optimises material layout within a given design space for a given set of loads, boundary conditions, and constraints, with the goal of maximising the performance of the system. This could be useful, because some of the predetermined conditions could be mechanical properties. However, Guessasma et al. concluded that not enough is understood about the macro structures of the various 3D printing materials to reliably apply this method to build orientation optimisation (2015).

Leutenecker-Twelsiek, Klahn, and Meboldt propose a method which analyses each design element of a part to determine its best orientation. They do this by first deconstructing the part into each of its design elements, analysing them, and then reassembling them in the most appropriate way to best suit 3D printing (see Figure 2.33).

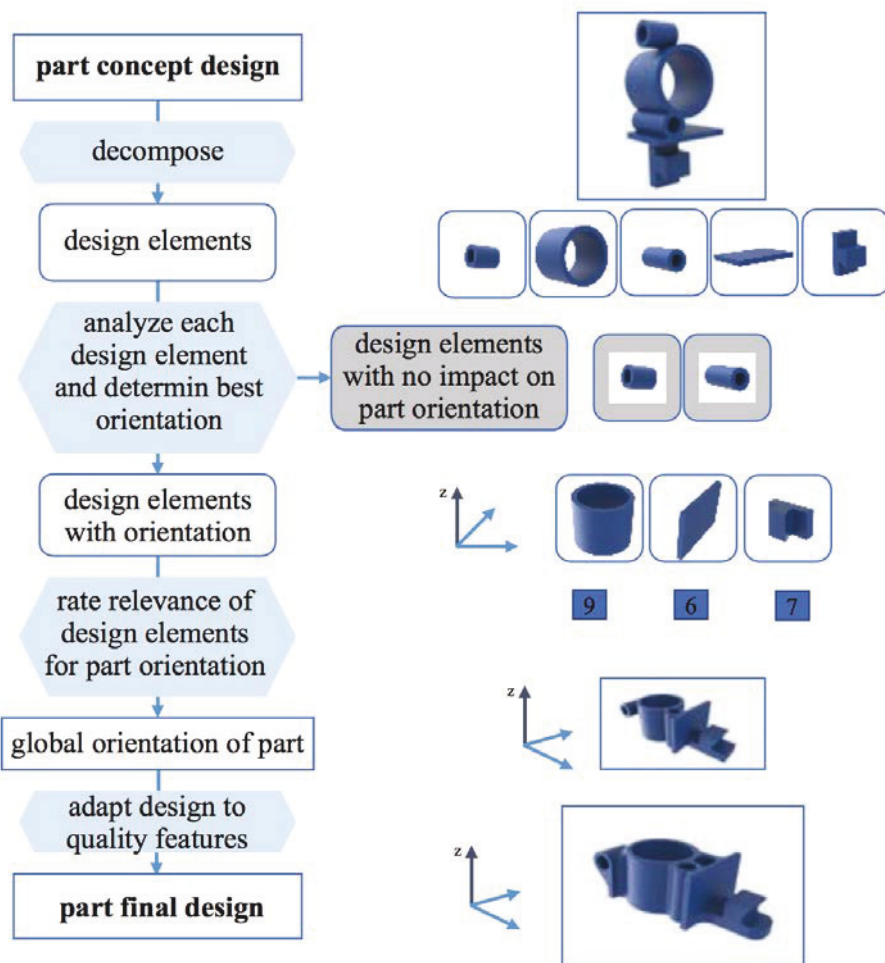


Figure 2.33: Flow chart of Leutenecker-Twelsiek, Klahn, and Meboldt's method (2016, p. 411).

This is similar to how a product designer would optimise any part for production, given they have an in-depth understanding of the manufacturing process they are going to employ. Leutenecker-Twelsiek, Klahn and Meboldt (2016) support this by stating that the developer [designer] must of course know the process characteristics of 3D printing before he [she] enters the design process, and that there is a challenge to develop a design guideline for 3D printing which can be used in industry and is based on industrial experience. They go on to say that the different publications of design rules for 3D printing are usually driven scientifically (see also Wohlers 2016) and follow a systematic scientific structure which doesn't necessarily match the workflow of practitioners (2016). This statement indicates an understanding of the product design process, and the resulting method they propose is based on this understanding.

Moroni, Syam and Perto propose a methodology that attempts to optimise the orientation of assemblies containing three moving parts, which are to be built assembled (2015). Once built, the parts can be removed from the build chamber as a complete functioning unit that does not require assembling. As such, they are mostly concerned with the accuracy of the parts, and specifically the tolerances necessary to allow the parts to move correctly.

Zhang et al. investigated optimising the build orientation for multi-part production in 3D printing (Zhang et al. 2017) by applying an improved genetic algorithm. By multi-part, they mean several parts that are all different from one another. They concluded that it is still uncertain whether the obtained solution is the best solution or not for the application context (Zhang et al. 2017). This is not surprising, because dealing with several different parts at the same time in one build orientation is a complicated task.

2.4.1 Discussion of strategies to optimise part orientation

The work in Section 2.4: Strategies to optimise part orientation, was reviewed to discover if there were any strategies or algorithms to optimise a part's orientation in relation to its mechanical properties. As such, none of it can be applied to the research presented in this thesis, because none of the work reviewed included mechanical properties or part strength as part of their process parameters in any of the methods or algorithms. This is not surprising, because a multitude of variables have a bearing on a 3D printed parts' mechanical properties (see Section 2.3.4: Discussion of end-use products made through 3D printing) and not enough is known about the materials' properties in relation to build orientation to make informed, knowledge-directed decisions. The reviewed methods and algorithms also have rigid step by step structures which are at odds with the way product design practitioners work, where the process is more holistic and less structured.

However, the research challenges this thesis is addressing, namely balancing part strength with surface texture, could be solved with an approach using tools, methods, or algorithms if it were possible to know exactly what the mechanical properties of a part are in any given build orientation.

2.5 Interacting with products

When we interact with products, we transition through three levels of experience, namely, visceral, behavioural and reflective (Norman 2004). The visceral level deals with immediate (non-reflective) sensations inspired by physical product characteristics, such as the soft pleasant feel of linen (Ludden & van Rompay 2015). The behavioural level deals with how easy or hard it is to use the product. Appearance and rationale don't really matter, but performance does (Norman 2004). Finally, the reflective level deals with attributions of symbolic meaning and people's resulting tendency to perceive products as embodying values, personality, and hence as a means for self-expression (Ludden & van Rompay 2015). Of course, the degree of influence each level has over the way we experience a product will change over time. For example, if a product is familiar to us, we already know many things about it, such as how it will feel, how to use it, and perhaps how much we like it and why. If we come in contact with a product for the first time, we will draw on past experiences we've had with similar objects, situations, and materials, and will construct a conceptual model of it, in the hope that this will enable us to anticipate what our experience will be. Norman states that a conceptual model is the underlying belief structure held by a person about how something works (Norman 2010). Because of this, the ways in which individual people will experience the same products can differ considerably. Designers can heavily influence this process of experiencing a product, because they can choose to design the product, even if it has never existed before, in ways that can help us understand both its function and use, as well as how it will feel, before we come in contact with it. Designers do this through the clever application of affordances, which are based on what an object affords us to do with it. The noun affordance, derived from the verb afford (Gibson 1977), was created by the American psychologist James J. Gibson, who predominantly worked in the field of visual perception. Gibson explains the theory of affordances as follows (Gibson 1977):

If an object that rests on the ground has a surface that is itself sufficiently rigid, level, flat, and extended, *and if this surface is raised approximately at the height of the knees of the human biped*, then it affords *sitting-on*. We call the object a seat, stool, bench or chair. It affords support for the

rump, whether or not it affords support for the back. If these five properties coexist the object is in fact sit-on-able; they combine to yield a higher-order property for the human observer. The object may then be perceived as sit-on-able without much attention being paid to the five properties in isolation. Note that knee-high for a child is not the same as knee-high for an adult so that sit-on-ability must be taken with reference to a subclass of the human species. The surface layout may be a natural seat like a log or a ledge or an artificial seat like a chair or a couch; the affordance is the same. (p. 68).

We know that chairs are made for us to sit on them and therefore afford sitting, however they also afford standing on, and for small children, they afford getting underneath, and so forth. So, some of the affordances of chairs known to us are sitting, standing and getting underneath, and we know this through our experience with chairs. However, if a designer wants to design a product that is new and unfamiliar s/he can use affordances to help people understand what it could be, how it may feel and how it would be used. The two products shown in Figure 2.34 are a good example of this.



Figure 2.34: Salt and Pepper Maracas by Naoto Fukasawa (courtesy of *Plus Minus Zero*).

Even though there is very little reference to scale it can be assumed that the objects are likely to be maracas due to their overall shape, as well as the glossy highlights on the large elliptical shapes at the top ends of the sticks, which indicates that those are elliptical volumes. If this is correct and they are maracas they would be used by holding them by the stick ends and shaking them. The holes, or more importantly their combination and arrangement, are the main reference to scale, because they are recognisable as a salt and pepper hole pattern, which, together with the colours, indicates that these are a set of salt and pepper shakers. The last question is the material they are made from which, judging by the glossy finish is plastic. There are other options, such as glazed ceramic, powder coated (enamelled) metal, or lacquered timber, but it is most likely to be plastic because that seems the most practical material to make salt and pepper maracas from. Knowing their size, function and material, it can now be assumed what it would be like to interact with them. One can imagine how they would feel in one's hand, how they might sound when shaken, and if they would be enjoyable and fun to use. The products were designed by Naoto Fukasawa in 2007 for Plus Minus Zero. Fukasawa is a visionary designer who uses affordances very effectively. From this example, it can be seen that the surface texture, geometry and colour of a product are all affordances, which means designers can use this to make a product easier to understand and use.

When 3D printing in a polymer is being considered for end-use part production, a considerable part of the discussion will usually centre around the surface quality of the product. These debates ensue due to the processes of 3D printing technologies, stemming from the ways the machines deposit the material or how the material is fused together, leading to stepping or rough surfaces (see Section 2.1: 3D printing). Because people are so accustomed to extremely sophisticated surface detailing and finishes on the products they use daily, which are usually made through a plastic moulding process, it may be the case that many designers assume a person's expectations of 3D printed products will be the same — that they will draw direct comparisons between the two. This is true if 3D printing in plastics is thought of and marketed as a replacement technology for moulding. However, this is an unhelpful perspective to consider 3D printing for manufacturing end-use products,

because 3D printing is not a manufacturing technology that was developed to replace established manufacturing technologies, but is rather a new one that should be treated as such. Therefore, its characteristics such as surface textures should be approached as elements that need to be considered during the various stages of the design process. Figures 2.35 and 2.36 show examples of products, in these cases jewellery, that were made using 3D printing. In all three examples, some build steps have not been removed during post-processing so they can be seen clearly and are used to amplify texture and surface contrast on the pieces. This is all that will be said about these examples for now, as they will be expanded on in Section 7.1: Selecting a surface appearance.



Figure 2.35: 3D printed nautilus shell jewellery piece showing build steps (courtesy of *Thingiverse*).



Figure 2.36: 3D printed jewellery pieces showing build steps (courtesy of *sculpteo*).

Therefore, if a 3D printing method has characteristics that cannot be avoided, such as a particular surface texture, those characteristics become an affordance, and it makes sense for designers to use these characteristics to their advantage as much as possible by integrating them into the design of the product in a meaningful way. To do this, designers would have to be able to visualise the effect a specific build orientation would have on the surface of a part prior to building it, which, according to Gibson, Rosen and Stucker's (2010) eight steps of AM, is step 3: Transfer to 3D printing machine and STL file manipulation. The STL file must be transferred to the 3D printing machine. Here there may be some general manipulation of the file so that it is the correct size, position and orientation for building, as discussed in Section 2.1. This is typically done through the software application used to interface with the 3D printing machine, as shown in figure 2.37; however, most people do not have access to the machines at this level, especially if a service provider is being engaged. In addition, the quality of the representation is low and nowhere near to a true visual representation of what the part will look like after printing.

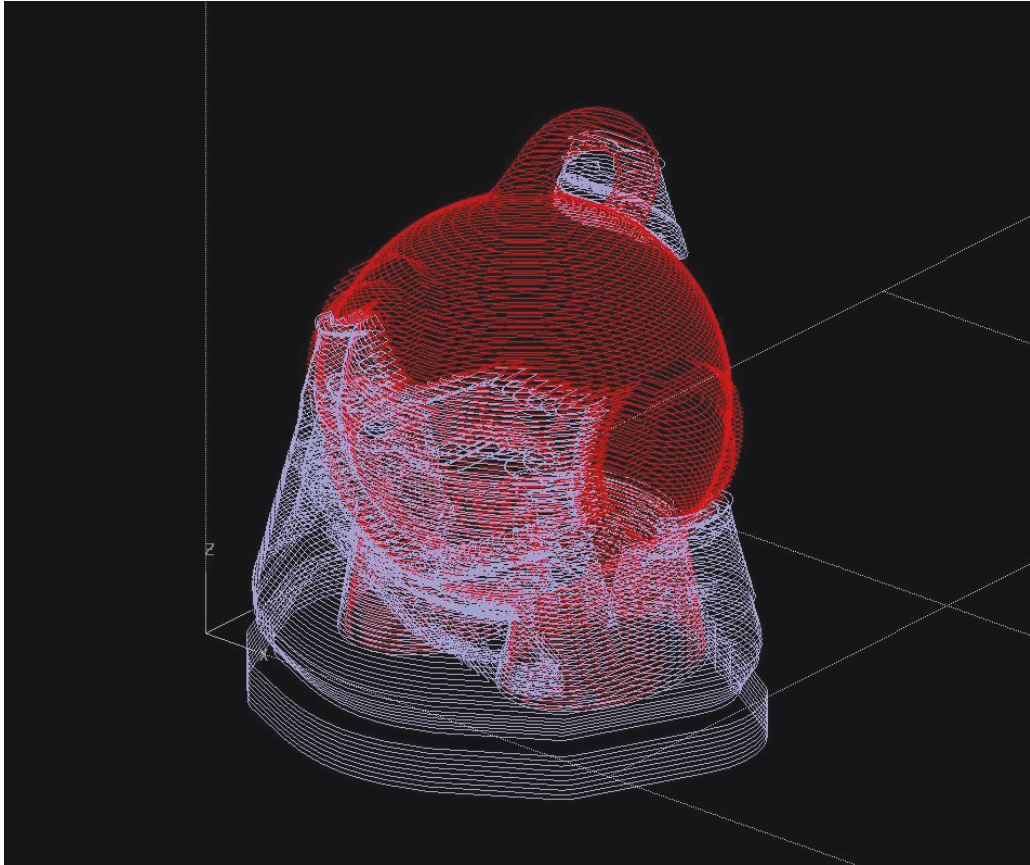


Figure 2.37: Toolpath visualisation through Stratasys Catalyst software.

As a consequence, research is being conducted that is attempting to make surface roughness and the visualisation thereof easier to manage. Because this is currently done through manipulating the orientation of the part in the build volume, there are parallels to the work reviewed in the previous Section 2.4: Strategies to optimise part orientation. Out of the twelve publications reviewed in Section 2.4, five considered either enhancing part finish (Thrimurthulu et al. 2004), averaging weighted surface roughness (Byun & Lee 2006), minimising post machining (Ahn et al. 2007), part surface finish (Pandey et al. 2007), and minimising staircase error (Patak & Pande 2012) as at least one of the variables for build orientation optimisation. Others have considered optimising the surface texture and/or quality as a standalone objective, such as Campbell, Martorelli and Lee, who state that conventional geometric CAD modellers that display a smooth, shaded image of the physical model provide the designer with no information on the surface roughness of the object (2002). They propose a method that uses a visualisation algorithm for surface roughness based on the slanted angle of STL facets, which allows the local surface roughness value applicable to each facet to be determined

(2002). Once their algorithm is applied to the STL model it shows through shading which areas on the surface will be rougher than others, as Figure 2.38 shows. The darker the shading, the rougher the surface will be.

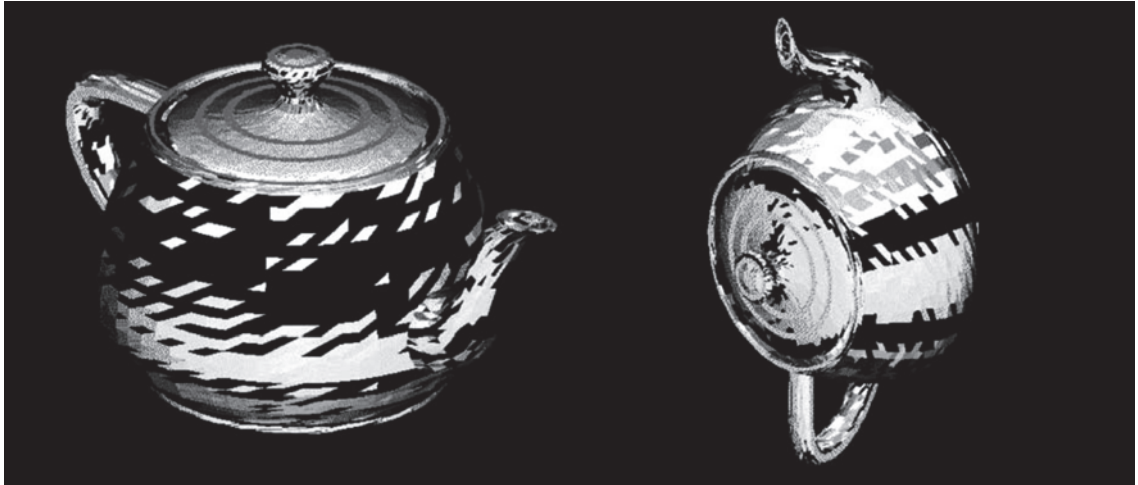


Figure 2.38: Effect of orientation upon surface roughness visualisation (Campbell, Martorelli & Lee 2002, p. 723).

As can be seen in Figure 2.38, the visualisation is good enough to show what areas will be rougher than others, and which orientation will yield an overall better surface, but doesn't show the surface as it would appear after building the part.

Ahn et al. propose a theoretical model to express surface roughness distribution [for FDM] according to changes in surface angle, by considering the main factors that crucially affect surface quality. They did this through evaluating and analysing the effects of surface angle, layer thickness, cross-sectional shape of the filament, and overlap interval on surface roughness (2009). After comparing their theoretical model with the corresponding parts they physically built, Ahn et al. demonstrated that an elaborate prediction of the surface roughness of FDM parts can be performed with the presented surface roughness expression (2009). Unfortunately, the roughness data is presented in the form of a data table rather than a 3D virtual visualisation of the part, which makes applying this method to the workflow of a product design process challenging.

Boschetto, Giordano & Veniali (2013) developed a method to be applied in process planning to determine FDM manufacturing strategies. Through a case

study, they showed the capability of the approach to support the stage of a product by representing the attainable prototype roughness (2013). The most interesting element of this method is that it allows one to select the area on a model for which the best surface quality is required, as shown in Figure 2.39, where the face is the selected area. The graph to the right of Figure 2.39 shows the most beneficial orientation for the selected area, in this case at 104 deg. This is a useful method if a high surface quality is required for a particular area.

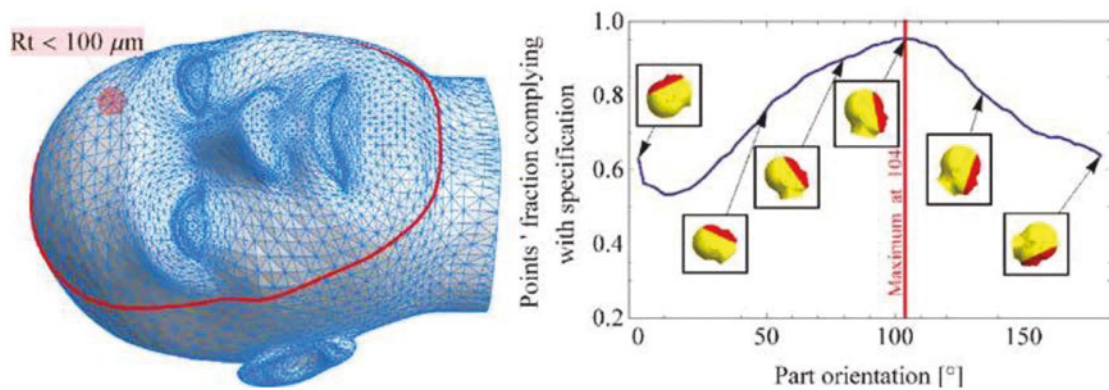


Figure 2.39: Best surface quality on a selected area of a model (Boschetto, Giordano & Veniali 2013, p. 250).

2.5.1 Discussion of interacting with products

The work in Section 2.5 was reviewed to find out what research has been conducted that would enable a designer to see what the surface of part would look like before the part is built. This would enable the designer to potentially use the surface of the part as an affordance, as well as decide which orientation they like best. The author would like to make clear at this point that his opinion regarding what constitutes an acceptable virtual representation of the surface of a part prior to building is subjective and based on what his preferences would be. The author's preference would be for him to be able to see how the build layers and stair-stepping will affect the visual appearance of the surface.

The primary focus of all work reviewed in Section 2.5 is to reduce overall surface roughness through manipulation of the orientation; this is with the

exception of Boschetto, Giordano and Veniali's (2013) method, which enables the selection of a specific area for treatment. None of the proposed methods are able to visually represent what the part will look like after building, although both methods developed by Campbell, Martorelli and Lee (2002) and Boschetto, Giordano and Veniali (2013) attempt to do so. Considering Campbell, Martorelli and Lee's method was published in 2002, their method seems to have been ahead of its time, and it is unfortunate that it was never further developed and refined. Nevertheless, their research does demonstrate that having the ability to visualise the surface of a part prior to 3D printing has been desirable for some time and provides a sound basis for the research presented here.

Ultimately, this is a challenge that needs to be addressed at the CAD level, so designers working on a part in CAD can efficiently visualise the surface of a part based on any given 3D printing process. As Thompson et al. (2016) state, producing digital models for 3D printing is challenging, because most commercially available CAD programs are parametric NURBS systems, which are well suited to modelling geometries associated with traditional manufacturing processes. They go on to say that to overcome these limitations, 3D printing CAD systems require an interface that can develop complex shapes and structures, and a data structure that can store their properties (2016).

2.6 Discussion of existing knowledge and related literature

The work reviewed in Chapter 2: Existing knowledge and related literature demonstrates that scholars understand the need for more knowledge in the area of 3D printing. They are conducting excellent research, the results of which are the foundation upon which the research presented here is built. Of predominant relevance is the work that has been done by other scholars in the areas of DFAM (see Section 2.2.2: Designing for 3D printing/additive manufacturing (DFAM)), the static mechanical properties of 3D printed polymers (see Section 2.3.3: AM polymer specific studies) and part orientation (see Section 2.4: Strategies to optimise part orientation). The preceding work made it possible for the author to build his knowledge in those areas and without the preceding work would not have been able to identify where more

work needs to be done. Upon contemplation of the reviewed literature it becomes clear that from the point of view of a product designer who uses 3D printing in polymers to produce end-use products for clients, the reviewed literature does not provide enough information to enable them to make informed decisions regarding the build orientation of a part in relation to its mechanical properties. To begin with, much of the information is not comparable, because different testing procedures were used as well as different materials and testing machines or equipment. And even if all data could be cross-referenced accurately, only the difference in mechanical properties between horizontal and vertical oriented parts would be known. This, in turn, would be acceptable if all parts were either longitudinal beam structures or structures with 90 deg angle features, such as L-shaped or U-shaped parts. However, most of the parts that are produced are far more complex than that, with curved surfaces and angled features. It would therefore be an advantage to have a better understanding of how the mechanical properties of the materials change if the build orientation is changed to an angle, so it is not just horizontal or vertical, but also at an incline. To that end, no one appears to have conducted tests where specimens were built at an incline, at, for example, 45 deg in the Z orientation, which being halfway between 0 and 90 degs, would be a good orientation to start with. Having said this, it is possible that research in this area is currently being conducted but has not been published yet.

Chapter 3. Research questions and methodology

As to methods there may be a million and then some, but principles are few. The [person] who grasps principles can successfully select [their] own methods. The [person] who tries methods, ignoring principles, is sure to have trouble.

— Emerson Harrington (1911)

The review of existing work and knowledge revealed that predicting the mechanical properties of 3D printed polymers can be likened to a “dark art”, because there are many factors at play, ranging from the EO (end of vector) effect for SLS (selective laser sintering) to filament bonding for FDM (fused deposition modelling). If someone is the designer as well as the producer of a product they are directly responsible for its performance, because there are no other professionals involved that share the responsibility and the associated risks with them. An example of a case where the responsibility and risks are shared is injection moulding, where toolmakers and production engineers are involved in the process, as discussed in Section 2.2: The process of designing a product. Considering that all mechanical property testing to date has only been done in various horizontal and vertical orientations, it would be useful to start testing on an incline, halfway between vertical and horizontal at 45 deg. To do this, test specimens for each test should be built in HF (Horizontal Flat), HoE (Horizontal on Edge), I 45 (incline 45 deg) and V (Vertical) orientations and tested under the same conditions. In addition, to ensure the resulting test data can be cross referenced and compared from material to material, it would be advantageous to test all three polymers under the same conditions using only one standard. To enable this, ensuring that the test specimens are built in the correct orientations and from the required materials is important. As shown in Section 2.3.3: Material/process specific studies, two seemingly identical 3D printing machines operated by the same bureau, building the same part with the same settings (e.g. material and orientation), are likely to produce parts with different properties and characteristics. Furthermore, there is anecdotal evidence to suggest similar occurrences, where technicians that operate 3D

printing machines will, out of a pool of apparently identical 3D printing machines, recommend one machine over others because it “runs” better and produces more consistent parts. Monzon et al. reinforce this, stating that two manufacturers of 3D printed parts supplying the same product to final users, even using the same equipment and material, could supply parts with different characteristics, in terms of either mechanical properties or geometric tolerances and roughness (2015). Therefore, it is necessary to have a clear understanding of the types of machines and materials service providers such as 3D printing bureaus use to produce parts. In other words, it is necessary to build good relationships with the service providers so they can be asked to orient parts in specific build orientations. It is also helpful if they provide guarantees that the machines are being calibrated according to the manufacturer’s specifications, because this ensures all the resulting parts are produced as intended. This is akin to the relationship a designer would have with a more traditional craftsperson who produces products or parts thereof for them. To achieve this, it would be advantageous to work with local service providers and have test specimens built locally, so it can be ascertained exactly what type of part properties the machines that can be accessed will produce.

In summary three key observations can be made:

- Building knowledge of the mechanical properties of 3D printed polymers in more than horizontal and vertical orientations is necessary.
- There are no tools or methods to optimise the mechanical properties of a part based on build orientation. Developing an approach to enable this would assist product designers during the process of designing a product for 3D printing.
- No research is being conducted to ascertain what tools could enable a designer to see what the surface of part would look like prior to the part being built. Ascertaining what appropriate tools there are that enable designers to visually represent the surface of a part, virtually in 3D and prior to building it, would be of benefit.

3.1 Research questions

The previous section concluded with three observations that are key to assisting product designers who are designing an end-use product to be manufactured through 3D printing. Individually, those three observations could form a research question each. However, it was decided to use the observations as a basis to develop a new approach that will assist product designers when manufacturing through 3D printing. To develop the new approach, research questions were formulated so their results could be combined in a variation of ways depending on what a product designer may require. The various ways that the new approach can find application to product design practice are explored through case studies and scenarios in Chapter: 6.0 Analysis and communication of results. The research questions were also formulated so they, in combination with their results, can be used independently from each other for future publications.

Below are the research questions:

- 1a. For each of the 3D printed polymers ABS, TPGDA and PA:
How do the tensile, flexural and impact properties vary between test samples built in HF (Horizontal Flat), HoE (Horizontal on Edge), V (Vertical) and I 45 (Incline at 45 degrees) orientations?
- 1b. Based on the results from question 1a:
How do the tensile, flexural and impact properties of the 3D printed polymers ABS, TPGDA and PA compare from polymer to polymer?
2. Which software application provides the clearest visual representation of the surface of a part prior to building?

3.2 Methodology

The need for this research emerges from the lack of available data in relation to the mechanical properties of 3D printed polymers. To design and manufacture end use products made from 3D printed polymers, more material data is needed to ensure the products are safe to use, as well as developing an approach that makes the design process more efficient. After completing an in-depth study of the existing knowledge and related literature in the fields of

design, engineering, and science, with the focus on the strength of 3D printed polymers in relation to their build orientation (see Section 2.0: Existing knowledge and related literature), it became apparent that there were gaps in the knowledge of several areas, and therefore a lot of scope for conducting research. The research was focused on three areas that are relevant to product design practice and would benefit product designers working on products that are to be made from 3D printed polymers. Those three areas are: 1) the variations of the strength of 3D printed polymer parts built in horizontal, 45 deg incline, and vertical orientations; 2) the comparison to these strengths between three different polymers; and 3) the visualisation of a part prior to it being built. All three areas formed the basis for the research questions 1a, 1b and research question 2, listed in the previous Section 3.1: Research Questions.

The aim of this research is to make it easier for product designers to choose the type of 3D printing polymer and build orientation for end-use parts they have designed and want to manufacture using 3D printing. To achieve this, the methodology is split into two parts; please refer to the diagram shown in Figure 3.1. Each part of the methodology was developed so their combined results would suit the needs of product designers and allow them to apply and integrate the results into their product design process.

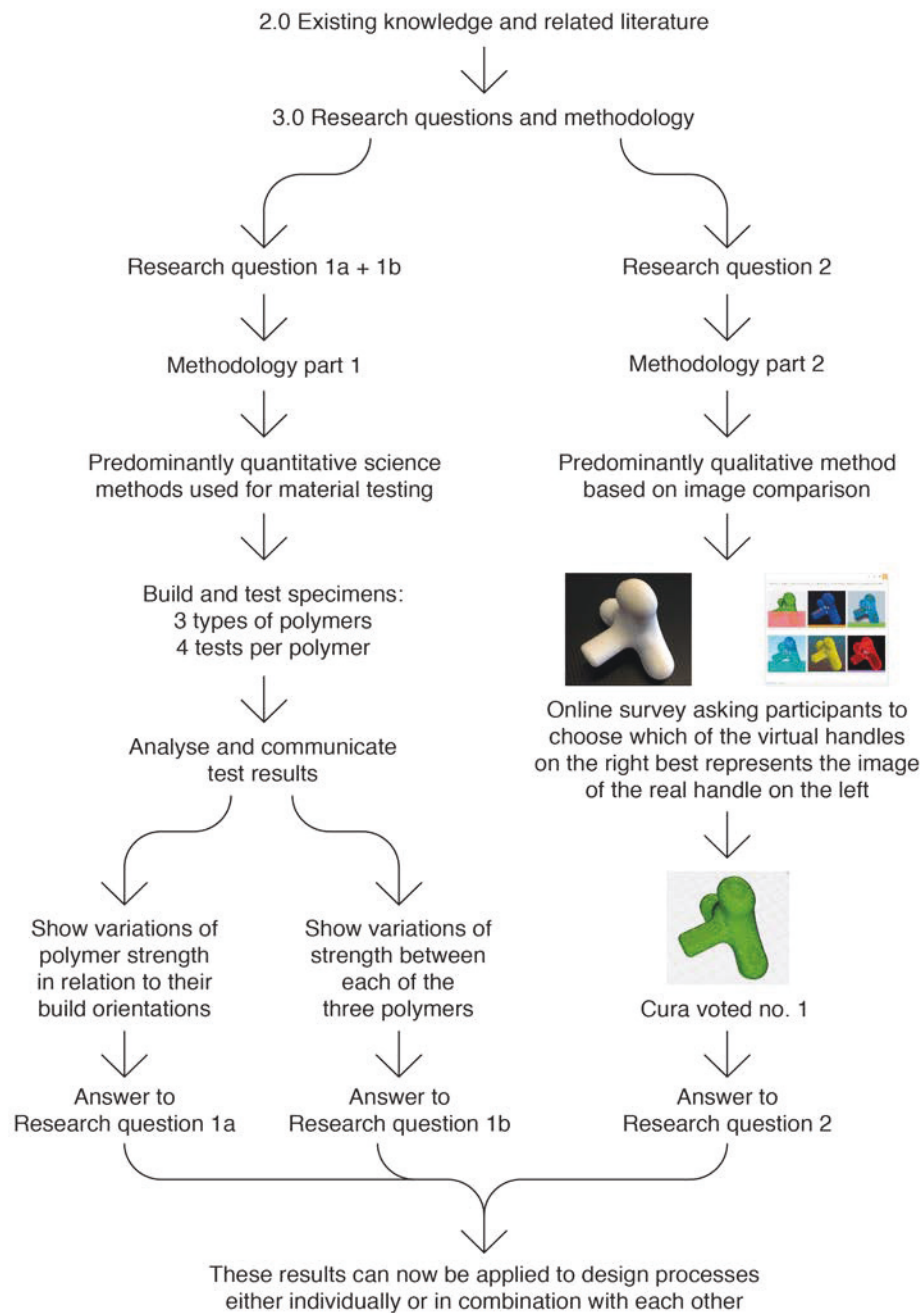


Figure 3.1: Diagram of the methodology.

Methodology Part 1 is predominantly quantitative and larger in scope than Part 2, and was developed to answer research questions 1a and 1b (see previous Section: 3.1 Research Questions).

Methodology 2 is predominantly qualitative and was developed to answer Research Question 2.

3.2.1 Methodology Part 1

Methodology Part 1 is based on scientific methods, which are predominantly quantitative; specifically, the methods used to test the strength of materials. However, the methodology itself is not a scientific one, such as is often used in science or engineering, where a typical approach is to construct or put forward a hypothesis based on existing knowledge. The hypothesis is then tested by conducting tests or experiments, the results of which are then compared with the hypothesis and conclusions are drawn based on how the results compare to the hypothesis. This scientific method forms part of a well-established traditional hierarchy, in which empirical knowledge is built through the process of one experiment and its results lead to the next. It is a process where the discovery of a result opens up new questions, which then inform and lead to the next hypothesis and experiment. Along the way, the results of the experiments and new knowledge they uncovered are published, usually through academic publication channels, and so transition from theory into practice where they can be applied to real world needs.

In Methodology Part 1, although scientific methods are used to build empirical knowledge, this traditional hierarchy is not present. The motivation that gave rise to this research came from a lack of information available to product designers about strength and build orientation, which is necessary to design end-use products made from 3D printed polymers. This lack of information was discovered while working on several real-world projects that involved designing end-use products that were produced using 3D printing; detailed descriptions of those projects can be found in Section 2.3: End-use products made from 3D printed polymers.

This has already been discussed in Section 2.3.1: Static mechanical properties of three 3D printed polymers and is repeated here to ensure clarity with regard to the notation of part orientation. The ASTM standards utilise the coordinate system X, Y, and Z to communicate the notation of part orientations; see Figure 3.2. However, people who are not accustomed to thinking in X, Y and Z coordinates may find this confusing. To assist people with comprehending build orientation more easily, the ASTM notations have been translated into acronyms for this research:

XYZ & YXZ = horizontal flat (HF)

XZY & YZX = horizontal on edge (HoE)

ZXY & ZYX = vertical (V)

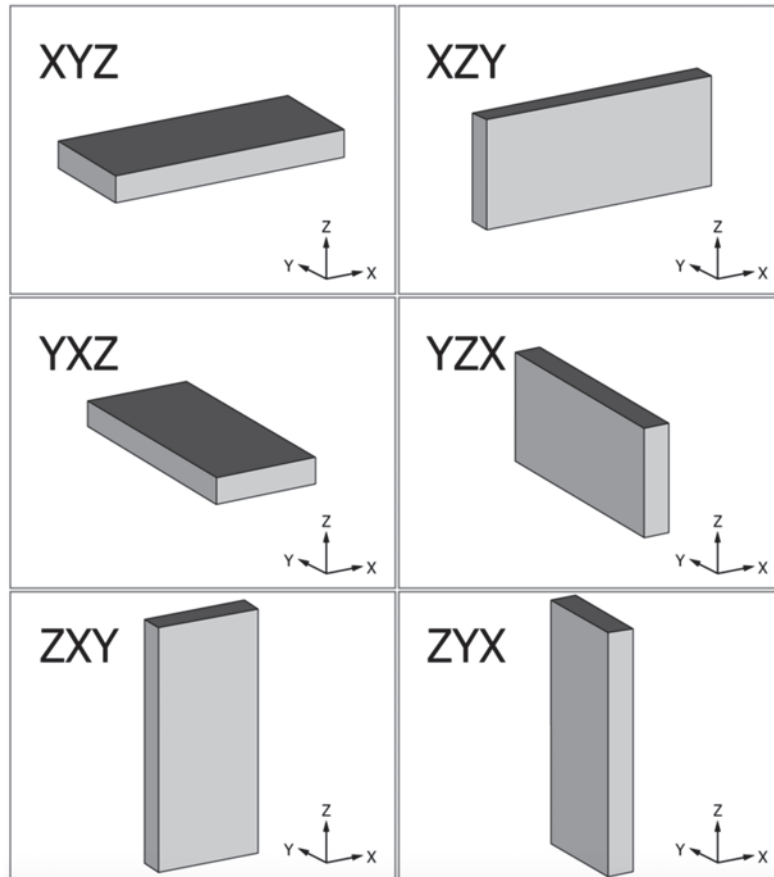


Figure 3.2: Orthogonal orientation notation (ASTM 2013b). The biggest dimension takes the 1st coordinate, the next biggest dimension the 2nd coordinate, and the smallest the 3rd coordinate.

At the time of writing, inclined (at an angle) build orientations did not yet have an ASTM notation, using X, Y and Z coordinates, which led to one being created for this research:

Incline 45 (I 45), see Figure 3.3.

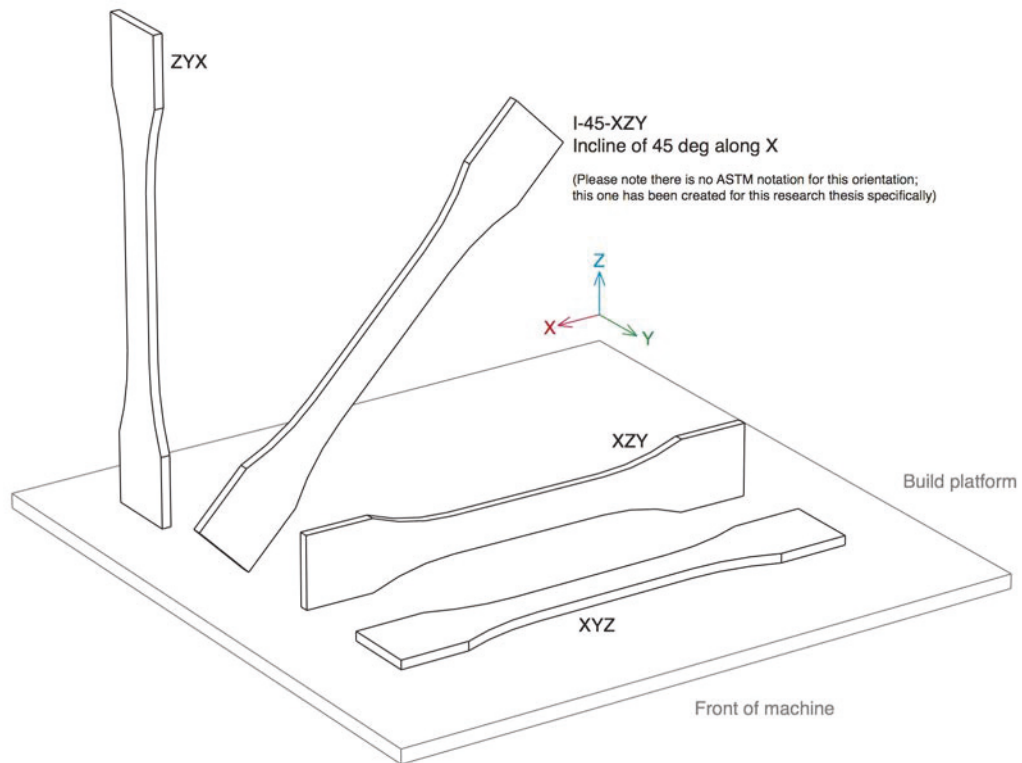


Figure 3.3: Inclined build orientations, such as I-45-XZY (I 45), do not have an ASTM notation, this notation has been created specifically for this research.

Methodology Part 1 is designed to answer Research Questions 1a and 1b which are:

- 1a. For each of the 3D printed polymers ABS, TPGDA and PA:

How do the tensile, flexural and impact properties vary between test samples built in HF (Horizontal Flat), HoE (Horizontal on Edge), V (Vertical) and I 45 (Incline at 45 degrees) orientations?
- 1b. Based on the results from question 1a:

How do the tensile, flexural and impact properties of the 3D printed polymers ABS, TPGDA and PA compare from polymer to polymer?

To achieve this, data was generated by first building test samples in each polymer in all the build orientations listed in Research Question 1a, and then destructively testing them using science-based material testing methods. The data was then analysed and interpreted in two different ways, where the first interpretation answers Research Question 1a and the second answers Research Question 1b.

Figure 3.4 shows the diagram which illustrates the path of Methodology Part 1 and at which point it addresses Research Question 1a and 1b.

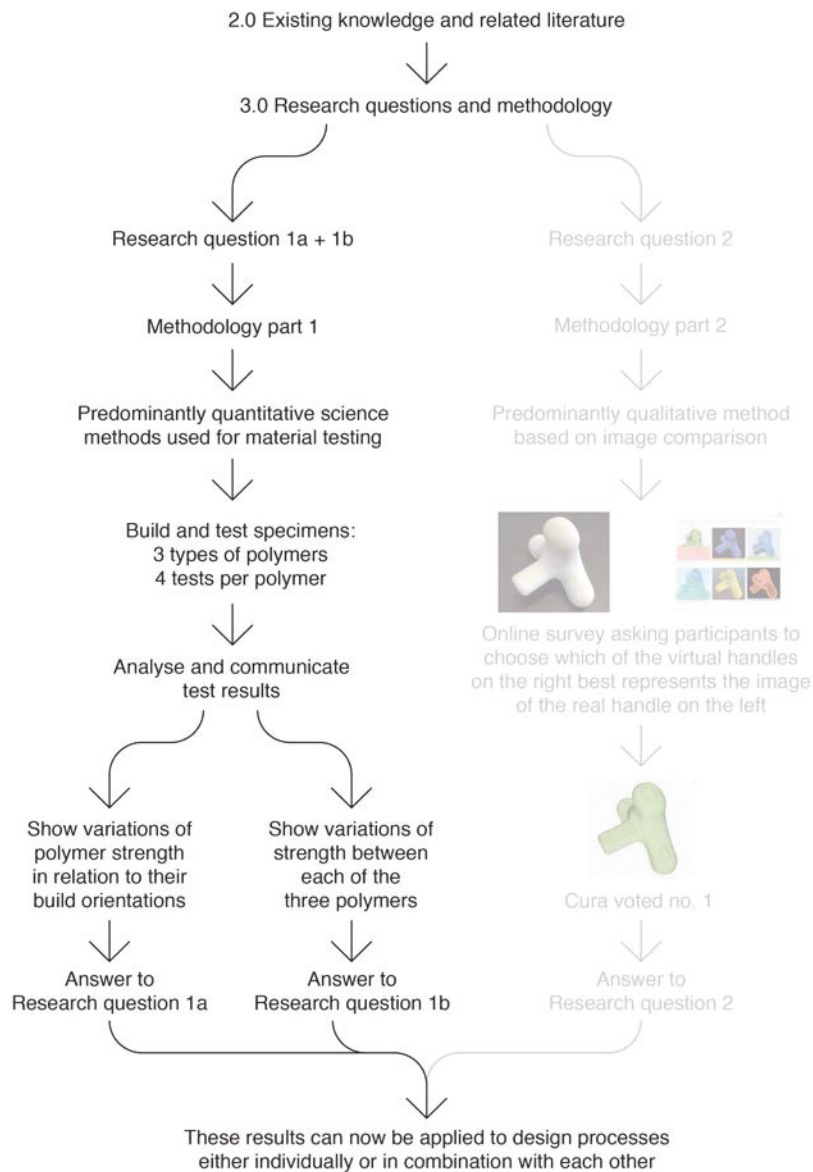


Figure 3.4: Diagram of Methodology Part 1.

3.2.2 Methodology Part 2

Methodology Part 2 is based on a predominantly qualitative method and is, as indicated earlier, designed to answer Research Question 2:

2. Which software application provides the clearest visual representation of the surface of a part prior to building?

To achieve this a test part was built in ABS on an FDM machine, photographed and then compared with six different software applications and their virtual representations of the test part. All virtual representations were set to the same parameters, such as build resolution and perspective (point of view) as the test part. A detailed description of all aspects of this methodology is provided in Section 4.2: Experiment to determine clear visual representation of the surface of a 3D printed part prior to building.

Figure 3.5 shows the diagram which illustrates the path of Methodology Part 2 and at which point it addresses Research Question 2.

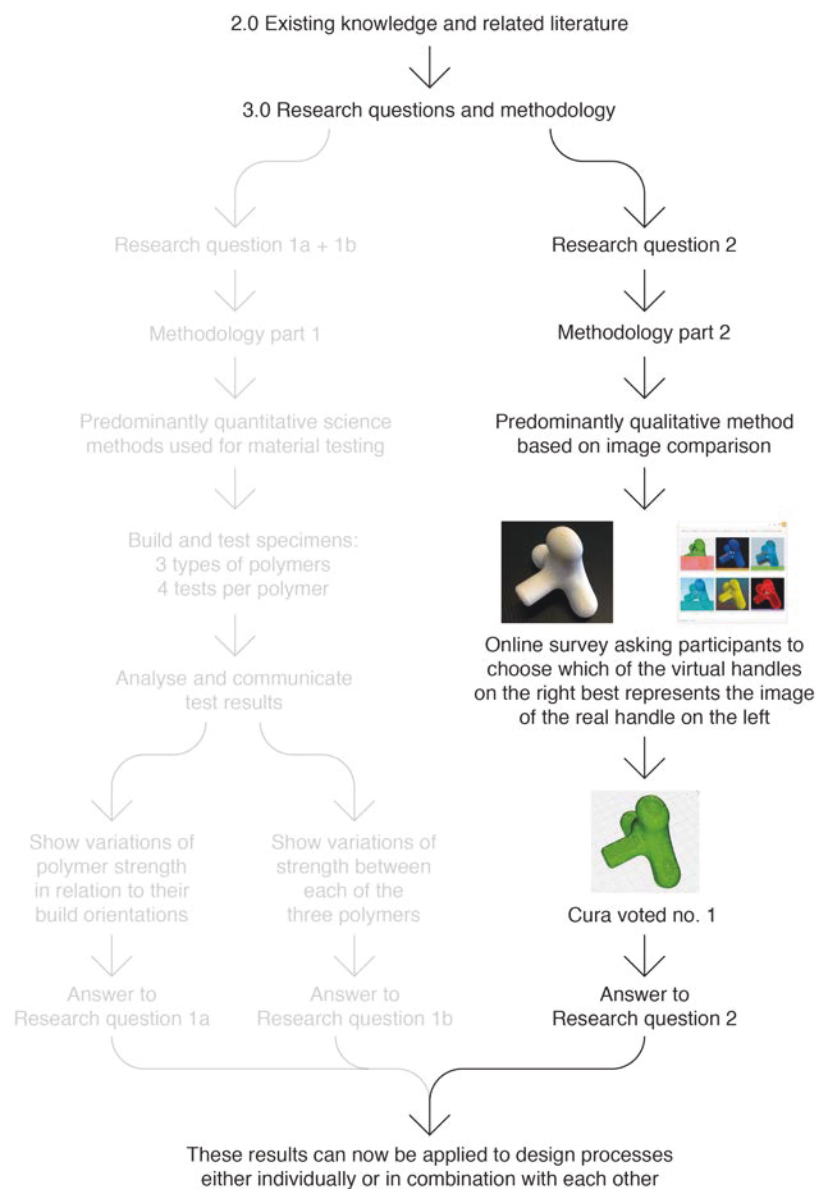


Figure 3.5: Diagram of Methodology Part 2.

3.3 Limitations of scope

As is the case with all projects, research or other, it is important that the scope of the project is limited to ensure its completion is achievable in the time allowed and on budget. With regard to this research, it was imperative to manage the scope of the experiments so that they provide a set of data and, more importantly, a way of interpretation that is useful to product designers and can be applied to product design practice.

The properties of materials can be experimented with and tested in a multitude of ways, ranging from several static and dynamic tests as well as thermal and chemical ones. For test results to be valid and repeatable, testing standards are used, and in Australia, ASTM (American Society for Testing Materials) standards are used. The ASTM recommends that for anisotropic materials, a minimum of 5 test specimens are tested per test in each material, and in the case of this research, each build orientation. The mean or average of the test data from the five test specimens is then calculated to account for the variations between test specimens. For this research, three build orientations are tested per polymer to ascertain the variations in strength between each build orientation. This means that to test one polymer, for example for impact strength, 15 test specimens need to be built and tested, 5 for each of the 3 build orientations. Therefore, to test 3 different polymers for impact strength, 45 test specimens need to be built and tested. This is both expensive and time consuming, which is why the scope of the material testing for this research has been limited as follows:

1. The scope has been limited to three rigid 3D printed polymers, namely ABS, TPGDA and PA; the reasons for this are as follows: 1) Testing materials is time consuming and expensive, so it was necessary to ensure the scope of the research was manageable in the time allowed, which is why the testing was limited to three materials. 2) The processes and materials suitable for end-use part production as recommended by the literature, such as Boeing's use of SLS in PA and FDM in ABS, and Starkey Hearing Technologies' use of TPGDA, as well as according to the author's experience. 3) Accessibility to 3D printing technology in the Sydney metro area. This is important because it ensures, as much as possible: consistency of material (proprietary for each brand of machine/process);

build orientation (important since the strength comparisons are centered around orientation); and build quality of the test parts produced. All of these things are easier to manage face-to-face rather than via email, phone or Skype. See also Section 2.3: End-use parts made from 3D printed polymers.

2. The testing is limited to static mechanical properties, namely: tensile, flexural and impact, as they are the three properties that are most useful to product designers when deciding what type of material to use. They are also the typical properties listed on data sheets for polymers, as well as being the most common tests applied to the materials tested in the majority of literature that was reviewed for this research.
3. The only two build process parameters that can be altered are layer height and build orientation. In the literature reviewed, several researchers experimented with the altering of additional parameters, such as: laser intensity with SLS, print head tracking speed for FDM, and UV light exposure in MJ, which are all parameters that cannot be altered if the parts are being supplied by a 3D print bureau. To change those sorts of parameters, access to the machines would be needed at a level that no print bureau would allow. It would also require detailed knowledge of the machines, which is not available. Another option would be for the print bureau to change parameters on request, however, it is unlikely that any 3D printing print bureau would do this, because it would alter the property of the part produced beyond the guarantee of the company supplying the machine and the material.

Under certain circumstances, the scope of a research project needs to be managed or decided upon within boundaries that are not clearly defined. This was the case with the experiment designed to determine which software tool provides the best representation of surface appearance prior to building. Things that were important for this experiment were: choice of software applications, the size and form of the part, and the material it was built from. The limitations that were applied to those aspects are outlined as follows:

4. The experiment is limited to six software applications, which were selected based on discussions with academics at the School of Design at UTS, 3D printing blogs, and the authors' experience. The 6 applications

are: 1) CatalystEx V3.5, 2) Cura V3.0.4, 3) Cubicreator3 V3.6, 4) Simplify3D V4.0.1, 5) Slic3r V1.2.9 and 6) Slicer for Fusion 360 V1.0.0.

5. The test part is built via FDM in ABS. The reason for focusing on an FDM in ABS part is because the stair stepping effect is visually more notable on FDM than on MJ and SLS parts. This is due to the layer height at 0.25mm, the smooth surface of the extruded filament, and the fact that ABS is 100% opaque. MJ parts have been excluded from the experiment, because the semi opaque appearance of the TPGDA cannot be represented through any of the six software applications. SLS parts have also been excluded due to the rough surface texture, representing suede or flocking, which, again, cannot be represented through any of the six software applications.
6. This research is centred around handheld products (a portable product that can be used while it is being held and carried by one or both hands) so the size of the part needs to be of a size appropriate to handheld products. There are two reasons why it was decided to limit the size of the products to handheld size. The first reason is that it was important to ensure that the build steps (stair stepping effect) could clearly be seen and identified by the naked eye. Handheld products are typically utilised in a hand-eye coordinated fashion and in close proximity to the person using it, so the look and feel of its surface is highly relevant. The second reason why it was decided to limit the size of the products to handheld size is the build volume of the 3D printers capable of printing in all three of the chosen materials. At the time of writing it was challenging to find 3D print bureaus in the Sydney metropolitan area with build volumes larger than 300mm x 300mm x 300mm (width x length x height).

3.4 Research hypothesis

As discussed at the beginning of this chapter the research questions were formulated based on three key observations that came out of what was discovered in Chapter 2: Existing knowledge and related literature. Those three key observations were:

- Building knowledge of the mechanical properties of 3D printed polymers in more than horizontal and vertical orientations is necessary.

- There are no tools or methods to optimise the mechanical properties of a part based on build orientation. Developing an approach to enable this would assist product designers during the process of designing a product for 3D printing.
- No research is being conducted to ascertain what tools could enable a designer to see what the surface of part would look like prior to the part being built. Ascertaining what appropriate tools there are that enable designers to visually represent the surface of a part, virtually in 3D and prior to building it, would be of benefit.

The formulation of the research questions was done in such a way so their results could be used to develop a new approach to assist product designers manufacturing end-use products from 3D printed polymers. The other aspect that the results of the research questions need to satisfy is that they can be used independently from each other for future publications purely from the perspective of what will be learnt about the mechanical properties of each polymer.

The research questions are:

- 1a. For each of the 3D printed polymers ABS, TPGDA and PA:

How do the tensile, flexural and impact properties vary between test samples built in HF (Horizontal Flat), HoE (Horizontal on Edge), V (Vertical) and I 45 (Incline at 45 degrees) orientations?
- 1b. Based on the results from question 1a:

How do the tensile, flexural and impact properties of the 3D printed polymers ABS, TPGDA and PA compare from polymer to polymer?
2. Which software application provides the clearest visual representation of the surface of a part prior to building?

To answer the research questions the research methodology was developed which comprises of two parts. Methodology Part 1, shown in the left channel of Figure 3.6, was developed to answer research question 1a and 1b. It is based on scientific methods that, through the destructive testing of the material samples, will yield quantitative data of the mechanical properties of the three

polymers. Methodology Part 2, shown on the right channel of Figure 3.6, was developed to answer research question 2. It is based on qualitative methods that, through an online survey, will yield qualitative data of the software application that best represents the surface of a part prior to printing.

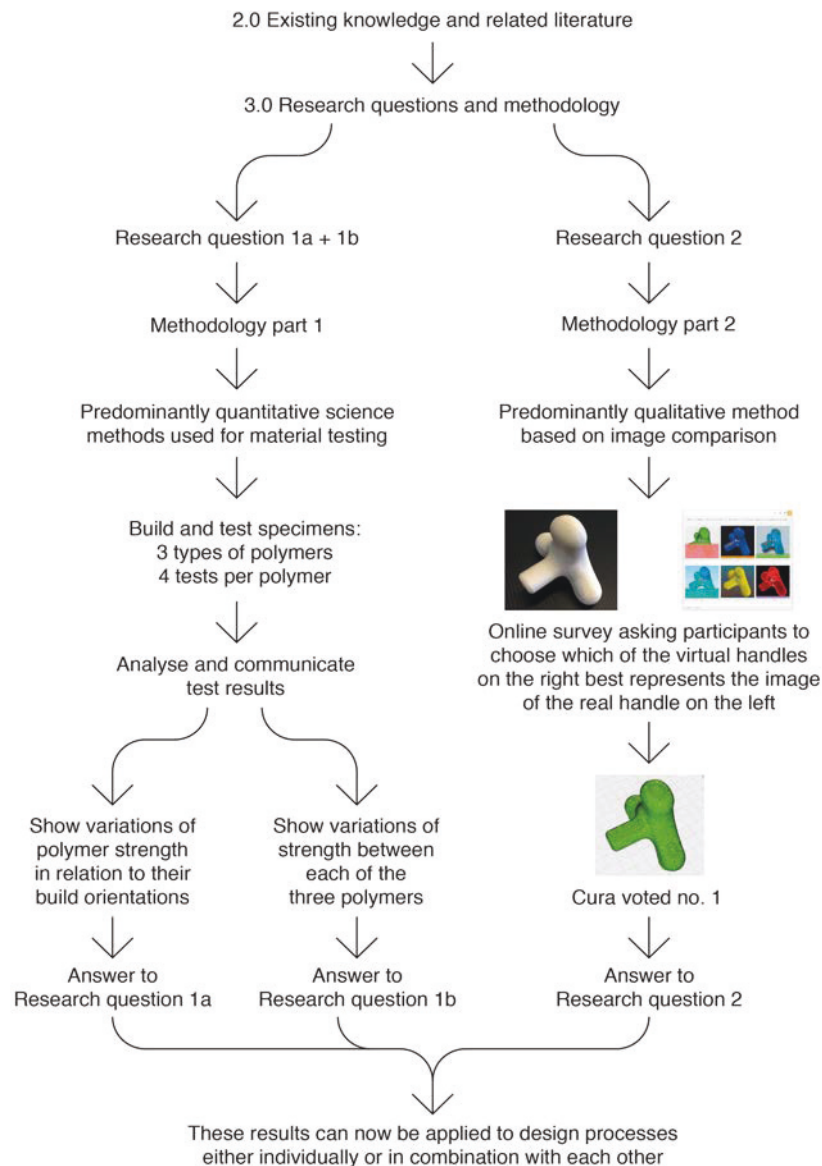


Figure 3.6: Diagram of the methodology.

The methodology diagram (see Figure 3.6) ends with the statement:

These results can now be applied to design processes either individually or in combination with each other.

This statement forms the research hypothesis which is anticipating that the data resulting from the experiments (see Chapter 5: Results) can be applied to and will be useful for the process of designing end use products to be manufactured through 3D printing. The hypothesis makes a distinction between the results being applied either individually or in combination with each other. What is meant by this is that the resulting data can be used as tools in various combinations depending on what the designer may require. The aim of this, as discussed at the beginning of this chapter, is to develop a new approach that will assist product designers designing end use products to be manufactured through 3D printing. To test the hypothesis the resulting test data was first analysed and translated into a set of tools (see Chapter 6: Analysis and communication of results) and then tested by applying them to a series of case studies and scenarios (see Chapter 7: Discussion).

Chapter 4. Experiments

Experiments is split into two sections: 4.1 Experiments Part 1: Determining the mechanical properties of three 3D printed polymers at a 45 deg incline; and 4.2 Experiments Part 2: Determining clear visual representation of the surface of a 3D printed part prior to building. Section 4.1 is predominantly quantitative basic research and 4.2 is predominantly qualitative applied research.

4.1 Experiments to determine the mechanical properties of the three 3D printed polymers at a 45 deg incline

The purpose of these experiments is to generate data to determine two things that will enable Research Questions 1a and 1b to be answered:

1. How much stronger, or weaker, is each of the three 3D printed polymers if the test specimen is built at a 45 deg incline, when compared to the horizontal and vertical orientations? This is important for product designers to know, because many actual parts have complex geometries, meaning they are not just straight, flat sticks of L-shaped in form. Therefore, it is an advantage to be able to better understand the balance between orientation and strength.
2. How do the three properties of the polymers compare to each other? This is important because it enables product designers to make knowledge-directed decisions between the three polymers.

The guidelines applied to the following experiments are based on the procedures recommended in ASTM standards, which, as mentioned earlier, are the standards Australia adheres to. The mechanical properties of the materials are tested accordingly, so the data can be used by others and cross referenced, as well as allowing testing procedures to be replicated. Hence the choice of this methodology to answer research questions 1a and 1b (see Chapter 3.0). Since this methodology was specifically designed to generate new data on the mechanical properties of the three 3D printed polymers at a 45 deg incline, test samples needed to be built at 0 deg horizontal and 90 deg vertical as well as 45 deg incline. The reason for this is that 3D printed materials are anisotropic, so the new 45 deg incline data is only useful to this research and others who might want to use it in the future if it can be

compared to the mechanical properties of other build orientations. Therefore, to ensure that all data was comparable, the test samples for each material were built at the same time and tested under the same conditions.

In 2009, the ASTM (American Society for Testing and Materials) established the International Technical Committee F42 on AM Technologies; their scope is the promotion of knowledge, and stimulation and implementation of technology through the development of standards for AM technologies (ASTM 2009a). Within Committee F42 sits the Subcommittee F42.01 on Test Methods (ASTM 2009b), which lists ASTM 52910:2017 Standard Guidelines for Design for Additive Manufacturing (ASTM 2017) as the top-level standard relating to AM testing procedures as well as other things such as terminology. The following standards were used in this methodology and are all in accordance with ASTM 2017.

For tensile, flexural and impact test procedures:

- ASTM D638 – 14
Standard Test Method for Tensile Properties of Plastics (ASTM 2014)
- ASTM D256 – 10
Standard Test Methods for Determining the Izod Pendulum Impact Resistance of Plastics (ASTM 2010)
- ASTM D790 – 15
Standard Test Methods for Flexural Properties of Unreinforced and Reinforced Plastics and Electrical Insulating Materials (ASTM 2015a)

Copies of the testing standards listed above can be found in Appendix H.

For the conditioning of test specimens for testing:

- ASTM D618 – 13
Standard Practice for Conditioning Plastics for Testing (ASTM 2013a)

For build orientation notation:

- ASTM 52921:2013
Standard Terminology for Additive Manufacturing – Coordinate Systems and Test Methodologies (ASTM 2013b)

All three of the main test procedure standards (ASTM D638 – 14, ASTM D790 – 15 and ASTM D256 – 10) stipulate that if the polymer to be tested is anisotropic, then a minimum of five specimens must be tested for each desired direction, which was done for this research.

4.1.1 Making the test specimens

The CAD models of all specimens were created in Shark CAD FX V 8.0.3 (now called SharkCAD Pro V 10.0); from there, they were exported as STL files, which were then sent to the 3D print bureaus via email. Each bureau was supplied with the same STL file for each test specimen grouping, with the specification to build them in the desired orientation. Because this was important, it was further reinforced by physically visiting the print bureaus and making follow-up calls over the phone. Figures 4.1 to 4.4 show how the test specimens were arranged on the build platforms.

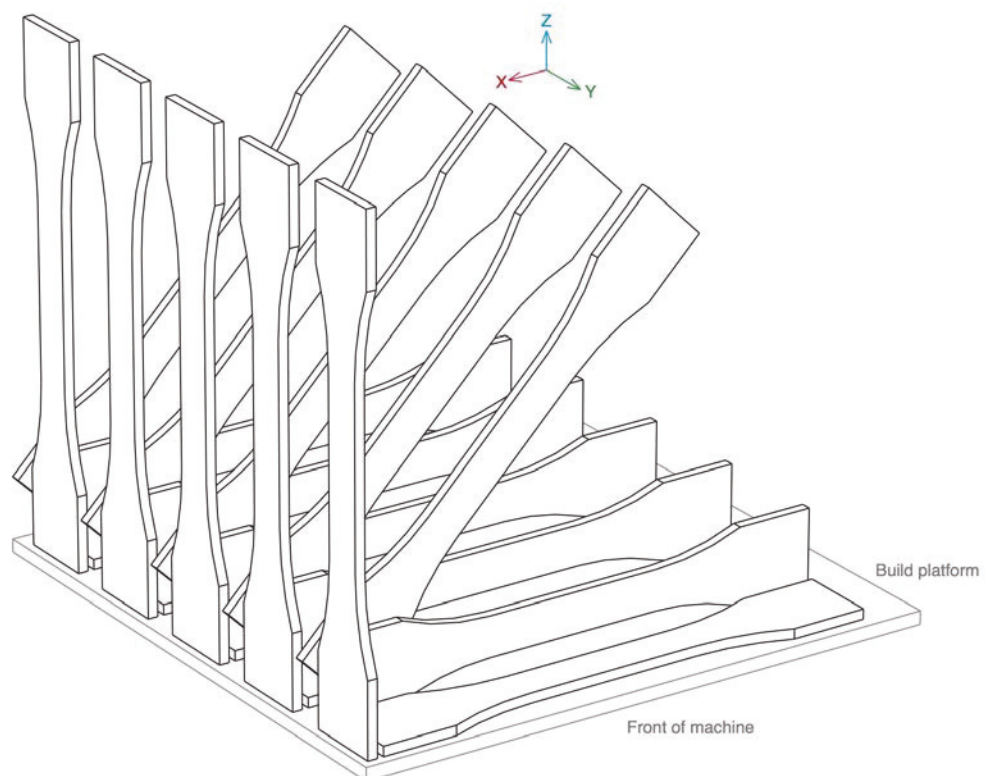


Figure 4.1: Tensile specimen build orientation and arrangement for ABS and TPGDA.

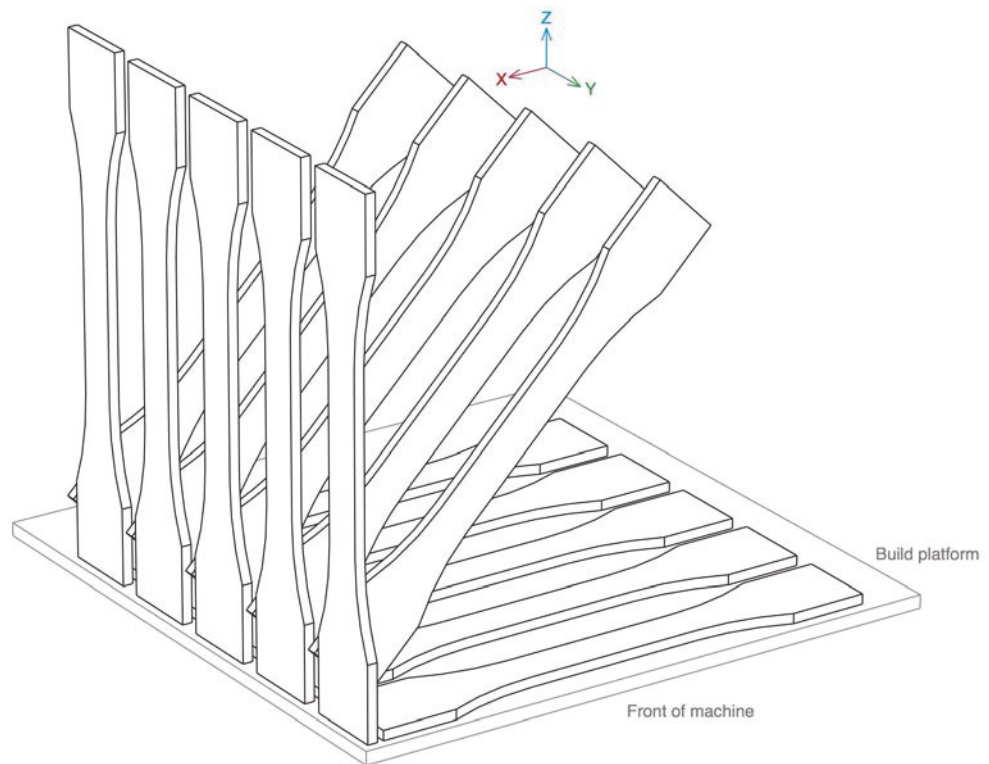


Figure 4.2: Tensile specimen build orientation and arrangement for PA.

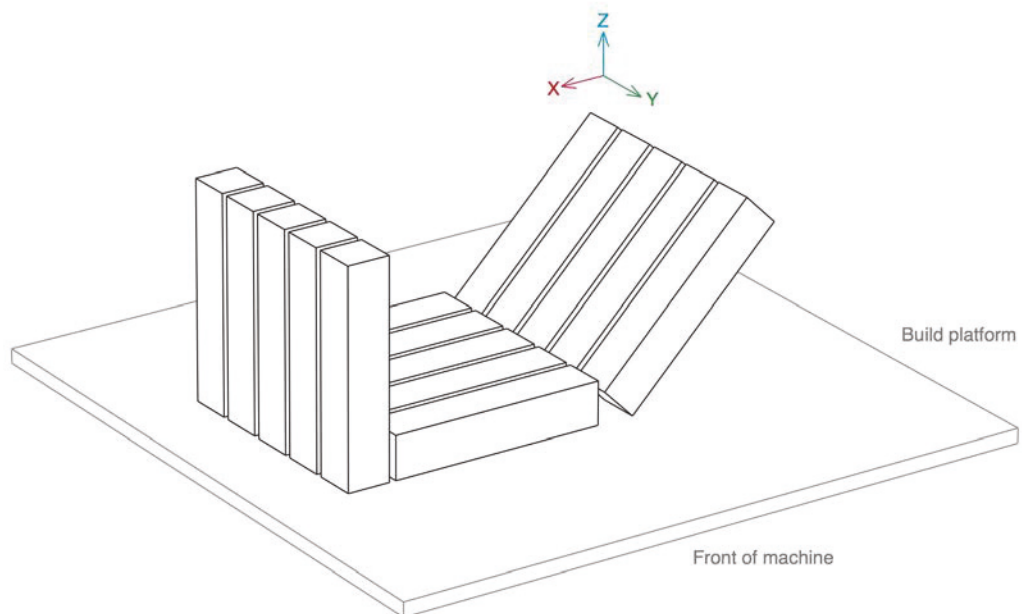


Figure 4.3: Izod impact specimen build orientation and arrangement for ABS, TPGDA and PA.

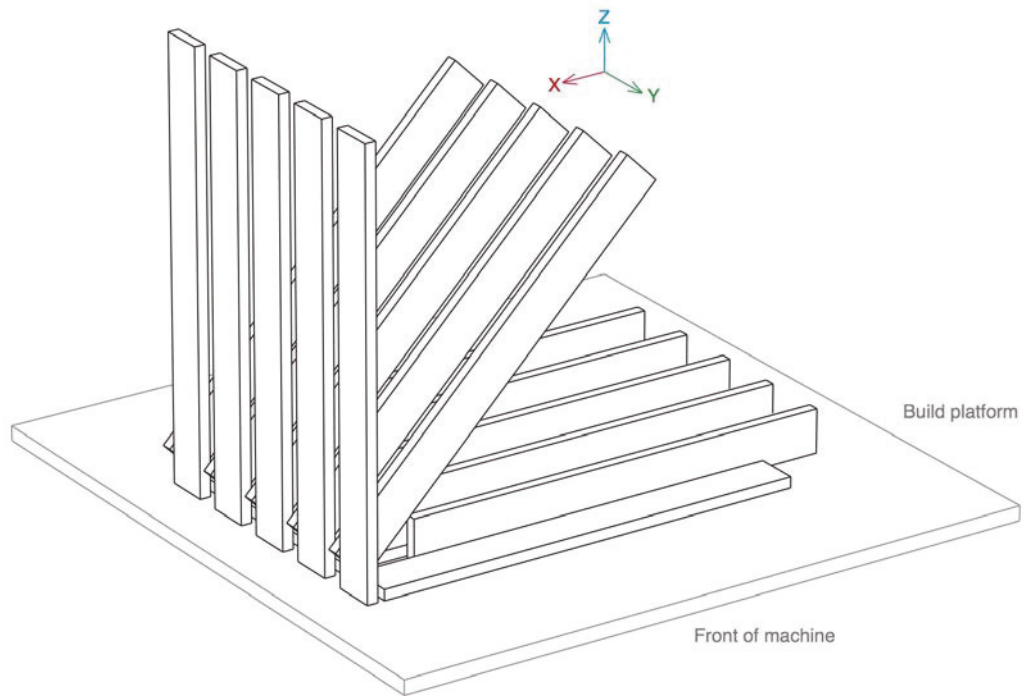


Figure 4.4: Flexural specimen build orientation and arrangement for ABS, TPGDA and PA.

Listed below are the details of each 3D printing process and polymer, including the settings used to build the test samples as well as the 3D printing bureau (service provider) who built them.

Fused Deposition Modelling

Machine: Stratasys FMD Dimension SE 1200
 Material: ABS-P430 XL Model, ivory
 Support: SR-30 XL (soluble support)
 Settings: Solid build
 Layer thickness: 0.25mm
 Samples built by: DAB Digital Workshop
 University of Technology Sydney
 702-730 Harris Street
 Ultimo 2007 NSW

Material jetting

Machine: 3D Systems ProJet 3510 SD
Material: VisiJet M3 Crystal (TPGDA)
Support: Wax
Setting: Solid build
Layer thickness: 0.01mm
Samples built by: DAB Digital Workshop
University of Technology Sydney
702-730 Harris Street
Ultimo 2007 NSW

Selective Laser Sintering

Machine: EOS Eosint P 380i
Material: PA 2200, (PA)
Support: N/A
Settings: Laser Spot Diameter: 0.6mm
Layer Thickness: 0.1 mm
Samples built by: Advanced Manufacturing Services
45 Lancaster Street
Ingleburn 2565 NSW

All general post-processing was done by each respective bureau.

4.1.2 Tensile testing

The tensile test is the benchmark test performed on most materials, even though, in many applications, the materials we use are much more likely to be under compressive, impact or flexural loads. As the name suggests, a test sample undergoing a tensile test is to be put under tension, or in other words, pulled apart until it breaks. The two main things we can learn from performing a tensile test on a material are its tensile strength, or toughness to resist being pulled apart, and its modulus of elasticity, or how elastic it is. Product designers will use the tensile data of a material to gauge its comparative strength from one material to another, but will rarely integrate actual data for it into the design of a part. According to Davis (2004), tensile tests are performed for several reasons: the results of tensile tests are used in selecting

materials for engineering applications. Tensile properties are frequently included in material specifications to ensure quality. Tensile properties are often measured during development of new materials and processes, so that different materials and processes can be compared. Finally, tensile properties are often used to predict the behaviour of a material under forms of loading other than uniaxial tension (Davis 2004).

The specimen type is the Type I (ASTM 2013a), the dimensions of which are shown in Figure 4.5. The build orientations of the tensile test specimens for each polymer were selected based on the findings discussed in Section 2.3.4: Discussion of end use products made through 3D printing; they vary between materials (see Figure 4.6 and 4.7). For each build orientation, five test specimens were built.

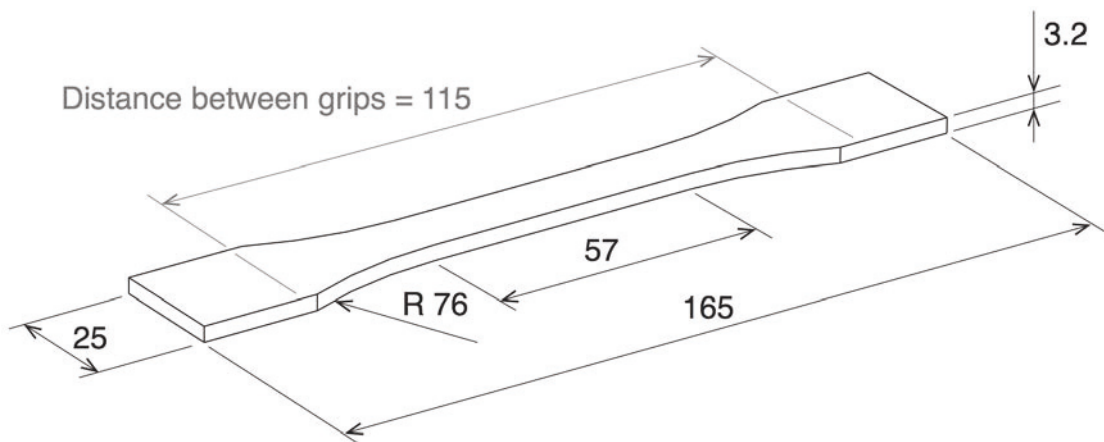


Figure 4.5: Dimensions of tensile test specimens (all dimensions in mm).

The test specimens for FDM in ABS and MJ in TPGDA were built in the four build orientations, as shown in Figure 4.6. For SLS in PA, there were only three orientations needed; see Figure 4.7. The reason that the XYZ (HoE) orientation was excluded for PA was because the work of several scholars reviewed in Chapter 2: Existing knowledge and related literature, showed that there was no

difference in the tensile strength of PA between the XYZ (HF) and XZY (HoE) orientations. Therefore, it was decided to only build test specimens in one of those orientations which was XYZ (HF).

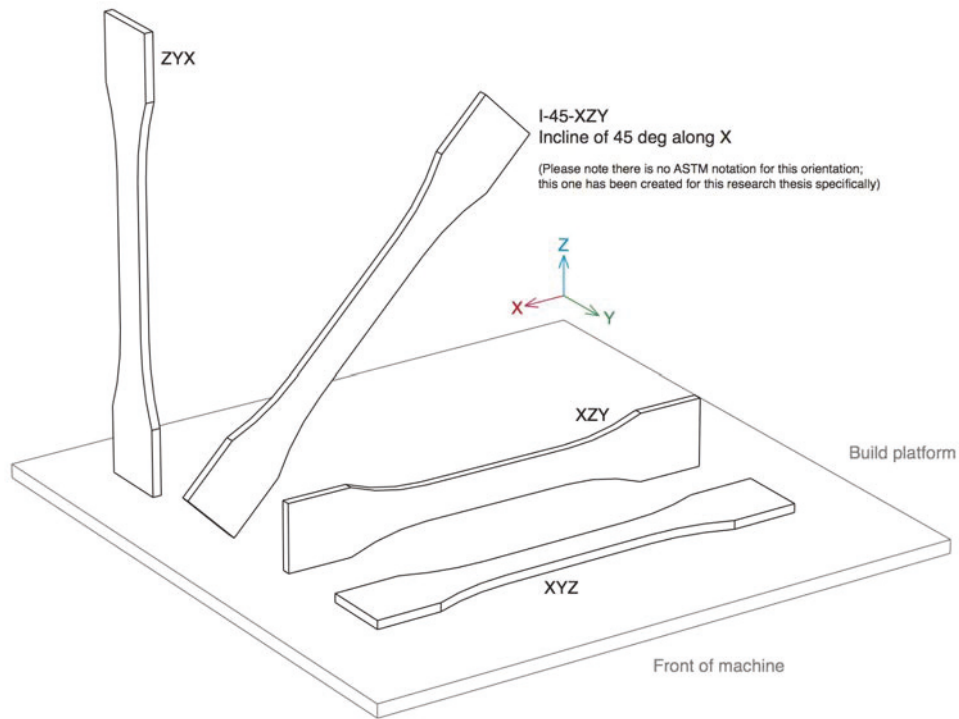


Figure 4.6: Tensile specimen build orientations for ABS and TPGDA.

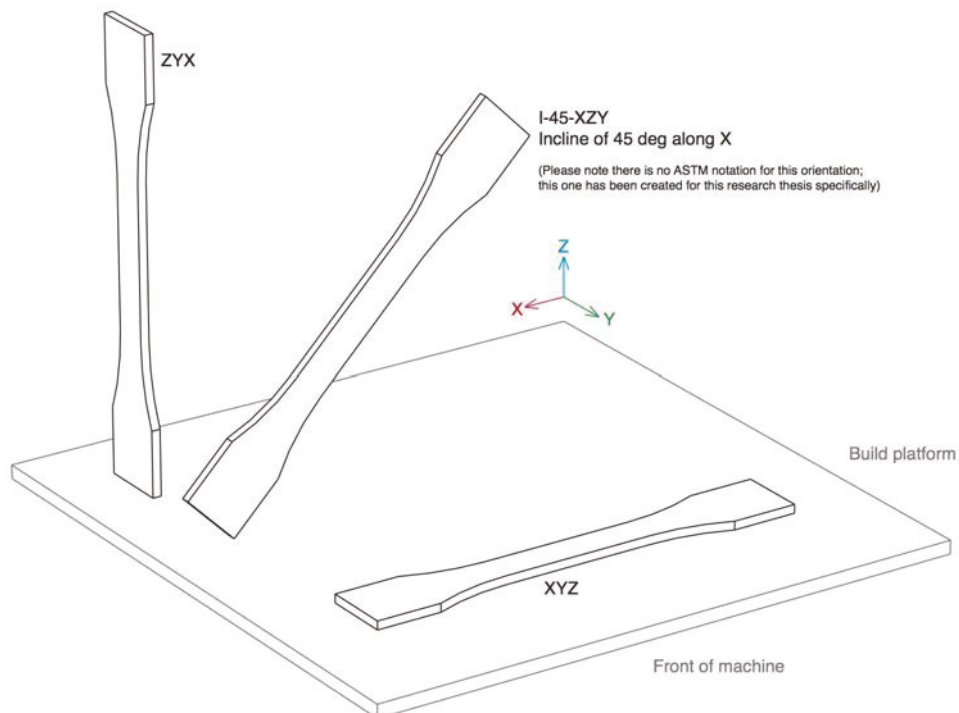


Figure 4.7: Tensile specimen build orientations for SLS in PA.

The tensile tests were conducted in the Faculty of Science at UTS on a Shimadzu ASG-X 10kN Tabletop model machine and a video extensometer TRView X800D with dual camera. The software used was Trapezium X version 1.4.2 and the load cell was certified by Australian Calibration Services (see Appendix C for certificate). The test setup is shown in Figure 4.8.

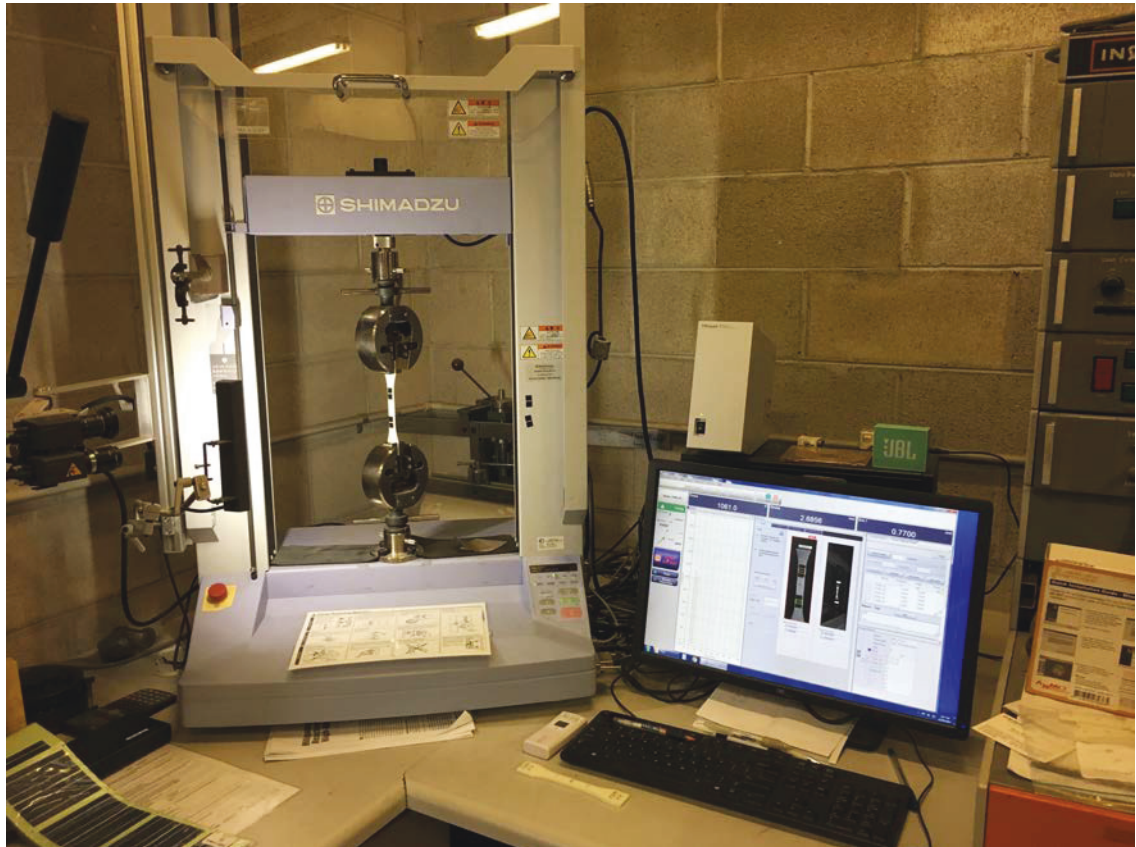


Figure 4.8: Tensile test set up on Shimadzu ASG-X.

Conditioning of specimens prior to test:
48 h at 24 deg C and 51% relative humidity.

Measuring of specimens prior to test:
The width and thickness were measured in the centre of each specimen and within 5mm of each end of the gauge length. All measurements were recorded in writing. See Appendix D for a sample spreadsheet.

Condition of specimens during the test:
24.4 – 25 deg C and 51% relative humidity.

Speed of testing:
3.75 mm/min, to rupture in 0.5 to 5 min

Please note: The speed was set as low as was allowed according to the standard, where the recommended speed is 5 mm +/-25% per min (ASTM 2014). This was done because pre-testing showed the FDM in ABS specimens built in ZYX (Vertical at 90 deg) at 5 mm/min ruptured before 0.5 min. So the speed was lowered to 3.75mm/min which is 25% less than 5 mm/min.

Between all three polymers 55 specimens were tested, not including pre-test specimens.

4.1.3 Izod impact testing (notched)

The impact strength of a material can be understood to be its resistance to being hit or knocked by something else, or being dropped onto a harder surface. As such, it is one of the material properties that are more interesting and relevant to product designers, because many product designers design housings for electrical appliances and tools such as cordless drills. One of the main functions of such a housing is to protect the internal components from damage that may occur due to the product being dropped or hit. Impact strength is also less abstract than tensile strength and can therefore be more easily integrated into the design process and applied to practice. Gerdeen & Rorrer explain that the ability of a polymer to absorb energy under impact is important in design applications, for reasons both obvious (e.g., the design of a plastic composite bumper for an automobile) and not so obvious (e.g., the housing for an electric drill that might be accidentally dropped on the floor) (2012).

For this research, the Izod impact testing was outsourced to LMATS (Laboratories for Materials Advanced Testing Services) Pty Ltd, because UTS does not have the facilities to conduct such tests. The test specimen dimensions are shown in Figure 4.9, and build orientations in Figure 4.10. Because the specimens are square in cross-section, only three build orientations were needed, because at 0 deg the cross sections of HF and HoE are the same.

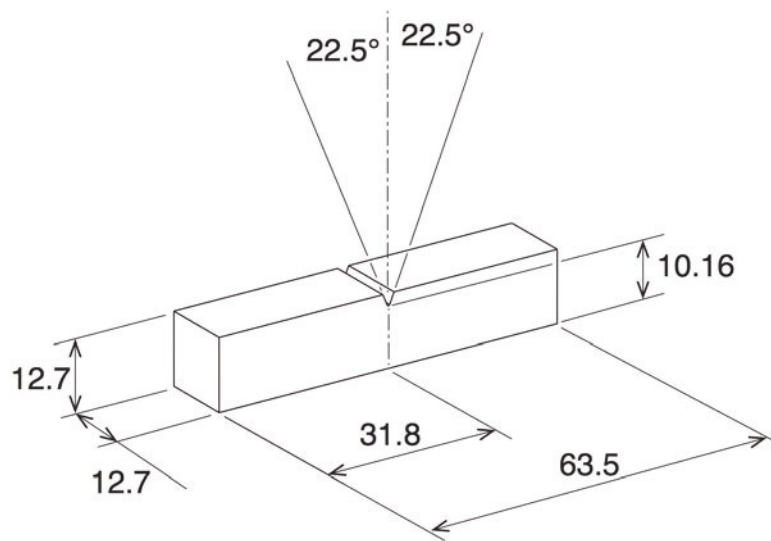


Figure 4.9: Dimensions of Izod test specimens (all dimensions in mm).

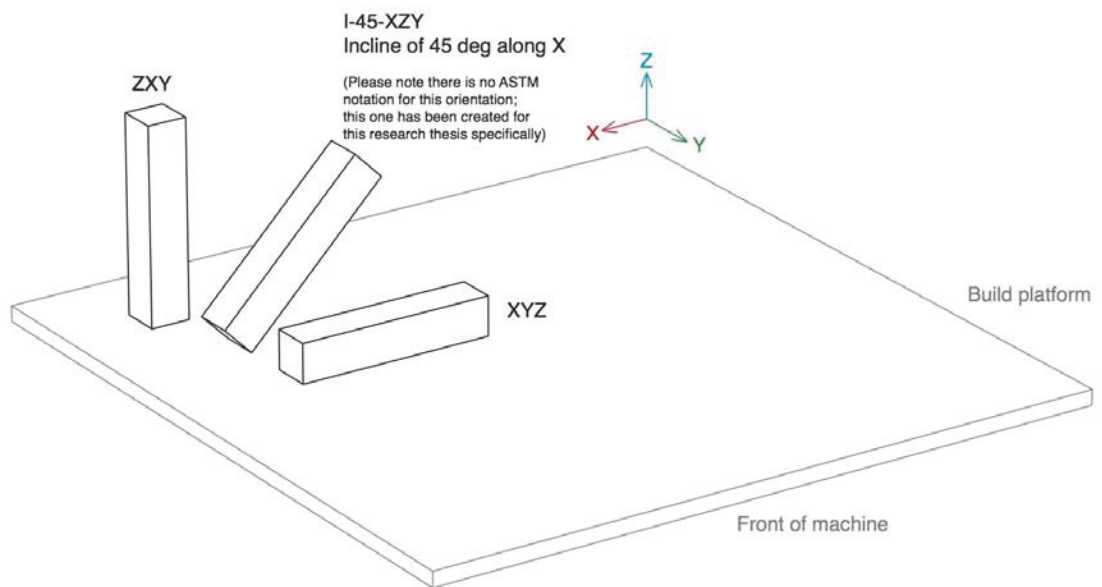


Figure 4.10: Izod specimen build orientations for ABS, TPGDA and PA.

LMATS Pty Ltd conducted the testing in their laboratories in Melbourne according to ASTM D256, using test method A. The test setup is shown in Figure 4.11.



Figure 4.11: Izod test set up at LMATS Pty Ltd.

Preparation of specimens prior to test:

Specimens were notched by LMATS Pty Ltd using the impact specimen notcher (International Equipment's S/N 221).

Conditioning of specimens prior to test:

Following notching the specimens were conditioned for 40 h at 24 deg C and 51% relative humidity.

Between all three polymers 45 specimens were tested.

The complete report compiled by LMATS Pty Ltd can be found in Appendix E.

4.1.4 Flexural or 3-point bend testing

The flexural strength of a material is its resistance to bending. There are two types of properties of a material we can learn about by testing it for flexural strength. The first is the maximum load a material can withstand while still returning to its original state if released; this can also be understood as the point at which it will bounce back. The second is the point at which the material remains permanently deformed. Flexural strength, also known as breaking strength, is the strength determined from the load and the test piece dimensions in a flexural test (Whelan 2012). It is important for product designers to understand how much flexural strength a material has that is being considered for use with products where a part may need to flex and/or bend. Examples of such products are door handles, eyewear, and products that are designed to snap together like Lego, or the caps on pens.

The test specimen dimensions are shown in Figure 4.12. The build orientations of the flexural test specimens for each polymer (see Figure 4.13) were selected based on the findings discussed in Section 2.3.4: Discussion of end use products made through 3D printing. For each build orientation, five test specimens were built.

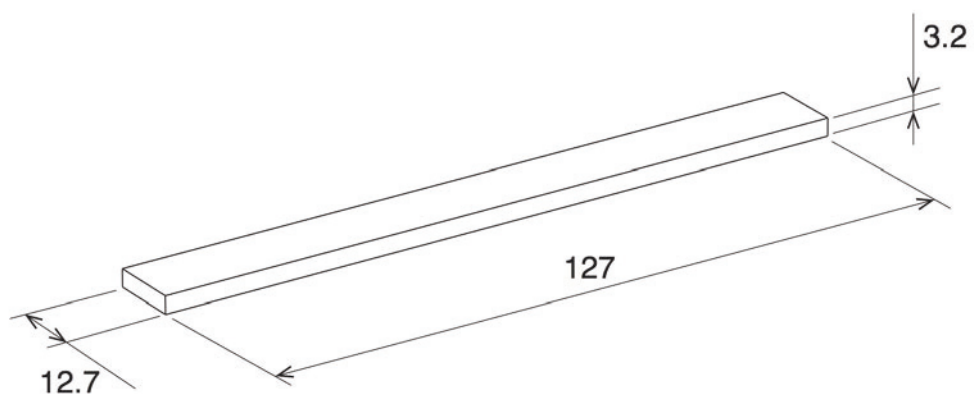


Figure 4.12: Dimensions of flexural test specimens (all dimensions in mm).

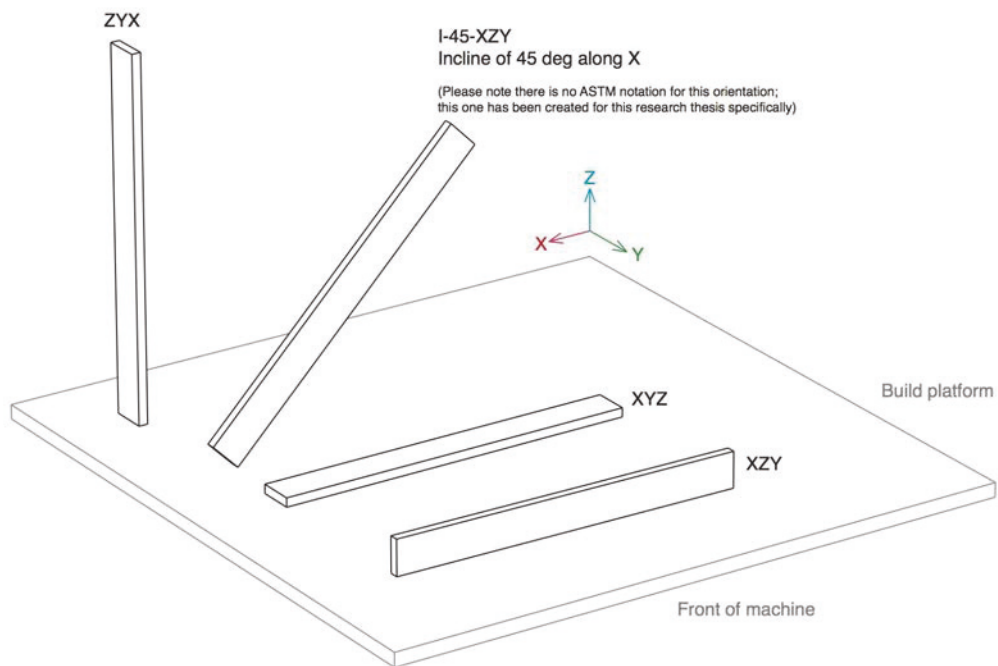


Figure 4.13: Flexural test specimens for ABS, TPGDA and PA.

As with the tensile testing, the flexural tests were conducted in the Faculty of Science at UTS, on a Shimadzu ASG-X 500N Tabletop, and the software used was Trapezium X Lite. Test method A was used and the test setup is shown in Figure 4.14.

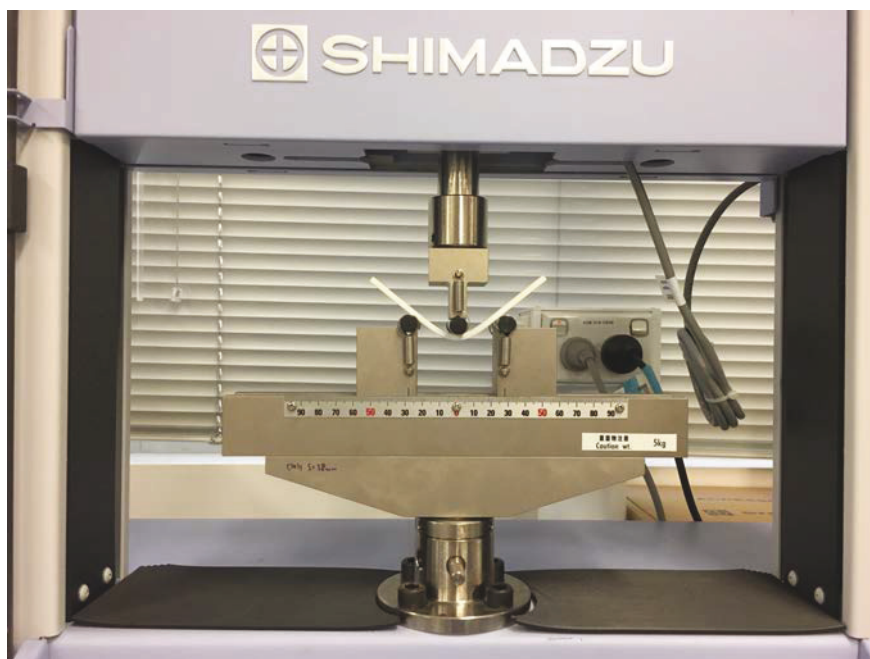


Figure 4.14: Flexural test setup on Shimadzu ASG-X.

Conditioning of specimens prior to test:

The specimens were conditioned for 48 h at 22.7 deg C and 69% relative humidity.

Measuring of specimens prior to test:

The width and thickness were measured at the centre of each specimen and at both points of the support span width (28mm from the centre), and recorded in writing.

A sample spreadsheet can be found in Appendix F.

Condition of specimens during the test:

22.7 – 25 deg C and 69% relative humidity.

Speed of crosshead motion:

1.5 mm/min

Depth of sample:

16 : 1

Span width:

56mm

Between all three polymers 60 specimens were tested.

The test results can be found in Section 5.1: Mechanical property test results of the three 3D printed polymers.

4.2 Experiment to determine clear visual representation of the surface of a 3D printed part prior to building

This section determines which software tool provides the clearest representation of the surface of a 3D printed part prior to the same part being built, in order to answer research question 2 (see Section 3.1: Research questions). As was discussed in Sections 2.5: Interacting with products, and 2.5.1: Discussion of interacting with products, the texture and appearance of the surface on a handheld product are important design considerations. Therefore, it would be an advantage to have tools that enable designers to visually represent what the surface may look like based on a chosen build

orientation and layer height. As the reviewed literature showed (see Section: 2.6: Discussion of existing knowledge and related literature), no tools are being developed or investigated that may enable designers to do this. However, there are software applications, referred to as 'slicing' software, that are specifically designed for 3D printing and sit between the 3D CAD software, where the digital file of the part is created, and the 3D printing machine that builds the physical part. They are referred to as slicing software because they slice a 3D CAD model into virtual horizontal layers and generate a toolpath for the 3D printing machines' toolhead to follow (more will be said about this below). Once a given part has been sliced, the software generates a 3D preview of the part to show how the material would be laid down during building. Slicing software is predominantly used to prepare parts to be built using FDM; however, the layer height or thickness of slices can be adjusted to any dimension. The useful element of slicing software for this research is that the 3D preview it generates provides designers with a visual representation of what the part will look like after it has been built. So once the part is in the desired orientation and the layer height has been set to suit any one of the three processes, for example 0.254mm for FDM, 0.1mm for SLS or 0.05mm for MJ, slicing software will generate a preview accordingly. At this point, it is important to note that none of the major 3D CAD applications, such as Solidworks or Rhinoceros CAD, are able to generate a preview of a part based on layer height and part orientation in their native environment. This is mainly because CAD software has been developed for the design of parts for many different methods of manufacture. However, in recent years, 3D printing technology has been advancing faster than 3D CAD software developers can keep up with; therefore, there is a lag in developing additional functionalities that may serve 3D printing technologies. As a result, the manufacturers of 3D printing hardware have stepped in and developed their own software applications. Below is a recap of the eight steps needed to create a 3D printed part, according to Gibson, Rosen and Stucker (2010):

- Step 1, CAD. All 3D printed parts must start from a virtual 3D software model that fully describes the external geometry.
- Step 2, Conversion to STL. The CAD file is converted to STL (Standard Triangulation Language), which is the file format accepted by nearly

every 3D printing machine. This file forms the external closed surfaces of the original CAD model and forms the basis for calculation of the slices.

- Step 3, Transfer to 3D printing machine and STL file manipulation. The STL file must be transferred to the 3D printing machine. Here there may be some general manipulation of the file so that it is the correct size, position and orientation for building.
- Step 4, Machine set up. The 3D printing machine must be properly set up prior to the build process. Such settings would relate to build parameters such as the material constraints, energy source, layer thickness, timing etc.
- Step 5, Build. Building of the part is mainly an automated process and the machine can largely carry on without supervision. Only superficial monitoring of the machine needs to take place at this time, to ensure no errors have taken place, such as running out of material, power or software glitches, etc.
- Step 6, Removal. Once the build is completed, the parts must be removed.
- Step 7, Postprocessing. Once removed from the machine, parts may require additional cleaning up before they are ready for use (see also Section 2.1.2).
- Step 8, Application. Parts are now ready to be used (2010).

The slicing software typically covers steps 3 and 4; what it does is slice the STL file into horizontal layers based on the specified layer thickness, and then generate a toolpath for each layer. A toolpath is the path the extrusion head (for FDM), the laser (for SLS), or the printhead (for MJ), follows to fill in each layer. The best way to think of slicing software is as a print dialogue interface, much like the ones used for print previews of 2D printing on paper. Many suppliers of 3D printing machines provide their own version of slicing software, such as Catalyst by Stratasys. For this project, six software applications were chosen through consultation with 3D printing experts within the University of Technology Sydney, from the Faculty of Design Architecture & Building (DAB) and the Faculty of Engineering & Information Technology (FEIT). The professions those experts are engaged in range from technical personnel

managing and operating 3D printing facilities within the university, to academics specialising in 3D printing.

Based on their recommendations, the following six 3D printing slicing software applications were selected:

1. CatalystEx V3.5 (by Stratasys, only available with the purchase of Stratasys machine)
2. Cura V3.0.4 (for Ultimaker, free, open source)
3. Cubicreator3 V3.6 (by Cubicon, only available with the purchase of a Cubison machine)
4. Simplify3D V4.0.1 (cost AU\$195)
5. Slic3r V1.2.9 (by Slic3r, free)
6. Slicer for Fusion 360 V1.0.0 (by Autodesk, free).

To be able to ascertain which one of the six applications would provide the best virtual representation of a real part, it was necessary to compare them with a real part that had been made using a 3D printing process. To facilitate this, a part was built from ABS on an FDM machine, with a 0.254mm step height. The part is a handheld, three-pronged turning handle (see Figure 4.15); its dimensions are 78mm (width) x 71mm (length) x 50.5mm (height), and it is a part of a compost aerator, which is a real product.



Figure 4.15: Image of the real turning handle.

This particular part was chosen because it belongs to a handheld device and has several rounded surfaces, which made the build steps more recognisable. After the part had been built and post-processed, which in this case meant removing the support material, it was placed in the specific orientation and photographed; see Figure 4.15. The original CAD file of the part was then imported into each of the six slicing software applications, and the part's layer height and build orientation were matched to that of the photograph of the real part. Figures 4.16 to 4.21 show screen shots of the part in each of the six software applications.



Figure 4.16: Software: Slicer (for Fusion 360 V1.0.0 by Autodesk).

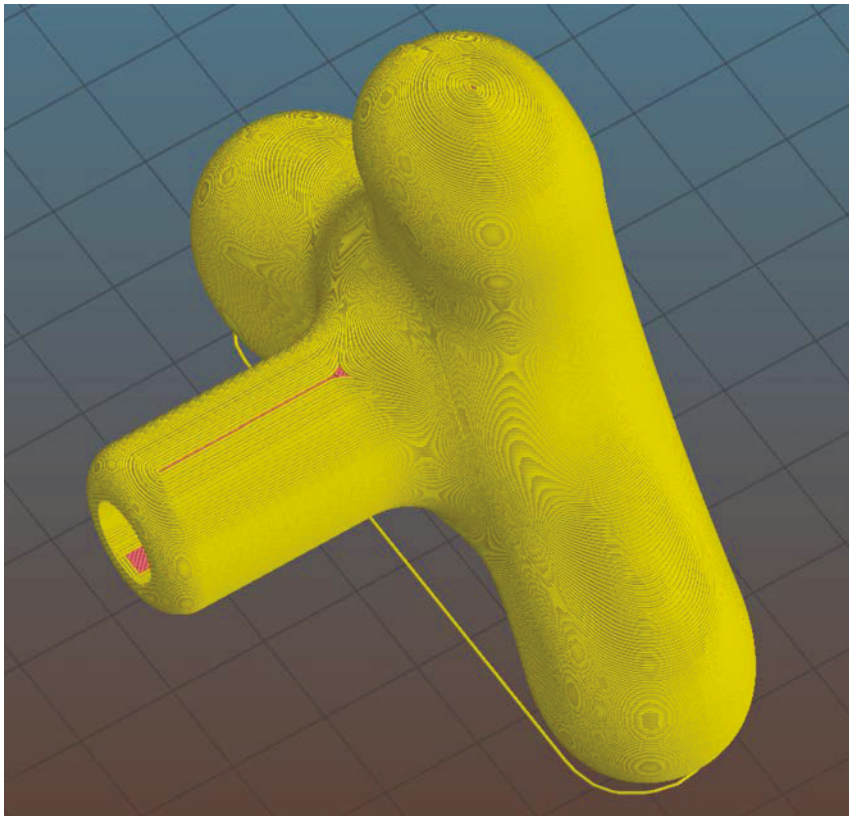


Figure 4.17: Software: Slic3r V1.2.9.



Figure 4.18: Software: Simplify3D V4.0.1.

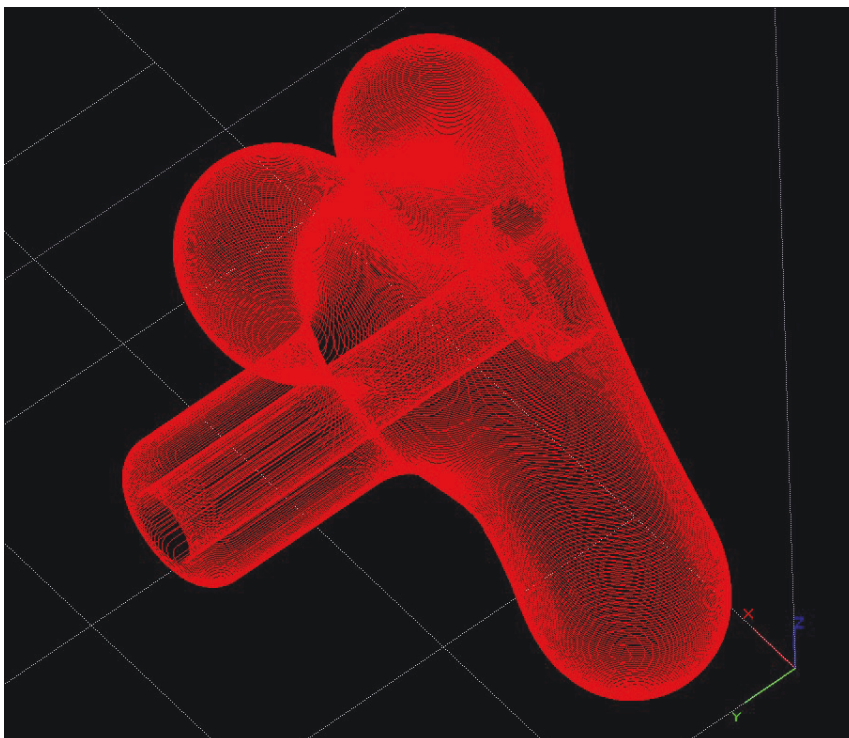


Figure 4.19: Software: CatalystEx V3.5 (by Stratasys).

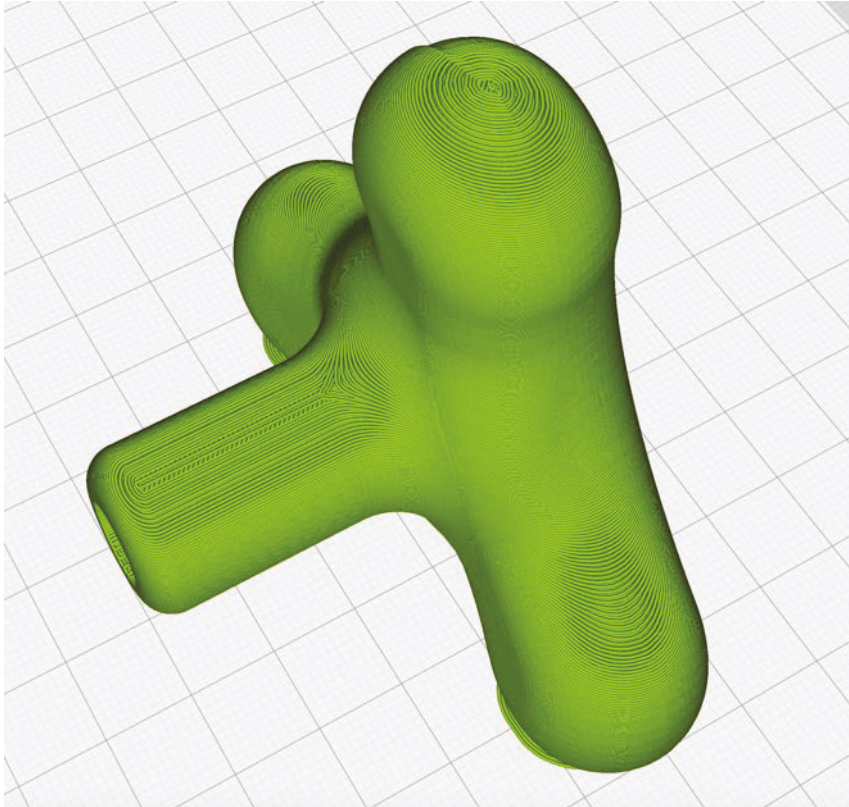


Figure 4.20: Software: Cura V3.0.4 (for Ultimaker).

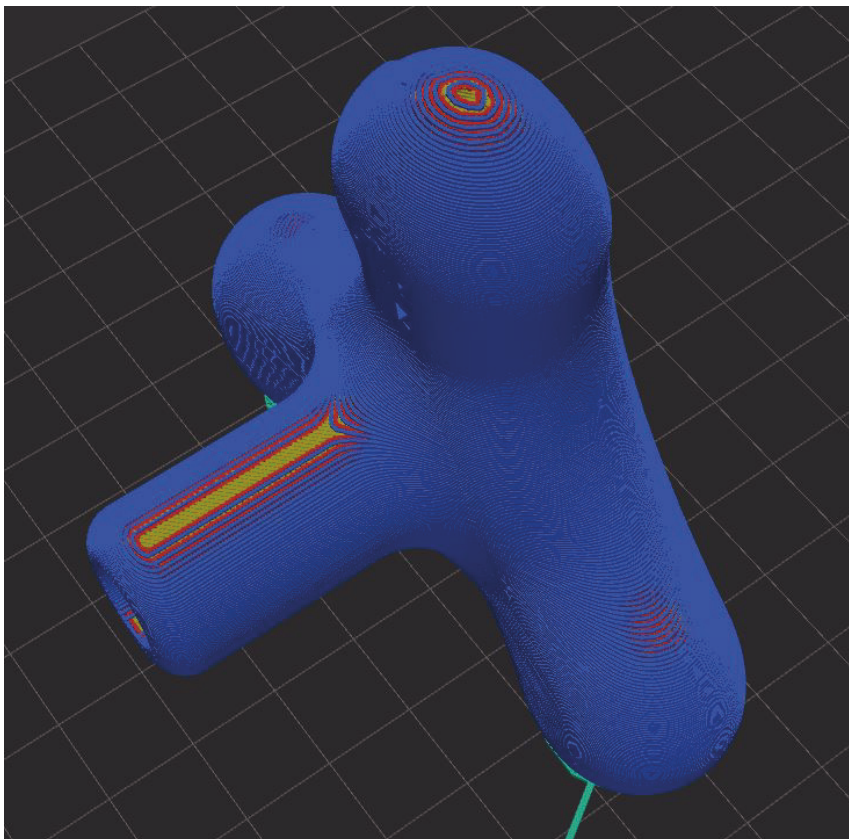


Figure 4.21: Software: Cubicreator3 V3.6 (by Cubicon).

The colour of the part and background in those six images are the default settings for each software application. We attempted to make them uniform across all six applications, but this proved challenging, because in some cases the colours could not be matched, and for this reason, all parameters were left in the default settings. An online survey using the seven images was then created using the online survey tool, Survey Legend. On the survey page (see Figure 23) the first image was that of the real part and the six images below it were images of the virtual representations as displayed in the slicing software applications. The people participating in the survey were then asked to compare the image of the real part with the six images of the virtual parts, and decide which one of the six matched the image of the real part the best.

The question participants were asked was: “Which one of images A to F is the clearest representation of the surface on the object shown in the main photo directly below?”. Each of the six images had a specific letter, A to F, attached to it, but the sequence in which the images were displayed was randomised every time a new survey was opened (see Figure 4.22). This ensured that there was no preference given to which of the images A to F would be seen first. 75 participants were invited to take part in the survey via email. All 75 participants were known to the author through his professional network in industrial and product design. The results are anonymous, in that it is not known which participant chose which image. Because this research method involved people, ethical clearance from the Human Research Ethics Committee (HREC) at UTS was sought. Because the survey was to be conducted anonymously, the advice was that there was nil to negligible risk to anyone participating in it. This meant that it was sufficient to lodge a Nil/Negligible Risk Declaration through the Research Manager in our faculty, which was accepted and filed under the code ETH17-2075 (see Appendix G for approved human ethics application). As mentioned earlier, participants were invited to participate through an email which contained a link to the survey welcome page (see Figure 4.22).

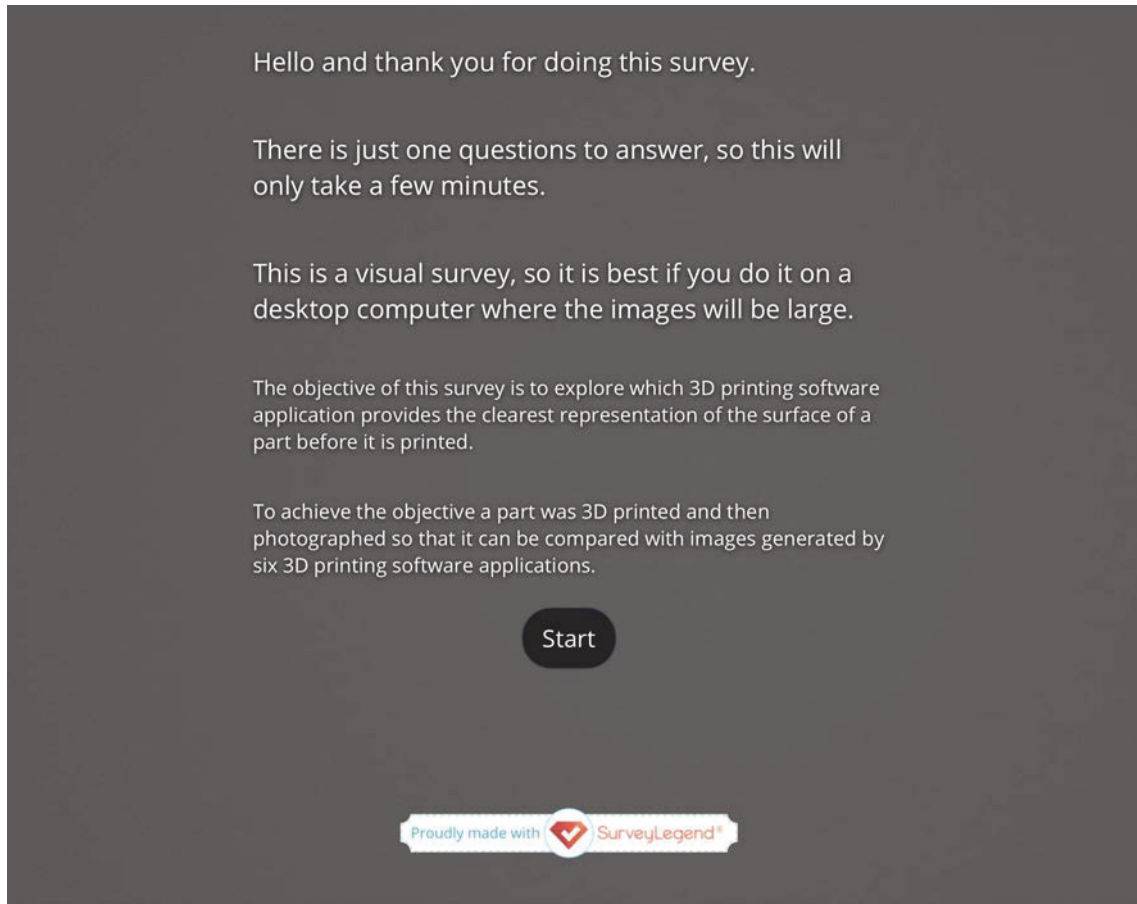


Figure 4.22: Survey Welcome page.

If a participant decided to participate and clicked on the Start button, the main survey page opened (see Figure 4.23) and the survey could be conducted by comparing the main image at the top to the six below it. Each of the six images could be enlarged by clicking on the magnifying glass “+” icon in the top right-hand corner of each image.



Figure 4.23: Main survey page.

The chosen image was selected by clicking on it and the result was recorded by clicking the Submit button, which took participants to the Thank you page (see Figure 4.24).

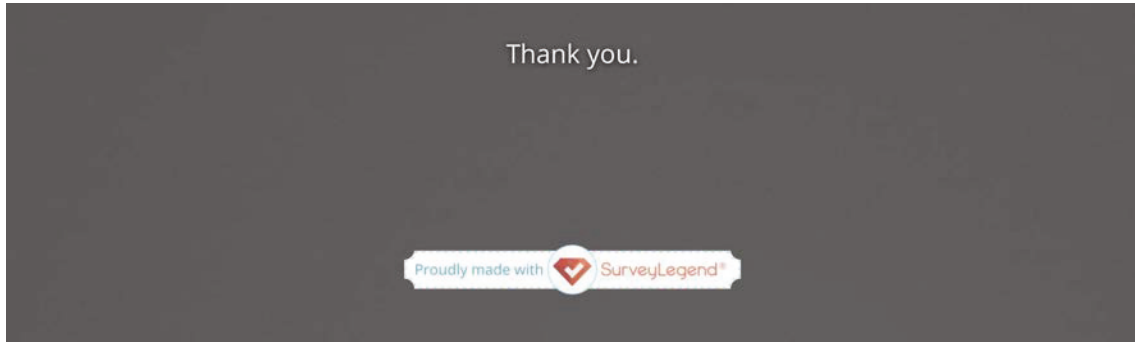


Figure 4.24: Survey thank you page.

Please refer to Section 5.2: Results for a clear visual surface representation, to see the test results.

Chapter 5. Results

This chapter presents the results in their basic form as they were generated from the experiments. The results are presented in this way so that others who may want to use them for their own research or compare them to the results generated through their own studies can do so.

5.1 Mechanical property test results of the three 3D printed polymers

The test results listed in Sections 5.1.1, 5.1.2, and 5.1.3 are reported in accordance with the testing standards relevant to each test method, which are:

- ASTM D638 – 14
Standard Test Method for Tensile Properties of Plastics (ASTM 2014)
- ASTM D256 – 10
Standard Test Methods for Determining the Izod Pendulum Impact Resistance of Plastics (ASTM 2010)
- ASTM D790 – 15
Standard Test Methods for Flexural Properties of Unreinforced and Reinforced Plastics and Electrical Insulating Materials (ASTM 2015a).

The results were generated by first importing the raw test data as generated by the Trapezium X software (an example of how Trapezium X outputs the data is shown in Figure 5.1) into Excel spreadsheets, and then calculating them using the formulae specified in each of the standards (see Figure 5.2 to see how the data was presented in Excel after calculation). Trapezium X is the software used in combination with the Shimadzu testing machine. An individual spreadsheet was created for each test and build orientation.

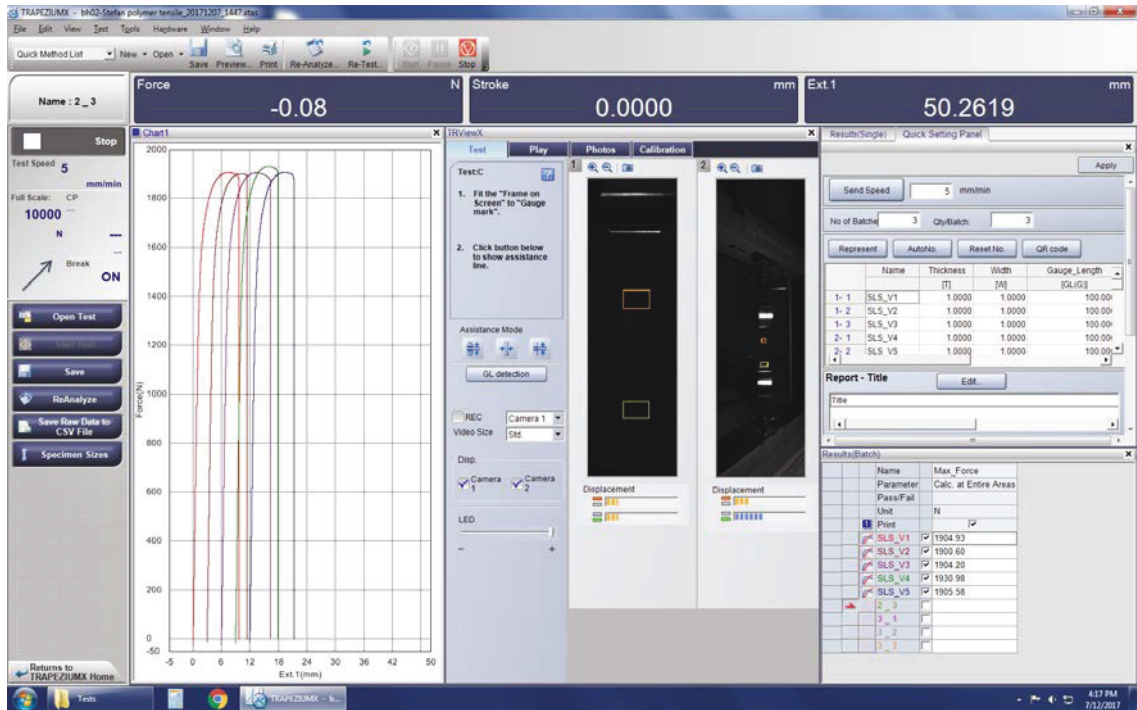


Figure 5.1: Raw data of test on SLS in V as output by Trapezium X.

Sample	GL	area, mm	max load, N	ext at max load, mm	max strength, Mpa	load at fracture, N	ext at fracture, mm	fracture strength, MPa	E, GPa
SLS V1	50.3	41.79	1929.967	7.516	46.182	1896.085	9.613	45.372	1.477
SLS V2	50.4	41.39	1913.559	7.115	46.232	1894.412	8.434	45.770	1.593
SLS V3	50.6	41.85	1927.346	7.283	46.054	1874.004	10.384	44.779	1.549
SLS V4	50	41.84	1950.526	7.053	46.619	1896.305	8.896	45.323	1.574
SLS V5	50	41.61	1920.743	7.389	46.161	1879.878	9.263	45.179	1.561
Mean			1928.43	7.27	46.25	1888.14	9.32	45.28	1.55

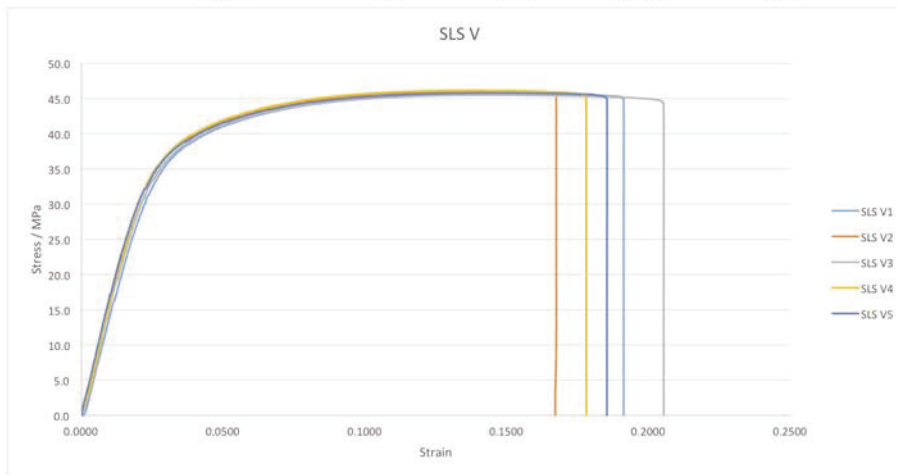


Figure 5.2: Calculated data for SLS in V as presented in Excel.

5.1.1 Results for tensile testing

For each of the three polymers, there are three tables. Tables 5.1, 5.4 and 5.7 list the test results for ABS, TPGDA and PA respectively for max. load in N,

extension at max. load in mm, and max. strength in MPa. Tables 5.2, 5.5 and 5.8 list the test results for ABS, TPGDA and PA respectively for load at fracture in N, extension at fracture in mm, and fracture strength in MPa. Tables 5.3, 5.6 and 5.9 list the test results for ABS, TPGDA and PA respectively for Young's modulus in GPa. Each result listed is the mean of five specimens tested in every single orientation.

Table 5.1:
ABS results for max. load, extension at max. load and max. strength

Orientation	Max. load N	Extension at max. load mm	Max. strength MPa
HF (XYZ)	1106.21	1	26.68
HoE (XZY)	1313.9	0.92	30.04
I 45 (I-45-XZY)	1168.78	0.95	27.3
V (ZXY)	1061.5	0.88	24.91

Table 5.2:
ABS results for load at fracture, extension at fracture and fracture strength

Orientation	Load at fracture N	Extension at fracture mm	Fracture strength MPa
HF (XYZ)	1037.58	3.13	24.99
HoE (XZY)	1144.37	5.42	26.16
I 45 (I-45-XZY)	1098.94	1.68	25.67
V (ZXY)	1043.32	1.03	24.48

Table 5.3:
ABS results for Young's modulus

Orientation	Young's GPa
HF (XYZ)	1.91
HoE (XZY)	2.02
I 45 (I-45-XZY)	1.99
V (ZXY)	1.89

Table 5.4:

TPGDA results for max. load, extension at max. load and max. strength

Orientation	Max. load N	Extension at max. load mm	Max. strength MPa
HF (XYZ)	1255	2.91	29.82
HoE (XZY)	944.29	3.1	22.35
I 45 (I-45-XZY)	866.23	1.78	20.33
V (ZXY)	1059.6	1.87	24.42

Table 5.5:

TPGDA results for load at fracture, extension at fracture and fracture strength

Orientation	Load at fracture N	Extension at fracture mm	Fracture strength MPa
HF (XYZ)	1254.25	2.98	29.8
HoE (XZY)	942.88	2.67	22.32
I 45 (I-45-XZY)	865.1	1.78	20.30
V (ZXY)	1058.79	1.87	24.4

Table 5.6:

TPGDA results for Young's modulus

Orientation	Young's GPa
HF (XYZ)	1.26
HoE (XZY)	0.88
I 45 (I-45-XZY)	0.86
V (ZXY)	1.07

Table 5.7:

PA results for max. load, extension at max. load and max. strength

Orientation	Max. load N	Extension at max. load mm	Max. strength MPa
HF (XYZ)	2153.58	7.1	46.9
I 45 (I-45-XZY)	1928.9	7.31	46.3
V (ZXY)	1928.43	7.27	46.25

Table 5.8:

PA results for Load at fracture, Extension at fracture and Fracture strength

Orientation	Load at fracture N	Extension at fracture mm	Fracture strength MPa
HF (XYZ)	1961.23	12.24	42.71
I 45 (I-45-XZY)	1891.36	9.34	45.4
V (ZXY)	1888.14	9.32	45.28

Table 5.9:

PA results for Young's modulus

Orientation	Young's GPa
HF (XYZ)	1.54
I 45 (I-45-XZY)	1.52
V (ZXY)	1.55

5.1.2 Results for Izod impact testing

For each of the three polymers, there is one table. Tables 5.10, 5.11, and 5.12 list the test results listed for ABS,TPGDA and PA respectively for Izod impact (notched) in J/m. Each result listed is the mean of 5 specimens tested in every single orientation.

Table 5.10:

ABS results for Izod impact (notched) testing

Orientation	Impact J/m
HF/HoE (XYZ/XZY)	89.2
I 45 (I-45-XZY)	63.7
V (ZXY)	32.3

Table 5.11:

TPGDA results for Izod impact (notched) testing

Orientation	Impact J/m
HF/HoE (XYZ/XZY)	11.5
I 45 (I-45-XZY)	12.1
V (ZXY)	10.2

Table 5.12:

PA results for Izod impact (notched) testing

Orientation	Impact J/m
HF/HoE (XYZ/XZY)	52.9
I 45 (I-45-XZY)	49.2
V (ZXY)	47.9

5.1.3 Results for flexural or 3-point bend testing

For each of three polymers there is one table. Tables 5.13, 5.14, and 5.15 list the test results listed for ABS, TPGDA and PA respectively for max. load in N, stroke at max. load in mm, and flexural stress in MPa. Each result listed is the mean of five specimens tested in every single orientation.

Table 5.13:

ABS results for max. load, stroke at max. load and flexural stress

Orientation	Max. Load N	Stroke at max. load mm	Flexural stress MPa
HF (XYZ)	93.89	7.65	49.89
HoE (XZY)	88.47	7.94	56.27
I 45 (I-45-XZY)	82.6	7.04	48.17
V (ZXY)	50.98	3.44	29.06

Table 5.14:

TPGDA results for max. load, stroke at max. load and flexural stress

Orientation	Max. Load N	Stroke at max. load mm	Flexural stress MPa
HF (XYZ)	68.78	9.91	41.92
HoE (XZY)	45.95	11.36	30.27
I 45 (I-45-XZY)	44.57	8.04	27.53
V (ZXY)	53.75	7.13	32.83

Table 5.15:

PA results for max. load, stroke at max. load and flexural stress

Orientation	Max. Load N	Stroke at max. load mm	Flexural stress MPa
HF (XYZ)	97.09	12.25	53.87
HoE (XZY)	96.47	12.11	57.77
I 45 (I-45-XZY)	79.37	12.7	48.8
V (ZXY)	77.54	12.34	48.54

5.2 Results for a clear visual surface representation

Out of the 75 participants invited, 48 completed the online survey. The breakdown of the results can be seen in Table 5.16 below.

Table 5.16:

Breakdown of the results from the online survey

Software	Votes	%	Rank
A (Cura V3.0.4)	21	43%	1
B (Cubicreator3 V3.6)	3	6%	4
C (Slicer, Autodesk)	6	12%	3
D (Simplify3D V4.0.1)	14	29%	2
E (Slic3r V1.2.9)	1	2%	5
F (CatalystEx V3.5)	3	6%	4

The following figures show how the survey software communicated: the number of participants' preference for a particular representation as well as percentage (Figure 5.3); how many of the 73 participants completed and submitted it (Figure 5.4); and a sample of time spent on the page by one participant (Figure 5.5).

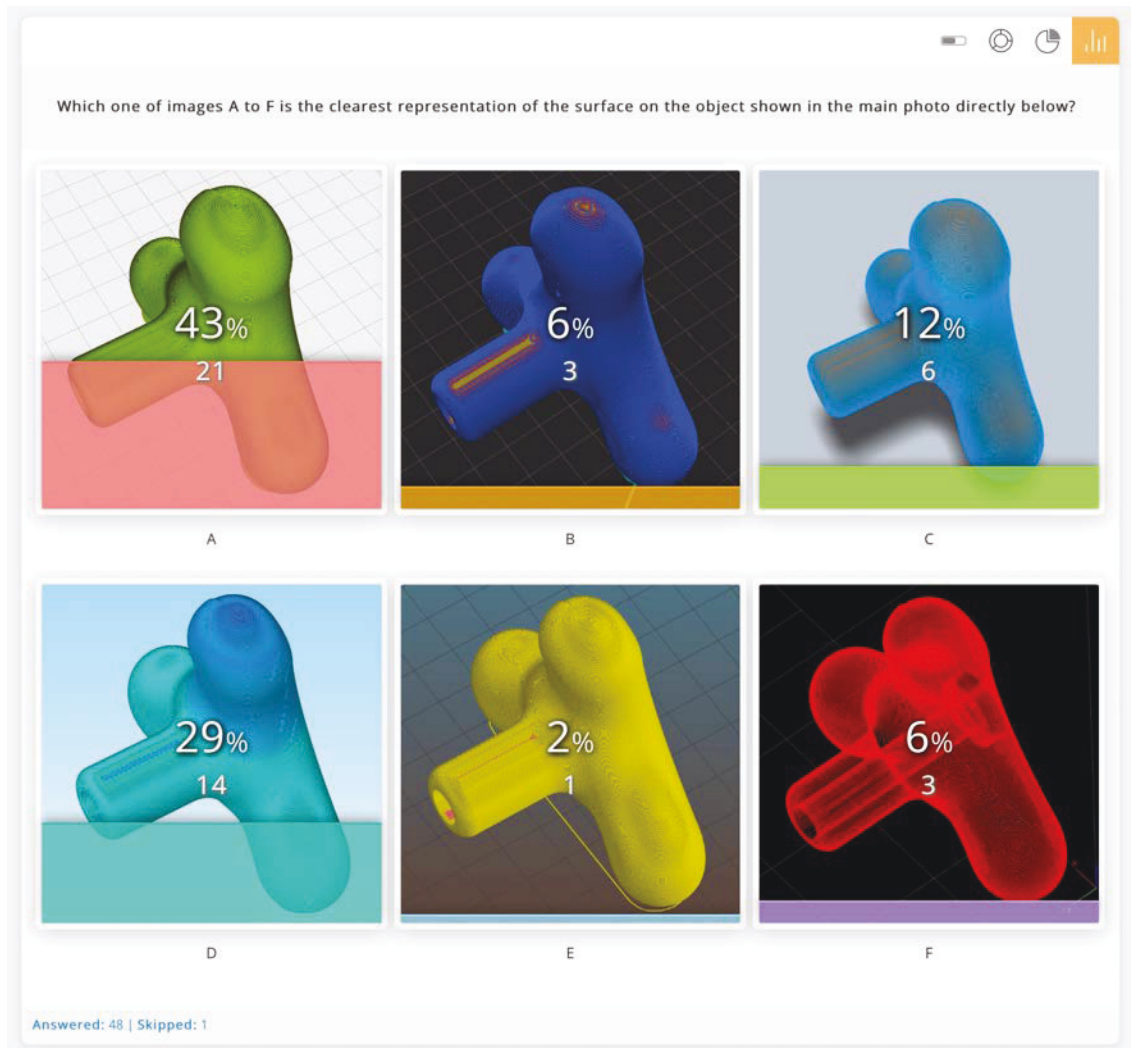


Figure 5.3: Results of survey in terms of preference and percentage.

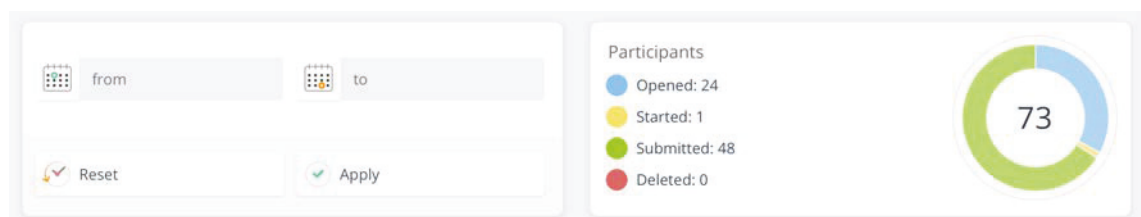


Figure 5.4: Number of participants who completed and submitted the survey.

Metrics Progress Manage

Opened 2018-01-07 07:53:50 Time Spent 00:02:02


Started 2018-01-07 07:53:52 Answered 1 / 1

Submitted 2018-01-07 07:55:54

Responses Responded questions

*
Which one of images A to F is the clearest representation of the surface on the object shown in the main photo directly below?

Please scroll down, choose an image by clicking on it and then clicking Submit.
You can enlarge images A to F by clicking on the magnifier in the top right corner of each image. The colours of the generated images are the default colours assigned by each software application.



A

Figure 5.5: Sample of individual response Progress (time spent on survey).

Chapter 6. Analysis and communication of results

In this chapter, the results are analysed and reported to answer the research questions. Section 6.1 responds to research question 1a; Section 6.2 to research question 1b; and Section 6.3 to research question 2.

On its own, data is simply data, with limited scope for practical application to the design process and project work. The data in the previous chapter was generated to answer the research questions, but it needs to be analysed and communicated so it can be applied efficiently to the product design process. The experiments that provided the data on the variations in strength between the build orientations as well as the different kinds of polymers is interesting and valuable, but is it abstract if represented solely as a list of numbers. Throughout this thesis, attention has been drawn to the fact that material testing data presented in lists in engineering and science literature is challenging for non-engineers and non-scientists such as product designers to interpret and apply to practice. A new approach tailored to the needs of product designers is required. To facilitate the interpretation of the data for this research, it has been represented visually, which makes it easier to understand and apply to practice. This was done through radar charts by layering the various material properties, specific to the research questions, over each other (see Figure 6.1). This clearly communicates how one set of data compares to another, or one strength compares to another in terms of magnitude. The radar charts are an effective way to compare several quantitative variables with one another. They are easy to read and understand and their use is widespread.

6.1 Analysis of the results in response to research question 1a

Reiterating the research question:

- 1a. For each of the 3D printed polymers ABS, TPGDA and PA:
How do the tensile, flexural and impact properties vary between test samples built in HF (Horizontal Flat), HoE (Horizontal on Edge), V (Vertical) and I 45 (Incline at 45 degrees) orientations?

To facilitate the comparison from one build orientation to another, the results are presented in two forms for each polymer. First, each polymer is

represented graphically in radar charts. See Figure 6.1 for the ABS build orientation chart, Figure 6.2 for the TPGDA build orientation chart, and Figure 6.3 for the PA build orientation chart. In each chart, all four build orientations and three mechanical properties are overlaid to show their magnitude and variation. This helps to provide a clear and general overview of each polymer. The results are also presented in tables: three tables per polymer, one for each mechanical property. In each of these tables, every build orientation is compared to all others and evaluated based on percentage. This helps to understand exactly by how many percent one build orientation varies from another. Tables 6.1, 6.2 and 6.3 show the percentage variations of the mechanical properties of ABS; Tables 6.4, 6.5, and 6.6 show these for TPGDA; and Tables 6.7, 6.8, and 6.9 show the percentage variations for PA.

6.1.1 Variations of ABS properties based on build orientation

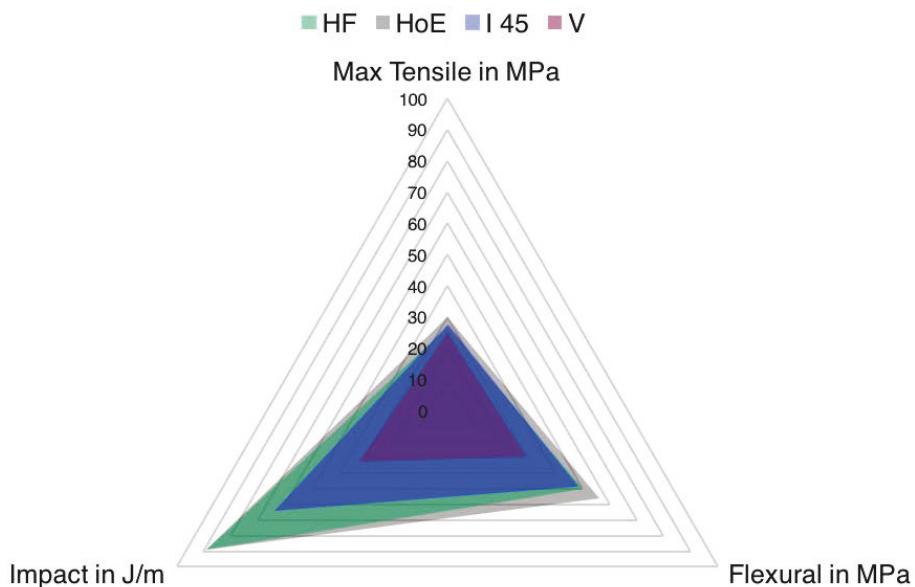


Figure 6.1: ABS build orientation chart.

The ABS build orientation chart shown in Figure 6.1 illustrates that the build orientation has the smallest effect on maximum tensile strength but a considerable effect on flexural strength and in particular on impact strength. Therefore, if a part needs to have some degree of flexibility and or impact resistance it is beneficial to pay attention to how the part is oriented.

Table 6.1:

ABS build orientation variations of max. tensile strength

Orientation	HF	HoE	I 45	V
HF		11.8% < HoE	2.3% < I 45	6.6% > V
HoE	11.8% > HF		9.1% > I 45	17% > V
I 45	2.3% > HF	9.1% < HoE		8.8% > V
V	6.6% < HF	17% < HoE	8.8% < I 45	

Table 6.2:

ABS build orientation variations of impact strength

Orientation	HF/HoE	I 45	V
HF/HoE		28.6% > I 45	63.8% > Vert.
I 45	28.6% < HF		49.3% > Vert.
V	63.8% < HF	49.3% < I 45	

Table 6.3:

ABS build orientation variations of max. flexural strength

Orientation	HF	HoE	I 45	V
HF		11.3% < HoE	3.4% > I 45	41.8% > Vert.
HoE	11.3% > HF		14.4% > I 45	48.4% > Vert.
I 45	3.4% < HF	14.4% < HoE		39.7% > Vert.
V	41.8% < HF	48.4% > HoE	39.7% < I 45	

6.1.2 Variations of TPGDA properties based on build orientation

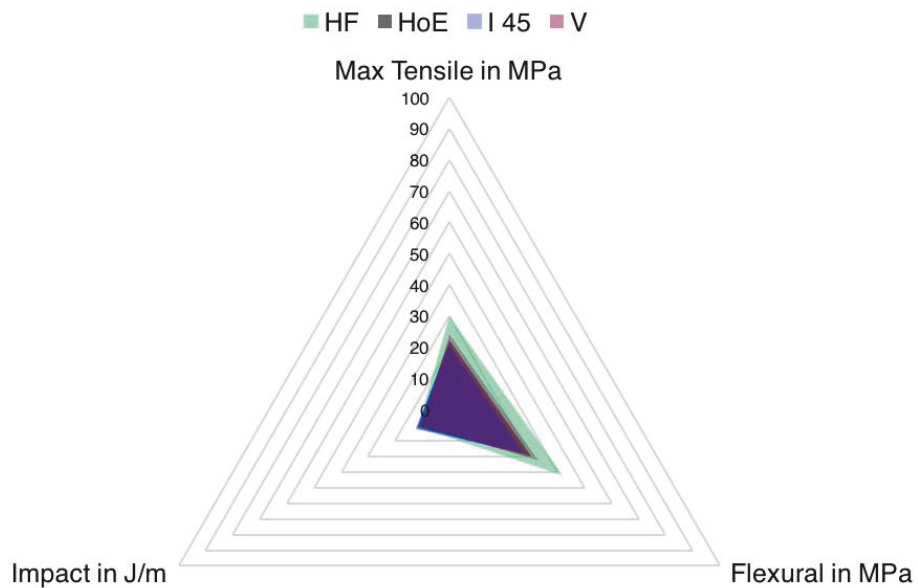


Figure 6.2: TPGDA build orientation chart.

Table 6.4:

TPGDA, build orientation variations of max. tensile strength

Orientation	HF	HoE	I 45	V
HF		25% > HoE	31.8% > I 45	18.1% > Vert.
HoE	25% < HF		9% > I 45	8.5% < Vert.
I 45	31.8% < HF	9% < HoE		16.7% < Vert.
V	18.1% < HF	8.5% > HoE	16.7% > I 45	

Table 6.5:

TPGDA build orientation variations of impact strength

Orientation	HF/HoE	I 45	V
HF/HoE		5% < I 45	11.3% > Vert.
I 45	5% > HF		15.7% > Vert.
V	11.3% < HF	15.7% < I 45	

Table 6.6:

TPGDA build orientation variations of max. flexural strength

Orientation	HF	HoE	I 45	V
HF		27.8% > HoE	34.3% > I 45	21.7% > Vert.
HoE	27.8% < HF		9% > I 45	7.8% < Vert.
I 45	34.3% < HF	9% < HoE		16.1% > Vert.
V	21.7% < HF	7.8% < HoE	16.1% > I 45	

6.1.3 Variations of PA properties based on build orientation

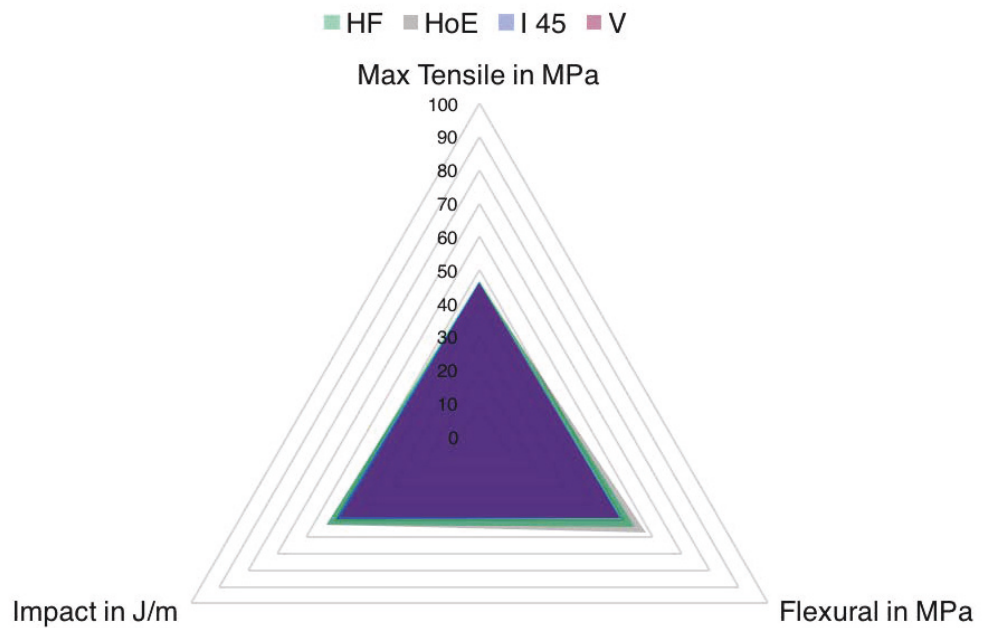


Figure 6.3: PA build orientation chart.

Table 6.7:

PA build orientation variations of max. tensile strength

Orientation	HF	I 45	V
HF		1.3% > I 45	1.4% > Vert.
I 45	1.3% < HF		0.1% > Vert.
V	1.4% < HF	0.1% < I 45	

Table 6.8:

PA build orientation variations of impact strength

Orientation	HF/HoE	I 45	V
HF/HoE		7% > I 45	5% > Vert.
I 45	7% < HF		2.7% > Vert.
V	5% < HF	2.7% < I 45	

Table 6.9:

PA build orientation variations of max. flexural strength

Orientation	HF	HoE	I 45	V
HF		6.8% < HoE	9.4% > I 45	9.9% > Vert.
HoE	6.8% > HF		15.5% > I 45	16% > Vert.
I 45	9.4% < HF	15.5% < HoE		0.5% > Vert.
V	9.9% < HF	16% < HoE	0.5% < I 45	

6.2 Analysis of the results in response to research question 1b

Reiterating the research question:

1b. Based on the results from question 1a:

How do the tensile, flexural and impact properties of the 3D printed polymers ABS, TPGDA and PA compare from polymer to polymer?

To facilitate the comparison between each polymer, the results have again been analysed and graphically using radar charts, although in a different way to the charts presented in Section 6.1. Here, each chart represents a property where each polymer is represented with a colour and each build orientation has a corner. Figure 6.4 shows the comparison chart of tensile strength between the three polymers; Figure 6.5 shows the comparison chart of impact strength between the three polymers; and Figure 6.6 shows the comparison chart of flexural strength between the three polymers.

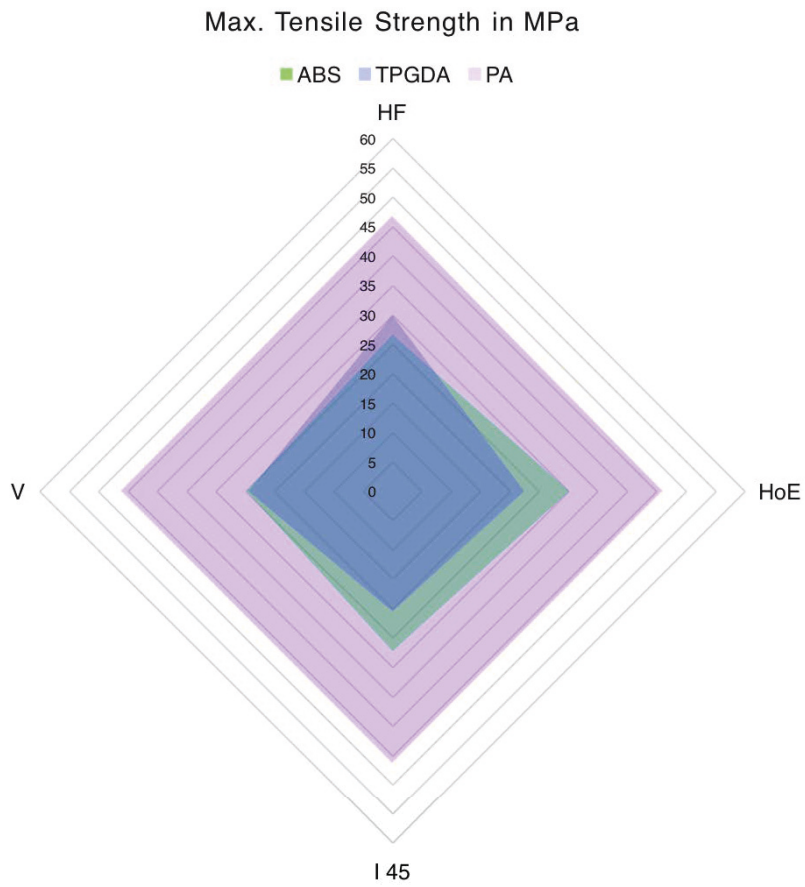


Figure 6.4: Comparison of tensile strength between the three polymers.

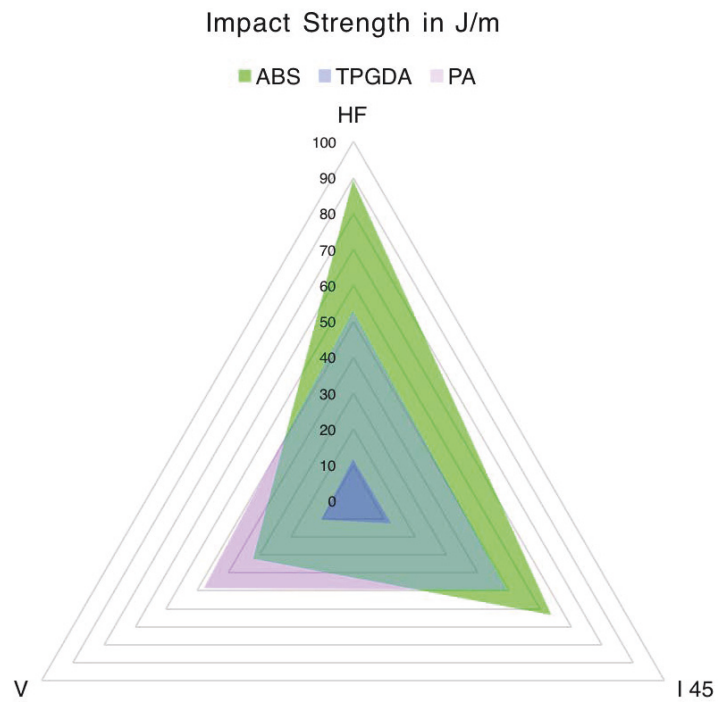


Figure 6.5: Comparison of impact strength between the three polymers.

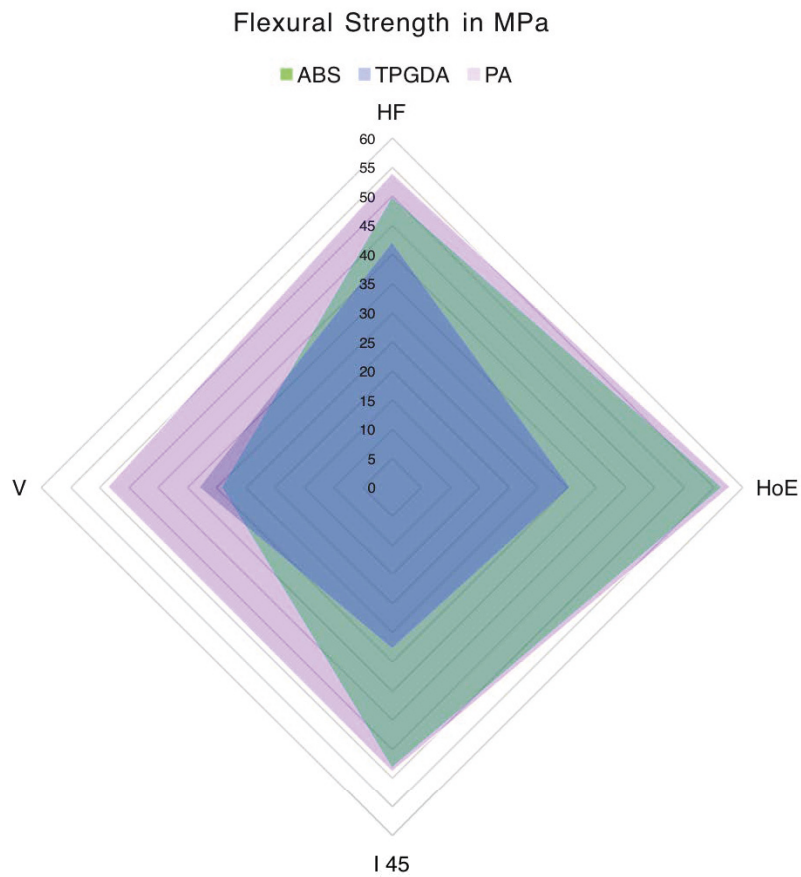


Figure 6.6: Comparison of flexural strength between the three polymers.

6.3 Analysis of the results in response to research question 2

Reiterating the research question:

2. Which software application provides the clearest visual representation of the surface of a part prior to building?

The results show that out of the six software applications reviewed, Cura V3.0.4 was chosen as the best at providing the clearest visual representation of the surface of a part prior to building it.

Chapter 7. Discussion

The purpose of this section is to demonstrate how the radar charts and Cura can be understood and used as an approach or a set of tools during the process of designing a product that is to be made from one of the three 3D printed polymers. This could be done via a combination of a radar chart and Cura, or using each tool on its own. There are several possible combinations of these tools that will help designers during the design process, such as in reviewing the appearance of the surface of a part prior to building it, or in deciding which one of the three polymers most suits the product that is being designed. Depending on how these tools are used, they will apply to different stages of the design process, and attention will be drawn to this in the course of this discussion. To help with this, the steps in the process of designing and producing a 3D printed product are reiterated here:

1. Opportunity identification
2. Research
3. The brief
4. Concept design
5. Design development
6. Detail design (for AM this is done in CAD)
7. Production (building the part with AM)
8. Sale or distribution
9. Service and repair
10. Safe disposal

Steps 1 to 7 are according to Milton & Rodgers' (2013) model, and are relevant for the traditional DFM (design for manufacture) approach, which stops at production; each of these seven steps is described in detail in Section 2.2: The process of designing a product. The additional three steps, 8–10, have been added to the process by the author. This has been done because, when the part is made by its designer using 3D printing, the responsibility for the products after-sale life falls on the designer (see also Section 2.2.3: Discussion of product design process).

7.1 Selecting a surface appearance

In this section, the use of Cura as a standalone tool is discussed to show how it can be used to preview the surface of a product prior to it being built.

For some products, for example, jewellery or ornamental artefacts, mechanical properties can be of negligible importance. They do need to have the strength to perform their intended functions, but the designer will account for this during the design process. For example, a ring to be worn on a finger will need to be strong enough to hold its shape and stay on the finger, but the forces exerted on it are typically not of significance. Similarly, an ornamental artefact needs to be able to stand up and hold its own. However, because their function is something that is potentially looked at on a regular basis or is admired at close proximity, the appearance of the surface becomes an important consideration for the designers of such products. Thus, the appearance of the surface of a product after it has been built is completely at the discretion of the designer, and is therefore entirely subjective.

Following are case studies of jewellery where the build steps can clearly be seen on the surface, which adds character and meaning to each piece. Figure 7.1 is of a necklace pendant in the form of a Nautilus shell that was 3D printed in ABS. It measures approximately 87mm across the longest distance, so would fit comfortably in the palm of an adult hand. The height of each build layer is 0.2mm and one can clearly see the build layer steps, which appear to be following the spiral of the shell from the outside to the centre. Even though this pendant is computer generated and completely artificial, the build steps add to its organic appearance. Although it can't be said for certain, it is likely that the designer of this product chose to build it in this orientation because they liked the way the build steps added visual interest or meaning to the overall form. The designer didn't do much post processing, such as smoothing the surface by sanding off the build steps, which, on an object of this size would have been fairly easy. This again could mean that the designer liked the build steps and left them there intentionally.



Figure 7.1: 3D printed Nautilus shell pendant showing spiralling build steps (courtesy of *Thingiverse*).

It is also not known if the designer of this product used Cura to visualise the piece prior to building it. However, the digital file can be accessed, and therefore, the use of Cura can demonstrate what it looked like prior to building. See Figure 7.2; and for what it would have looked like in another build orientation, see Figure 7.3. Please note that Figures 7.1, 7.2 and 7.3 are deliberately shown large so the detail on the surface can be seen clearly.



Figure 7.2: Nautilus shell pendant in Cura as it was built.

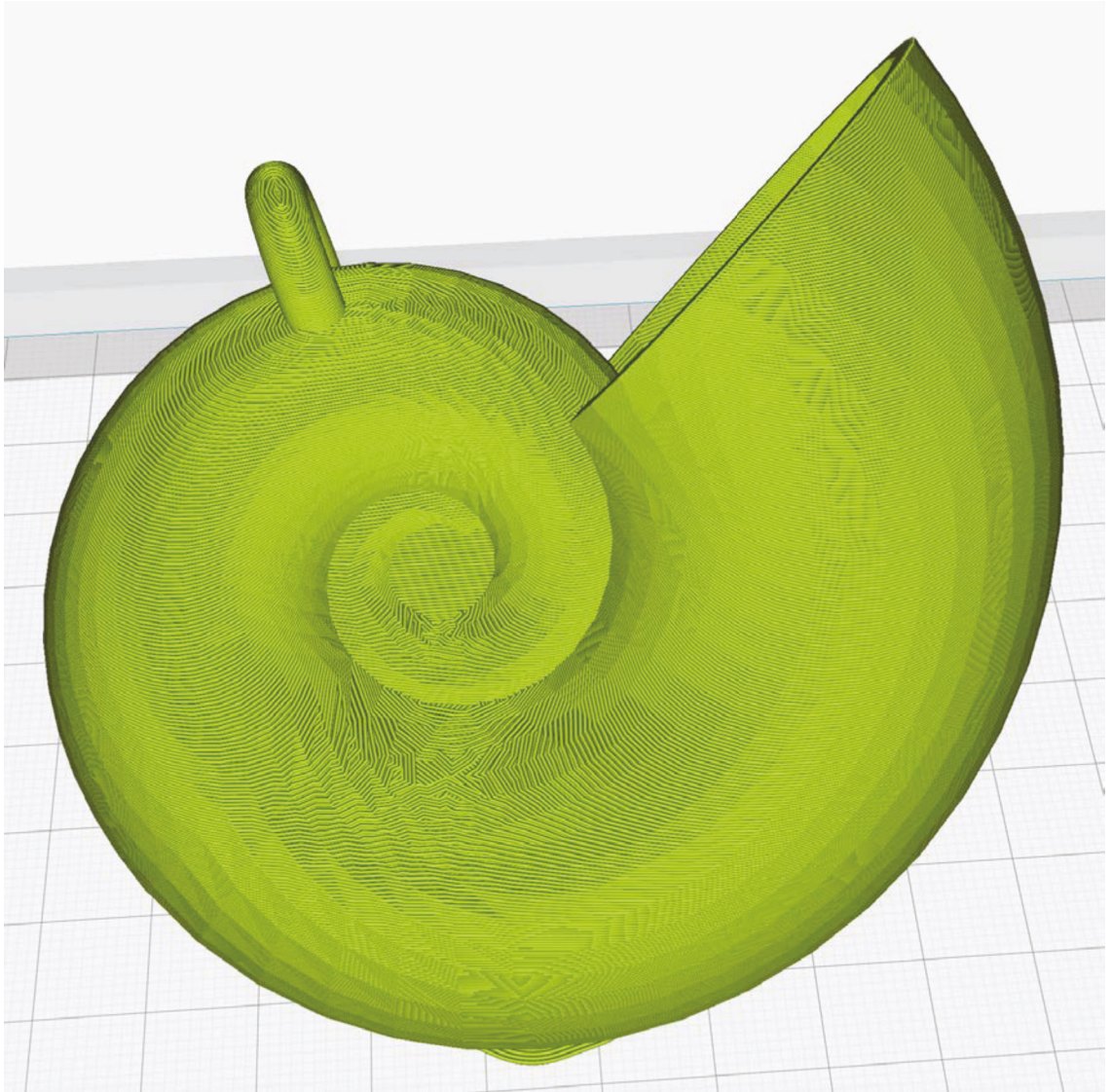


Figure 7.3: Nautilus shell pendant in Cura in a different orientation.

The precise details of the different build orientation, as depicted in figure 7.3, don't really matter in this case. What is important is that one can clearly see the difference in surface appearance between Figure 7.2 and Figure 7.3, as shown in Cura.

Figure 7.4 depicts two brooches. They are both made from metal; the one on the left is solid gold, and the one on the right is solid silver. However, they were manufactured by first building models of each of them in a polymer such as ABS, which was then used to make a mould, from which the final versions were cast in gold and silver. On both of them, the build steps can still be seen. On the gold piece, which looks to be a stylised four-leaf clover, the build steps radiate out from the main heart shapes on each clover leaf, and in so doing,

add texture to each leaf. On the silver piece, which looks like a stylised seed pod, the build steps can be seen on the left and right faces of each arch. Interestingly, the very outside ridge of each arch appears to have been polished to a high gloss and to the point at which the build steps have been removed. On each arch, this produces a visual and tangible contrast between the outside ridge and its faces.



Figure 7.4: Gold and silver broaches showing build steps (courtesy of *sculpteo*).

Again, it is not known for certain, but it is likely that in both cases the designer left the build steps behind intentionally, because, as this is precious metal jewellery, it would have been easy to polish the steps off. The digital files of either of these products cannot be accessed, so their appearances can't be simulated in Cura.

Application to practice through design process

It is not possible to contact the designers who designed the objects above, so it is impossible to know at which point in the design process they decided on

the build orientation. However, it can be assumed with a degree of certainty that all three designers intended to use 3D printing to manufacture them from the outset, so the build orientation would have been a constant consideration throughout the entire design process.

7.2 Selecting the most suitable polymer based on a mechanical property

In this section, the discussion centres on how each of the radar charts that depict the comparison of the three polymers to each other can be used as standalone tools to select the most appropriate polymer for a product. As shown in Section 6.2: Analysis of the results in response to research question 1a, one chart was designed for max tensile strength, one for impact strength, and one for flexural strength.

In most cases it is known what the purpose of a product will be, even before the designer starts designing it. It is known how it will need to work and how it is likely to be used, so it is known which particular mechanical properties it will need to have so it can best perform its function. The shell of a cordless drill will need to be impact resistant so it can protect its internal components in case it is dropped, whereas the frame and temples of eyewear will need to be able to bend and flex in case they are sat upon. So, from the outset there are clear indicators of what mechanical properties are required to satisfy the product's use, and if we combine that with tools that can help us choose the most appropriate polymer, there is a higher degree of certainty that the product will perform better.

7.2.1 Example of selecting a polymer based on max tensile strength

The radar chart shown in Figure 7.5 shows the comparison of the maximum tensile strength between each of the three polymers in relation to their build orientation. Maximum tensile strength is the amount of force a material can withstand while being pulled apart before it breaks. Concrete has a low max. tensile strength of approximately 5 MPa (mega pascals), whereas mild steel is higher at around 440 MPa. Max tensile strength is mainly used by engineers when designing for structural applications, and it is one of the most important and widely measured properties of materials included on most material data

sheets, which is why they were tested for it in this research. However, it is rare that a product designer will need to take tensile strength into consideration when designing a handheld product. As mentioned in Section 4.1.2: Tensile testing, product designers will use the tensile properties of a material to gauge how one material compares to another, but impact and flexural properties are typically more directly relevant considerations when designing a product.

Two things that stand out from the radar chart shown in Figure 7.5 are that, out of the three polymers, PA (Polyamide) has the highest max tensile strength, and that there is little variation between all four build orientations of PA. This means that if the tensile strength in a part is of importance, PA is a safe choice, and the build orientation will not make much difference to the tensile strength. In contrast to this, ABS, and in particular, TPGDA, are approximately 15–20 MPa weaker, and the build orientation will make a difference. For ABS, HoE is the best choice of orientation for tensile strength and HF for TPGDA; see Figure 7.5.

This chart is useful if there is a choice between PA and one or two of the other polymers, because it shows that PA is the best choice if the part needs to display the highest tensile strength in comparison to the other two. If we take PA out of the equation, ABS is the best choice in all orientations except one which is HF.

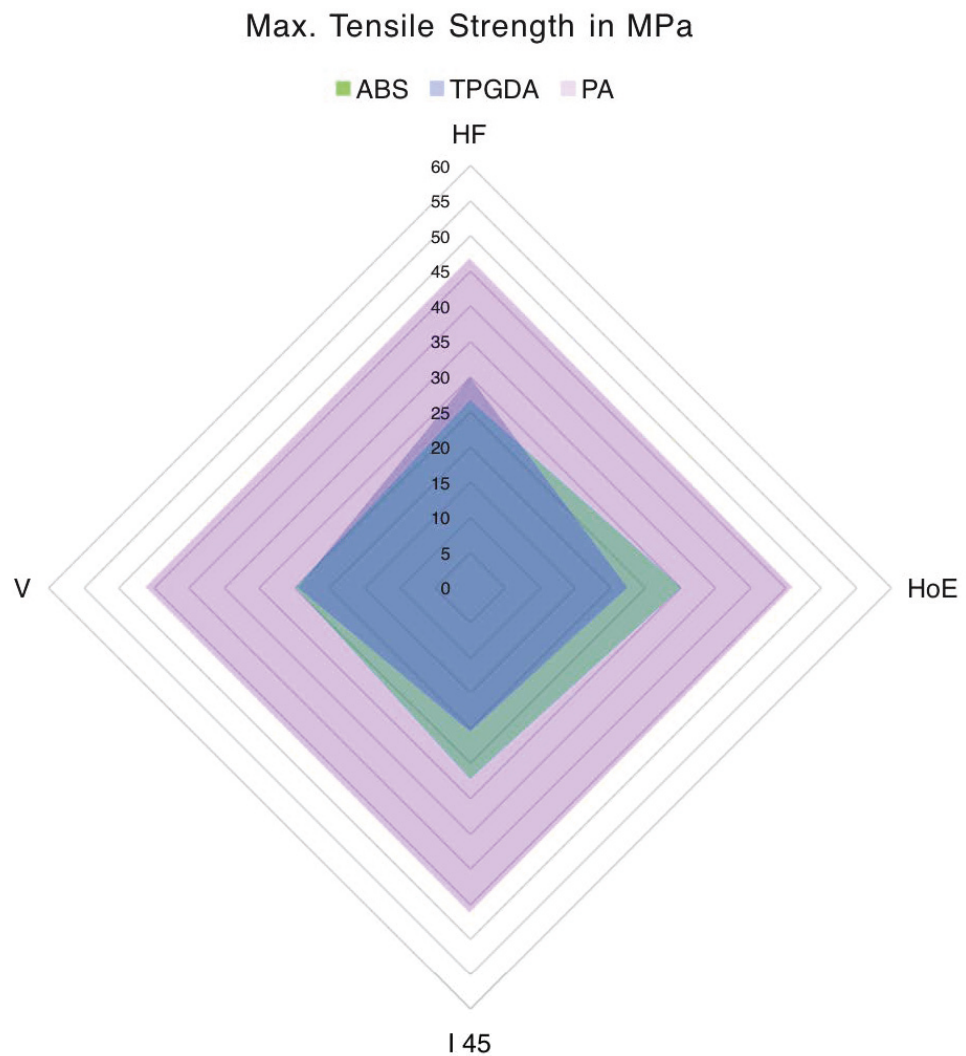


Figure 7.5: Comparison of tensile strength between the three polymers.

Application to practice through design process

In the design process the tensile chart could find application during step 5, design development, or step 7, production. If the part is to be made from ABS or TPGDA the chart would be used during design development, because it allows the optimisation of a part's geometry based on build orientations. If a part is ready for production and it is no longer possible to optimise its geometry for a particular build orientation, then it would be best built in PA if possible and in ABS if not PA.

7.2.2 Example of selecting a polymer based on impact strength

Impact strength is in general an important mechanical property for product designers to consider, and in particular for handheld products. This is because the outside shell of a product is typically designed to protect its internal components from impact if it is dropped or knocked. Examples are, handheld power tools such as the aforementioned cordless drill, handheld hair dryers, electric shavers, mobile phones, gaming controllers, and even ski boots.

The chart in Figure 7.6 shows how the impact strength of the three polymers compare; it can be seen that TPGDA has extremely low impact resistance in all three build orientations, and, if possible, should not be used to build a part if it needs to be impact resistant in any way. For both TPGDA and PA, the build orientation doesn't matter, since the impact resistance is similar across all three build orientations. Compared to TPGDA, the impact resistance of PA is approximately five times higher, but ABS is the one to design for if high impact strength is required. To achieve high impact strength in ABS, the build orientation of a part can range from HF to I 45, but anything above I 45 towards V should be avoided. This is because the build layers are horizontal in V and in the same direction as the line of impact. If, however, for some reason, that cannot be avoided, a part must be built in the V orientation, and PA would be a better material to choose.

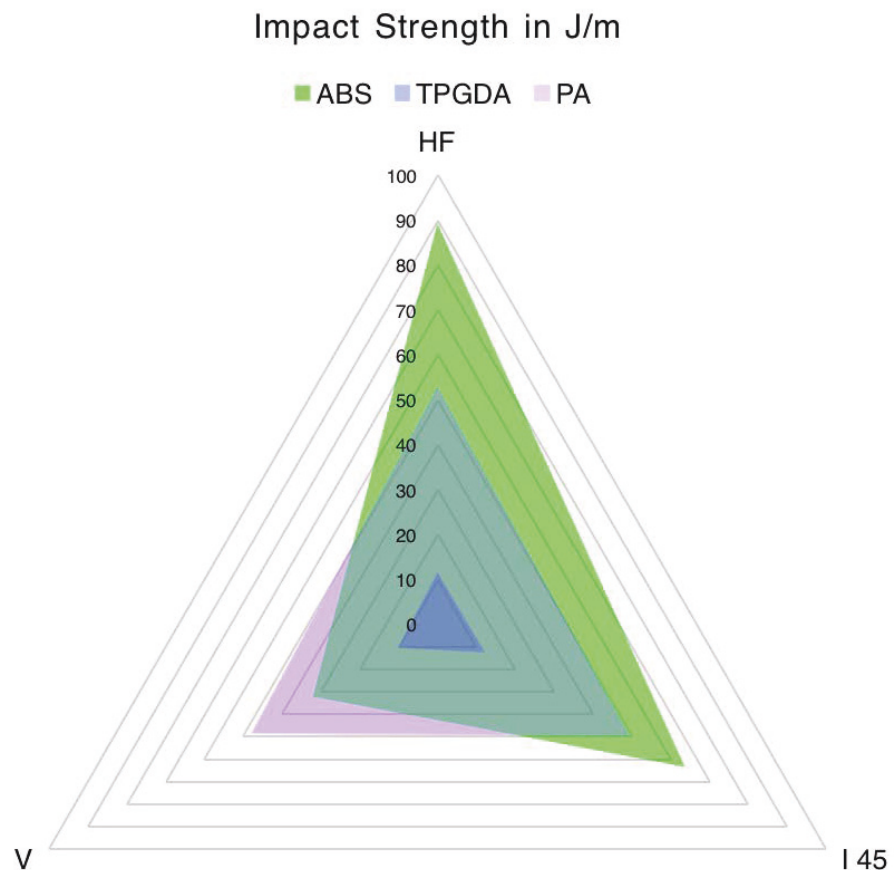


Figure 7.6: Comparison of impact strength between the three polymers.

Application to practice through design process

The impact chart in Figure 7.6 can be applied to the design process if production has already been reached and no more changes can be made in CAD, in which case it is recommended to have the part built from ABS in a build orientation ranging from HF to I 45. The chart could also be used as early concept development and definitively during design detailing, because this would enable the designer to pay particular attention to form development in relation to build orientation.

7.2.3 Example of selecting a polymer based on flexural strength

As mentioned in Section 4.1.4: Flexural or 3-point bend testing, the flexural strength of a material is its resistance to bending, which for product designers is important to consider if a component of the product they are designing needs to flex and or bend in some way and then return to its original position.

Examples are snap buckles on the chin straps of helmets, pen caps on pens, and battery cover clips; see Figure 7.7, remote controls for TVs etc.

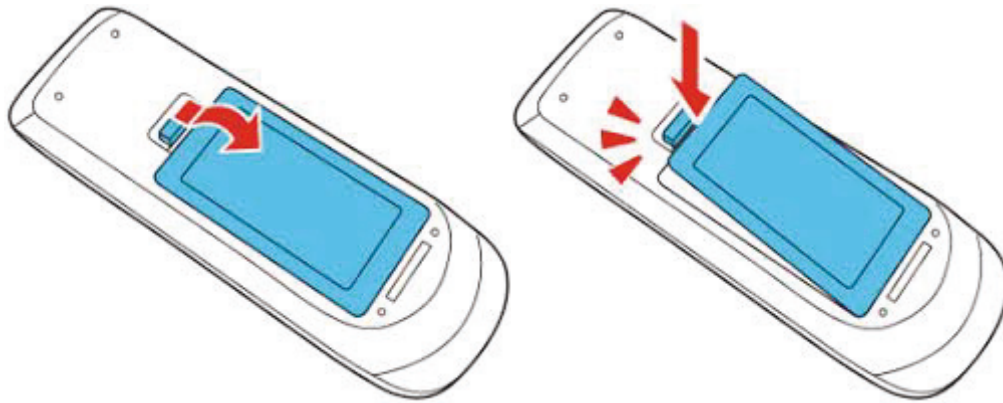


Figure 7.7: Flexing clip on the battery cover of a remote (courtesy of *Epson*).

Then there are products that need to have a degree of flex so they don't break if they are accidentally twisted or bent, such as eyewear. The chart in Figure 7.8 shows that, with regard to flexural strength, there are several options to choose from. To begin with, PA has the best flexural strength across all four build orientations. ABS comes close to PA in HF and HoE, and is almost as strong as PA in I 45. TPGDA does not flex well, except in V, where it fares better than ABS. Therefore, if the choice is between all three polymers, then PA is the one to use in any orientation, TPGDA in V, and ABS anywhere in the range of HF to I 45. Again, as with impact strength, ABS is the weakest in V because the build layers are horizontal in V, which is in the same direction as the flexing occurs. If the highest possible flexural strength for a part needs to be ensured, TPGDA should be disregarded altogether, and either PA in any orientation or ABS in the range of HF to I 45 considered instead.

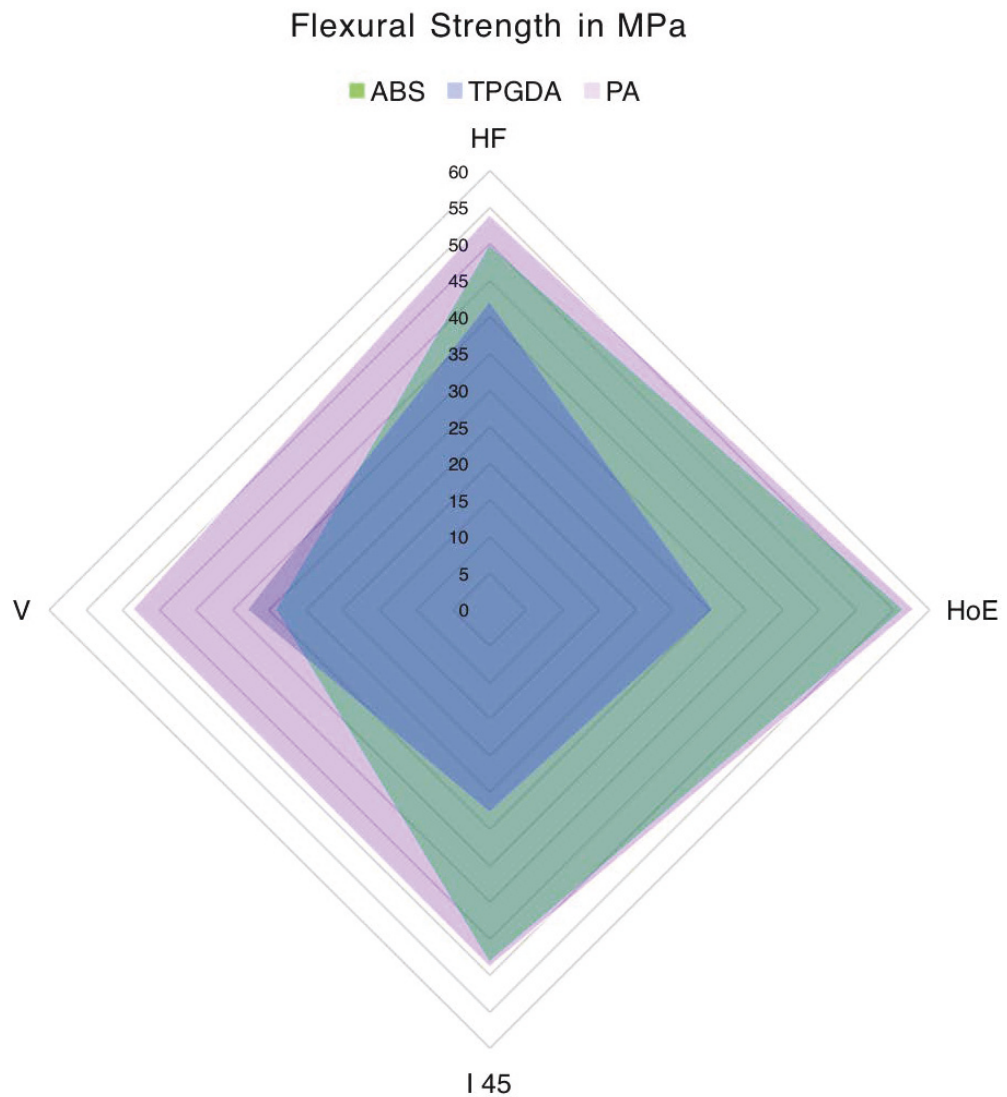


Figure 7.8: Comparison of flexural strength between the three polymers.

Application to practice through design process

In terms of design process, if the intention is to build the part in ABS, it would be advisable to integrate the flexural chart shown in Figure 7.8 during design development, and optimise its geometry to suit a build orientation ranging from HF to I 45. If the part is to be built in PA, then it can be designed without regard to build orientation.

7.3 Selecting the most suitable build orientation for each polymer

This section looks at how to select a build orientation if one of the three polymers has already been decided on. This may be because only one type of

3D printing technology or polymer can be accessed, or because there is a preference for a particular polymer. There follows a brief discussion of how to choose build orientations for each polymer based on specific properties that may be required. Briefly, because this has already been touched on in Section 6.1: Analysis of the results in response to research question 1a; but it needs to be expanded on more here to provide clarity with regard to the design process, as well as setting the context for Section 7.4: Balancing mechanical properties with surface appearance.

7.3.1 Scenario 1: Selecting a build orientation for ABS

The chart in Figure 7.9 represents the mechanical properties of ABS in relation to the four build orientations. Each corner of the lined triangle stands for a mechanical property; each coloured triangle for a build orientation and each corner of a coloured triangle gives us the value of the property it is pointing to. For example, in the HF orientation, the max tensile strength of ABS is approximately 27 MPa; its flexural strength is approximately 50 MPa; and its impact strength 90 J/m. In practice, an example could be that if a part needs to have good impact and flexural strength, it would be best to have it built in the range from HF to I 45.

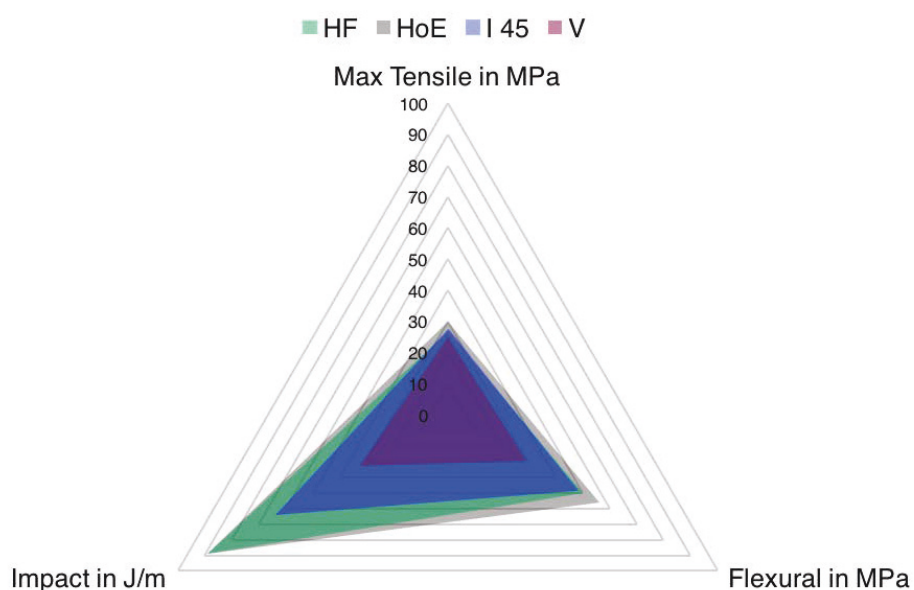


Figure 7.9: ABS Build Orientation Chart.

The product that has been chosen as an example is eyewear in the form of aviator sunglasses designed by the author, which will be used for Scenarios 1 and 2; see Section 7.3.1: Scenario 1: Selecting a build orientation for ABS; and Section 7.4.1: Scenario 2: Visualisation of a polymer based on max tensile strength. In the context of this research, the Cambridge English Dictionary's definition of a scenario will be used: A description of possible actions of events in the future (Cambridge English Dictionary 2018).

This particular product was chosen for the following reasons:

1. Its scale will be immediately apparent to most people because most people are familiar with the size of eyewear through their experience with sunglasses and eyewear designed to enhance sight.
2. In the context of mechanical forces, eyewear is a product that most people will be able to relate to, because many people will have accidentally broken a pair by either dropping them on the ground (impact strength) and or twisted/bent them (flexural strength) by sitting on them.
3. With regard to the appearance and texture of a surface, eyewear again lends itself well, because products such as this sit at the intersection of functionality and personal adornment, so the detailing on the surface can matter a lot to people.
4. The form of aviator eyewear is an iconic shape that is easily recognisable and is worn by both women and men alike.

To demonstrate how this will apply in practice, the ABS Build Orientation Chart (Figure 7.9) was used together with a CAD application to show the range of build orientations available in this case. Figure 7.10 provides an overview of how the chart connects to the range of build orientations for the aviator frame. The acceptable range is the range within which there is freedom of choice to select an orientation; this will be explained in more detail below.

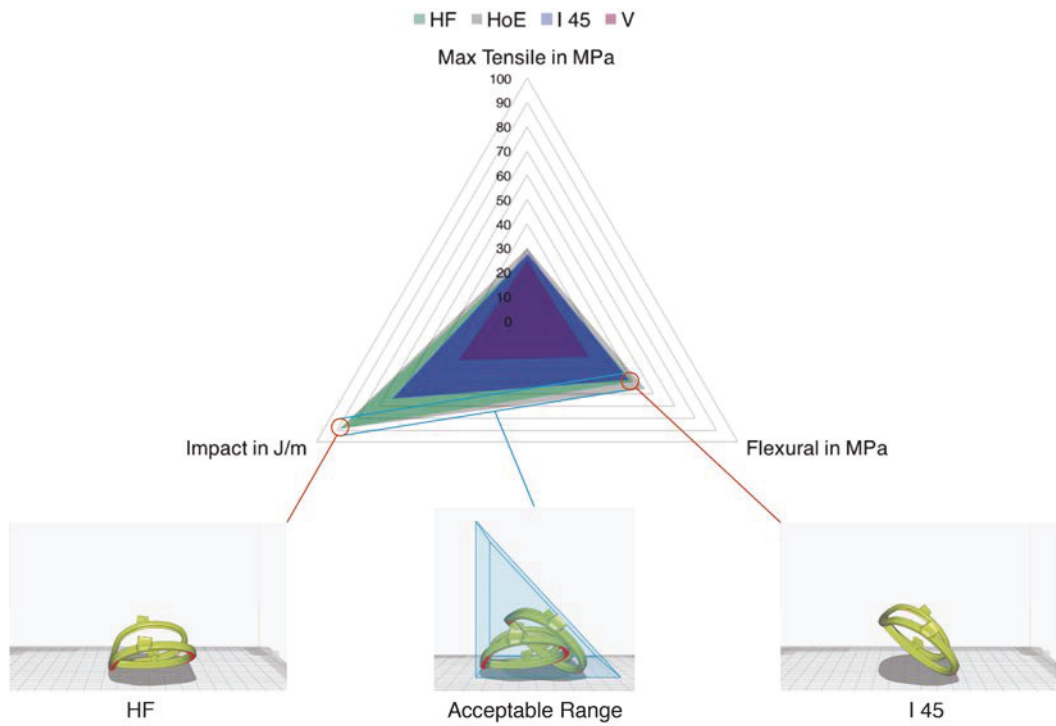


Figure 7.10: ABS Impact Chart and views of acceptable range.

Following are more detailed images of the Aviator Frame in both the HF (see Figure 7.11) and I 45 (see Figure 7.12) orientations.

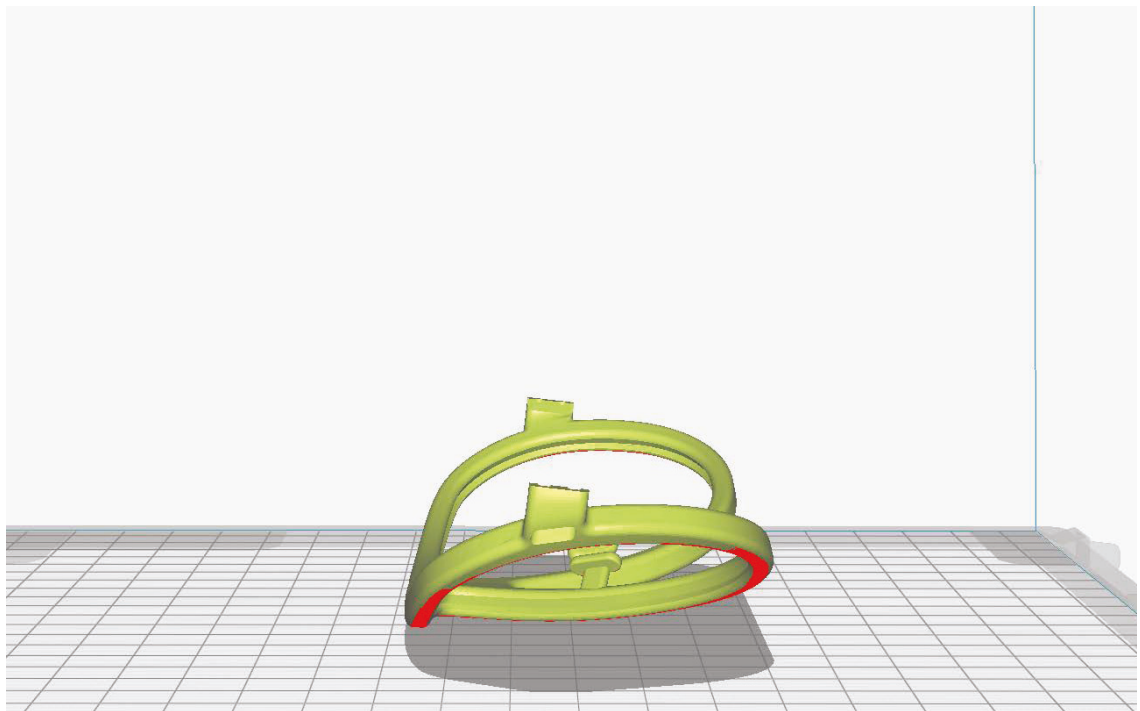


Figure 7.11: Aviator Frame shown in HF orientation.

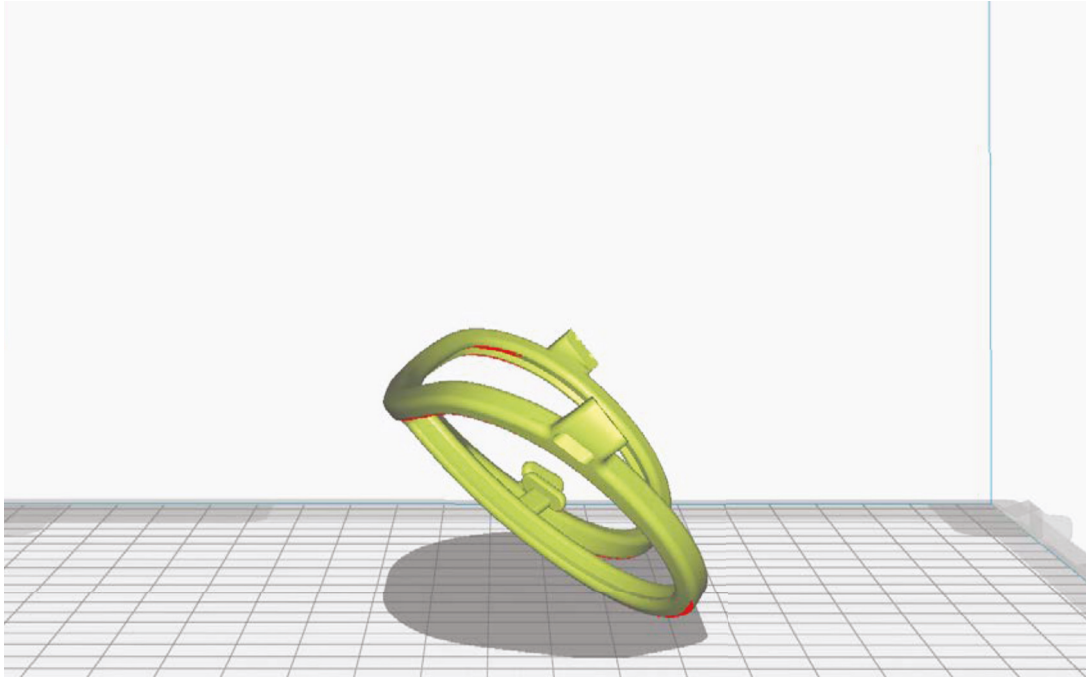


Figure 7.12: Aviator Frame shown in I 45 orientation.

The chart in figure 7.11 indicates that in these two orientations, HF and I 45, and at any angle within them ranging from 0 to 45 degrees, both the impact and flexural strength will be as good as ABS has to offer. If the part were to be rotated any further, beyond 45 degrees and towards 90 degrees, it would become weaker and weaker and would be weakest in the V orientation at 90 degrees (see Figure 7.13).

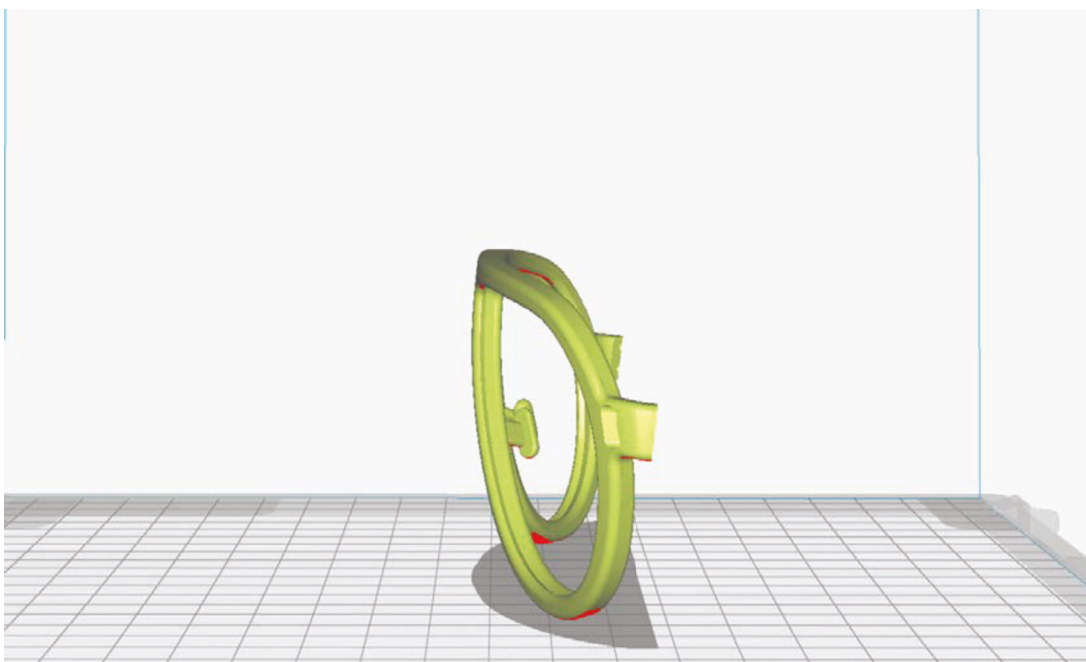


Figure 7.13: Aviator frame shown in V orientation, which would produce the weakest part.

Henceforth, the term “acceptable range” will be used to describe the range of orientation in which a part can be built to ensure its mechanical properties are as good as possible. In the aviator frame example, the acceptable range of orientation is from HF to I 45, but for future examples it is likely to be different. In Figure 7.14, a semi translucent volume in the shape of a blue wedge has been superimposed over the HF to I 45 orientation to illustrate where the acceptable range is approximately in this case.

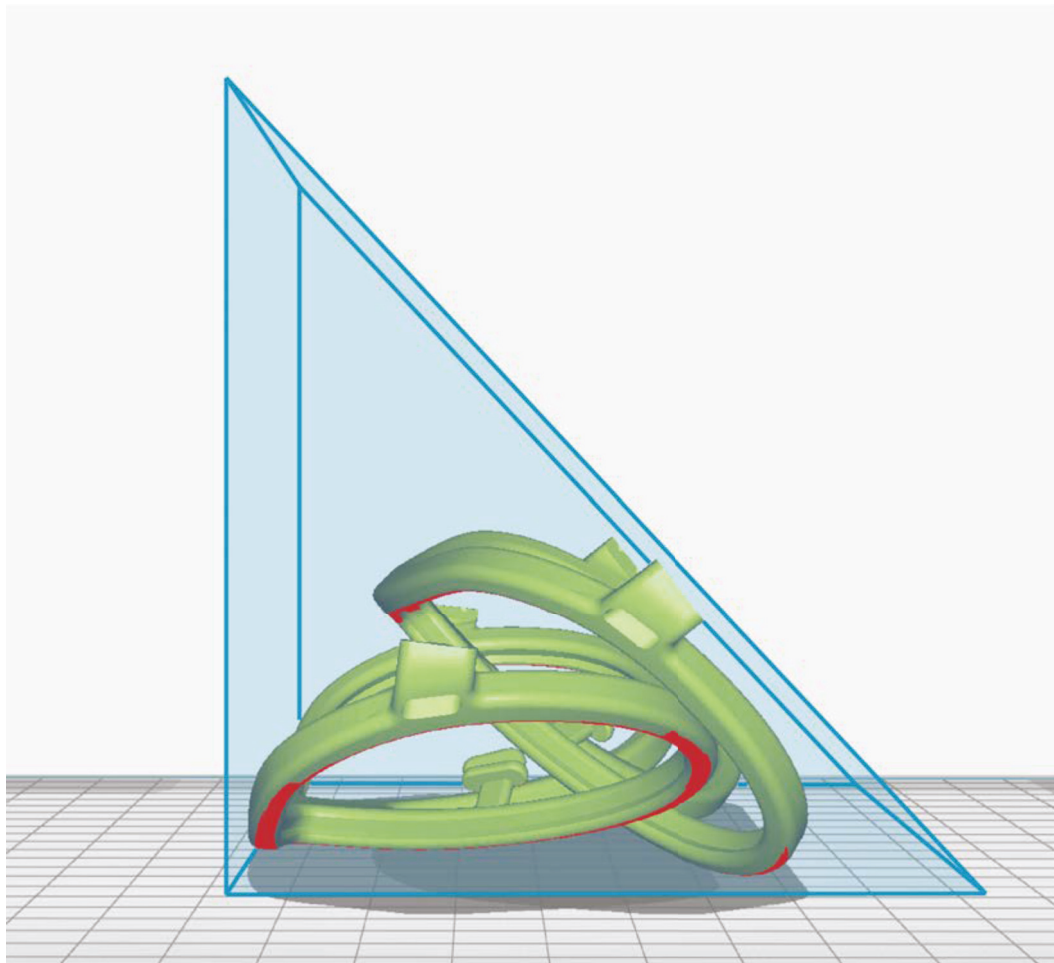


Figure 7.14: HF to I 45 acceptable range of orientation shown in blue.

The information that the chart in figure 7.9 provides for ABS is useful. The same goes for the charts for TPGDA and PA. Those charts were developed to function as quick visual reference guides that allow product designers to make timely assessments, and the charts can be used on their own. If more accurate information is required, one or more of the percentage tables (Table 7.1, for example) lists how much weaker or stronger a property, in this case impact strength, is in relation to other build orientations based on percentage.

Table 7.1:

ABS build orientation variations of impact strength

Orientation	HF/HoE	I 45	V
HF/HoE		28.6% > I 45	63.8% > Vert.
I 45	28.6% < HF		49.3% > Vert.
V	63.8% < HF	49.3% < I 45	

If we revisit the aviator frame example discussed earlier in this section, using Table 7.1, it can be seen that the HF orientation is 28% stronger than I 45 and 63% stronger than V. It was already known that the HF orientation would provide the best impact strength and that up to I 45 was still in the acceptable range, but it was not known how big the difference between the two would be. 28% is a substantial amount, and this additional information may be important if it is necessary to know how much strength a part may gain or lose depending on a particular build orientation.

7.3.2 Selecting a build orientation for TPGDA and PA

Since the previous section provided an example for ABS, the process will not be repeated for TPGDA and PA, because although the build orientations and percentages may be different, the approach would be the same. However, the charts have been included below so it is not necessary to revisit Section 6.1 to review them; see Figures 7.15 and 7.16, which show the properties of TPGDA and PA respectively.

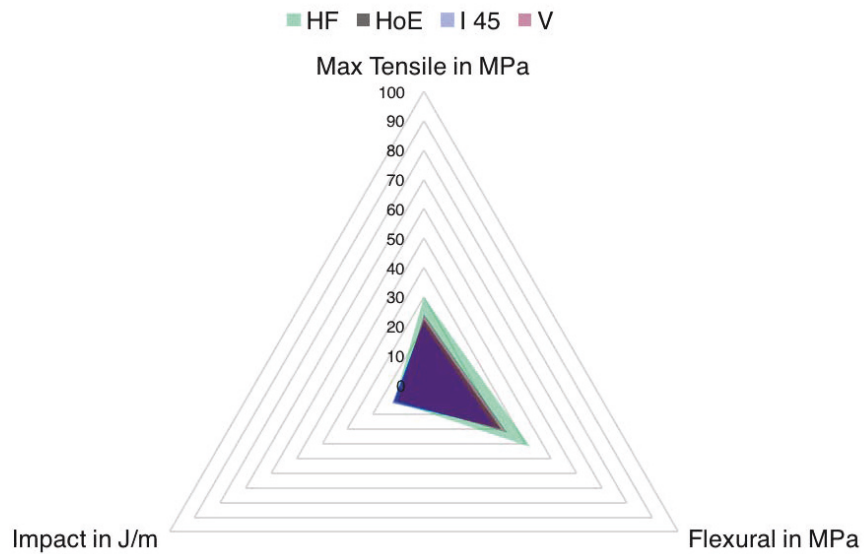


Figure 7.15: Four build orientations in relation to mechanical properties of TPGDA.

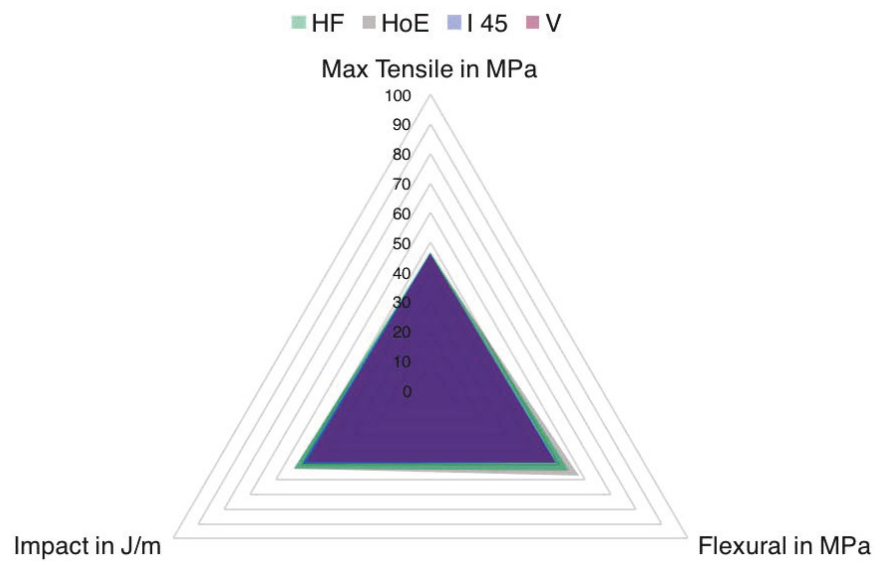


Figure 7.16: Four build orientations in relation to mechanical properties of PA.

Application to practice through design process

The charts (see Figures 7.9, 7.15 and 7.16) could find application during design development, design detailing, and for production. During design development they could help with form development through part geometry to optimise a part for a particular mechanical property. This would still apply to design detailing, but depends on how far the form development has progressed. If the part reaches production and has at no point been optimised, then the chart will still help to make knowledge-directed decisions.

The percentage tables (see Table 7.1) would be best applied during design development, in cases where a product designer needs to know exactly how much strength the part is set to gain or lose, based on a build orientation.

7.4 Balancing mechanical properties with surface appearance

This is what it's all come down to!

It will now be discussed how the tools created (radar charts and percentage tables) by this research can be combined with Cura in an approach that enables product designers to make sure that the part they are working on has the best mechanical properties for its intended use, as well as the surface appearance that most suits its application. Or, in other words, how can the tools to be utilised to find a balance between the two? Once again, this will be done by working through scenarios that have been broken down into stages and by explaining at what stage in each scenario which tool needs to be considered, and how to use them alongside each other. Listed here are the stages:

Stage1: select polymer using 3 x polymer max tensile chart

Stage 2: check Acceptable Range using ABS, PA or TPGDA build orientation chart

Stage 3: experiment with build orientations in Cura

Stage 4: select final build orientation

Stage 5: build part.

As before, the eyewear will be used as the case study, for the reasons outlined in Section 7.3.1: Scenario 1: Selecting a build orientation for ABS.

7.4.1 Scenario 2: Visualisation of a polymer based on max tensile strength

In this scenario, it is assumed that the design detailing of the part that is being worked on has been completed and its form can no longer be altered, therefore it is ready for step 7 in the design process, which is production. As this scenario is being worked through, each stage will be explained in detail;

however, the diagram in Figure 7.17 provides a clear overview of Scenario 2 and can serve as a reference guide.

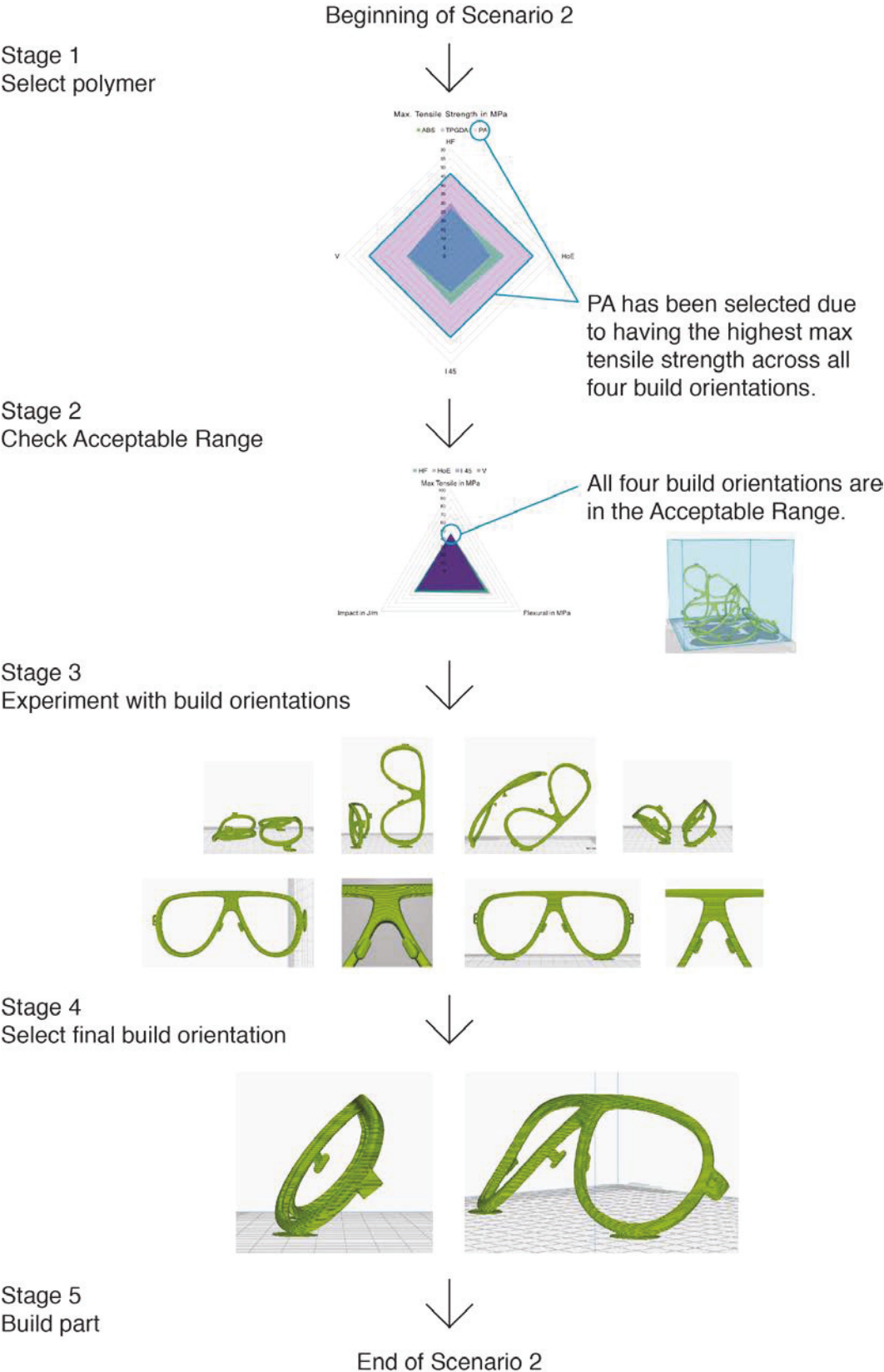


Figure 7.17: Diagram of Scenario 2.

For this scenario, the material PA will be used, because it has the highest max tensile strength in all four build orientations, as the chart in Figure 7.18 shows.

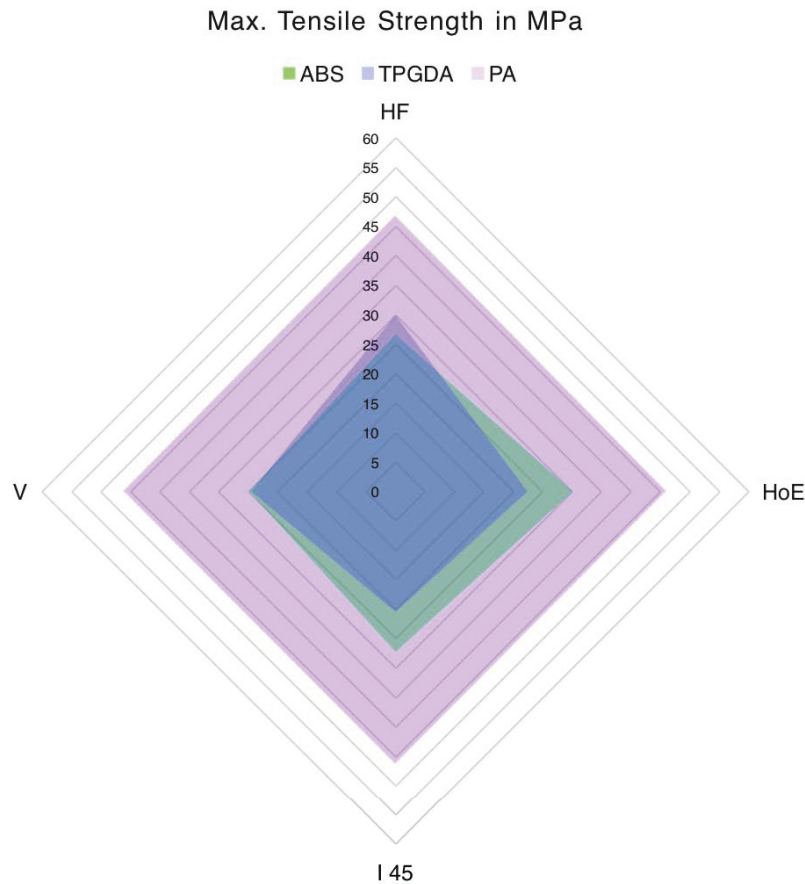


Figure 7.18: Comparison of tensile strength between the three polymers.

Stage 1: select polymer

Using the comparison of tensile strength between the three polymers chart (see Figure 7.18) PA has been selected. Not only does it have the highest max tensile strength across all four build orientations, but PA also displays, at approximately 46 MPa, the same max tensile strength across all four build orientations. Therefore, the build orientation will have no effect on the max tensile strength, which means that there is complete freedom of choice regarding how the part is oriented.

Stage 2: check acceptable range

This stage is important, because it is here that the acceptable range is decided on, which ultimately guarantees the part's best possible performance in relation to the strength(s) for which it is being optimised. Since PA has been

chosen, the PA build orientation chart (see figure 7.19) can be used to check what the acceptable range of build orientations is. It can be seen that, with regard to max tensile strength, the part can be oriented from HF to V or anything in between. At this stage, there is also the opportunity to review the two other properties, namely flexural and impact, to see how a build orientation may affect them in relation to max tensile strength. It can be seen that if flexural and impact strength were important, it would be wise to build in the HF orientation; however, in this scenario this will be disregarded and the sole focus will be on max tensile strength.

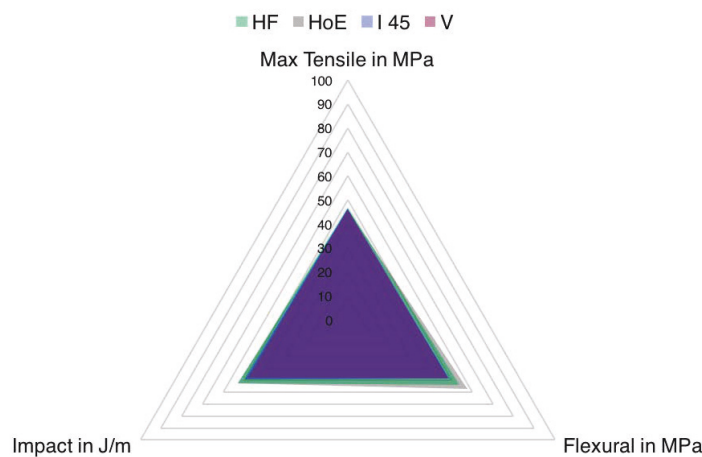


Figure 7.19: PA build orientation chart.

One last measure that can be applied to this stage is to check what the difference between each build orientation is with greater numerical accuracy than the chart allows. This can be done using Table 7.2, which shows in percentages what the difference in strength between each build orientation is. It can be seen that the difference is less than 1.5% between all build orientations, which is negligible and therefore won't be taken into account when the acceptable range for this particular scenario is defined.

Table 7.2:

PA build orientation variations of max. tensile strength

Orientation	HF	I 45	V
HF		1.3% > I 45	1.4% > Vert.
I 45	1.3% < HF		0.1% > Vert.
V	1.4% < HF	0.1% < I 45	

After consideration of the two charts and table, it can be concluded that the acceptable range that will guarantee the best max tensile strength in PA will be from HF to V.

Stage 3: experiment with build orientations in Cura

To ensure Cura represents the surface of a part as close as possible to the way it would look after building, the build layer height in Cura needs to be set to the same height the part is to be built at. For this scenario, the build layer height in Cura is set to 0.1mm, because this is the layer height used to build the PA test specimens for testing (see Chapter 4.0: Experiments).

Since, in this scenario, the acceptable range allows for any orientation, as shown in Figure 7.20, there is complete freedom when it comes to selecting a build orientation. This is both a disadvantage and an advantage at the same time. It is a disadvantage in that there are too many options to choose from, which may make the decision harder; on the other hand, it is an advantage because there is no need to worry that an orientation outside the acceptable range is chosen.

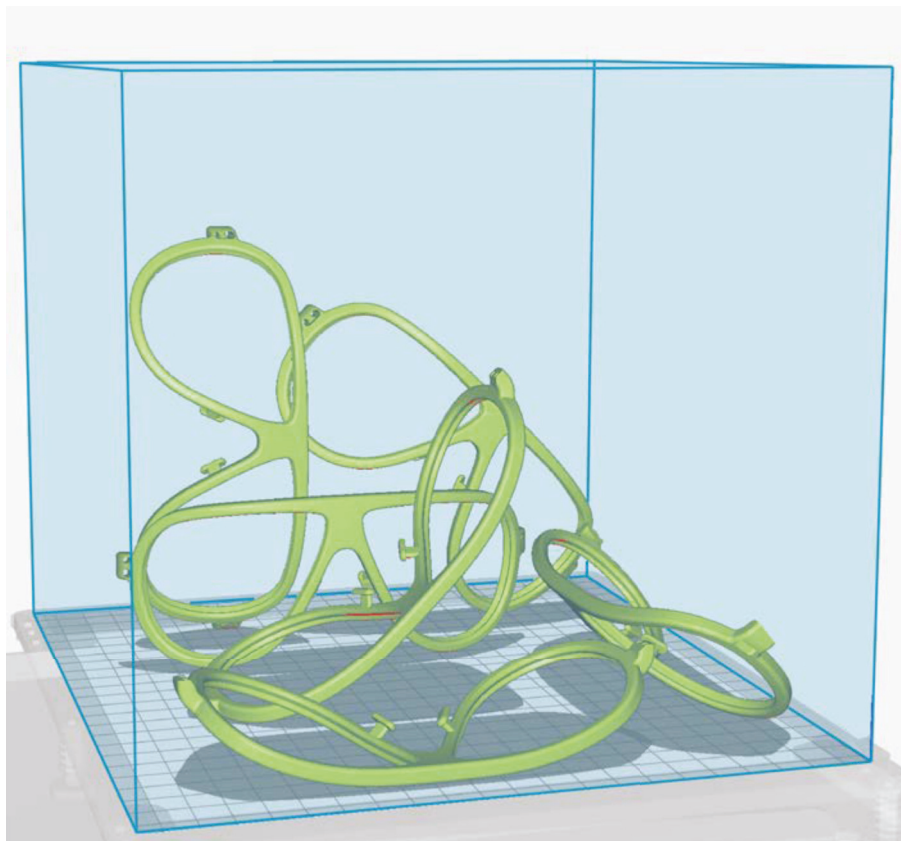


Figure 7.20: The acceptable range, shown in blue, for max tensile in PA.

It is important to note that most orientations have at least two ways a part can be placed, some examples of which are shown in Figures 7.21 and 7.22. In Figure 7.21, the part is placed in the HF orientation, facing up as well as down, and in Figure 7.22, the orientation is I 45, also facing both up as well as down. In both cases the part's mechanical properties and surface texture will turn out to be the same, regardless of whether it is built facing up or down.



Figure 7.21: HF facing up and down.



Figure 7.22: I 45 facing up and down.

This gets more interesting in situations where the orientation allows for different placements that do not affect the mechanical properties, but will affect the surface texture, as shown in Figures 7.23 and 7.24.



Figure 7.23: V option 1.



Figure 7.24: V option 2.

The difference between V options 1 and 2 will be that once the frames are being worn by someone, option 1 will have the build steps running horizontally across the frame, whereas in option 2 the steps will run vertically across the frame; see Figures 7.25 and 7.26 respectively. The difference is a subtle one, but to many product designers this would matter.

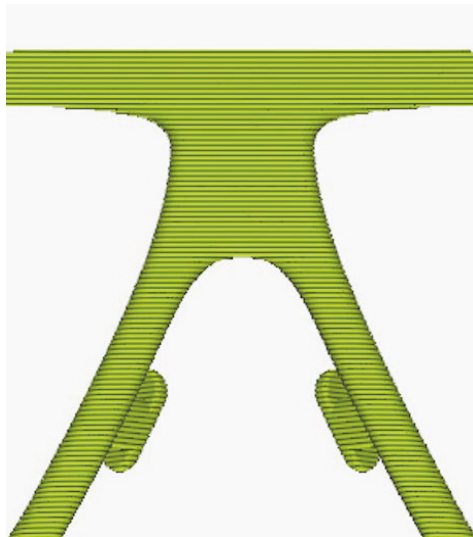


Figure 7.25: Horizontal build steps.



Figure 7.26: Vertical build steps.

At this point Stage 3 is still being worked through and build orientations are being experimented with in Cura. The surface texture of a product is for the most part subjective and depends on the preference of the product designer who may have a set of criteria that s/he may apply to a product. Examples of such criteria are: comfort — will the surface be comfortable to use? will it feel good to the touch? Maintenance — will the surface be easy to keep clean? and appearance — will the surface give the product a visually pleasing appearance overall? In this scenario, comfort is considered as the most important criterion because the product is eyewear and needs to feel comfortable while sitting on the bridge of the nose and while resting against the forehead. Visually, symmetry could also be a major factor to consider, because eyewear is typically symmetrical, as are faces, so people are likely to prefer symmetrical eyewear. If symmetry is considered first, this rules out several build orientations, such as the ones shown in Figure 7.27.

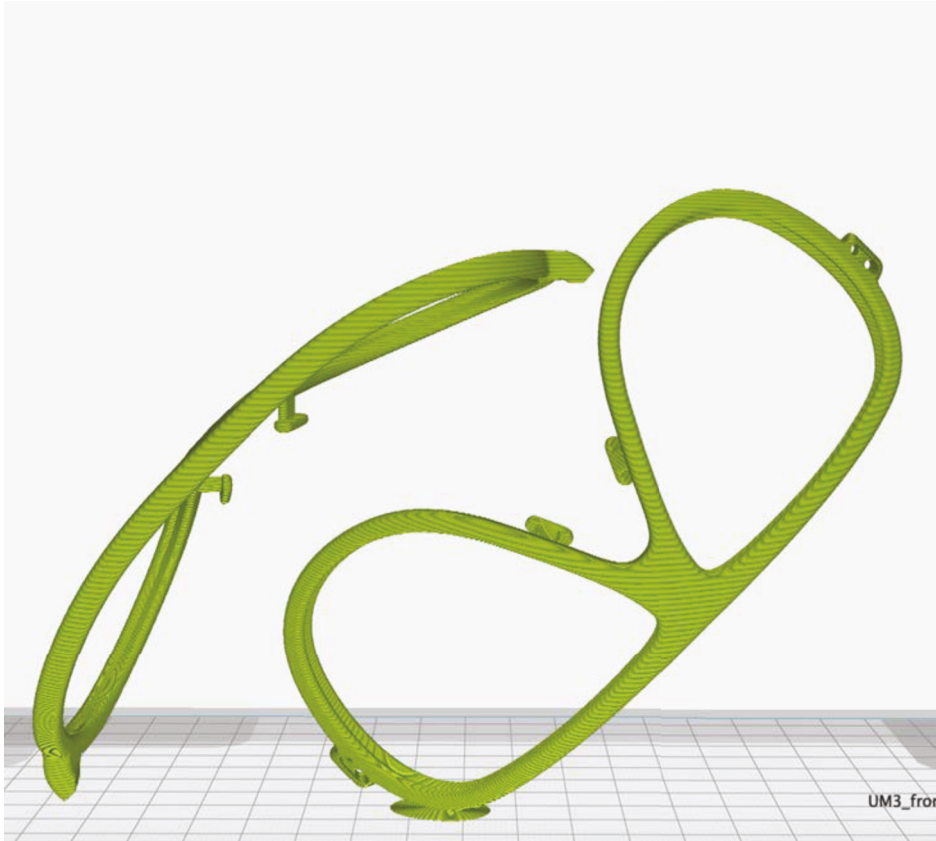


Figure 7.27: I 45 options 1 and 2, both of which are asymmetrical.

These build orientations would produce an asymmetrical appearance, because the build steps would run diagonally across the front of the frame and would make the left side of the frame look different from the right, as can be seen in Figure 7.28.



Figure 7.28: Frame with diagonal build steps.

Stage 4: select final build orientation

One criterion was that the orientation has to be such that it produces a symmetrical frame. The other criterion was comfort around the bridge of the nose and in the area of the forehead between the eyes of the person wearing the eyewear. To achieve this, it would be best to place the frame in an I 45 orientation, as shown in Figure 7.29, because this will minimise rough surface transitions and produce comfortable surfaces where the frame comes in contact with the skin; see Figure 7.30.

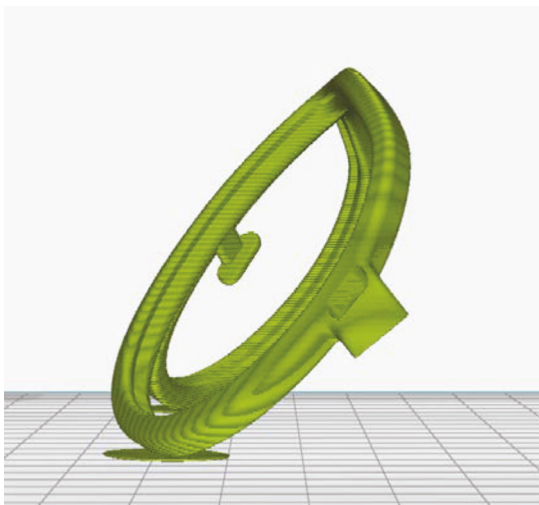


Figure 7.29: I 45 orientation.

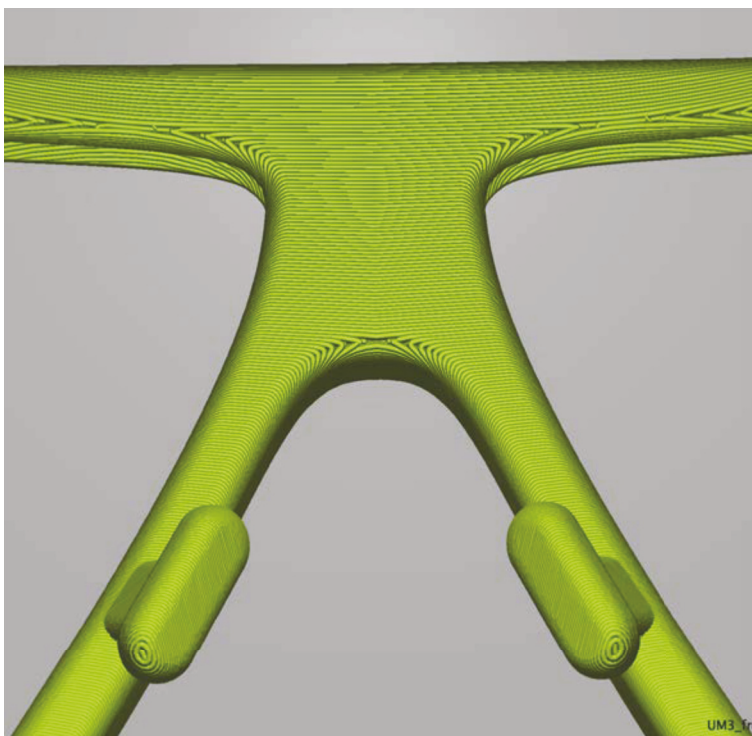


Figure 7.30: View of the section of the frame that will come in contact with the skin.

Stage 5: build part

Now that a build orientation has been decided on, this information needs to be included when the digital stl file of the part is sent to the 3D print bureau that will be producing the part. To ensure the correct build orientation is selected, it helps to send a screen grab (Figure 7.31) together with an explanation, so the operator of the 3D printing machine has a visual reference to work with as well as the written one.

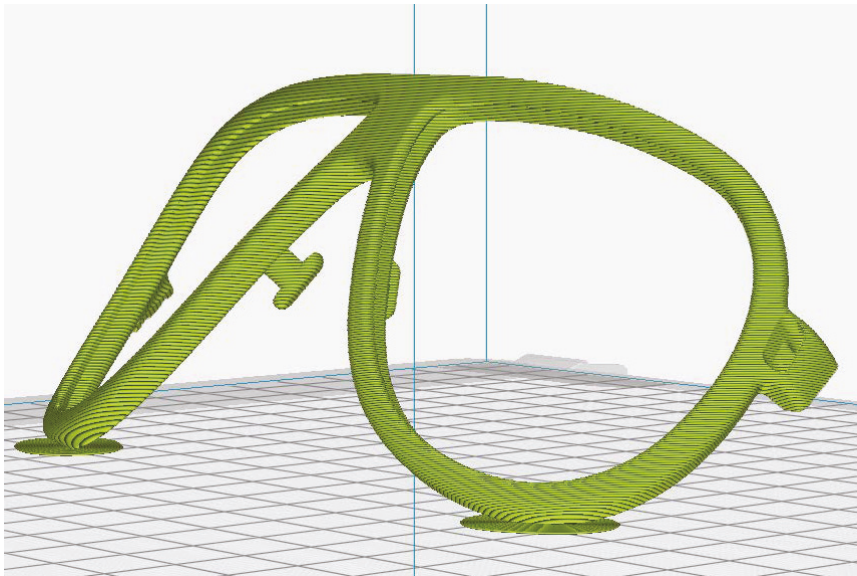


Figure 7.31: Screen grab for print bureau operator.

Application to practice through design process

At the beginning of this section, it was stated that for this scenario, it would be assumed that the part was ready for production (step 7 in the design process) and that it was no longer possible to alter the design in CAD. In practice, many designers are likely to find themselves in this scenario. For example, they may need to supply a replacement part to a customer because the original part failed in some way and broke. Perhaps the original part was built in a different material which turned out to be too weak for its intended purpose, and can now be re-evaluated through the application of the approach and tools presented here, enabling the production of a new, more reliable part.

7.4.2 Scenario 3: Redesign of a product to suit a specific polymer

For the third and final scenario, a product shall be revisited that was introduced earlier in this thesis in Section 2.3: End-use products made from 3D printed polymers. The scenario will commence by showing the product in its current state, evaluating it, and then redesigning it, using the approach and tools developed through this research to suit one of the three polymers. The product is the Visionsearch Head Distancer (see Figure 7.32), which the author designed for the company Visionsearch.



Figure 7.32: The Visionsearch Head Distancer; the black component (excluding the strap) is 3D printed.

Visionsearch is a company that engineers and distributes a system that helps people with certain visual impairments to get an accurate diagnosis and then receive therapy for their visual impairment. Part of people's interaction with the system involves them looking at a screen and reacting to cues displayed on the screen. As they go through this process, it is important that they remain at an exact distance between their eyes and the screen. The Visionsearch Head Distancer is the device designed to ensure that this distance is maintained, as shown in Figure 7.33. The distinct curve of the form is to ensure that it does not

obstruct the field of vision of a person using it while focusing on the screen. For a more detailed explanation of this project, please see Section 2.3: End-use products made from 3D-printed polymers.

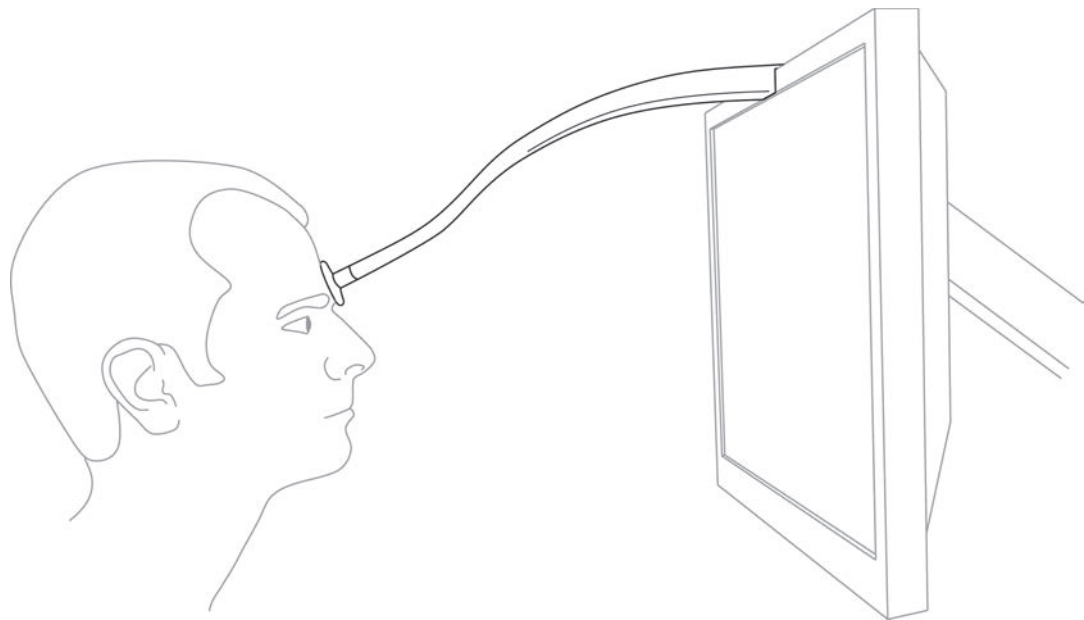


Figure 7.33: The Visionsearch Head Distancer in use.

The version of the Head Distancer, as shown in Figure 7.32, dates back to 2014 and was designed to be 3D-printed in PA using SLS. In 2014 there was not as much information about 3D printing available, which is part of the reason for conducting this research. See also Section 1.1: Background and motivation. In 2014, 3D printing in PA was much more expensive than it is now, so the Head Distancer was designed with a focus on reducing material volume, which saves cost and has less impact on the environment. Much of the decisions made while designing it were based on the product designer's pre existing experience with PA and data obtained from material data sheets. For example, it was known from the material data sheet on PA that PA parts built in the HF orientation display better tensile properties than in the V orientation. This led to the area of the part that was going to be under tension being designed as thin as was thought possible. Figure 7.34 shows a CAD image of the Head Distancer, and the area which was to be under tension is outlined in red. That area is under tension because it is used to secure the Head Distancer onto the screen by an elastic strap. The strap,

which can be seen in Figure 7.32, attaches the back end of the Head Distancer to the back of the screen, and is therefore under constant tension.

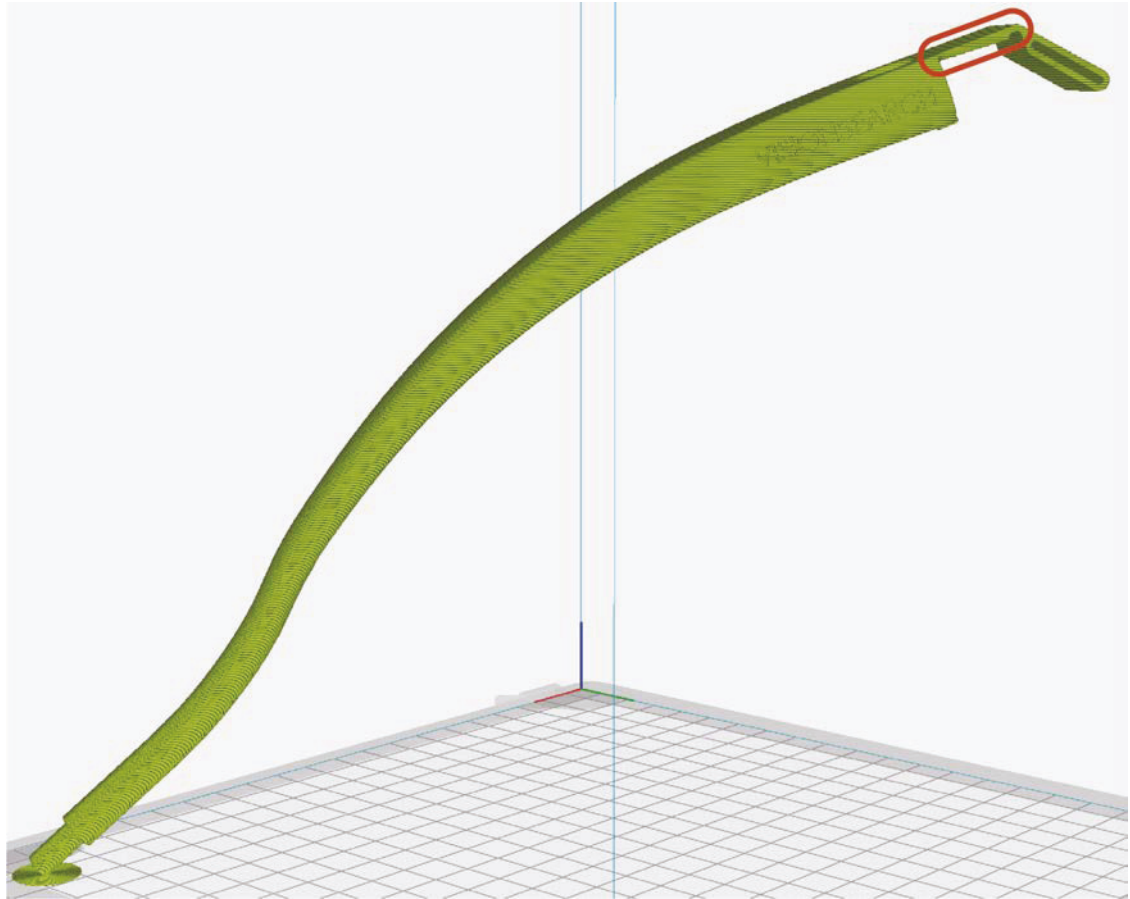


Figure 7.34: Outlined in red is the section of Head Distancer to be under tension.

Another design feature of the Head Distancer that is worth mentioning is that it was not solid but hollow; see Figure 7.35; this was done to reduce material volume which saves material and cost.

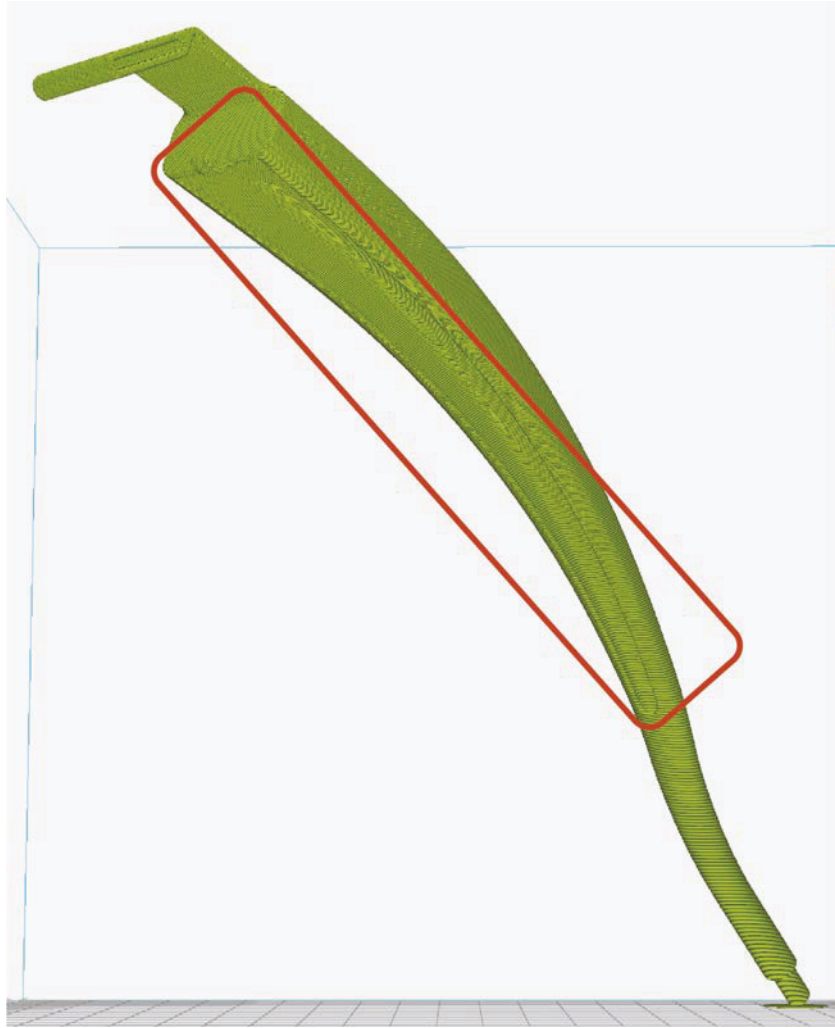


Figure 7.35: Outline in red shows how the main body was hollowed out to reduce volume.

Having established how and why the Head Distancer was designed in the way it was, the tools will be now combined into an approach that will evaluate the existing design and then redesign it to suit a different polymer. For this scenario, TPGDA will be selected, because it has not been used in any of the previous scenarios so far. Furthermore, it is the polymer that performs the worst out of the three across almost all material properties and build orientations, which makes it an interesting material to design for, because more attention needs to be paid to areas on the part that may fail due to its properties. As before, in Scenarios 1 and 2 (see Sections 7.3.1 and 7.4.1 respectively), this scenario will be worked through in stages and the decision making processes will be explained along the way. The diagram in Figure 7.36 provides a clear overview of Scenario 3 and can serve as a reference guide if anything becomes unclear.

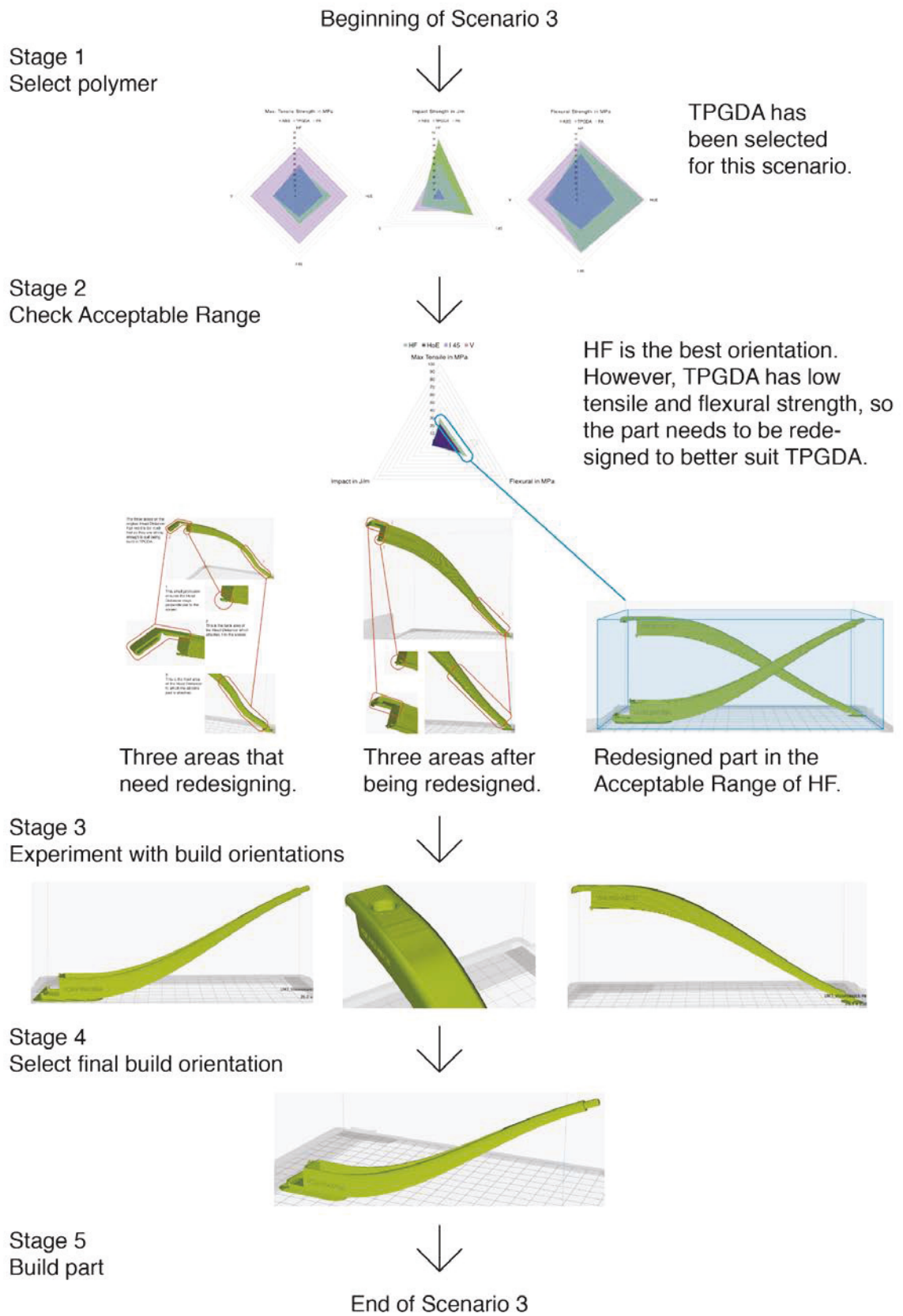


Figure 7.36: Diagram of Scenario 3.

Stage 1: select polymer

As mentioned above, TPGDA has been selected as the polymer to redesign the Head Distancer for. However, a brief comparison from the point of view of TPGDA with the other two polymers is nonetheless interesting. Due to the way the Head Distancers are used, they may need to flex and perhaps stretch, so tensile and in particular flexural properties are more important than impact. The comparison charts of the three polymers for max tensile, impact and flexural properties (see Figure 7.37) show that TPGDA doesn't perform very well when compared with ABS and PA. TPGDA is by far the worst with regard to impact strength, but for tensile strength, it is better than ABS in the HF orientation, and for flexural strength, it is again the weakest, but is best built in the HF orientation.

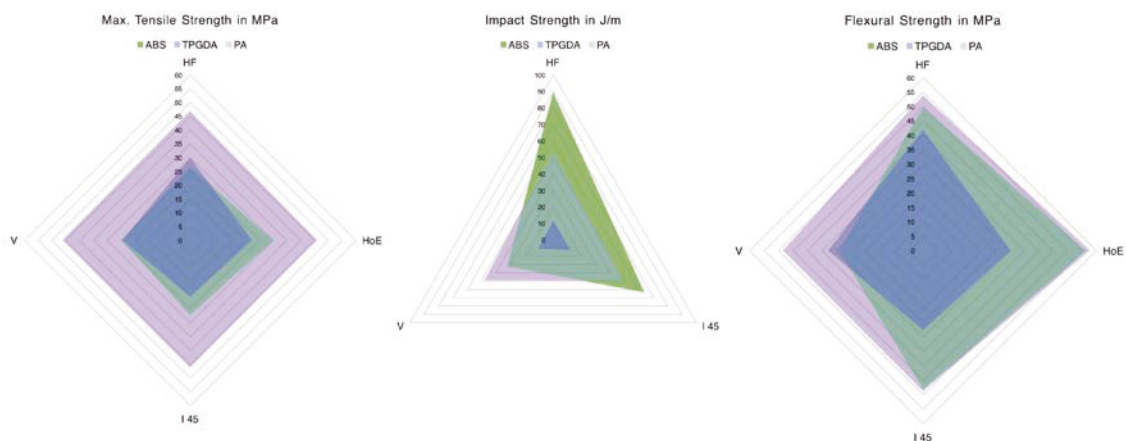


Figure 7.37: Comparison charts of the three polymers for max tensile, impact and flexural properties.

Stage 2: check the acceptable range

With the help of the TPGDA build orientation chart (see Figure 7.38) it can be confirmed that the best orientation for flexural and tensile strength is HF. In addition, the chart shows that even though HF is the best build orientation, TPGDA's flexural strength isn't very high at just over 40 MPa, and its tensile strength is not much better at 30 MPa. For these reasons, it is advisable to redesign the original version of the Head Distancer and optimise it so it better suits TPGDA.

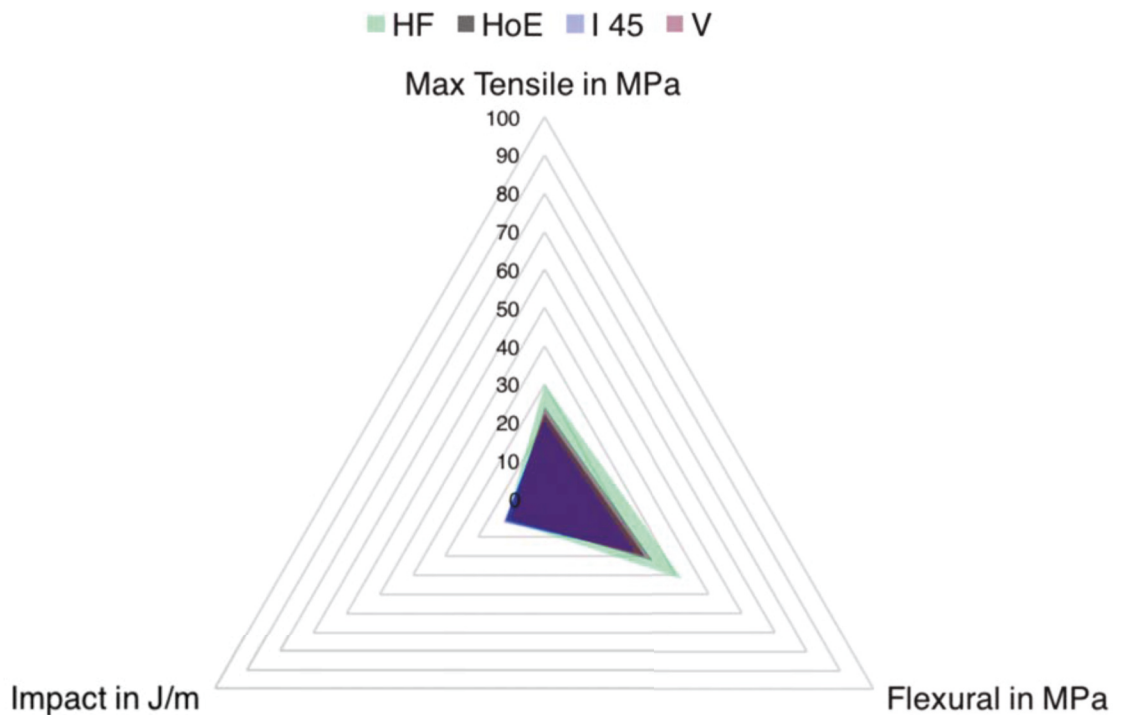


Figure 7.38: TPGDA build orientation chart.

Based on what is known about how a Head Distancer needs to perform, three areas have been identified on the original design, shown in Figure 7.39, that would be too weak if it were to be built in TPGDA, and therefore need to be modified and strengthened:

1. This is the protrusion that ensures the Head Distancer remains perpendicular to the screen by holding onto the screen bezel. Due to this it is constantly under flexural strain, and in its current form, it is likely that it will not be strong enough in TPGDA.
2. This area secures the Head Distancer to the screen with the help of the elastic strap. It is constantly under tension as well as flexural strain, and is to break if built from TPGDA.
3. This area holds the silicone pad against which people place their head while using the Visionsearch system. People need to remain in constant contact with the pad to ensure the correct distance between the person's eyes and the screen is maintained; see also Figure 7.33. For that reason, this area of the Head Distancer is under flexural strain while in use. In its

current form, this area may be strong enough in TPGDA, but it will be redesigned to ensure it won't break.

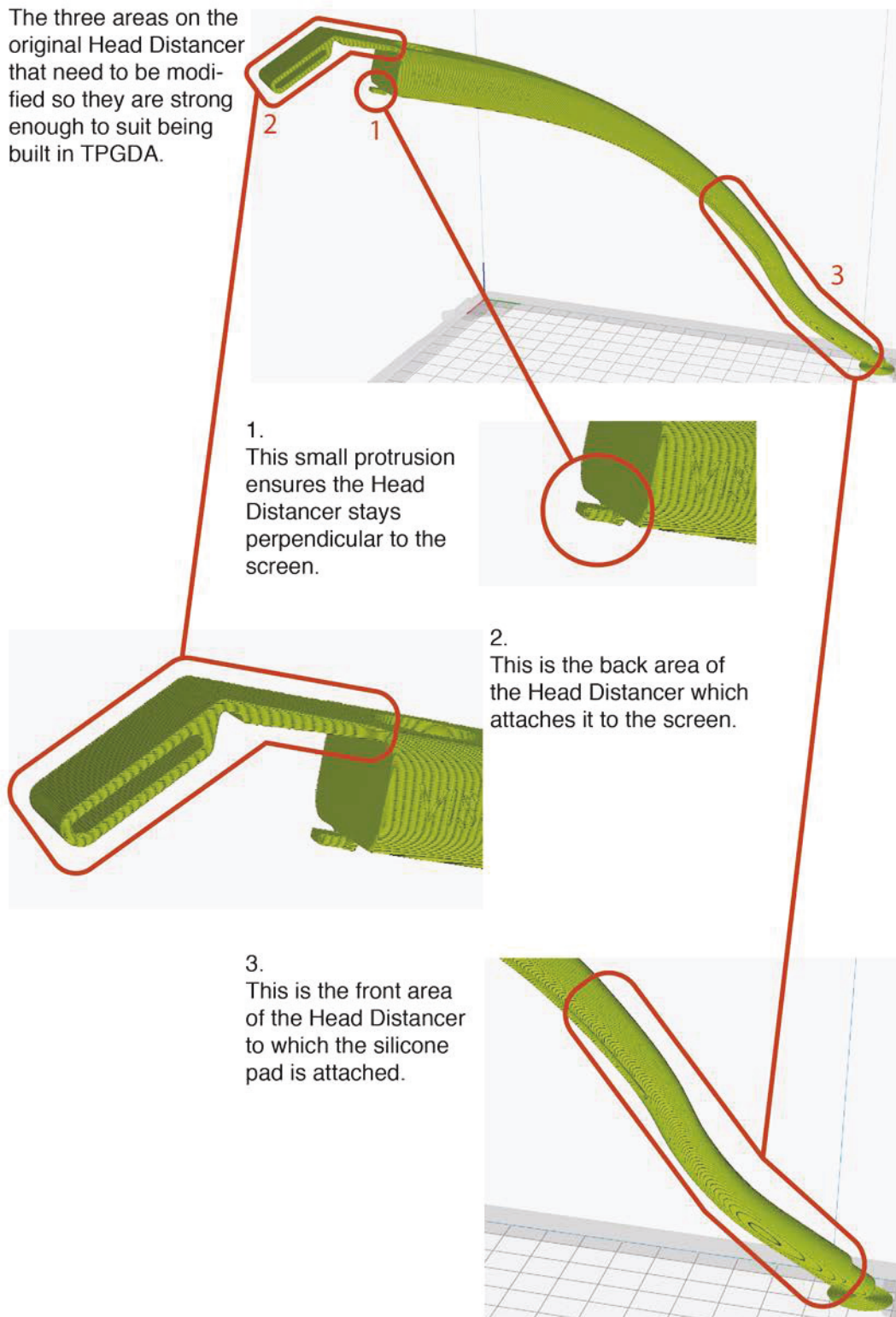


Figure 7.39: The three areas on the original design that will need to be redesigned to suit 3D printing in TPGDA.

During the redesign process, the predominant focus was on optimising the three areas discussed above. However, it wasn't possible to address and redesign each of the areas in isolation, because two of them, namely area 2 and area 3, had an effect on the overall form. This meant the redesign had to be conducted holistically, taking all necessary changes into account simultaneously. Figure 7.40 shows the final result of the Head Distancer after it was redesigned.

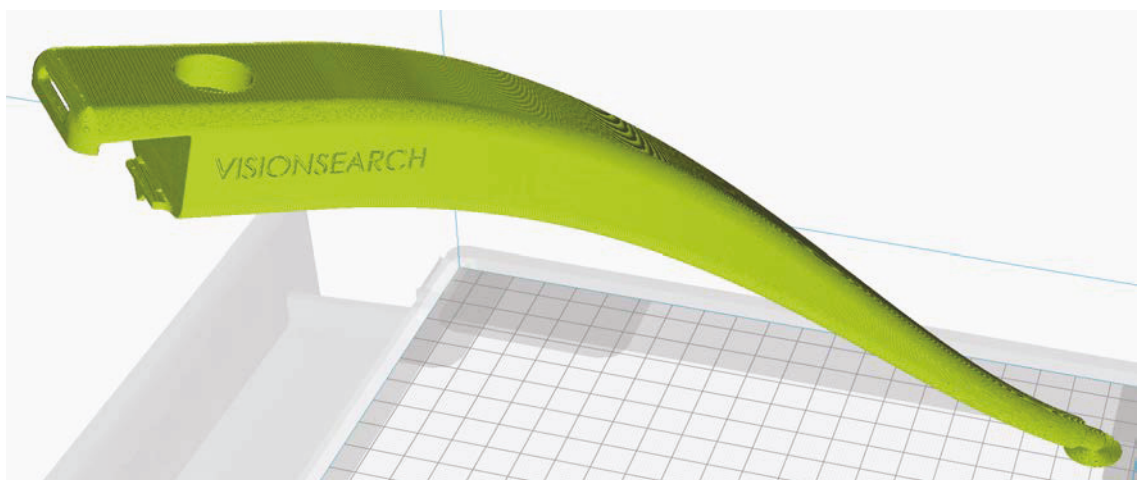


Figure 7.40: The redesigned Head Distancer.

The image is a screenshot of the CAD model; but there was more to the redesign process than simply remodelling the part in CAD. During the redesign process, several hand drawings on paper, such as sketches and orthographic drawings, were completed to evaluate the overall form, and two cardboard models were made to review crucial measurements. Considering the three areas individually, as shown in Figure 7.41, the changes can be rationalised as follows:

1. The protrusion that ensures the Head Distancer remains perpendicular to the screen was redesigned to be wider and thicker, to ensure it is less likely to crack or fracture completely.
2. Substantial changes were made to the area that secures the Head Distancer to the screen, because in its original form it was inadequate for TPGDA. Most notably, side walls were added to either side, which can be seen in the lower left of figure 7.41. However, there are elements that

can't be clearly seen in the image, such as a thicker wall thickness, and radii on the underside of the aforementioned sidewalls.

3. This is the area that holds the silicone pad against which people place their forehead; it was redesigned so the curve is less pronounced or smoother, as well as ensuring it tapers in a more gradual way towards the tip that holds the silicone pad. Both of these changes will ensure that the Head Distancer is less likely to break in this area.

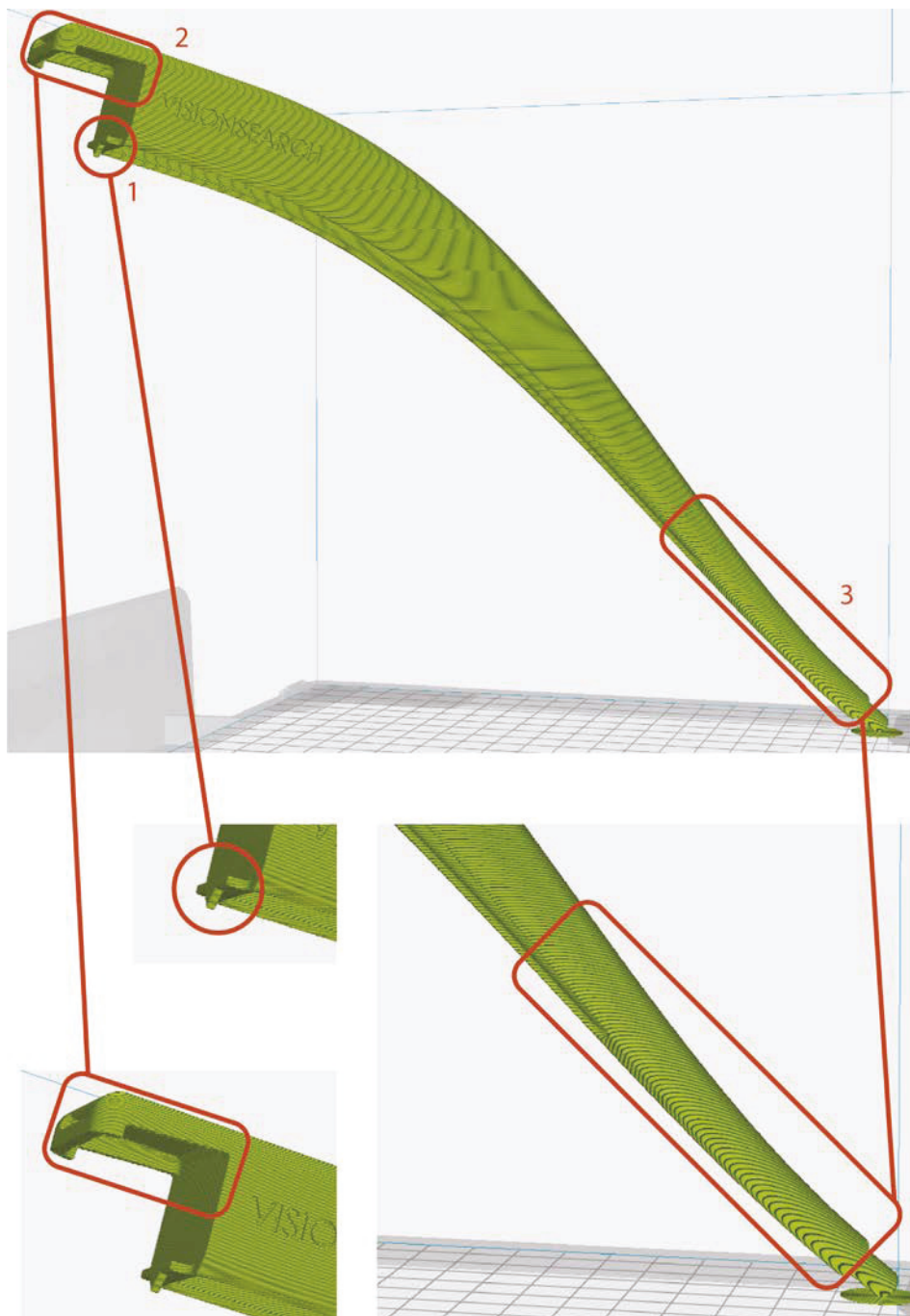


Figure 7.41: The changes to the three areas after redesigning the Head Distancer to suit TPGDA.

Having completed the redesign of the Head Distancer, Stage 2 can now be continued, and the acceptable range can be checked. The mechanical properties that are of most interest for this part are flexural and tensile, and it is known through the TPGDA build orientation chart (see Figure 7.38) that the HF orientation offers the best flexural and tensile strengths. The chart also shows that the next best option would be HoE, although the part would be somewhat weaker. To check how much weaker Tables 7.3 and 7.4, see below, will be consulted which are the tables that show the exact variation between all build orientations for tensile and flexural strength respectively.

Table 7.3:

TPGDA build orientation variations of max. tensile strength

Orientation	HF	HoE	I 45	V
HF		25% > HoE	31.8% > I 45	18.1% > Vert.
HoE	25% < HF		9% > I 45	8.5% < Vert.
I 45	31.8% < HF	9% < HoE		16.7% < Vert.
V	18.1% < HF	8.5% > HoE	16.7% > I 45	

Table 7.4:

TPGDA, build orientation variations of max. flexural strength

Orientation	HF	HoE	I 45	V
HF		27.8% > HoE	34.3% > I 45	21.7% > Vert.
HoE	27.8% < HF		9% > I 45	7.8% < Vert.
I 45	34.3% < HF	9% < HoE		16.1% > Vert.
V	21.7% < HF	7.8% < HoE	16.1% > I 45	

As the tensile strength table (see Table 7.3) shows, when compared with HF, all other build orientations are between 18.1% (for V) and 31.8% (for I 45) weaker than HF. And in the case of flexural strength, Table 7.4 shows that HF is between 21.7% (for V) and 43.3% (for I 45) stronger than all other build orientations. The lowest variation is 18%, which is considerably weaker, and too much of a risk if it needs to be ensured that the part is strong enough. As a result, the acceptable range is limited to the HF orientation.

Considering the Head Distancer is not straight or flat, what HF could mean for this part is open to interpretation. It could be in any of the orientations shown in Figure 7.42, or on its side, as seen in Figure 7.43.

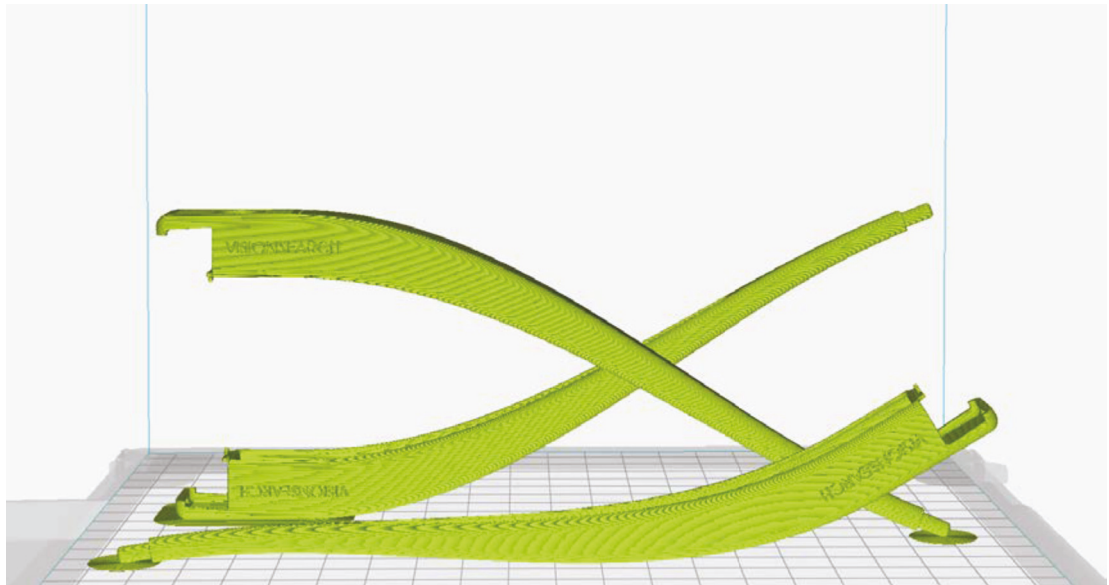


Figure 7.42: Possible HF orientations.

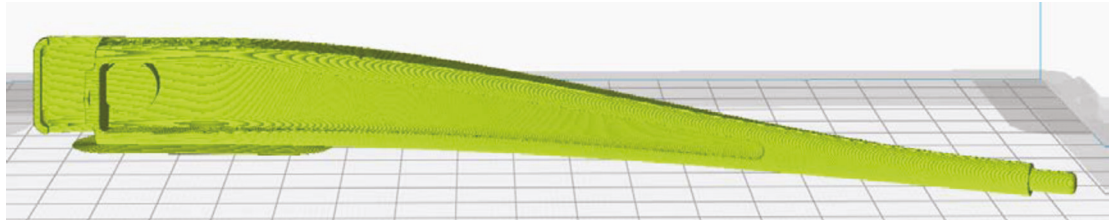


Figure 7.43: On its side could also be considered HF.

In a case such as this, a sensible strategy is to pay attention to the area that needs to be the strongest, and then make that area the focal point for the build orientation. In this case, the area framed in red in Figure 7.44 will be the focal point, because it is the area on the Head Distancer that will be under the largest amount of flexural and tensile strain, for the reasons discussed earlier; see also Figure 7.39.

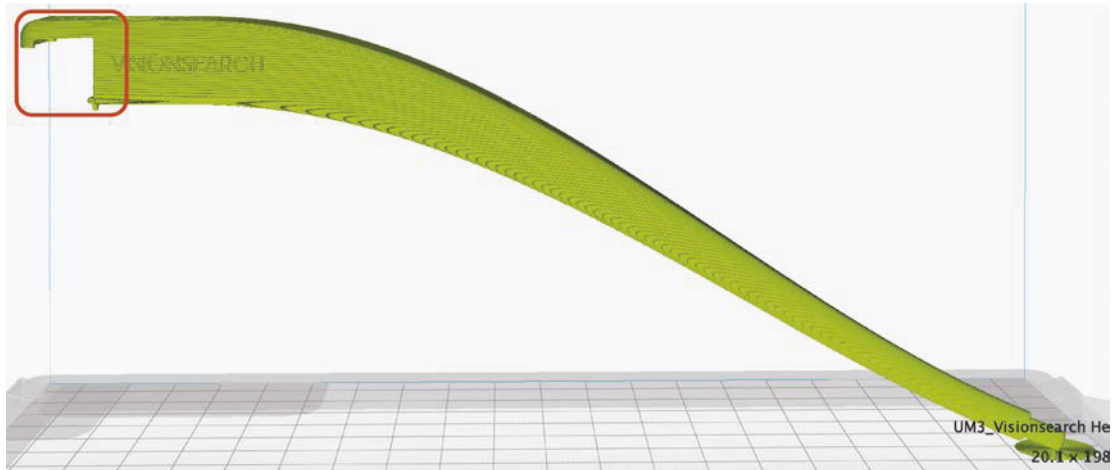


Figure 7.44: The area of focus for selection of build orientation.

If the possible HF orientations are now revisited purely from the point of view of the focal area, and in so doing, ensuring that predominantly the focal area is in the HF orientation, then the acceptable range is limited to the two orientations shown in Figure 7.45.

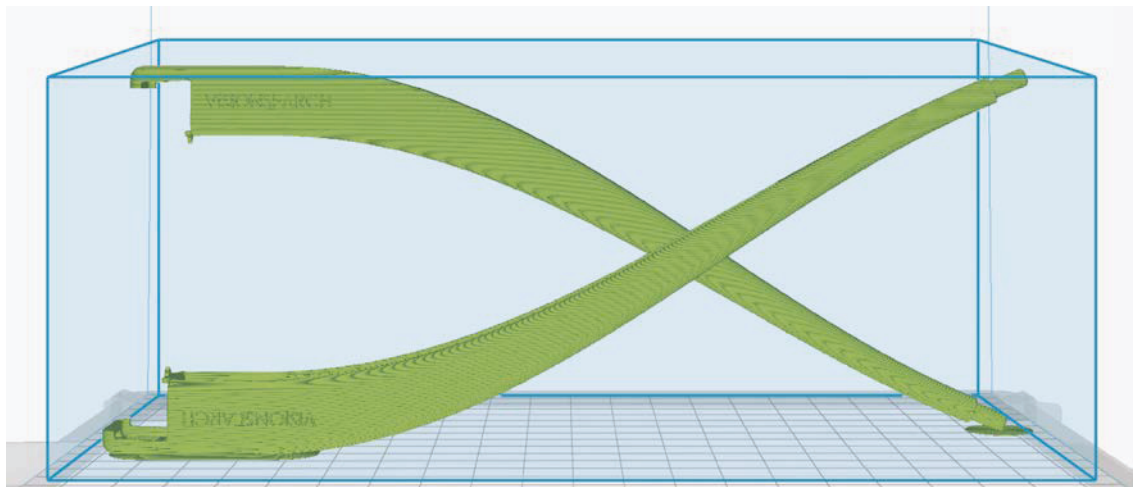


Figure 7.45: Acceptable range for scenario 3.

Stage 3: experiment with build orientations in Cura

Since the acceptable range has been limited to the HF build orientations, as shown in Figure 7.45, the opportunity to experiment with build orientations in combination with surface appearance is also limited to the two build orientations shown in Figure 7.45. For both of those orientations, the surface appearance (the appearance of the build steps) will be the same, so it is of no consequence which of the two orientations the part is built in.

Stage 4: select final build orientation

The final build orientation that has been selected for this scenario is shown in Figure 7.46. In the process, little attention has been paid to the surface appearance, because the material TPGDA chosen for this part from is rather weak. It can therefore be argued that it is more important to pay attention to the part's strength than its appearance.

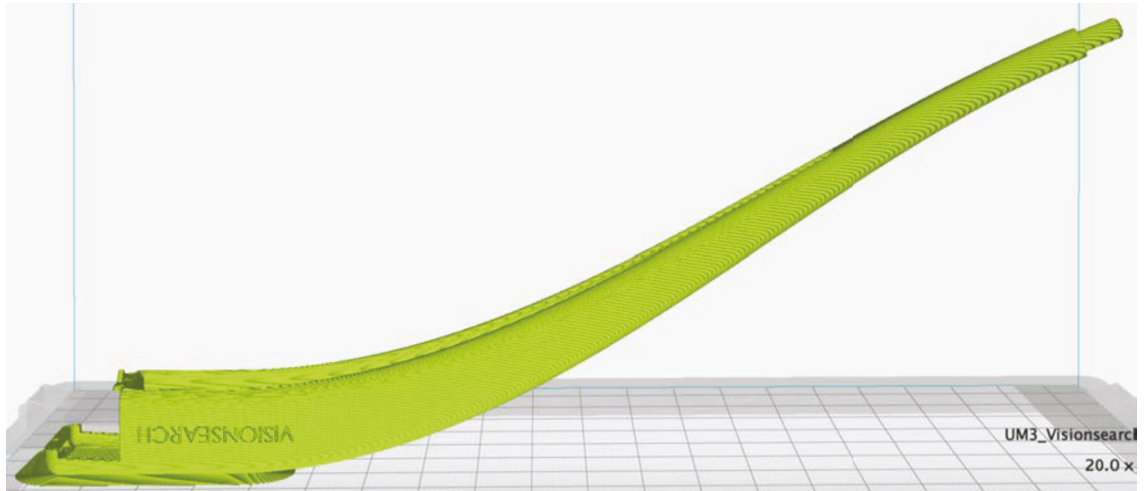


Figure 7.46: Final build orientation.

However, if desired, Cura can still be used to preview what the surface of this part will look like after it has been built. As was done during scenario 2 with the aviator frame, the CAD model can be zoomed in on in Cura to show a close-up and reveal what the surface of the Head Distancer will look like prior to building; see Figure 7.47 for an example of this.

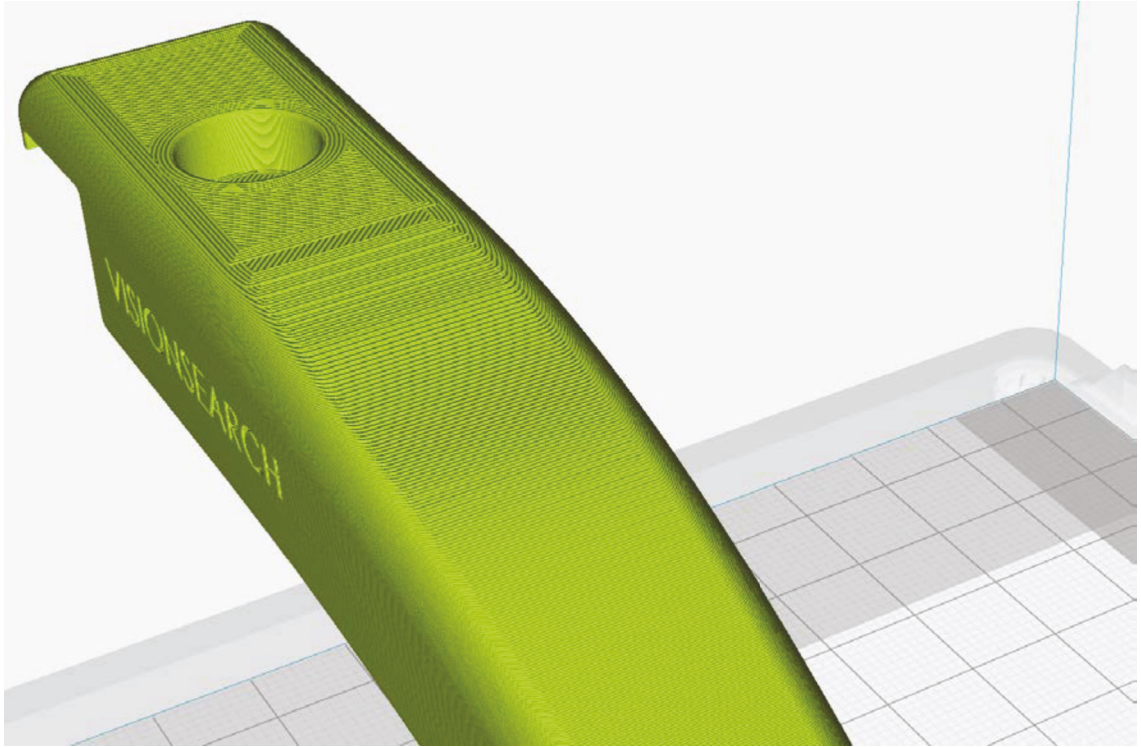


Figure 7.47: Close-up showing surface detail.

Stage 5: build part

The stl file of the Head Distancer can now be sent to a 3D printing bureau for building. To ensure that there is no misunderstanding regarding the required build orientation, it is advisable to send a screen grab (see Figure 7.48) together with the stl file.

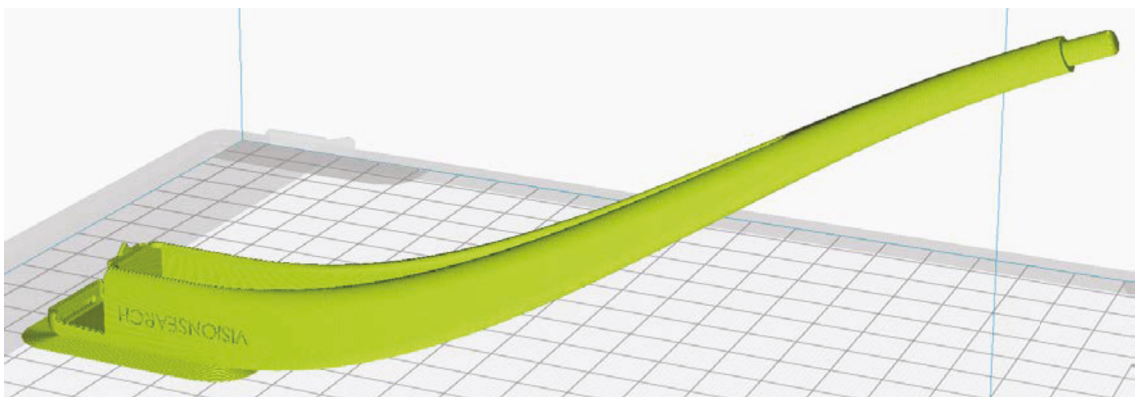


Figure 7.48: Screen grab for 3D print bureau operator.

Application to practice through design process

The focus of this scenario was the redesign of a part due to a change in polymer. The original version of the part, the Visionsearch Head Distancer, was designed to be 3D printed in PA, but it was decided to switch to TPGDA. Due to this, the part needed to be redesigned to suit TPGDA. A redesign such as this would typically occur during design development (step 5 in the design process) because, even though the form and function of the Head Distancer remained the same, the properties of the two materials are so different the design needed to be redeveloped. It would be similar to designing a part to be made in steel and then changing the material to aluminium; because the properties of the materials are very different, the part would require redevelopment. In practice, this is a scenario that many designers may find themselves in. For example, a part may have been designed to be printed in a particular material which then turns out to be too expensive, and a cheaper, less strong material is selected instead. This would mean that the part needs to be redesigned to suit the weaker material, taking a similar path to that taken in scenario 3, as discussed above.

7.5 The approach and tools in review

This chapter discusses the approach and the possible applications of all the tools developed as part of this research. This was done through case studies (see Section 7.1: Selecting a surface appearance), examples (see Section 7.2: Selecting the most suitable polymer based on a mechanical property) and by creating three scenarios (see Section 7.3.1: Scenario 1: Selecting a build orientation for ABS, Section 7.4.1: Scenario 2: Visualisation of a polymer based on max tensile strength, and Section 7.4.2: Scenario 3: Redesign of a product to suit a specific polymer). These scenarios include all three polymers and several different products and their parts. It is understood that there will be many more ways to shape an approach through the use of the tools and applying them to a multitude of different products. It is also understood that several of the decisions that were made throughout the scenarios are subjective, and that other product designers might have different opinions and will make other decisions in certain situations. For example, a different product designer may be of the opinion that tensile strength is more important than

impact strength when designing eyewear. Or they may consider the surface appearance of jewellery to be of little significance. Regardless of the situation, the approach presented here, including the tools in any kind of combination, will help designers in the future make better, more knowledge-directed decisions when it comes to finding a balance between strength, build orientation and surface appearance.

Chapter 8. Conclusion

The thesis will conclude by starting with a recap (see the following section) that explains the significance of each chapter to the research and how each chapter connects to the next. This will then lead into Section 8.2: Contribution to knowledge, which elaborates on the claimed contribution to knowledge, how it links to practice, what it can and cannot do, and what to avoid if similar research were to be conducted in the future. The Conclusion will end with Section 8.3: Wider reaching implications, that explores how this research may apply to emerging developments of 3D printing.

8.1 Thesis recap

The intention of the research presented in this thesis was to create new knowledge that makes the design process more efficient, and the decision-making process knowledge-directed for designers who are using 3D printing in polymers to manufacture handheld products for end-use.

Chapter 1.0: Introduction introduces the research in general terms and leads into Background and motivation (Section 1.1) which explains that the motivation to conduct research in this area came from the author's experience as an academic design practitioner who frequently uses 3D printing in polymers to manufacture handheld products for end-use. The specific research intention was to ascertain which build orientation would suit a part best, based on polymer selection, how strong the part needs to be based on its intended use, and how well the part's surface texture can be visualised prior to building it. To achieve this research intention, an in-depth review of the existing knowledge was conducted in Chapter 2.0: Existing knowledge and related literature, covering the topics: 3D printing (Section 2.1); The process of designing a product (Section 2.2); End-use products made from 3D printed polymers (Section 2.3); Strategies to optimise part orientation (Section 2.4); and Interacting with products (Section 2.5). Section 2.1: 3D printing, reviews: the various steps that need to be taken in the process of manufacturing a part using 3D printing technology; all current 3D printing processes; their available materials and typical applications; and how much post processing each 3D printing process requires.

The purpose of Section 2.1: 3D printing, was to build an understanding of 3D printing technology and clearly identify at which point in the manufacturing process the product designer is best placed to make decisions on material, build orientation, and surface texture. While reviewing material for Section 2.1, it became clear that decisions relating to material, build orientation and surface texture needed to be made earlier in the process, before the part is built; this led to Section 2.2: The process of designing a product.

Section 2.2 revealed that the earlier in the design process the designer knows what 3D-printing method/material is to be used, the better — preferably during concept development. This is because the strength of 3D-printed materials and orientations varies substantially, which affects the part's geometry and therefore its shape and potentially, its function.

Section 2.3: End-use products made from 3D printed polymers, begins by expanding on several case studies for which 3D-printed polymers were used to produce end-use products, and serves to highlight where the gaps in the existing knowledge were. This made it clearer what areas the research needed to focus on during the review of existing literature, to ascertain what is known about the mechanical properties of 3D-printed polymers in relation to their build orientations. By the end of Section 2.3, it is understood that, other than comparisons between horizontal and vertical build orientations, there is no existing research with regard to strength variations of 3D-printed parts that are built at an incline, and there are no studies that allow direct comparisons between the mechanical properties of polymers.

Section 2.4 Strategies to optimise part orientation, investigates whether there are any known methods and or tools that enable someone to optimise part orientation based on the mechanical properties a part might need to have. Although there are several good methods and algorithms to optimise part orientation based on parameters such as building efficiency, no one has used mechanical properties as parameters. This is not surprising, if one considers how challenging it is to be certain of the polymer's strength based on its build orientation, as highlighted in Section 2.3.

The surface texture of a product, in particular hand-held products, is important, because it has an effect on how people initially perceive it visually

and then interact with it physically, which is the focus of Section 2.5: Interacting with products. Because 3D printing technologies produce distinct surface characteristics, such as layer steps, these become design considerations that need to be incorporated into the design process. To do this, designers need to be able to see a virtual representation of the part prior to building it so they can decide how to orient the part such that it looks and feels the way they want it to. This led to a review of the methods and tools that make it possible to look at the surface of a part prior to building it. As the review shows, there are some methods that will indicate where the surface will be roughest through shaded sections on a CAD model, but there are no methods or tools that show the surface of part in the way it will actually look.

Based on what was learnt in Chapter 2.0, Chapter 3: Research questions and methodology, frames the Research Questions (Section 3.1) and the Methodology (Section 3.2) devised to answer them, and discusses where the Limitations of the scope (Section 3.3) lie for this research. Because what was learnt in Chapter 2.0 directly informs the formulation of the research questions, Chapter 3.0 begins with a discussion of the findings from Chapter 2. Based on this, two research questions were formulated:

- 1a. For each of the 3D printed polymers ABS, TPGDA and PA:
How do the tensile, flexural and impact properties vary between test samples built in HF (Horizontal Flat), HoE (Horizontal on Edge), V (Vertical) and I 45 (Incline at 45 degrees) orientations?
- 1b. Based on the results from question 1a:
How do the tensile, flexural and impact properties of the 3D printed polymers ABS, TPGDA and PA compare from polymer to polymer?
2. Which software application provides the clearest visual representation of the surface of a part prior to building?

Because the two research questions are different from one another, a methodology was developed that has two parts to it, as shown in the methodology diagram in Figure 8.1 (please note, a larger version of the diagram can be found in Chapter 3.0 under Section 3.2: Methodology).

Methodology Part 1 answers Research Question 1a and 1b, and Methodology Part 2 answers Research Question 2.

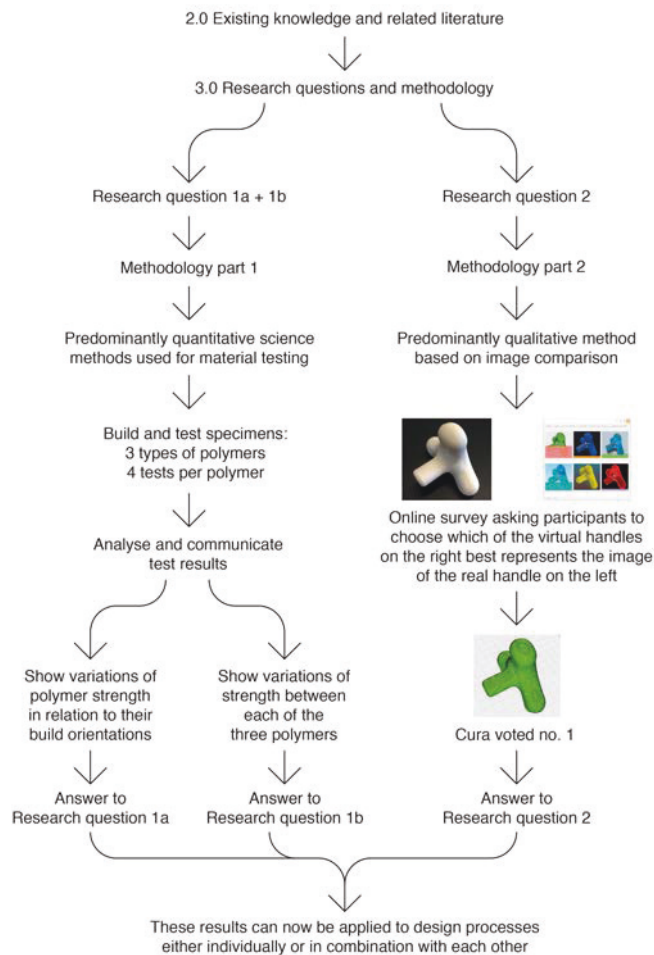


Figure 8.1: Methodology Diagram.

Chapter 3.0 concludes with three limitations that were put in place to assist with managing the scope of the research. The first limits the research to three polymers/processes, namely ABS for FDM, PA for SLS and TPGDA for MJ. The second limitation is to only test the material samples for their tensile, impact and flexural properties, and the third limitation was that the only two build parameters that could be influenced or altered were layer height and build orientation.

Chapter 4.0: Experiments is split into two sections, namely Section 4.1: Experiments to determine the mechanical properties of the three 3D printed polymers at a 45 deg incline, executing Methodology part 1, and Section 4.2:

Experiment to determine clear visual representation of the surface of a 3D-printed part prior to building, executing Methodology part 2. Section 4.1 details the ASTM standards the testing is based on, the exact dimensions of the test specimens, and how the test specimens were arranged on the build plates, to ensure the orientation of all test specimens were consistent across all required build orientations. The remainder of Section 4.1 explains the testing set up on the Shimadzu machines for the tensile and flexural tests which were done at UTS, as well as the impact testing done externally by LMats Pty Ltd. Chapter 4.0 ends with Section 4.2, which describes the process of setting up the online survey designed to determine which software provides the clearest visual representation of the surface of a 3D-printed part prior to it being built.

Chapters 5.0: Results, and 6.0: Analysis and communication of results, is where the test results are listed, first, in their elemental form (Chapter 5.0), and then, thorough analysis, are translated into data visualisations, which are easier to read, and present the results in a more communicable way (Chapter 6.0). Listing the mechanical testing results in their elemental form in Section 5.1 Mechanical property test results of the three 3D printed polymers, is useful because it will enable other researchers to use them for their own purposes. However, in their elemental form, the results couldn't answer Research Question 1a or 1b, so they were analysed and translated into radar graphs and tables in answer to the Research Question, as shown in Chapter 6.0. The radar graphs and tables can now be understood and used as a set of tools that enable product designers to make knowledge-directed decisions when it comes to designing parts to be printed in one of the three polymers. Based on the results for determining a clear visual representation of the surface of a 3D printed part prior to building which was obtained in Section 5.2: Results for a clear visual surface representation, the answer to Research Question 2 was Cura.

The title of this thesis takes on meaning in Chapter 7.0 Discussion, because this is where several new approaches using the tools developed as part of this research could find application in the design process of 3D-printed handheld products. This is done by first giving examples of how each tool can be used on its own: see Section 7.1 Selecting a surface appearance, and Section 7.2: Selecting the most suitable polymer based on a mechanical property. With the

help of three scenarios (Section 7.3: Selecting the most suitable build orientation for each polymer, and Section 7.4: Balancing mechanical properties with surface appearance) it is then demonstrated how these new approaches are applied to practice, using the tools in various combinations with each other. In so doing they achieve potential outcomes that are likely to occur when a product designer is working on a part and preparing it for 3D printing. Chapter 7.0 ends with a review of the tools with regard to their various applications; see 7.5 The approach and tools in review.

Chapter 8.0: Conclusion, commenced with a thesis recap. Section 8.2: Contribution to knowledge, will summarise the contribution that this research makes and recommend what to avoid in future research of a similar kind.

8.2 Contribution to knowledge

In this section, the significance of the findings is explained and linked to product design practice, albeit at a more general level than in the detailed examples, case studies, and scenarios presented in Chapter 7.0: Discussion.

8.2.1 A new approach for product design

This research is a significant contribution to knowledge because it provides product designers with a new approach to finding a balance between the strength and surface texture of handheld products and parts thereof to be 3D printed in polymers. This new approach consists of a set of tools in the form of data visualisations (radar graphs), tables, and software recommendations, as presented and discussed in Chapters 6.0 and 7.0 respectively, that will assist product designers with making knowledge-directed decisions when needing to optimise a part prior to 3D printing it. Before this research, not much attention has been paid to the needs of product designers in this area, despite the fact that this need is growing rapidly. This rapid growth is due to 3D printing becoming more accepted for end-use part production, and product designers realising that 3D printing has turned into a feasible manufacturing method. Until now, the research that has been conducted in this area was focused on the needs of science and engineering. Consequently, it has been conducted *by* scientists and engineers *for* scientists and engineers, and is disseminated and presented to suit their requirements; and thus could not be

linked to product design practice. This is highlighted by the fact that the vast majority of the research reviewed in Chapter 2.0 Existing knowledge and related literature, was conducted by scientists and engineers and not by product designers. This is an important distinction, because the information and tools a product designer requires are different from those of a scientist or engineer. In general terms, the research scientists and engineers conduct seeks answers to specific questions. An example of this is the work by Leutenecker-Twelsiek et al. (2016) reviewed in Section: 2.4 Strategies, to optimise part orientation. They devised a method that analyses each component of a part to determine its best orientation based on strength. Leutenecker-Twelsiek et al. did this by first deconstructing the part into each of its components, analysing each one according to the properties they required, and then reassembling the components in the most optimal way to suit 3D printing. As they worked on a product, they would tackle a question in isolation from other aspects of the product. In so doing, they did not consider the entire product in the process, but limited themselves to the specific question. In Leutenecker-Twelsiek et al.'s case they were only looking to optimise the part for its strength and not for anything else, such as overall appearance, surface texture, or usability. In practice, product designers work in a different way to this. They rarely consider a question in isolation from the other aspects of the product they are working on. During the design process, product designers are constantly attempting to find a balance between all the requirements that the product needs to meet. The approach presented here enables that to be done in a manner where product design is central to the process; previous approaches do not do that.

The approach comprises of three tools, the first and most significant of which are the radar graphs that translate the material testing results into data visualisations. They are tools that can be used by practising product designers during the design process of a product. The radar graphs provide complex information in a comprehensible way that enables product designers to make timely and knowledge-directed decisions as they work on a product. If a designer needs to compare the mechanical properties of one of the three polymers to another, the polymer comparison charts (see Figures 6.1, 6.2 and 6.3) enable them to do that. If the individual mechanical properties of one of the three polymers need to be compared, then the build orientation charts (see

Figures 6.4, 6.5 and 6.6) will facilitate that. In more general terms the data visualisation tools could be translated into other areas of product design. Here they are presented as part of an approach to designing for 3D printing. However, there are other areas of product design where designers may want to balance other types of performance criteria of the parts and products they are working on. This could be done by using the data visualisation techniques presented here in other ways by assigning different sets of criteria.

The second tool is a set of nine tables, three for each polymer (see Tables 6.1–6.9). The tables have been devised to provide accurate information regarding the differences in strength between build orientations specific to each polymer and their mechanical properties. This difference in strength is represented in percentages; for example, the impact strength of ABS is 28.6% higher in HF than in I 45. When applied to product design practice, this is valuable information that helps designers understand the relative loss or gain of a part's strength based on build orientations.

The third and last tool the approach comprises is the software application, Cura. Through Cura, parts can be manipulated to change their build orientation in the build volume, and they can be viewed and assessed for their surface texture prior to building. In this way, Cura acts as the interface of the approach, and helps translate the information from the other two tools into possible outcomes. Although it was useful to ascertain that Cura works best for this (see Section 5.2: Results for a clear visual surface representation), viewing parts can be done using other software applications that have similar capabilities to Cura. It also needs to be anticipated that software applications such as Cura will likely be outdated or superseded in the near future. This will mean that other tools that enable a clear visual surface representation of parts prior to 3D printing will take its place. Therefore, the significance of the third tool of the approach lies less in what software application is used but rather how future software applications represent the surface texture of a part.

Perhaps the most useful aspect of the approach presented here is that product designers can apply it to other materials and combinations of materials. This could be done by collecting existing data on material properties from tests

others have conducted, providing the data is verified and reliable, and translating it into a different set of radar graphs and percentage tables. In situations where the material property data is insufficient, the research presented here can be used by others to conduct their own tests on materials they are interested in using. Another aspect that is gaining momentum and is specific to 3D printing on FDM machines is that of designers creating their own materials, and more will be said about this in Section 8.3: Wider reaching implications. Designers are experimenting with recycled polymers, biodegradable polymers, and a multitude of other material combinations and composites, and if these experimental materials are to be used in live situations, they need to be tested. The approach presented here provides a methodological framework and processes within which the testing of such new material can occur.

8.2.2 Material property data

The material property data that was collected during the testing of the polymers in the various build orientations (see Chapter 4.0: Experiments) is a significant contribution to knowledge for two reasons. First, the results made it possible to develop the new approach and tools discussed in Section 8.2.1 above. This approach could not have been developed without the material property data generated through the research presented here. However, the impetus to conduct the material testing to begin with came from the realisation that material data for the three polymers was only available for horizontal and vertical orientations and no other orientations, such as at an incline. This is important, because a 3D printing machine deposits its material in horizontal layers, one on top of the previous. This makes 3D-printed materials anisotropic, which means the material will display different physical properties in one direction than in another, similar to wood. The fact that most parts are not flat or L-shaped but are curved and angled meant that having more information about the properties of materials built at an incline would be an advantage. The review of the existing knowledge and related literature (see Chapter 2.0) confirmed that no data existed for test specimens built at an incline, which led to the testing of specimens at a 45 degree incline. To ensure that the test results of specimens built at an incline could be verifiably

compared to the results of those built in horizontal and vertical orientations, all specimens for each of the three polymers were built at the same time in the same build volume, and were then all tested under the same conditions. To date, there have been no other studies on the three 3D printed polymers that are as comprehensive as this one. The second significant contribution of the material property data to knowledge is that the three different tests were conducted on each of the three polymers (ABS, TPGDA and PA) in several build orientations (HF, HoE, I 45 and V). Researchers that have limited use for or no interest in the approach discussed in Section 8.2.1 above will be able to use the test data as it is presented in Chapter 5.0: Results, for their own purposes. The data could be used to compare it with the data shown on MDS (material data sheets) that are supplied by the manufacturers of the materials. Or the test data could be cross referenced with similar studies others might conduct in the future. It is likely that researchers are currently in the process or have recently conducted studies like this one on the same or similar materials. If this is the case, then the results presented here could act as a reference point to build upon.

8.2.3 Unanticipated discoveries

There are parts of this research that were surprising. It was not expected that the maximum tensile strength of PA in SLS would be almost homogeneous across all variations of build orientation. The largest difference was between HF and V, where HF was 1.4% stronger than V, which is almost negligible. Bearing that in mind, the difference of maximum flexural strength of PA in SLS built in V was 16% weaker than HoE. Looking at those two cases side by side, the results appear to make no sense. If the tensile strength is homogeneous across all build orientations then the flexural strength should be similar. In contrast to this, the comparison of the results of the tensile and flexural properties of ABS in FDM make more sense. It was also not expected that out of all three polymers, ABS in FDM would have by far the highest impact strength in both HF and I 45 orientations.

If this research were to be repeated, the inclusion of TPGDA is not recommended. Compared to ABS and PA, it is a weak material only suitable for small parts. TPGDA was included in this research because it has found

application in many end use products in the past. However, it was found to be a volatile material that discolours in a matter of weeks and has a limited shelf life. Furthermore, it is difficult to work with, especially when it comes to general post processing, where the wax support material has first to be melted off the parts in an oven, then the parts need to be degreased by washing them by hand with detergent. Another concerning aspect to products made from 3D printed photopolymers such as TPGDA is their biocompatibility (the need to be not harmful or toxic to living tissue). Alifui-Segbaya et al. (2017) studied the health effects of TPGDA on Zebrafish embryos and concluded that is not safe to use in situation where biocompatibility is required. The minimum mortality rate of the zebrafish embryos kept in photopolymer petri dishes ranged from 15% to 100% depending on the type of photopolymer. Furthermore, Zebrafish larvae showed malformations of the tails and heads within a period of 96 hours (Alifui-Segbaya et al. 2017). The material testing for this research had been conducted before Alifui-Segbaya et al. published their research. However, if the health concerns regarding 3D printed photopolymers had been known prior to the testing, TPGDA would have been excluded from this research, and due to its adverse health effects, is not recommended to be used for any application at all.

8.3 Wider reaching implications

The above recommendation, not to use 3D-printed photopolymers at all, points to other aspects that product designers have control over and can consider when using 3D printing as a way to manufacture a product or parts thereof. Traditional DFM (design for manufacture) processes are geared towards the mass-production of products. This can limit the product designers' choice of materials and control over the manufacturing process, because it is optimised to suit mass production. There are also several other professionals involved, such as production engineers, who manage the production of the products and wholesale to retail entities that control the sale and distribution (see also Section 2.2.1: Design for Manufacturing (DFM)). Those other professionals have a say in how things are produced and how they are priced. A situation might occur where a product designer has specified a material that can be recycled, but if others involved in the process deem it

necessary to use a different material that is cheaper but cannot be recycled, there may be little the product designer can do about it. DFAM (design for additive manufacturing), in comparison, gives product designers complete control over material choice and other aspects of manufacturing the products they have designed. It will be many decades before 3D printing surpasses mass production processes such as injection moulding or die casting, if it surpasses them at all. However, the 3D printing industry is advancing rapidly. Since this research was commenced, new processes have become available that are relevant to FDM and SLS. For example, there are now FDM machines that are capable of building parts at 0.06 mm layer height, which is finer than the standard layer heights of 0.25mm to 0.1mm. This gives parts a smoother surface and allows for more detailed features on parts. Also, in the FDM, space research is being conducted into multi-axis toolpath variation, predominantly through the use of robots as 3D printers. Multi-axis toolpath variation allows the toolpath of the extrusion head to be changed from horizontal to angled and curved layers (Murtezaoglu et al. 2018). Even though multi-axis toolpath variation has developed rapidly in recent years, the idea is not new and was investigated by Singamneni et al. in 2010, although they referred to it as 'curved-layer fused deposition modelling' (Singamneni et al. 2010). This is an interesting direction, because it can both reduce the stair stepping effect to produce a smoother surface, and enhance the flexural strength of parts fabricated by curved layer, fused deposition modeling (Guan et al. 2015). New SLS processes have also emerged, such as HP's Multi-Jet Fusion technology; this is capable of exposing an entire layer of powder in one pass, as opposed to conventional SLS technology that requires a single laser beam to melt the layer by tracking the entire cross section of a layer. This makes HP's Multi-Jet Fusion technology much faster and more time efficient than conventional SLS machines. Those examples, of finer surface detail, multi-axis toolpath variation, and shorter build time, give an indication of how rapidly 3D printing technology is advancing. Contemporaneous to this are the new materials that are being developed as well as existing materials that are being made 3D printable. Materials ranging from high end polymers such as Polycarbonate (PC) to composite materials such as Polyamide-Carbon Fiber composites are now commonplace. This offers product designers more materials to choose from, which gives them a higher degree of control, but also, a higher degree of

responsibility. For example, if a product designer wants to only use biocompatible polymers that are 100% recyclable and/or 100% biodegradable, then that is possible without the need to involve anyone else in that decision.

There have also been disruptions within the 3D printing industry itself. Since 2015, several patents around 3D printing technology held by large 3D printing corporations, such as Stratasys and EOS, have expired. This has created a “free market” type of environment, and as a result, a multitude of new 3D printing businesses have emerged who are taking advantage of the now freely available technology, and are manufacturing and supplying 3D printing machines at a much lower cost than the larger corporations. This in turn has begun to make 3D printing technology accessible to businesses, which are now able to purchase machines and produce parts at a much lower cost; this means more and more businesses are able to use 3D printing as a manufacturing method. This reduction in the cost of 3D printing machines has also led to other avenues of experimentation. Because the machines are less expensive, there is less risk or loss of capital investment if a machine is damaged. As a result, product designers are conducting research into non-proprietary, or homemade, materials where materials are being invented to suit the needs of product designers. These materials are then experimented with and tested on the cheaper machines. An example of this is the work by Rael & San Fratello, who use industrial waste such as sawdust and discarded car tyres to create new materials and 3D print new products from them (2018).

3D printing is a digital manufacturing method. Product designers designing products to be made using 3D printing depend on CAD software applications such as Solidworks to design the parts. Because 3D printing machines require a digital file to print the physical part, the design process cannot be done without CAD. Considering that the approach and tools presented here make the designing of end-use parts to be 3D printed easier, and since CAD is a necessary part of the process, it would be worth considering combining the two. As was discussed in Section 2.2.2: Designing for 3D printing/additive manufacturing (DFAM), one of the main challenges DFAM faces is that the CAD tools used in product design, such as, Solidworks Rhinoceros and SharkCAD Pro, were not developed with 3D printing in mind, and therefore do not accommodate or support the needs a product designer might have when

designing a product for 3D printing. Product designers need CAD software that assesses the microstructure of a material based on a 3D printed material. For example, the microstructure of the material and the desired behaviour or physical requirements of the product are automatically matched to a chosen build orientation in CAD, which then is able to provide information about part strength and surface texture. This is currently possible with finite element analysis (FEA) tools in CAD, but is limited to homogeneous materials that are not anisotropic. Other CAD applications that are heading in the right direction are based on mathematical methods such as topology optimisation that optimises material distribution within a given part based on predetermined constraints.

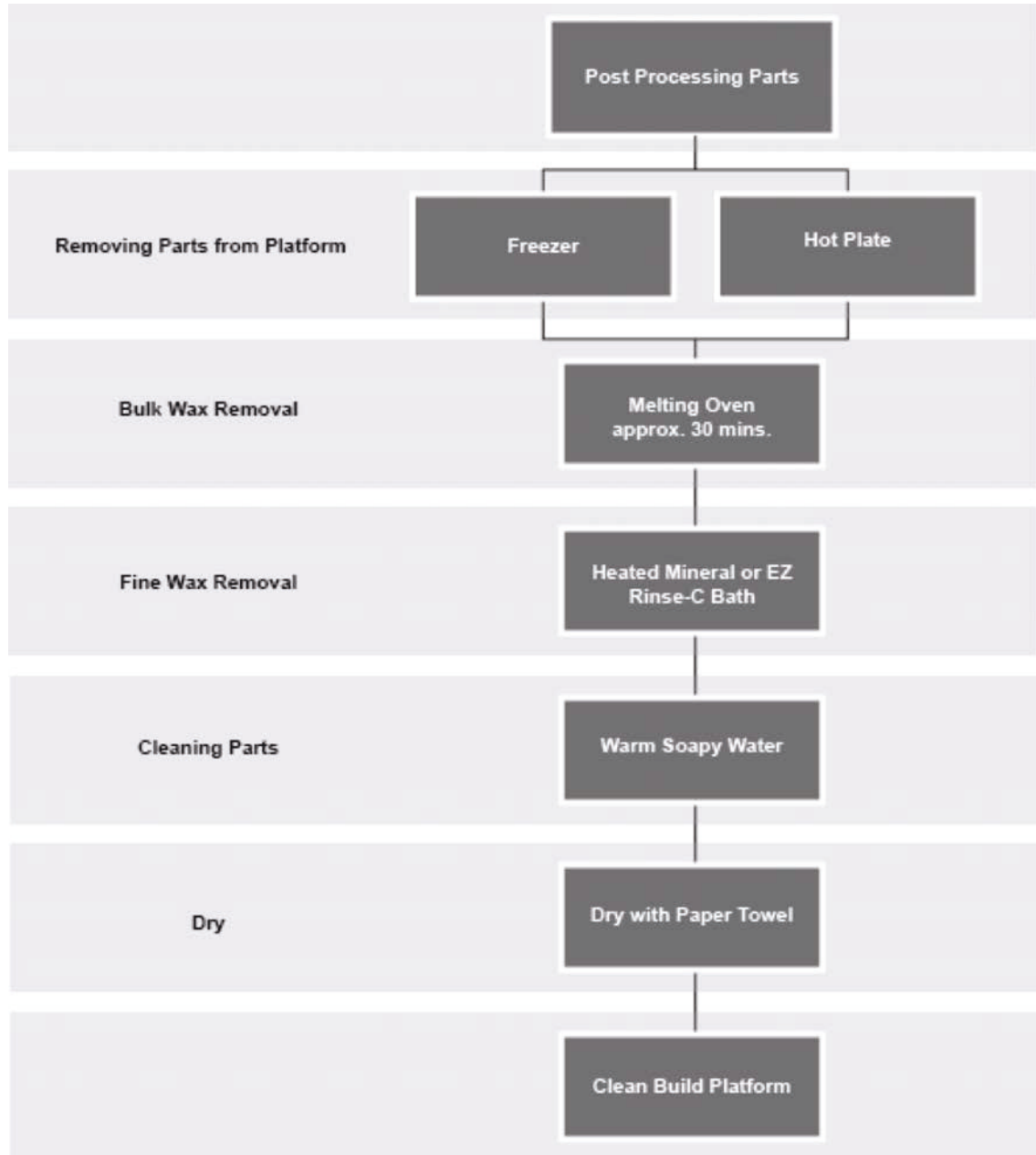
In the context of these developments, it will be challenging for research in this area to keep up with the pace. However, because the use of 3D printing to manufacture end-use products will continue to increase, product designers will need to find ways to ensure they can guarantee that the products they design and make are safe to use, and can be repaired, recycled and disposed of in ways that are safe for our natural environment. For this reason, continued research and experimentation in this area remains important.

End

Appendices

Appendix A

ProJet (Material Jetting) general post processing wax removal process.



Appendix B

Supplier material data sheets for ABS, TPGDA and PA.



ABSplus™ is a true production-grade thermoplastic that is durable enough to perform virtually the same as production parts. When combined with Design Series 3D Printers, ABSplus is ideal for building 3D models and prototypes in an office environment.

MECHANICAL PROPERTIES	TEST METHOD	ENGLISH	METRIC
		XZ AXIS	XZ AXIS
Tensile Strength, Ultimate (Type 1, 0.125", 0.2"/min)	ASTM D638	4,700 psi	33 MPa
Tensile Strength, Yield (Type 1, 0.125", 0.2"/min)	ASTM D638	4,550 psi	31 MPa
Tensile Modulus (Type 1, 0.125", 0.2"/min)	ASTM D638	320,000 psi	2,200 MPa
Tensile Elongation at Break (Type 1, 0.125", 0.2"/min)	ASTM D638	6%	6%
Tensile Elongation at Yield (Type 1, 0.125", 0.2"/min)	ASTM D638	2%	2%
IZOD Impact, notched (Method A, 23°C)	ASTM D256	2.0 ft-lb/in	106 J/m

MECHANICAL PROPERTIES	TEST METHOD	ENGLISH		METRIC	
		XZ AXIS	ZX AXIS	XZ AXIS	ZX AXIS
Flexural Strength (Method 1, 0.05"/min)	ASTM D790	8,450 psi	5,050 psi	58 MPa	35 MPa
Flexural Modulus (Method 1, 0.05"/min)	ASTM D790	300,000 psi	240,000 psi	2,100 MPa	1,650 MPa
Flexural Strain at Break (Method 1, 0.05"/min)	ASTM D790	4%	4%	2%	2%

THERMAL PROPERTIES ¹	TEST METHOD	ENGLISH	METRIC
Heat Deflection (HDT) @ 66 psi	ASTM D648	204°F	96°C
Heat Deflection (HDT) @ 264 psi	ASTM D648	180°F	82°C
Glass Transition Temperature (T _g)	DSC (SSYS)	228°F	108°C
Melting Point	-----	Not Applicable ²	Not Applicable ³
Coefficient of Thermal Expansion	ASTM E831	4.90x10 ⁻⁶ in/in/°F	8.82x10 ⁻⁶ mm/mm/°C

STRATASYS.COM

stratasys

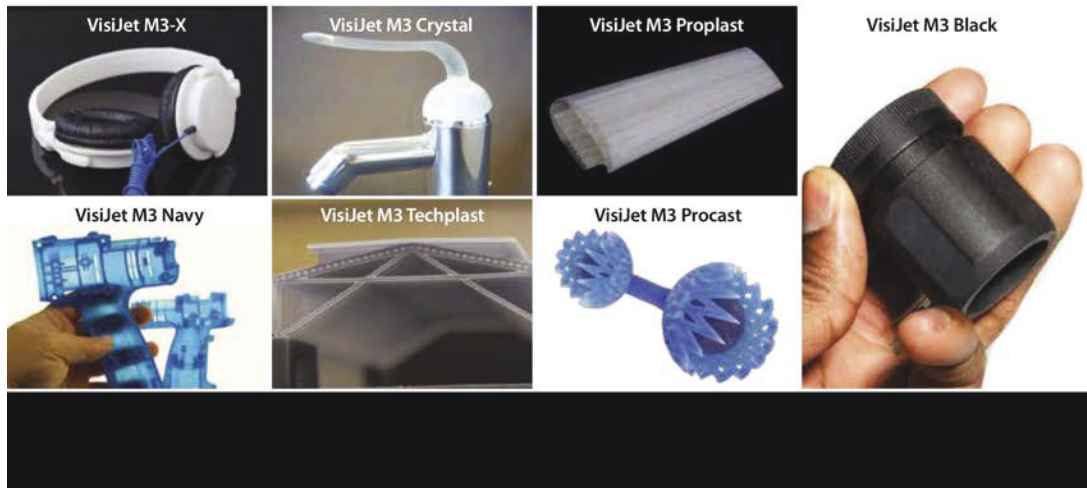
THE 3D PRINTING SOLUTIONS COMPANY

VisiJet® M3 Materials for ProJet SD & HD Printers

The VisiJet line of plastic materials offers numerous capabilities to meet a variety of commercial applications. 3D Systems' ProJet 3500 3D printers use VisiJet M3 materials to build accurate, high-definition models and prototypes for proof of concept, functional testing, master patterns for moldmaking, and direct investment casting. Vertical markets for the ProJet 3500 line include transportation, energy, consumer products, recreation, healthcare and education. Toughness, high temperature resistance, durability, stability, watertightness, biocompatibility and castability are a few of the key attributes you will find within the VisiJet M3 materials line. Parts can be drilled, glued, painted, plated, etc. Support material offers easy, non-hazardous post-processing and preserves delicate features.

Properties	Condition	VisiJet M3-X	VisiJet M3 Black	VisiJet M3 Crystal	VisiJet M3 Proplast	VisiJet M3 Navy	VisiJet M3 Techplast	VisiJet M3 Procast	VisiJet® S300
Composition		UV Curable Plastic							Wax Support Material
Color		White	Black	Natural	Natural	Blue	Gray	Dark Blue	White
Bottle Quantity		2 kg	2 kg	2 kg	2 kg	2 kg	2 kg	2 kg	2 kg
Density @ 80 °C (liquid)	ASTM D4164	1.04 g/cm ³	1.02 g/cm ³	1.02 g/cm ³	1.02 g/cm ³	1.02 g/cm ³	1.02 g/cm ³	1.02 g/cm ³	N/A
Tensile Strength	ASTM D638	49 MPa	35.2 MPa	42.4 MPa	26.2 MPa	20.5 MPa	22.1 MPa	32 MPa	N/A
Tensile Modulus	ASTM D638	2168 MPa	1594 MPa	1463 MPa	1108 MPa	735 MPa	866 MPa	1724 MPa	N/A
Elongation at Break	ASTM D638	8.3 %	19.7 %	6.83 %	8.97 %	8 %	6.1 %	12.3 %	N/A
Flexural Strength	ASTM D790	65 MPa	44.5 MPa	49 MPa	26.6 MPa	28.1 MPa	28.1 MPa	45 MPa	N/A
Heat Distortion Temperature @ 0.45MPa	ASTM D648	88 °C	57 °C	56 °C	46 °C	46 °C	46 °C	N/A	N/A
Ash Content		N/A	N/A	N/A	0.01 %	0.01 %	0.01 %	0.01 %	N/A
Melting Point		N/A	N/A	N/A	N/A	N/A	N/A	N/A	60 °C
Softening Point		N/A	N/A	N/A	N/A	N/A	N/A	N/A	40 °C
USP Class VI Certified*		No	No	Yes	No	No	No	No	N/A
ProJet Compatibility		SD, HD	SD, HD	SD, HD	SD, HD	SD, HD	SD, HD	HD	SD, HD
Description		ABS-like Plastic	High strength & flexibility plastic	Tough Plastic, Translucent	Plastic, Natural	Plastic, Blue	Plastic, Gray	Castable Plastic	Non-toxic wax material for hands-free melt-away supports

DISCLAIMER: It is the responsibility of each customer to determine that its use of any VisiJet® material is safe, lawful and technically suitable to the customer's intended applications. The values presented here are for reference only and may vary. Customers should conduct their own testing to ensure suitability for their intended application.



Material Data Sheet

Fine Polyamide PA 2200 for EOSINT P

Application:

PA 2200 is suitable for use in all EOSINT P systems with fine polyamide option. The recommended layer thickness is 0.15 mm. Unexposed powder can be reused. Depending on building time it has to be mixed with fresh powder by a ratio of 2:1 to 1:1 (old : new) in order to guarantee constant process parameters and persisting part quality.

Typical applications of the material are fully functional prototypes with high end finish right from the process. They easily withstand high mechanical and thermal load.

Material Properties:

Average grain size	Laser diffraction	60	µm
Bulk density	DIN 53466	0,435 - 0,445	g/cm ³
Density of laser-sintered part	EOS-Method	0,9 - 0,95	g/cm ³

Mechanical Properties:*

Tensile Modulus	DIN EN ISO 527	1700 ± 150	N/mm ²
Tensile strength	DIN EN ISO 527	45 ± 3	N/mm ²
Elongation at break	DIN EN ISO 527	20 ± 5	%
Flexural Modulus	DIN EN ISO 178	1240 ± 130	N/mm ²
Charpy - Impact strength	DIN EN ISO 179	53 ± 3,8	kJ/m ²
Charpy - Notched impact	DIN EN ISO 179	4,8 ± 0,3	kJ/m ²
Izod – Impact Strength	DIN EN ISO 180	32,8 ± 3,4	kJ/m ²
Izod – Notched Impact Strength	DIN EN ISO 180	4,4 ± 0,4	kJ/m ²
Ball indentation hardness	DIN EN ISO 2039	77,6 ± 2	
Shore D - hardness	DIN 53505	75 ± 2	

Appendix C

Load cell certification by Australian Calibration Services.



**AUSTRALIAN
CALIBRATING
SERVICES (A'SIA) PTY. LTD.**
A.B.N. 33 623 153 735

23 / 31 Wentworth Street, Greenacre
P.O. Box 439, Greenacre, NSW. 2190, Australia
Phone: +61 2 9642 6588, Fax: +61 2 9742 6454

File No.: N148A-F-1
Issue Date: 27 Jul 2016
Page 1 of 2

SCN020v3.37

CALIBRATION REPORT A UNIVERSAL TESTING MACHINE

FOR: UNIVERSITY OF TECHNOLOGY SYDNEY
MICROSTRUCTURAL ANALYSIS UNIT
BUILDING 2, 745 HARRIS STREET
ULTIMO NSW 2007

LOCATION: Level 1, Room 43A Materials Testing Laboratory

DATE OF TEST: 27 July 2016

EQUIPMENT DETAILS:	Machine	Load Cell	Load Cell
Maker:	SHIMADZU	SHIMADZU	SHIMADZU
Serial Number:	133075030426	700235	12061018
Plant Number:	Nil		
Type:	AGS-X	AGSX 10kN	AGS-X 500N
Ranges:	10 kN x 0.001 kN,	500 N x 0.01 N	

Aux Equipment: 500 N Load Cell & Computer VDU
Force Application: Screw Actuated
Force Indication: Digital Indicator with Trapezium Lite X Software

TEST DETAILS:

- Australian Standard AS 2193 - 2005 "Force Measuring Systems of Testing Machines."
- The testing machine was calibrated in tension & compression over a series of three tests.
- The method of calibration adopted was in accordance with clause 3.3.6.2.(a).
- The ambient temperature at the time of calibration was $22.5^{\circ}\text{C} \pm 1^{\circ}\text{C}$.
- Approved Devices were used.
Reference Numbers. N.AC/0001-9La&9Lb-3, N.AC/0001-9Na&9Nb-3 & N.AC/0001-9Ka&9Kb-3.
- Uncertainty Confidence Level = 95%

PRELIMINARY INSPECTION:
The Equipment was in an operational condition as found

Signed
G. Ainsworth

Approved Signatory

AUSTRALIAN CALIBRATING SERVICES (A'SIA) PTY LIMITED



NATA Accredited Laboratory Number 1239. Accredited for compliance with ISO/IEC 17025.
The results of the tests, calibrations and/or measurements included in this document are traceable to Australian/National Standards.
This Report shall not be reproduced except in full.

Appendix D

Sample spreadsheet of recorded tensile specimen dimensions.

07/12/2017: Tensile strength (rate = 5mm/min)

Sample	Temp. (celcius)	Humidityt(%)	GL	Position	Thickness (mm)
FDM V1	27	11	50.58	Top	3.23
				centre	3.24
				bottom	3.23
FDM V2	27	11	49.39	Top	3.3
				centre	3.32
				bottom	3.31
FDM V3	27	11	49.77	Top	3.3
				centre	3.31
				bottom	3.28
FDM V4	27	11	49.93	Top	3.24
				centre	3.26
				bottom	3.25
FDM V5	27	44	49.25	Top	3.28
				centre	3.3
				bottom	3.31
FDM A1	27	44	49.43	Top	3.3
				centre	3.26
				bottom	3.26
FDM A2	27	44	50.48	Top	3.26
				centre	3.27
				bottom	3.28
FDM A3	27	44	49.03	Top	3.26
				centre	3.25
				bottom	3.3
FDM A4	27	44	51.3	Top	3.28
				centre	3.26
				bottom	3.27
FDM A5	27	45	50.8	Top	3.26
				centre	3.27
				bottom	3.28
FDM HF1	26	45	49	Top	3.17
				centre	3.19
				bottom	3.19

Appendix E

Izod impact testing report by LMATS Pty Ltd.



- ✓ NDT & Inspection
- ✓ Hydrostatic testing
- ✓ Weld qualification
- ✓ Concrete testing
- ✓ Mechanical testing
- ✓ Metallurgical services
- ✓ Chemical analysis & PMI
- ✓ Pressure plant inspection

IZOD IMPACT STRENGTH MEASUREMENT OF: 3D Printed Polymer Samples



Client:

University Of Technology Sydney
15 Broadway
Ultimo NSW 2007
Customer ABN: 77 257 686 961

Job Details

LMATS Job Number: LS16-1079
Client Purchase Order: STEFAN
LMATS Quote Ref: QS15-0514
LMATS Invoice: 00023747
Test Date: 19th October 2016
Scope: 15 FDM Samples (5 Angle, 5 Horizontal, 5 Vertical)
15 Resin Samples (5 Angle, 5 Horizontal, 5 Vertical)
15 SLS Samples (5 Angle, 5 Horizontal, 5 Vertical)

LS15-1079 University Of Technology Sydney

LMATS Pty Ltd
ABN: 41 107 100 925
www.lmats.com.au

Melbourne 03 9399 8145
Sydney 02 9648 1989
Brisbane 07 3875 2070
Albury 02 9648 1989

6 Techno Park Drive, Williamstown, VIC - 3016
1C/137 Silverwater Road, Silverwater, NSW - 2128
14/121 Kerry Road, Archerfield, QLD - 4108
Suite 4/10-12 High Street, Wodonga VIC 3690

1. Objective

The objective of this study is to measure the Izod impact strength of polymer samples.

2. Samples Supplied

45 samples of block polymers were supplied for izod impact strength testing.

The identifications of the samples were:

15 FDM Samples (5 Angle Samples, 5 Horizontal Samples, 5 Vertical Samples)

15 Resin Samples (5 Angle Samples, 5 Horizontal Samples, 5 Vertical Samples)

15 SLS Samples (5 Angle Samples, 5 Horizontal Samples, 5 Vertical Samples)

3. Testing Undertaken

Izod Impact Strength measurement testing was undertaken according to ASTM D 256 using Test Method A

4. Specimen Preparation

The Izod Impact strength specimens were provided by customer and notched by using Izod impact specimen notcher (International Equipment's S/N 221)

5. Specimen Conditioning

The specimens were conditioned for 40 hours at 24°C and 51% R.H. following notching.

Izod Impact (ASTM D 256) V3 20160712 RP



Accredited Laboratory
ISO/IEC 17025

6. Test Results

FDM Samples (5 Angle Samples)

Pendulum Correction : 0.01J

Specimen	Specimen Width at Notch (mm)	Notch Depth (mm)	Impact Energy (Joule)	Corrected Impact Energy (Joule)	Izod Impact (J/m)	Failure Type*
1	12.76	10.14	0.78	0.77	60.3	C
2	12.74	10.17	0.78	0.77	60.4	C
3	12.72	10.19	0.86	0.85	66.8	C
4	12.69	10.18	0.86	0.85	67.0	C
5	12.70	10.15	0.83	0.81	63.8	C
Mean					63.7	
Standard Deviation					3.3	

*C = Complete Break— A break where the specimen separates into two or more pieces.

H = Hinge Break— An incomplete break, such that one part of the specimen cannot support itself above the horizontal when the other part is held vertically (less than 90° included angle).

P = Partial Break— An incomplete break that does not meet the definition for a hinge break but has fractured at least 90 % of the distance between the vertex of the notch and the opposite side.

NB = Non-Break— An incomplete break where the fracture extends less than 90 % of the distance between the vertex of the notch and the opposite side.

Accredited Laboratory
ISO/IEC 17025

Izod Impact (ASTM D 256) V3 20160712 RP

6. Test Results (cont.)

FDM Samples (5 Horizontal Samples)

Pendulum Correction : 0.01J

Specimen	Specimen Width at Notch (mm)	Notch Depth (mm)	Impact Energy (Joule)	Corrected Impact Energy (Joule)	Izod Impact (J/m)	Failure Type*
1	12.66	10.50	1.12	1.11	87.7	C
2	12.67	10.50	1.23	1.22	96.3	C
3	12.63	9.31	1.12	1.11	87.9	C
4	12.68	10.60	1.18	1.17	92.3	C
5	12.69	10.70	1.05	1.04	82.0	C
Mean					89.2	
Standard Deviation					5.4	

*C = *Complete Break*— A break where the specimen separates into two or more pieces.
H = *Hinge Break*— An incomplete break, such that one part of the specimen cannot support itself above the horizontal when the other part is held vertically (less than 90° included angle).
P = *Partial Break*— An incomplete break that does not meet the definition for a hinge break but has fractured at least 90 % of the distance between the vertex of the notch and the opposite side.
NB = *Non-Break*— An incomplete break where the fracture extends less than 90 % of the distance between the vertex of the notch and the opposite side

Izod Impact (ASTM D 256) V3 20160712 RP



6. Test Results (cont.)

FDM Samples (5 Vertical Samples)

Pendulum Correction : 0.01J

Specimen	Specimen Width at Notch (mm)	Notch Depth (mm)	Impact Energy (Joule)	Corrected Impact Energy (Joule)	Izod Impact (J/m)	Failure Type*
1	12.64	10.17	0.40	0.39	30.9	C
2	12.64	10.16	0.36	0.35	27.7	C
3	12.63	10.16	0.53	0.52	41.2	C
4	12.62	10.20	0.42	0.41	32.5	C
5	12.69	10.14	0.38	0.37	29.2	C
Mean					32.3	
Standard Deviation					5.3	

*C = Complete Break— A break where the specimen separates into two or more pieces.
H = Hinge Break— An incomplete break, such that one part of the specimen cannot support itself above the horizontal when the other part is held vertically (less than 90° included angle).
P = Partial Break— An incomplete break that does not meet the definition for a hinge break but has fractured at least 90 % of the distance between the vertex of the notch and the opposite side.
NB = Non-Break— An incomplete break where the fracture extends less than 90 % of the distance between the vertex of the notch and the opposite side.

Izod Impact (ASTM D 256) V3 20160712 RP



Accredited Laboratory
ISO/IEC 17025

6. Test Results

Resin Samples (5 Angle Samples)

Pendulum Correction : 0.01J

Specimen	Specimen Width at Notch (mm)	Notch Depth (mm)	Impact Energy (Joule)	Corrected Impact Energy (Joule)	Izod Impact (J/m)	Failure Type*
1	12.60	10.30	0.18	0.17	13.5	C
2	12.54	10.30	0.16	0.15	12.0	C
3	12.65	9.30	0.13	0.12	9.5	C
4	12.64	10.17	0.16	0.15	11.9	C
5	12.54	9.25	0.18	0.17	13.6	C
Mean					12.1	
Standard Deviation					1.7	

*C = Complete Break— A break where the specimen separates into two or more pieces.
H = Hinge Break— An incomplete break, such that one part of the specimen cannot support itself above the horizontal when the other part is held vertically (less than 90° included angle).
P = Partial Break— An incomplete break that does not meet the definition for a hinge break but has fractured at least 90 % of the distance between the vertex of the notch and the opposite side.
NB = Non-Break— An incomplete break where the fracture extends less than 90 % of the distance between the vertex of the notch and the opposite side.



Accredited Laboratory
ISO/IEC 17025

Izod Impact (ASTM D 256) V3 20160712 RP

6. Test Results (cont.)

Resin Samples (5 Horizontal Samples)

Pendulum Correction : 0.01J

Specimen	Specimen Width at Notch (mm)	Notch Depth (mm)	Impact Energy (Joule)	Corrected Impact Energy (Joule)	Izod Impact (J/m)	Failure Type*
1	12.52	10.27	0.18	0.17	13.6	C
2	12.60	9.20	0.16	0.15	11.9	C
3	12.52	10.00	0.13	0.12	9.6	C
4	12.60	10.04	0.16	0.15	11.9	C
5	12.54	10.14	0.14	0.13	10.4	C
Mean					11.5	
Standard Deviation					1.5	

*C = Complete Break— A break where the specimen separates into two or more pieces.
H = Hinge Break— An incomplete break, such that one part of the specimen cannot support itself above the horizontal when the other part is held vertically (less than 90° included angle).
P = Partial Break— An incomplete break that does not meet the definition for a hinge break but has fractured at least 90 % of the distance between the vertex of the notch and the opposite side.
NB = Non-Break— An incomplete break where the fracture extends less than 90 % of the distance between the vertex of the notch and the opposite side.

Izod Impact (ASTM D 256) V3 20160712 RP



6. Test Results (cont.)

Resin Samples (5 vertical Samples)

Pendulum Correction : 0.01J

Specimen	Specimen Width at Notch (mm)	Notch Depth (mm)	Impact Energy (Joule)	Corrected Impact Energy (Joule)	Izod Impact (J/m)	Failure Type*
1	12.64	10.15	0.18	0.17	13.4	C
2	12.63	10.14	0.12	0.11	8.7	C
3	12.54	10.11	0.13	0.12	9.6	C
4	12.55	10.25	0.13	0.12	9.6	C
5	12.53	10.16	0.13	0.12	9.6	C
Mean					10.2	
Standard Deviation					1.9	

*C = Complete Break— A break where the specimen separates into two or more pieces.
H = Hinge Break— An incomplete break, such that one part of the specimen cannot support itself above the horizontal when the other part is held vertically (less than 90° included angle).
P = Partial Break— An incomplete break that does not meet the definition for a hinge break but has fractured at least 90 % of the distance between the vertex of the notch and the opposite side.
NB = Non-Break— An incomplete break where the fracture extends less than 90 % of the distance between the vertex of the notch and the opposite side.

Izod Impact (ASTM D 256) V3 20160712 RP

Accredited Laboratory
ISO/IEC 17025

6. Test Results (cont.)

Nylon Samples (5 Angle Samples)

Pendulum Correction : 0.01J

Specimen	Specimen Width at Notch (mm)	Notch Depth (mm)	Impact Energy (Joule)	Corrected Impact Energy (Joule)	Izod Impact (J/m)	Failure Type*
1	12.79	10.15	0.59	0.58	45.3	C
2	12.64	10.13	0.71	0.70	55.4	C
3	12.70	10.21	0.63	0.62	48.8	C
4	12.67	10.16	0.63	0.62	48.9	C
5	12.62	10.01	0.61	0.60	47.5	C
Mean					49.2	
Standard Deviation					3.7	

*C = Complete Break— A break where the specimen separates into two or more pieces.
H = Hinge Break— An incomplete break, such that one part of the specimen cannot support itself above the horizontal when the other part is held vertically (less than 90° included angle).
P = Partial Break— An incomplete break that does not meet the definition for a hinge break but has fractured at least 90 % of the distance between the vertex of the notch and the opposite side.
NB = Non-Break— An incomplete break where the fracture extends less than 90 % of the distance between the vertex of the notch and the opposite side.

Izod Impact (ASTM D 256) V3 20160712 RP



Accredited Laboratory
ISO/IEC 17025

6. Test Results (cont.)

Nylon Samples (5 Horizontal Samples)

Pendulum Correction : 0.01J

Specimen	Specimen Width at Notch (mm)	Notch Depth (mm)	Impact Energy (Joule)	Corrected Impact Energy (Joule)	Izod Impact (J/m)	Failure Type*
1	12.64	10.13	0.73	0.72	57.0	C
2	12.79	10.19	0.65	0.64	50.0	C
3	12.92	10.24	0.73	0.72	55.7	C
4	12.72	10.21	0.67	0.66	51.9	C
5	12.60	9.25	0.65	0.63	50.0	C
Mean					52.9	
Standard Deviation					3.2	

*C = Complete Break— A break where the specimen separates into two or more pieces.
H = Hinge Break— An incomplete break, such that one part of the specimen cannot support itself above the horizontal when the other part is held vertically (less than 90° included angle).
P = Partial Break— An incomplete break that does not meet the definition for a hinge break but has fractured at least 90 % of the distance between the vertex of the notch and the opposite side.
NB = Non-Break— An incomplete break where the fracture extends less than 90 % of the distance between the vertex of the notch and the opposite side.

Izod Impact (ASTM D 256) V3 20160712 RP



6. Test Results (cont.)

Nylon Samples (5 Vertical Samples)

Pendulum Correction : 0.01J

Specimen	Specimen Width at Notch (mm)	Notch Depth (mm)	Impact Energy (Joule)	Corrected Impact Energy (Joule)	Izod Impact (J/m)	Failure Type*
1	12.61	10.34	0.57	0.56	44.4	C
2	12.81	10.05	0.59	0.58	45.3	C
3	12.62	10.15	0.67	0.66	52.3	C
4	12.66	10.18	0.59	0.58	45.8	C
5	12.61	10.01	0.67	0.65	51.5	C
Mean					47.9	
Standard Deviation					3.7	

*C = *Complete Break*— A break where the specimen separates into two or more pieces.
H = *Hinge Break*— An incomplete break, such that one part of the specimen cannot support itself above the horizontal when the other part is held vertically (less than 90° included angle).
P = *Partial Break*— An incomplete break that does not meet the definition for a hinge break but has fractured at least 90 % of the distance between the vertex of the notch and the opposite side.
NB = *Non-Break*— An incomplete break where the fracture extends less than 90 % of the distance between the vertex of the notch and the opposite side.



Accredited Laboratory
ISO/IEC 17025

Izod Impact (ASTM D 256) V3 20160712 RP



Rod Parry, B. Sc., MBA (Tech Mgmt)
Laboratory & Technical Manager
ExcelPlas Pty. Ltd. for LMATS Pty Ltd

Terms & Conditions:

The testing herein is based upon accepted industry practice as well as the test methods listed.

Test results reported herein do not apply to samples other than those tested.

LMATS neither accepts responsibility for nor makes claim as to the final use and purpose of the material.

It is up to the client to validate the suitability of any material recommendations contained in this report by conducting proper product field trials to establish 'fitness for purpose' to their satisfaction.

LMATS shall not be liable for any losses, costs, damages or expenses incurred by the recipient or any other person or entity resulting from the use of any information or interpretation given in this report.

LMATS observes and maintains client confidentiality.

LMATS limits reproduction of this report, except in full, without prior approval of ExcelPlas.

Unless otherwise negotiated with the client, test samples will be disposed of 90 days after the report has been issued.

Izod Impact (ASTM D 256) V3 20160712 RP



Accredited Laboratory
ISO/IEC 17025

Appendix F

Sample spreadsheet of recorded 3-point bend specimen dimensions.

12/01/2017: 3 pt bend (speed = 1.5mm/min, span = 56mm , 16:1 dep

Sample	Temp. (celcius)	Humidity(%)	Position	Thickness (mm)	Width (mm)
FDM V1	22.7	69	Top	3.38	12.92
			centre	3.38	12.92
			bottom	3.38	12.9
FDM V2	22.7	69	Top	3.36	12.9
			centre	3.38	12.92
			bottom	3.38	12.94
FDM V3	22.7	69	Top	3.38	12.86
			centre	3.38	12.9
			bottom	3.38	12.9
FDM V4	22.7	69	Top	3.36	12.9
			centre	3.4	12.9
			bottom	3.38	12.9
FDM V5	22.7	69	Top	3.38	12.9
			centre	3.38	12.9
			bottom	3.38	12.94
FDM A1	22.7	69	Top	3.3	12.96
			centre	3.3	12.96
			bottom	3.32	13.04
FDM A2	22.7	69	Top	3.36	12.76
			centre	3.36	12.9
			bottom	3.34	12.84
FDM A3	22.7	69	Top	3.28	12.96
			centre	3.28	12.96
			bottom	3.3	12.96
FDM A4	22.7	69	Top	3.4	12.8
			centre	3.34	12.86
			bottom	3.34	12.86
FDM A5	22.7	69	Top	3.4	12.94
			centre	3.4	12.96
			bottom	3.4	12.84
FDM HF1	22.7	69	Top	3.4	12.8
			centre	3.42	12.8
			bottom	3.44	12.8

Appendix G

Screenshot of approved human ethics application with Nil/Neg risk to participants.

The screenshot displays the UTS ResearchMaster Enterprise System interface for an ethics application. The header includes the UTS logo and the text "ResearchMaster Enterprise System". Navigation links for "Home", "Projects", "Ethics", "Agreements", and "Personnel" are visible, along with "System", "Help", and "Logout". The current page is titled "Ethics (5/6)" and includes a "Back" link.

The application details are as follows:

- Ethics Category:** Human
- Application Code:** ETH17-2075
- Version:** (empty field)
- Application Title:** Which way works best? Assisting product designers with balancing strength and surface texture of handheld products made from polymers through additive manufacturing
- Primary Contact:** Mr Stefan Lie
- Primary Committee:** (empty field)
- Primary Org. Unit:** DAB.School of Design
- Start Date:** 16/03/2018
- End Date:** 16/03/2023
- Status:** Neg Risk Approved
- Current?:**

Ethics Dates

Submission date	<input type="text"/>	Date Approved	16/03/2018
Date Withdrawn	<input type="text"/>	Review Date	16/03/2018
Date Rejected	<input type="text"/>		

Ethics Summary

Approval Purpose: Nil/Negligible Risk

Conditions of Approval: (empty text area)

Appendix H

ASTM standard: D638-14 (tensile), D256 – 10 (Izod impact) and D790 – 15 (flexural)



Designation: D638 – 14

Standard Test Method for Tensile Properties of Plastics¹

This standard is issued under the fixed designation D638; the number immediately following the designation indicates the year of original adoption or, in the case of revision, the year of last revision. A number in parentheses indicates the year of last reapproval. A superscript epsilon (ϵ) indicates an editorial change since the last revision or reapproval.

This standard has been approved for use by agencies of the U.S. Department of Defense.

1. Scope*

1.1 This test method covers the determination of the tensile properties of unreinforced and reinforced plastics in the form of standard dumbbell-shaped test specimens when tested under defined conditions of pretreatment, temperature, humidity, and testing machine speed.

1.2 This test method is applicable for testing materials of any thickness up to 14 mm (0.55 in.). However, for testing specimens in the form of thin sheeting, including film less than 1.0 mm (0.04 in.) in thickness, ASTM standard D882 is the preferred test method. Materials with a thickness greater than 14 mm (0.55 in.) shall be reduced by machining.

1.3 This test method includes the option of determining Poisson's ratio at room temperature.

NOTE 1—This standard and ISO 527-1 address the same subject matter, but differ in technical content.

NOTE 2—This test method is not intended to cover precise physical procedures. It is recognized that the constant rate of crosshead movement type of test leaves much to be desired from a theoretical standpoint, that wide differences may exist between rate of crosshead movement and rate of strain between gage marks on the specimen, and that the testing speeds specified disguise important effects characteristic of materials in the plastic state. Further, it is realized that variations in the thicknesses of test specimens, which are permitted by these procedures, produce variations in the surface-volume ratios of such specimens, and that these variations may influence the test results. Hence, where directly comparable results are desired, all samples should be of equal thickness. Special additional tests should be used where more precise physical data are needed.

NOTE 3—This test method may be used for testing phenolic molded resin or laminated materials. However, where these materials are used as electrical insulation, such materials should be tested in accordance with Test Methods D229 and Test Method D651.

NOTE 4—For tensile properties of resin-matrix composites reinforced with oriented continuous or discontinuous high modulus >20 -GPa ($>3.0 \times 10^5$ -psi) fibers, tests shall be made in accordance with Test Method D3039/D3039M.

1.4 Test data obtained by this test method have been found to be useful in engineering design. However, it is important to

consider the precautions and limitations of this method found in Note 2 and Section 4 before considering these data for engineering design.

1.5 The values stated in SI units are to be regarded as standard. The values given in parentheses are for information only.

1.6 *This standard does not purport to address all of the safety concerns, if any, associated with its use. It is the responsibility of the user of this standard to establish appropriate safety and health practices and determine the applicability of regulatory limitations prior to use.*

2. Referenced Documents

2.1 ASTM Standards:²

- D229 Test Methods for Rigid Sheet and Plate Materials Used for Electrical Insulation
- D412 Test Methods for Vulcanized Rubber and Thermoplastic Elastomers—Tension
- D618 Practice for Conditioning Plastics for Testing
- D651 Test Method for Test for Tensile Strength of Molded Electrical Insulating Materials (Withdrawn 1989)³
- D882 Test Method for Tensile Properties of Thin Plastic Sheet
- D883 Terminology Relating to Plastics
- D1822 Test Method for Tensile-Impact Energy to Break Plastics and Electrical Insulating Materials
- D3039/D3039M Test Method for Tensile Properties of Polymer Matrix Composite Materials
- D4000 Classification System for Specifying Plastic Materials
- D4066 Classification System for Nylon Injection and Extrusion Materials (PA)
- D5947 Test Methods for Physical Dimensions of Solid Plastics Specimens
- E4 Practices for Force Verification of Testing Machines

¹ This test method is under the jurisdiction of ASTM Committee D20 on Plastics and is the direct responsibility of Subcommittee D20.10 on Mechanical Properties.

Current edition approved Dec. 15, 2014. Published March 2015. Originally approved in 1941. Last previous edition approved in 2010 as D638 - 10. DOI: 10.1520/D0638-14.

² For referenced ASTM standards, visit the ASTM website, www.astm.org, or contact ASTM Customer Service at service@astm.org. For *Annual Book of ASTM Standards* volume information, refer to the standard's Document Summary page on the ASTM website.

³ The last approved version of this historical standard is referenced on www.astm.org.

*A Summary of Changes section appears at the end of this standard

Copyright © ASTM International, 100 Barr Harbor Drive, PO Box C700, West Conshohocken, PA 19428-2959. United States

Copyright ASTM International
Provided by IHS under license with ASTM
No reproduction or networking permitted without license from IHS

Licensee=Uni of Technology Sydney/5928310001
Not for Resale, 10/21/2015 22:52:16 MDT

E83 Practice for Verification and Classification of Extensometer Systems

E132 Test Method for Poisson's Ratio at Room Temperature

E691 Practice for Conducting an Interlaboratory Study to Determine the Precision of a Test Method

2.2 ISO Standard.⁴

ISO 527-1 Determination of Tensile Properties

3. Terminology

3.1 *Definitions*—Definitions of terms applying to this test method appear in Terminology D883 and Annex A2.

4. Significance and Use

4.1 This test method is designed to produce tensile property data for the control and specification of plastic materials. These data are also useful for qualitative characterization and for research and development.

4.2 Some material specifications that require the use of this test method, but with some procedural modifications that take precedence when adhering to the specification. Therefore, it is advisable to refer to that material specification before using this test method. Table 1 in Classification D4000 lists the ASTM materials standards that currently exist.

4.3 Tensile properties are known to vary with specimen preparation and with speed and environment of testing. Consequently, where precise comparative results are desired, these factors must be carefully controlled.

4.4 It is realized that a material cannot be tested without also testing the method of preparation of that material. Hence, when comparative tests of materials per se are desired, exercise great care to ensure that all samples are prepared in exactly the same way, unless the test is to include the effects of sample preparation. Similarly, for referee purposes or comparisons within any given series of specimens, care shall be taken to secure the maximum degree of uniformity in details of preparation, treatment, and handling.

4.5 Tensile properties provide useful data for plastics engineering design purposes. However, because of the high degree of sensitivity exhibited by many plastics to rate of straining and environmental conditions, data obtained by this test method cannot be considered valid for applications involving load-time scales or environments widely different from those of this test method. In cases of such dissimilarity, no reliable estimation of the limit of usefulness can be made for most plastics. This sensitivity to rate of straining and environment necessitates testing over a broad load-time scale (including impact and creep) and range of environmental conditions if tensile properties are to suffice for engineering design purposes.

NOTE 5—Since the existence of a true elastic limit in plastics (as in many other organic materials and in many metals) is debatable, the propriety of applying the term “elastic modulus” in its quoted, generally accepted definition to describe the “stiffness” or “rigidity” of a plastic has been seriously questioned. The exact stress-strain characteristics of plastic materials are highly dependent on such factors as rate of application of

⁴ Available from American National Standards Institute (ANSI), 25 W. 43rd St., 4th Floor, New York, NY 10036, <http://www.ansi.org>.

stress, temperature, previous history of specimen, etc. However, stress-strain curves for plastics, determined as described in this test method, almost always show a linear region at low stresses, and a straight line drawn tangent to this portion of the curve permits calculation of an elastic modulus of the usually defined type. Such a constant is useful if its arbitrary nature and dependence on time, temperature, and similar factors are realized.

5. Apparatus

5.1 *Testing Machine*—A testing machine of the constant-rate-of-crosshead-movement type and comprising essentially the following:

5.1.1 *Fixed Member*—A fixed or essentially stationary member carrying one grip.

5.1.2 *Movable Member*—A movable member carrying a second grip.

5.1.3 *Grips*—Grips for holding the test specimen between the fixed member and the movable member of the testing machine can be either the fixed or self-aligning type.

5.1.3.1 Fixed grips are rigidly attached to the fixed and movable members of the testing machine. When this type of grip is used take extreme care to ensure that the test specimen is inserted and clamped so that the long axis of the test specimen coincides with the direction of pull through the center line of the grip assembly.

5.1.3.2 Self-aligning grips are attached to the fixed and movable members of the testing machine in such a manner that they will move freely into alignment as soon as any load is applied so that the long axis of the test specimen will coincide with the direction of the applied pull through the center line of the grip assembly. Align the specimens as perfectly as possible with the direction of pull so that no rotary motion that may induce slippage will occur in the grips; there is a limit to the amount of misalignment self-aligning grips will accommodate.

5.1.3.3 The test specimen shall be held in such a way that slippage relative to the grips is prevented insofar as possible. Grip surfaces that are deeply scored or serrated with a pattern similar to those of a coarse single-cut file, serrations about 2.4 mm (0.09 in.) apart and about 1.6 mm (0.06 in.) deep, have been found satisfactory for most thermoplastics. Finer serrations have been found to be more satisfactory for harder plastics, such as the thermosetting materials. It is important that the serrations be kept clean and sharp. Should breaking in the grips occur, even when deep serrations or abraded specimen surfaces are used, other techniques shall be used. Other techniques that have been found useful, particularly with smooth-faced grips, are abrading that portion of the surface of the specimen that will be in the grips, and interposing thin pieces of abrasive cloth, abrasive paper, or plastic, or rubber-coated fabric, commonly called hospital sheeting, between the specimen and the grip surface. No. 80 double-sided abrasive paper has been found effective in many cases. An open-mesh fabric, in which the threads are coated with abrasive, has also been effective. Reducing the cross-sectional area of the specimen may also be effective. The use of special types of grips is sometimes necessary to eliminate slippage and breakage in the grips.

5.1.4 *Drive Mechanism*—A drive mechanism for imparting a uniform, controlled velocity to the movable member with

respect to the stationary member. This velocity is to be regulated as specified in Section 8.

5.1.5 Load Indicator—A suitable load-indicating mechanism capable of showing the total tensile load carried by the test specimen when held by the grips. This mechanism shall be essentially free of inertia lag at the specified rate of testing and shall indicate the load with an accuracy of $\pm 1\%$ of the indicated value, or better. The accuracy of the testing machine shall be verified in accordance with Practices E4.

NOTE 6—Experience has shown that many testing machines now in use are incapable of maintaining accuracy for as long as the periods between inspection recommended in Practices E4. Hence, it is recommended that each machine be studied individually and verified as often as may be found necessary. It frequently will be necessary to perform this function daily.

5.1.6 The fixed member, movable member, drive mechanism, and grips shall be constructed of such materials and in such proportions that the total elastic longitudinal strain of the system constituted by these parts does not exceed 1 % of the total longitudinal strain between the two gage marks on the test specimen at any time during the test and at any load up to the rated capacity of the machine.

5.1.7 Crosshead Extension Indicator—A suitable extension indicating mechanism capable of showing the amount of change in the separation of the grips, that is, crosshead movement. This mechanism shall be essentially free of inertial lag at the specified rate of testing and shall indicate the crosshead movement with an accuracy of $\pm 10\%$ of the indicated value.

5.2 Extension Indicator (extensometer)—A suitable instrument shall be used for determining the distance between two designated points within the gauge length of the test specimen as the specimen is stretched. For referee purposes, the extensometer must be set at the full gage length of the specimen, as shown in Fig. 1. It is desirable, but not essential, that this instrument automatically record this distance, or any change in it, as a function of the load on the test specimen or of the elapsed time from the start of the test, or both. If only the latter is obtained, load-time data must also be taken. This instrument shall be essentially free of inertia at the specified speed of testing. Extensometers shall be classified and their calibration periodically verified in accordance with Practice E83.

5.2.1 Modulus-of-Elasticity Measurements—For modulus-of-elasticity measurements, an extensometer with a maximum strain error of 0.0002 mm/mm (in./in.) that automatically and continuously records shall be used. An extensometer classified by Practice E83 as fulfilling the requirements of a B-2 classification within the range of use for modulus measurements meets this requirement.

5.2.2 Low-Extension Measurements—For elongation-at-yield and low-extension measurements (nominally 20 % or less), the same above extensometer, attenuated to 20 % extension, is acceptable. In any case, the extensometer system must meet at least Class C (Practice E83) requirements, which include a fixed strain error of 0.001 strain or $\pm 1.0\%$ of the indicated strain, whichever is greater.

5.2.3 High-Extension Measurements—For making measurements at elongations greater than 20 %, measuring techniques with error no greater than $\pm 10\%$ of the measured value are acceptable.

5.3 Micrometers—Apparatus for measuring the width and thickness of the test specimen shall comply with the requirements of Test Method D5947.

6. Test Specimens

6.1 Sheet, Plate, and Molded Plastics:

6.1.1 Rigid and Semirigid Plastics—The test specimen shall conform to the dimensions shown in Fig. 1. The Type I specimen is the preferred specimen and shall be used where sufficient material having a thickness of 7 mm (0.28 in.) or less is available. The Type II specimen is recommended when a material does not break in the narrow section with the preferred Type I specimen. The Type V specimen shall be used where only limited material having a thickness of 4 mm (0.16 in.) or less is available for evaluation, or where a large number of specimens are to be exposed in a limited space (thermal and environmental stability tests, etc.). The Type IV specimen is generally used when direct comparisons are required between materials in different rigidity cases (that is, nonrigid and semirigid). The Type III specimen must be used for all materials with a thickness of greater than 7 mm (0.28 in.) but not more than 14 mm (0.55 in.).

6.1.2 Nonrigid Plastics—The test specimen shall conform to the dimensions shown in Fig. 1. The Type IV specimen shall be used for testing nonrigid plastics with a thickness of 4 mm (0.16 in.) or less. The Type III specimen must be used for all materials with a thickness greater than 7 mm (0.28 in.) but not more than 14 mm (0.55 in.).

6.1.3 Reinforced Composites—The test specimen for reinforced composites, including highly orthotropic laminates, shall conform to the dimensions of the Type I specimen shown in Fig. 1.

6.1.4 Preparation—Methods of preparing test specimens include injection molding, machining operations, or die cutting, from materials in sheet, plate, slab, or similar form. Materials thicker than 14 mm (0.55 in.) shall be machined to 14 mm (0.55 in.) for use as Type III specimens.

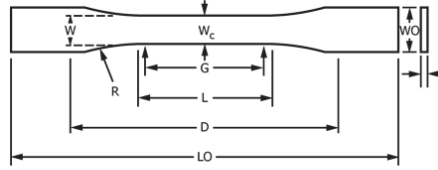
NOTE 7—Test results have shown that for some materials such as glass cloth, SMC, and BMC laminates, other specimen types should be considered to ensure breakage within the gage length of the specimen, as mandated by 7.3.

NOTE 8—When preparing specimens from certain composite laminates such as woven roving, or glass cloth, exercise care in cutting the specimens parallel to the reinforcement. The reinforcement will be significantly weakened by cutting on a bias, resulting in lower laminate properties, unless testing of specimens in a direction other than parallel with the reinforcement constitutes a variable being studied.

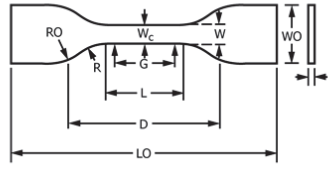
NOTE 9—Specimens prepared by injection molding may have different tensile properties than specimens prepared by machining or die-cutting because of the orientation induced. This effect may be more pronounced in specimens with narrow sections.

6.2 Rigid Tubes—The test specimen for rigid tubes shall be as shown in Fig. 2. The length, L , shall be as shown in the table in Fig. 2. A groove shall be machined around the outside of the specimen at the center of its length so that the wall section after

ASTM D638 – 14



TYPES I, II, III & V



TYPE IV

Specimen Dimensions for Thickness, T , mm (in.)^A

Dimensions (see drawings)	7 (0.28) or under		Over 7 to 14 (0.28 to 0.55), incl	4 (0.16) or under		Tolerances
	Type I	Type II	Type III	Type IV ^B	Type V ^{C,D}	
W —Width of narrow section ^{E,F}	13 (0.50)	6 (0.25)	19 (0.75)	6 (0.25)	3.18 (0.125)	± 0.5 (± 0.02) ^{B,C}
L —Length of narrow section	57 (2.25)	57 (2.25)	57 (2.25)	33 (1.30)	9.53 (0.375)	± 0.5 (± 0.02) ^C
WO —Width overall, min ^G	19 (0.75)	19 (0.75)	29 (1.13)	19 (0.75)	...	+ 6.4 (+ 0.25)
WO —Width overall, min ^G	9.53 (0.375)	+ 3.18 (+ 0.125)
LO —Length overall, min ^H	165 (6.5)	183 (7.2)	246 (9.7)	115 (4.5)	63.5 (2.5)	no max (no max)
G —Gage length ^I	50 (2.00)	50 (2.00)	50 (2.00)	...	7.62 (0.300)	± 0.25 (± 0.010) ^C
G —Gage length ^I	25 (1.00)	...	± 0.13 (± 0.005)
D —Distance between grips	115 (4.5)	135 (5.3)	115 (4.5)	65 (2.5) ^J	25.4 (1.0)	± 5 (± 0.2)
R —Radius of fillet	76 (3.00)	76 (3.00)	76 (3.00)	14 (0.56)	12.7 (0.5)	± 1 (± 0.04) ^C
RO —Outer radius (Type IV)	25 (1.00)	...	± 1 (± 0.04)

^AThickness, T , shall be 3.2 ± 0.4 mm (0.13 ± 0.02 in.) for all types of molded specimens, and for other Types I and II specimens where possible. If specimens are machined from sheets or plates, thickness, T , shall be the thickness of the sheet or plate provided this does not exceed the range stated for the intended specimen type. For sheets of nominal thickness greater than 14 mm (0.55 in.) the specimens shall be machined to 14 ± 0.4 mm (0.55 ± 0.02 in.) in thickness, for use with the Type III specimen. For sheets of nominal thickness between 14 and 51 mm (0.55 and 2 in.) approximately equal amounts shall be machined from each surface. For thicker sheets both surfaces of the specimen shall be machined, and the location of the specimen with reference to the original thickness of the sheet shall be noted. Tolerances on thickness less than 14 mm (0.55 in.) shall be those standard for the grade of material tested.

^BFor the Type IV specimen, the internal width of the narrow section of the die shall be 6.00 ± 0.05 mm (0.250 ± 0.002 in.). The dimensions are essentially those of Die C in Test Methods D412.

^CThe Type V specimen shall be machined or die cut to the dimensions shown, or molded in a mold whose cavity has these dimensions. The dimensions shall be:

- $W = 3.18 \pm 0.03$ mm (0.125 ± 0.001 in.),
- $L = 9.53 \pm 0.08$ mm (0.375 ± 0.003 in.),
- $G = 7.62 \pm 0.02$ mm (0.300 ± 0.001 in.), and
- $R = 12.7 \pm 0.08$ mm (0.500 ± 0.003 in.).

The other tolerances are those in the table.

^DSupporting data on the introduction of the L specimen of Test Method D1822 as the Type V specimen are available from ASTM Headquarters. Request RR:D20-1038.

^EThe tolerances of the width at the center W_c shall be $+0.00$ mm, -0.10 mm ($+0.000$ in., -0.004 in.) compared with width W at other parts of the reduced section. Any reduction in W at the center shall be gradual, equally on each side so that no abrupt changes in dimension result.

^FFor molded specimens, a draft of not over 0.13 mm (0.005 in.) is allowed for either Type I or II specimens 3.2 mm (0.13 in.) in thickness. See diagram below and this shall be taken into account when calculating width of the specimen. Thus a typical section of a molded Type I specimen, having the maximum allowable draft, could be as follows:

^GOverall widths greater than the minimum indicated are used for some materials in order to avoid breaking in the grips.

^HOverall lengths greater than the minimum indicated are used for some materials to avoid breaking in the grips or to satisfy special test requirements.

^ITest marks or initial extensometer span.

^JWhen self-tightening grips are used, for highly extensible polymers, the distance between grips will depend upon the types of grips used and may not be critical if maintained uniform once chosen.

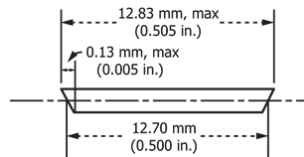
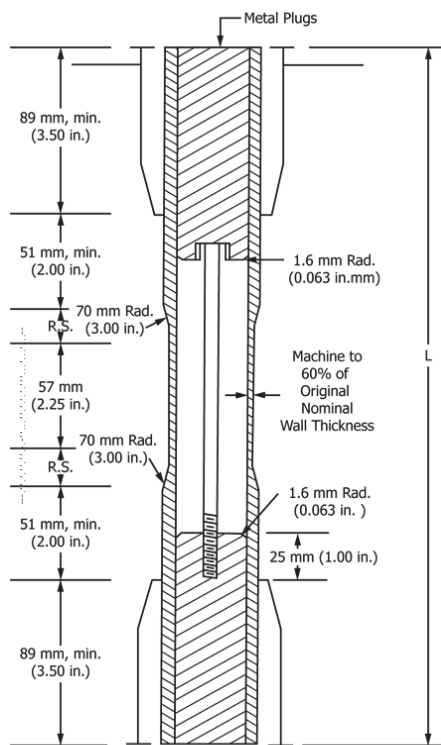


FIG. 1 Tension Test Specimens for Sheet, Plate, and Molded Plastics



DIMENSIONS OF TUBE SPECIMENS			
Nominal Wall Thickness	Length of Radial Sections, 2R.S.	Total Calculated Minimum Length of Specimen	Standard Length, L, of Specimen to Be Used for 89-mm (3.5-in.) Jaws ⁴
mm (in.)			
0.79 (1/32)	13.9 (0.547)	350 (13.80)	381 (15)
1.2 (1/8)	17.0 (0.670)	354 (13.92)	381 (15)
1.6 (1/16)	19.6 (0.773)	356 (14.02)	381 (15)
2.4 (3/32)	24.0 (0.946)	361 (14.20)	381 (15)
3.2 (1/8)	27.7 (1.091)	364 (14.34)	381 (15)
4.8 (3/16)	33.9 (1.333)	370 (14.58)	381 (15)
6.4 (1/4)	39.0 (1.536)	376 (14.79)	400 (15.75)
7.9 (5/16)	43.5 (1.714)	380 (14.96)	400 (15.75)
9.5 (3/8)	47.6 (1.873)	384 (15.12)	400 (15.75)
11.1 (7/16)	51.3 (2.019)	388 (15.27)	400 (15.75)
12.7 (1/2)	54.7 (2.154)	391 (15.40)	419 (16.5)

⁴For jaws greater than 89 mm (3.5 in.), the standard length shall be increased by twice the length of the jaws minus 178 mm (7 in.). The standard length permits a slippage of approximately 6.4 to 12.7 mm (0.25 to 0.50 in.) in each jaw while maintaining the maximum length of the jaw grip.

FIG. 2 Diagram Showing Location of Tube Tension Test Specimens in Testing Machine

machining shall be 60 % of the original nominal wall thick-

ness. This groove shall consist of a straight section 57.2 mm (2.25 in.) in length with a radius of 76 mm (3 in.) at each end joining it to the outside diameter. Steel or brass plugs having diameters such that they will fit snugly inside the tube and having a length equal to the full jaw length plus 25 mm (1 in.) shall be placed in the ends of the specimens to prevent crushing. They can be located conveniently in the tube by separating and supporting them on a threaded metal rod. Details of plugs and test assembly are shown in Fig. 2.

6.3 *Rigid Rods*—The test specimen for rigid rods shall be as shown in Fig. 3. The length, L, shall be as shown in the table in Fig. 3. A groove shall be machined around the specimen at the center of its length so that the diameter of the machined portion shall be 60 % of the original nominal diameter. This groove shall consist of a straight section 57.2 mm (2.25 in.) in length with a radius of 76 mm (3 in.) at each end joining it to the outside diameter.

6.4 All surfaces of the specimen shall be free of visible flaws, scratches, or imperfections. Marks left by coarse machining operations shall be carefully removed with a fine file or abrasive, and the filed surfaces shall then be smoothed with abrasive paper (No. 00 or finer). The finishing sanding strokes shall be made in a direction parallel to the long axis of the test specimen. All flash shall be removed from a molded specimen, taking great care not to disturb the molded surfaces. In machining a specimen, undercuts that would exceed the dimensional tolerances shown in Fig. 1 shall be scrupulously avoided. Care shall also be taken to avoid other common machining errors.

6.5 If it is necessary to place gage marks on the specimen, this shall be done with a wax crayon or India ink that will not affect the material being tested. Gage marks shall not be scratched, punched, or impressed on the specimen.

6.6 When testing materials that are suspected of anisotropy, duplicate sets of test specimens shall be prepared, having their long axes respectively parallel with, and normal to, the suspected direction of anisotropy.

7. Number of Test Specimens

7.1 Test at least five specimens for each sample in the case of isotropic materials.

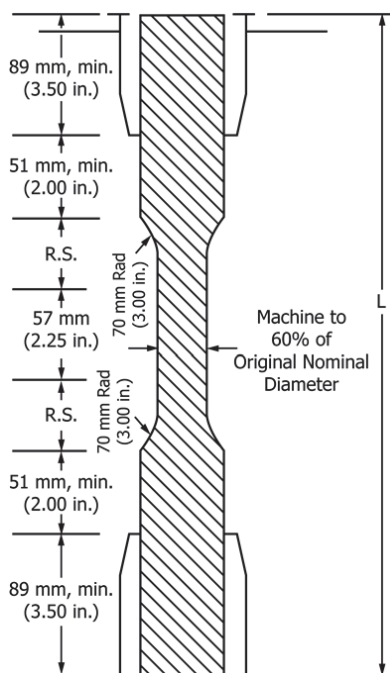
7.2 For anisotropic materials, when applicable, test five specimens, normal to, and five parallel with, the principle axis of anisotropy.

7.3 Discard specimens that break at some flaw, or that break outside of the narrow cross-sectional test section (Fig. 1, dimension “L”), and make retests, unless such flaws constitute a variable to be studied.

NOTE 10—Before testing, all transparent specimens should be inspected in a polariscope. Those which show atypical or concentrated strain patterns should be rejected, unless the effects of these residual strains constitute a variable to be studied.

8. Speed of Testing

8.1 Speed of testing shall be the relative rate of motion of the grips or test fixtures during the test. The rate of motion of the driven grip or fixture when the testing machine is running



DIMENSIONS OF ROD SPECIMENS

Nominal Diameter	Length of Radial Sections, 2R.S.	Total Calculated Minimum Length of Specimen	Standard Length, L, of Specimen to Be Used for 89-mm (3.5-in.) Jaws ^A
mm (in.)			
3.2 (1/8)	19.6 (0.773)	356 (14.02)	381 (15)
4.7 (1/4)	24.0 (0.946)	361 (14.20)	381 (15)
6.4 (1/4)	27.7 (1.091)	364 (14.34)	381 (15)
9.5 (3/8)	33.9 (1.333)	370 (14.58)	381 (15)
12.7 (1/2)	39.0 (1.536)	376 (14.79)	400 (15.75)
15.9 (5/8)	43.5 (1.714)	380 (14.96)	400 (15.75)
19.0 (3/4)	47.6 (1.873)	384 (15.12)	400 (15.75)
22.2 (7/8)	51.5 (2.019)	388 (15.27)	400 (15.75)
25.4 (1)	54.7 (2.154)	391 (15.40)	419 (16.5)
31.8 (1 1/4)	60.9 (2.398)	398 (15.65)	419 (16.5)
38.1 (1 1/2)	66.4 (2.615)	403 (15.87)	419 (16.5)
42.5 (1 3/4)	71.4 (2.812)	408 (16.06)	419 (16.5)
50.8 (2)	76.0 (2.993)	412 (16.24)	432 (17)

^AFor jaws greater than 89 mm (3.5 in.), the standard length shall be increased by twice the length of the jaws minus 178 mm (7 in.). The standard length permits a slippage of approximately 6.4 to 12.7 mm (0.25 to 0.50 in.) in each jaw while maintaining the maximum length of the jaw grip.

FIG. 3 Diagram Showing Location of Rod Tension Test Specimen in Testing Machine

idle may be used, if it can be shown that the resulting speed of testing is within the limits of variation allowed.

8.2 Choose the speed of testing from Table 1. Determine this chosen speed of testing by the specification for the material being tested, or by agreement between those concerned. When

TABLE 1 Designations for Speed of Testing^A

Classification ^B	Specimen Type	Speed of Testing, mm/min (in./min)	Nominal Strain ^C Rate at Start of Test, mm/mm·min (in./in.·min)
Rigid and Semirigid	I, II, III rods and tubes	5 (0.2) ± 25 %	0.1
		50 (2) ± 10 %	1
	500 (20) ± 10 %	10	
	IV	5 (0.2) ± 25 %	0.15
		50 (2) ± 10 %	1.5
Nonrigid	V	500 (20) ± 10 %	15
		1 (0.05) ± 25 %	0.1
	III	10 (0.5) ± 25 %	1
		100 (5) ± 25 %	10
		50 (2) ± 10 %	1
IV	500 (20) ± 10 %	10	
	50 (2) ± 10 %	1.5	
		500 (20) ± 10 %	15

^ASelect the lowest speed that produces rupture in 0.5 to 5 min for the specimen geometry being used (see 8.2).

^BSee Terminology D883 for definitions.

^CThe initial rate of straining cannot be calculated exactly for dumbbell-shaped specimens because of extension, both in the reduced section outside the gage length and in the fillets. This initial strain rate can be measured from the initial slope of the tensile strain-versus-time diagram.

the speed is not specified, use the lowest speed shown in Table 1 for the specimen geometry being used, which gives rupture within 0.5 to 5-min testing time.

8.3 Make modulus determinations at the speed selected for the other tensile properties when the recorder response and resolution are adequate.

9. Conditioning

9.1 *Conditioning*—Condition the test specimens in accordance with Procedure A of Practice D618, unless otherwise specified by contract or the relevant ASTM material specification. Conditioning time is specified as a minimum. Temperature and humidity tolerances shall be in accordance with Section 7 of Practice D618 unless specified differently by contract or material specification.

9.2 *Test Conditions*—Conduct the tests at the same temperature and humidity used for conditioning with tolerances in accordance with Section 7 of Practice D618, unless otherwise specified by contract or the relevant ASTM material specification.

10. Procedure

10.1 Measure the width and thickness of each specimen to the nearest 0.025 mm (0.001 in.) using the applicable test methods in D5947.

10.1.1 Measure the width and thickness of flat specimens at the center of each specimen and within 5 mm of each end of the gage length.

10.1.2 For injection molded specimens, the actual measurement of only one specimen from each sample will suffice when it has previously been demonstrated that the specimen-to-specimen variation in width and thickness is less than 1 %.

10.1.3 For thin sheeting, including film less than 1.0 mm (0.04 in.), take the width of specimens produced by a Type IV die as the distance between the cutting edges of the die in the

narrow section. For all other specimens, measure the actual width of the center portion of the specimen to be tested, unless it can be shown that the actual width of the specimen is the same as that of the die within the specimen dimension tolerances given in Fig. 1.

10.1.4 Measure the diameter of rod specimens, and the inside and outside diameters of tube specimens, to the nearest 0.025 mm (0.001 in.) at a minimum of two points 90° apart; make these measurements along the groove for specimens so constructed. Use plugs in testing tube specimens, as shown in Fig. 2.

10.2 Place the specimen in the grips of the testing machine, taking care to align the long axis of the specimen and the grips with an imaginary line joining the points of attachment of the grips to the machine. The distance between the ends of the gripping surfaces, when using flat specimens, shall be as indicated in Fig. 1. On tube and rod specimens, the location for the grips shall be as shown in Fig. 2 and Fig. 3. Tighten the grips evenly and firmly to the degree necessary to prevent slippage of the specimen during the test, but not to the point where the specimen would be crushed.

10.3 Attach the extension indicator. When modulus is being determined, a Class B-2 or better extensometer is required (see 5.2.1).

NOTE 11—Modulus of materials is determined from the slope of the linear portion of the stress-strain curve. For most plastics, this linear portion is very small, occurs very rapidly, and must be recorded automatically. The change in jaw separation is never to be used for calculating modulus or elongation.

10.4 Set the speed of testing at the proper rate as required in Section 8, and start the machine.

10.5 Record the load-extension curve of the specimen.

10.6 Record the load and extension at the yield point (if one exists) and the load and extension at the moment of rupture.

NOTE 12—If it is desired to measure both modulus and failure properties (yield or break, or both), it may be necessary, in the case of highly extensible materials, to run two independent tests. The high magnification extensometer normally used to determine properties up to the yield point may not be suitable for tests involving high extensibility. If allowed to remain attached to the specimen, the extensometer could be permanently damaged. A broad-range incremental extensometer or hand-rule technique may be needed when such materials are taken to rupture.

11. Calculation

11.1 Toe compensation shall be made in accordance with Annex A1, unless it can be shown that the toe region of the curve is not due to the take-up of slack, seating of the specimen, or other artifact, but rather is an authentic material response.

11.2 *Tensile Strength*—Calculate the tensile strength by dividing the maximum load sustained by the specimen in newtons (pounds-force) by the average original cross-sectional area in the gage length segment of the specimen in square metres (square inches). Express the result in pascals (pounds-force per square inch) and report it to three significant figures as tensile strength at yield or tensile strength at break, whichever term is applicable. When a nominal yield or break load less than the maximum is present and applicable, it is

often desirable to also calculate, in a similar manner, the corresponding tensile stress at yield or tensile stress at break and report it to three significant figures (see Note A2.8).

11.3 Elongation values are valid and are reported in cases where uniformity of deformation within the specimen gage length is present. Elongation values are quantitatively relevant and appropriate for engineering design. When non-uniform deformation (such as necking) occurs within the specimen gage length nominal strain values are reported. Nominal strain values are of qualitative utility only.

11.3.1 *Percent Elongation*—Percent elongation is the change in gage length relative to the original specimen gage length, expressed as a percent. Percent elongation is calculated using the apparatus described in 5.2.

11.3.1.1 *Percent Elongation at Yield*—Calculate the percent elongation at yield by reading the extension (change in gage length) at the yield point. Divide that extension by the original gage length and multiply by 100.

11.3.1.2 *Percent Elongation at Break*—Calculate the percent elongation at break by reading the extension (change in gage length) at the point of specimen rupture. Divide that extension by the original gage length and multiply by 100.

11.3.2 *Nominal Strain*—Nominal strain is the change in grip separation relative to the original grip separation expressed as a percent. Nominal strain is calculated using the apparatus described in 5.1.7.

11.3.2.1 *Nominal strain at break*—Calculate the nominal strain at break by reading the extension (change in grip separation) at the point of rupture. Divide that extension by the original grip separation and multiply by 100.

11.4 *Modulus of Elasticity*—Calculate the modulus of elasticity by extending the initial linear portion of the load-extension curve and dividing the difference in stress corresponding to any segment of section on this straight line by the corresponding difference in strain. All elastic modulus values shall be computed using the average original cross-sectional area in the gage length segment of the specimen in the calculations. The result shall be expressed in pascals (pounds-force per square inch) and reported to three significant figures.

11.5 *Secant Modulus*—At a designated strain, this shall be calculated by dividing the corresponding stress (nominal) by the designated strain. Elastic modulus values are preferable and shall be calculated whenever possible. However, for materials where no proportionality is evident, the secant value shall be calculated. Draw the tangent as directed in A1.3 and Fig. A1.2, and mark off the designated strain from the yield point where the tangent line goes through zero stress. The stress to be used in the calculation is then determined by dividing the load-extension curve by the original average cross-sectional area of the specimen.

11.6 For each series of tests, calculate the arithmetic mean of all values obtained and report it as the “average value” for the particular property in question.

11.7 Calculate the standard deviation (estimated) as follows and report it to two significant figures:

$$s = \sqrt{(\sum X^2 - n\bar{X}^2)/(n - 1)} \quad (1)$$

where:

- s = estimated standard deviation,
- X = value of single observation,
- n = number of observations, and
- \bar{X} = arithmetic mean of the set of observations.

11.8 See Annex A1 for information on toe compensation.

11.9 See Annex A3 for the determination of Poisson's Ratio.

12. Report

12.1 Report the following information:

- 12.1.1 Complete identification of the material tested, including type, source, manufacturer's code numbers, form, principal dimensions, previous history, etc.,
- 12.1.2 Method of preparing test specimens,
- 12.1.3 Type of test specimen and dimensions,
- 12.1.4 Conditioning procedure used,
- 12.1.5 Atmospheric conditions in test room,
- 12.1.6 Number of specimens tested; for anisotropic materials, the number of specimens tested and the direction in which they were tested,
- 12.1.7 Speed of testing,
- 12.1.8 Classification of extensometers used. A description of measuring technique and calculations employed instead of a minimum Class-C extensometer system,
- 12.1.9 Tensile strength at yield or break, average value, and standard deviation,
- 12.1.10 Tensile stress at yield or break, if applicable, average value, and standard deviation,
- 12.1.11 Percent elongation at yield, or break, or nominal strain at break, or all three, as applicable, average value, and standard deviation,
- 12.1.12 Modulus of elasticity or secant modulus, average value, and standard deviation,
- 12.1.13 If measured, Poisson's ratio, average value, standard deviation, and statement of whether there was proportionality within the strain range,
- 12.1.14 Date of test, and
- 12.1.15 Revision date of Test Method D638.

13. Precision and Bias⁵

13.1 Precision—Tables 2-4 are based on a round-robin test conducted in 1984, involving five materials tested by eight laboratories using the Type I specimen, all of nominal 0.125-in. thickness. Each test result was based on five individual determinations. Each laboratory obtained two test results for each material.

⁵ Supporting data are available from ASTM Headquarters. Request RR:D20-1125 for the 1984 round robin and RR:D20-1170 for the 1988 round robin.

TABLE 2 Modulus, 10⁶ psi, for Eight Laboratories, Five Materials

	Mean	S_r	S_R	I_r	I_R
Polypropylene	0.210	0.0089	0.071	0.025	0.201
Cellulose acetate butyrate	0.246	0.0179	0.035	0.051	0.144
Acrylic	0.481	0.0179	0.063	0.051	0.144
Glass-reinforced nylon	1.17	0.0537	0.217	0.152	0.614
Glass-reinforced polyester	1.39	0.0894	0.266	0.253	0.753

TABLE 3 Tensile Stress at Break, 10³ psi, for Eight Laboratories, Five Materials^A

	Mean	S_r	S_R	I_r	I_R
Polypropylene	2.97	1.54	1.65	4.37	4.66
Cellulose acetate butyrate	4.82	0.058	0.180	0.164	0.509
Acrylic	9.09	0.452	0.751	1.27	2.13
Glass-reinforced polyester	20.8	0.233	0.437	0.659	1.24
Glass-reinforced nylon	23.6	0.277	0.698	0.784	1.98

^ATensile strength and elongation at break values obtained for unreinforced propylene plastics generally are highly variable due to inconsistencies in necking or "drawing" of the center section of the test bar. Since tensile strength and elongation at yield are more reproducible and relate in most cases to the practical usefulness of a molded part, they are generally recommended for specification purposes.

TABLE 4 Elongation at Break, %, for Eight Laboratories, Five Materials^A

	Mean	S_r	S_R	I_r	I_R
Glass-reinforced polyester	3.68	0.20	2.33	0.570	6.59
Glass-reinforced nylon	3.87	0.10	2.13	0.283	6.03
Acrylic	13.2	2.05	3.65	5.80	10.3
Cellulose acetate butyrate	14.1	1.87	6.62	5.29	18.7
Polypropylene	293.0	50.9	119.0	144.0	337.0

^ATensile strength and elongation at break values obtained for unreinforced propylene plastics generally are highly variable due to inconsistencies in necking or "drawing" of the center section of the test bar. Since tensile strength and elongation at yield are more reproducible and relate in most cases to the practical usefulness of a molded part, they are generally recommended for specification purposes.

13.1.1 Tables 5-8 are based on a round-robin test conducted by the polyolefin subcommittee in 1988, involving eight polyethylene materials tested in ten laboratories. For each material, all samples were molded at one source, but the individual specimens were prepared at the laboratories that tested them. Each test result was the average of five individual determinations. Each laboratory obtained three test results for each material. Data from some laboratories could not be used for various reasons, and this is noted in each table.

13.1.2 Tables 9 and 10 are based on a round-robin test conducted by the polyolefin subcommittee in 1988, involving three materials tested in eight laboratories. For each material, all samples were molded at one source, but the individual specimens were prepared at the laboratories that tested them. Each test result was the average of five individual determinations. Each laboratory obtained three test results for each material.

TABLE 5 Tensile Yield Stress, for Ten Laboratories, Eight Materials

Material	Test Speed, in./min	Values Expressed in psi Units				
		Average	S_r	S_R	r	R
LDPE	20	1544	52.4	64.0	146.6	179.3
LDPE	20	1894	53.1	61.2	148.7	171.3
LLDPE	20	1879	74.2	99.9	207.8	279.7
LLDPE	20	1791	49.2	75.8	137.9	212.3
LLDPE	20	2900	55.5	87.9	155.4	246.1
LLDPE	20	1730	63.9	96.0	178.9	268.7
HDPE	2	4101	196.1	371.9	549.1	1041.3
HDPE	2	3523	175.9	478.0	492.4	1338.5

TABLE 6 Tensile Yield Elongation, for Eight Laboratories, Eight Materials

Material	Test Speed, in./min	Values Expressed in Percent Units				
		Average	S_r	S_R	r	R
LDPE	20	17.0	1.26	3.16	3.52	8.84
LDPE	20	14.6	1.02	2.38	2.86	6.67
LLDPE	20	15.7	1.37	2.85	3.85	7.97
LLDPE	20	16.6	1.59	3.30	4.46	9.24
LLDPE	20	11.7	1.27	2.88	3.56	8.08
LLDPE	20	15.2	1.27	2.59	3.55	7.25
HDPE	2	9.27	1.40	2.84	3.91	7.94
HDPE	2	9.63	1.23	2.75	3.45	7.71

TABLE 7 Tensile Break Stress, for Nine Laboratories, Six Materials

Material	Test Speed, in./min	Values Expressed in psi Units				
		Average	S_r	S_R	r	R
LDPE	20	1592	52.3	74.9	146.4	209.7
LDPE	20	1750	66.6	102.9	186.4	288.1
LLDPE	20	4379	127.1	219.0	355.8	613.3
LLDPE	20	2840	78.6	143.5	220.2	401.8
LLDPE	20	1679	34.3	47.0	95.96	131.6
LLDPE	20	2660	119.1	166.3	333.6	465.6

TABLE 8 Tensile Break Elongation, for Nine Laboratories, Six Materials

Material	Test Speed, in./min	Values Expressed in Percent Units				
		Average	S_r	S_R	r	R
LDPE	20	567	31.5	59.5	88.2	166.6
LDPE	20	569	61.5	89.2	172.3	249.7
LLDPE	20	890	25.7	113.8	71.9	318.7
LLDPE	20	64.4	6.68	11.7	18.7	32.6
LLDPE	20	803	25.7	104.4	71.9	292.5
LLDPE	20	782	41.6	96.7	116.6	270.8

TABLE 9 Tensile Stress at Yield, 10³ psi, for Eight Laboratories, Three Materials

	Mean	S_r	S_R	I_r	I_R
	Polypropylene	3.63	0.022	0.161	0.062
Cellulose acetate butyrate	5.01	0.058	0.227	0.164	0.642
Acrylic	10.4	0.067	0.317	0.190	0.897

13.1.3 Table 11 is based on a repeatability study involving a single laboratory. The two materials used were unfilled polypropylene types. Measurements were performed by a single technician on a single day. Each test result is an individual determination. Testing was run using two Type B-1 extensometers for transverse and axial measurements at a test speed of 5 mm/min.

13.1.4 In Tables 2-11, for the materials indicated, and for test results that derived from testing five specimens:

TABLE 10 Elongation at Yield, %, for Eight Laboratories, Three Materials

	Mean	S_r	S_R	I_r	I_R
Cellulose acetate butyrate	3.65	0.27	0.62	0.76	1.75
Acrylic	4.89	0.21	0.55	0.59	1.56
Polypropylene	8.79	0.45	5.86	1.27	16.5

TABLE 11 Poisson's Ratio Repeatability Data for One Laboratory and Two Polypropylene Materials

Materials	Values Expressed as a Dimensionless Ratio		
	Average	S_r	r
PP #1 Chord	0.412	0.009	0.026
PP #1 Least Squares	0.413	0.011	0.032
PP #2 Chord	0.391	0.009	0.026
PP #2 Least Squares	0.392	0.010	0.028

13.1.4.1 S_r is the within-laboratory standard deviation of the average; $I_r = 2.83 S_r$. (See 13.1.4.3 for application of I_r .)

13.1.4.2 S_R is the between-laboratory standard deviation of the average; $I_R = 2.83 S_R$. (See 13.1.4.4 for application of I_R .)

13.1.4.3 *Repeatability*—In comparing two test results for the same material, obtained by the same operator using the same equipment on the same day, those test results should be judged not equivalent if they differ by more than the I_r value for that material and condition.

13.1.4.4 *Reproducibility*—In comparing two test results for the same material, obtained by different operators using different equipment on different days, those test results should be judged not equivalent if they differ by more than the I_R value for that material and condition. (This applies between different laboratories or between different equipment within the same laboratory.)

13.1.4.5 Any judgment in accordance with 13.1.4.3 and 13.1.4.4 will have an approximate 95 % (0.95) probability of being correct.

13.1.4.6 Other formulations may give somewhat different results.

13.1.4.7 For further information on the methodology used in this section, see Practice E691.

13.1.4.8 The precision of this test method is very dependent upon the uniformity of specimen preparation, standard practices for which are covered in other documents.

13.2 *Bias*—There are no recognized standards on which to base an estimate of bias for this test method.

14. Keywords

14.1 modulus of elasticity; percent elongation; plastics; Poisson's Ratio; tensile properties; tensile strength

(Mandatory Information)

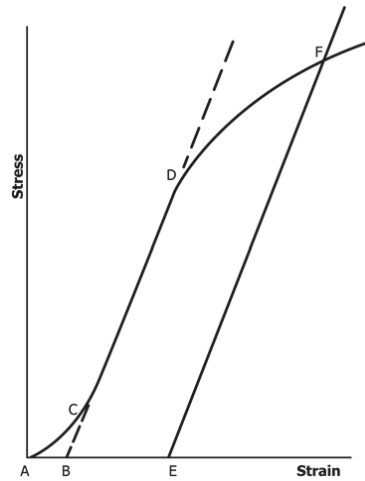
A1. TOE COMPENSATION

A1.1 In a typical stress-strain curve (Fig. A1.1) there is a toe region, AC, that does not represent a property of the material. It is an artifact caused by a take-up of slack and alignment or seating of the specimen. In order to obtain correct values of such parameters as modulus, strain, and offset yield point, this artifact must be compensated for to give the corrected zero point on the strain or extension axis.

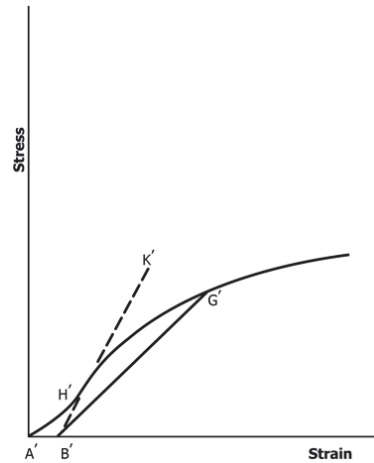
A1.2 In the case of a material exhibiting a region of Hookean (linear) behavior (Fig. A1.1), a continuation of the linear (CD) region of the curve is constructed through the zero-stress axis. This intersection (B) is the corrected zero-strain point from which all extensions or strains must be measured, including the yield offset (BE), if applicable. The

elastic modulus can be determined by dividing the stress at any point along the line CD (or its extension) by the strain at that point (measured from Point B, defined as zero-strain).

A1.3 In the case of a material that does not exhibit any linear region (Fig. A1.2), the same kind of toe correction of the zero-strain point can be made by constructing a tangent to the maximum slope at the inflection point (H'). This is extended to intersect the strain axis at Point B', the corrected zero-strain point. Using Point B' as zero strain, the stress at any point (G') on the curve can be divided by the strain at that point to obtain a secant modulus (slope of Line B'G'). For those materials with no linear region, any attempt to use the tangent through the inflection point as a basis for determination of an offset yield point may result in unacceptable error.



NOTE 1—
Some chart recorders plot the mirror image of this graph.
FIG. A1.1 Material with Hookean Region



NOTE 1—Some chart recorders plot the mirror image of this graph.
FIG. A1.2 Material with No Hookean Region

A2. DEFINITIONS OF TERMS AND SYMBOLS RELATING TO TENSION TESTING OF PLASTICS

A2.1 *elastic limit*—the greatest stress which a material is capable of sustaining without any permanent strain remaining upon complete release of the stress. It is expressed in force per unit area, usually megapascals (pounds-force per square inch).

NOTE A2.1—Measured values of proportional limit and elastic limit vary greatly with the sensitivity and accuracy of the testing equipment, eccentricity of loading, the scale to which the stress-strain diagram is plotted, and other factors. Consequently, these values are usually replaced by yield strength.

A2.2 *elongation*—the increase in length produced in the gage length of the test specimen by a tensile load. It is expressed in units of length, usually millimetres (inches). (Also known as *extension*.)

NOTE A2.2—Elongation and strain values are valid only in cases where uniformity of specimen behavior within the gage length is present. In the case of materials exhibiting necking phenomena, such values are only of qualitative utility after attainment of yield point. This is due to inability to ensure that necking will encompass the entire length between the gage marks prior to specimen failure.

A2.3 *gage length*—the original length of that portion of the specimen over which strain or change in length is determined.

A2.4 *modulus of elasticity*—the ratio of stress (nominal) to corresponding strain below the proportional limit of a material. It is expressed in force per unit area, usually megapascals (pounds-force per square inch). (Also known as *elastic modulus* or *Young's modulus*.)

NOTE A2.3—The stress-strain relations of many plastics do not conform to Hooke's law throughout the elastic range but deviate therefrom even at stresses well below the elastic limit. For such materials the slope of the tangent to the stress-strain curve at a low stress is usually taken as the modulus of elasticity. Since the existence of a true proportional limit in plastics is debatable, the propriety of applying the term "modulus of elasticity" to describe the stiffness or rigidity of a plastic has been seriously questioned. The exact stress-strain characteristics of plastic materials are very dependent on such factors as rate of stressing, temperature, previous specimen history, etc. However, such a value is useful if its arbitrary nature and dependence on time, temperature, and other factors are realized.

A2.5 *necking*—the localized reduction in cross section which may occur in a material under tensile stress.

A2.6 *offset yield strength*—the stress at which the strain exceeds by a specified amount (the offset) an extension of the initial proportional portion of the stress-strain curve. It is expressed in force per unit area, usually megapascals (pounds-force per square inch).

NOTE A2.4—This measurement is useful for materials whose stress-strain curve in the yield range is of gradual curvature. The offset yield strength can be derived from a stress-strain curve as follows (Fig. A2.1): On the strain axis lay off *OM* equal to the specified offset.

Draw *OA* tangent to the initial straight-line portion of the stress-strain curve.

Through *M* draw a line *MN* parallel to *OA* and locate the intersection of *MN* with the stress-strain curve.

The stress at the point of intersection *r* is the "offset yield strength." The specified value of the offset must be stated as a percent of the original gage length in conjunction with the strength value. Example: 0.1 % offset yield strength = ... MPa (psi), or yield strength at 0.1 % offset ... MPa (psi).

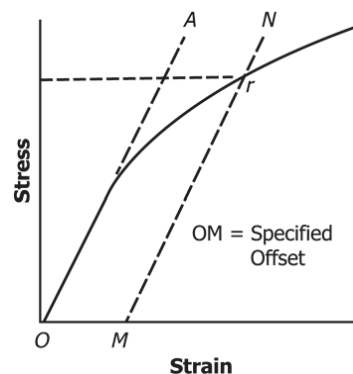


FIG. A2.1 Offset Yield Strength

A2.7 *percent elongation*—the elongation of a test specimen expressed as a percent of the gage length.

A2.8 *percent elongation at break and yield*:

A2.8.1 *percent elongation at break*—the percent elongation at the moment of rupture of the test specimen.

A2.8.2 *percent elongation at yield*—the percent elongation at the moment the yield point (A2.22) is attained in the test specimen.

A2.9 *percent reduction of area (nominal)*—the difference between the original cross-sectional area measured at the point of rupture after breaking and after all retraction has ceased, expressed as a percent of the original area.

A2.10 *percent reduction of area (true)*—the difference between the original cross-sectional area of the test specimen and the minimum cross-sectional area within the gage boundaries prevailing at the moment of rupture, expressed as a percentage of the original area.

A2.11 *Poisson's Ratio*—The absolute value of the ratio of transverse strain to the corresponding axial strain resulting from uniformly distributed axial stress below the proportional limit of the material.

A2.12 *proportional limit*—the greatest stress which a material is capable of sustaining without any deviation from proportionality of stress to strain (Hooke's law). It is expressed in force per unit area, usually megapascals (pounds-force per square inch).

A2.13 *rate of loading*—the change in tensile load carried by the specimen per unit time. It is expressed in force per unit time, usually newtons (pounds-force) per minute. The initial rate of loading can be calculated from the initial slope of the load versus time diagram.

A2.14 rate of straining—the change in tensile strain per unit time. It is expressed either as strain per unit time, usually metres per metre (inches per inch) per minute, or percent elongation per unit time, usually percent elongation per minute. The initial rate of straining can be calculated from the initial slope of the tensile strain versus time diagram.

NOTE A2.5—The initial rate of straining is synonymous with the rate of crosshead movement divided by the initial distance between crossheads only in a machine with constant rate of crosshead movement and when the specimen has a uniform original cross section, does not “neck down,” and does not slip in the jaws.

A2.15 rate of stressing (nominal)—the change in tensile stress (nominal) per unit time. It is expressed in force per unit area per unit time, usually megapascals (pounds-force per square inch) per minute. The initial rate of stressing can be calculated from the initial slope of the tensile stress (nominal) versus time diagram.

NOTE A2.6—The initial rate of stressing as determined in this manner has only limited physical significance. It does, however, roughly describe the average rate at which the initial stress (nominal) carried by the test specimen is applied. It is affected by the elasticity and flow characteristics of the materials being tested. At the yield point, the rate of stressing (true) may continue to have a positive value if the cross-sectional area is decreasing.

A2.16 secant modulus—the ratio of stress (nominal) to corresponding strain at any specified point on the stress-strain curve. It is expressed in force per unit area, usually megapascals (pounds-force per square inch), and reported together with the specified stress or strain.

NOTE A2.7—This measurement is usually employed in place of modulus of elasticity in the case of materials whose stress-strain diagram does not demonstrate proportionality of stress to strain.

A2.17 strain—the ratio of the elongation to the gage length of the test specimen, that is, the change in length per unit of original length. It is expressed as a dimensionless ratio.

A2.17.1 nominal strain at break—the strain at the moment of rupture relative to the original grip separation.

A2.18 tensile strength (nominal)—the maximum tensile stress (nominal) sustained by the specimen during a tension test. When the maximum stress occurs at the yield point (A2.22), it shall be designated tensile strength at yield. When the maximum stress occurs at break, it shall be designated tensile strength at break.

A2.19 tensile stress (nominal)—the tensile load per unit area of minimum original cross section, within the gage boundaries, carried by the test specimen at any given moment.

It is expressed in force per unit area, usually megapascals (pounds-force per square inch).

NOTE A2.8—The expression of tensile properties in terms of the minimum original cross section is almost universally used in practice. In the case of materials exhibiting high extensibility or necking, or both (A2.16), nominal stress calculations may not be meaningful beyond the yield point (A2.22) due to the extensive reduction in cross-sectional area that ensues. Under some circumstances it may be desirable to express the tensile properties per unit of minimum prevailing cross section. These properties are called true tensile properties (that is, true tensile stress, etc.).

A2.20 tensile stress-strain curve—a diagram in which values of tensile stress are plotted as ordinates against corresponding values of tensile strain as abscissas.

A2.21 true strain (see Fig. A2.2) is defined by the following equation for ϵ_T :

$$\epsilon_T = \int_{L_o}^L dL/L = \ln L/L_o \quad (A2.1)$$

where:

- dL = increment of elongation when the distance between the gage marks is L ,
- L_o = original distance between gage marks, and
- L = distance between gage marks at any time.

A2.22 yield point—the first point on the stress-strain curve at which an increase in strain occurs without an increase in stress (Fig. A2.2).

NOTE A2.9—Only materials whose stress-strain curves exhibit a point of zero slope may be considered as having a yield point.

NOTE A2.10—Some materials exhibit a distinct “break” or discontinuity in the stress-strain curve in the elastic region. This break is not a yield point by definition. However, this point may prove useful for material characterization in some cases.

A2.23 yield strength—the stress at which a material exhibits a specified limiting deviation from the proportionality of stress to strain. Unless otherwise specified, this stress will be the stress at the yield point and when expressed in relation to the tensile strength shall be designated either tensile strength at yield or tensile stress at yield as required in A2.18 (Fig. A2.3). (See *offset yield strength*.)



FIG. A2.2 Illustration of True Strain Equation

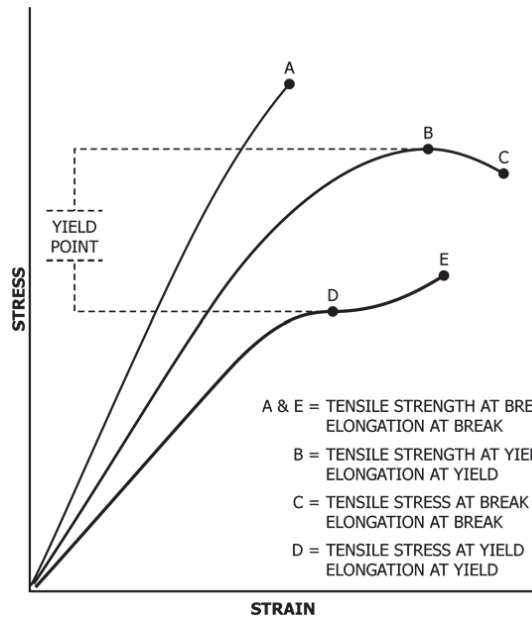


FIG. A2.3 Tensile Designations

A & E = TENSILE STRENGTH AT BREAK
 ELONGATION AT BREAK
 B = TENSILE STRENGTH AT YIELD
 ELONGATION AT YIELD
 C = TENSILE STRESS AT BREAK
 ELONGATION AT BREAK
 D = TENSILE STRESS AT YIELD
 ELONGATION AT YIELD

A2.24 Symbols—The following symbols may be used for the above terms:

Symbol	Term
W	Load
ΔW	Increment of load
L	Distance between gage marks at any time
L_o	Original distance between gage marks
L_u	Distance between gage marks at moment of rupture
ΔL	Increment of distance between gage marks = elongation

A	Minimum cross-sectional area at any time
A_o	Original cross-sectional area
ΔA	Increment of cross-sectional area
A_u	Cross-sectional area at point of rupture measured after breaking specimen
A_T	Cross-sectional area at point of rupture, measured at the moment of rupture
t	Time
Δt	Increment of time
σ	Tensile stress
$\Delta \sigma$	Increment of stress
σ_T	True tensile stress
σ_U	Tensile strength at break (nominal)
σ_{UT}	Tensile strength at break (true)
ϵ	Strain
$\Delta \epsilon$	Increment of strain
ϵ_U	Total strain, at break
ϵ_T	True strain
$\%EI$	Percentage elongation
Y.P.	Yield point
E	Modulus of elasticity

A2.25 Relations between these various terms may be defined as follows:

$$\begin{aligned} \sigma &= W/A_o \\ \sigma_T &= W/A \\ \sigma_U &= W/A_o \text{ (where } W \text{ is breaking load)} \\ \sigma_{UT} &= W/A_T \text{ (where } W \text{ is breaking load)} \\ \epsilon &= \Delta L/L_o = (L - L_o)/L_o \\ \epsilon_U &= (L_u - L_o)/L_o \\ \epsilon_T &= \int_{L_o}^L dL/L = \ln L/L_o \\ \%EI &= [(L - L_o)/L_o] \times 100 = \epsilon \times 100 \end{aligned}$$

Percent reduction of area (nominal) = $[(A_o - A_u)/A_o] \times 100$
 Percent reduction of area (true) = $[(A_o - A_T)/A_o] \times 100$
 Rate of loading = $\Delta W/\Delta t$
 Rate of stressing (nominal) = $\Delta \sigma/\Delta \epsilon = (\Delta W)/A_o/\Delta t$
 Rate of straining = $\Delta \epsilon/\Delta t = (\Delta L/L_o)/\Delta t$

For the case where the volume of the test specimen does not change during the test, the following three relations hold:

$$\sigma_T = \sigma(1 + \epsilon) = \sigma L/L_o \quad (A2.2)$$

$$\sigma_{UT} = \sigma_U(1 + \epsilon_U) = \sigma_U L_u/L_o$$

$$A = A_o/(1 + \epsilon)$$

A3. MEASUREMENT OF POISSON'S RATIO

A3.1. Scope

A3.1.1 This test method covers the determination of Poisson's ratio obtained from strains resulting from uniaxial stress only.

A3.1.2 Test data obtained by this test method are relevant and appropriate for use in engineering design.

A3.1.3 The values stated in SI units are regarded as the standard. The values given in parentheses are for information only.

NOTE A3.1—This standard is not equivalent to ISO 527-1.

A3.2. Referenced Documents

A3.2.1 ASTM Standards.²

D618 Practice for Conditioning Plastics for Testing

D883 Terminology Relating to Plastics

D5947 Test Methods for Physical Dimensions of Solid Plastics Specimens

E83 Practice for Verification and Classification of Extensometer Systems

E132 Test Method for Poisson's Ratio at Room Temperature

E691 Practice for Conducting an Interlaboratory Study to Determine the Precision of a Test Method

E1012 Practice for Verification of Testing Frame and Specimen Alignment Under Tensile and Compressive Axial Force Application

A3.2.2 ISO Standard:⁴

ISO 527-1 Determination of Tensile Properties

A3.3. Terminology

A3.3.1 *Definitions*—Definitions of terms applying to this test method appear in Terminology D883 and Annex A2 of this standard.

A3.4. Significance and Use

A3.4.1 When uniaxial tensile force is applied to a solid, the solid stretches in the direction of the applied force (axially), but it also contracts in both dimensions perpendicular to the applied force. If the solid is homogeneous and isotropic, and the material remains elastic under the action of the applied force, the transverse strain bears a constant relationship to the axial strain. This constant, called Poisson's ratio, is defined as the negative ratio of the transverse (negative) to axial strain under uniaxial stress.

A3.4.2 Poisson's ratio is used for the design of structures in which all dimensional changes resulting from the application of force need to be taken into account and in the application of the generalized theory of elasticity to structural analysis.

NOTE A3.2—The accuracy of the determination of Poisson's ratio is usually limited by the accuracy of the transverse strain measurements because the percentage errors in these measurements are usually greater than in the axial strain measurements. Since a ratio rather than an absolute quantity is measured, it is only necessary to know accurately the relative value of the calibration factors of the extensometers. Also, in general, the value of the applied loads need not be known accurately.

A3.5. Apparatus

A3.5.1 Refer to 5.1 and 5.3 of this standard for the requirements of the testing machine and micrometers.

A3.5.2 For measurement of Poisson's Ratio use either a bi-axial extensometer or an axial extensometer in combination with a transverse extensometer. They must be capable of recording axial strain and transverse strain simultaneously. The extensometers shall be capable of measuring the change in strains with an accuracy of 1 % of the relevant value or better.

NOTE A3.3—Strain gages are used as an alternative method to measure axial and transverse strain; however, proper techniques for mounting strain gauges are crucial to obtaining accurate data. Consult strain gauge suppliers for instruction and training in these special techniques.

A3.6. Test Specimen

A3.6.1 *Specimen*—The test specimen shall conform to the dimensions shown in Fig. 1. The Type I specimen is the preferred specimen and shall be used where sufficient material having a thickness of 7 mm (0.28 in.) or less is available.

A3.6.2 *Preparation*—Test specimens shall be prepared by machining operations, or die cutting, from materials in sheet, plate, slab, or similar form or be prepared by molding the material into the specimen shape to be tested.

NOTE A3.4—When preparing specimens from certain composite laminates such as woven roving, or glass cloth, care must be exercised in

cutting the specimens parallel to the reinforcement, unless testing of specimens in a direction other than parallel with the reinforcement constitutes a variable being studied.

NOTE A3.5—Specimens prepared by injection molding have different tensile properties than specimens prepared by machining or die-cutting because of the orientation induced. This effect is more pronounced in specimens with narrow sections.

A3.6.3 All surfaces of the specimen shall be free of visible flaws, scratches, or imperfections. Marks left by coarse machining operations shall be carefully removed with a fine file or abrasive, and the filed surfaces shall then be smoothed with abrasive paper (No. 00 or finer). The finishing sanding strokes shall be made in a direction parallel to the long axis of the test specimen. All flash shall be removed from a molded specimen, taking great care not to disturb the molded surfaces. In machining a specimen, undercuts that would exceed the dimensional tolerances shown in Fig. 1 shall be scrupulously avoided. Care shall also be taken to avoid other common machining errors.

A3.6.4 If it is necessary to place gage marks on the specimen, this shall be done with a wax crayon or India ink that will not affect the material being tested. Gauge marks shall not be scratched, punched, or impressed on the specimen.

A3.6.5 When testing materials that are suspected of anisotropy, duplicate sets of test specimens shall be prepared, having their long axes respectively parallel with, and normal to, the suspected direction of anisotropy.

A3.7 Number of Test Specimens

A3.7.1 Test at least five specimens for each sample in the case of isotropic materials.

A3.7.2 Test ten specimens, five normal to, and five parallel with, the principle axis of anisotropy, for each sample in the case of anisotropic materials.

A3.8. Conditioning

A3.8.1 Specimens shall be conditioned and tested in accordance with the requirement shown in Section 9 of this standard.

A3.9. Procedure

A3.9.1 Measure the width and thickness of each specimen to the nearest 0.025 mm (0.001 in.) using the applicable test methods in D5947. Follow the guidelines specified in 10.1.1 and 10.1.2 of this standard.

A3.9.2 Poisson's Ratio shall be determined at a speed of 5 mm/min.

A3.9.3 Place the specimen in the grips of the testing machine, taking care to align the long axis of the specimen and the grips with an imaginary line joining the points of attachment of the grips to the machine. The distance between the ends of the gripping surfaces, when using flat specimens, shall be as indicated in Fig. 1. Tighten the grips evenly and firmly to the degree necessary to prevent slippage of the specimen during the test, but not to the point where the specimen would be crushed.

A3.9.4 Attach the biaxial extensometer or the axial and transverse extensometer combination to the specimen. The transverse extensometer should be attached to the width of the specimen.

A3.9.5 Apply a small preload (less than 5 N) to the specimen at a crosshead speed of 0.1 mm/min. This preload will eliminate any bending in the specimens.

A3.9.6 Rebalance the extensometers to zero.

A3.9.7 Run the test at 5 mm/min out to a minimum of 0.5 % strain before removing the extensometers, simultaneously recording the strain readings from the extensometers at the same applied force. The precision of the value of Poisson's Ratio will depend on the number of data points of axial and transverse strain taken. It is recommended that the data collection rate for the test be a minimum of 20 points per second (but preferably higher). This is particularly important for materials having a non linear stress to strain curve.

A3.9.8 Make the toe compensation in accordance with Annex A1. Determine the maximum strain (proportional limit) at which the curve is linear. If this strain is greater than 0.25 % the Poisson's Ratio is to be determined anywhere in this linear portion of the curve below the proportional limit. If the material does not exhibit a linear stress to strain relationship the Poisson's Ratio shall be determined within the axial strain range of 0.0005 to 0.0025 mm/mm (0.05 to 0.25 %). If the ratio is determined in this manner it shall be noted in the report that a region of proportionality of stress to strain was not evident.

NOTE A3.6—A suitable method for determination of linearity of the stress to strain curve is by making a series of tangent modulus measurements at different axial strain levels. Values equivalent at each strain level indicate linearity. Values showing a downward trend with increasing strain level indicate non linearity.

A3.10. Calculation

A3.10.1 *Poisson's Ratio*—The axial strain, ϵ_a , indicated by the axial extensometer, and the transverse strain, ϵ_t , indicated by the transverse extensometers, are plotted against the applied load, P , as shown in Fig. A3.1.

A3.10.1.1 For those materials where there is proportionality of stress to strain and it is possible to determine a modulus of elasticity, a straight line is drawn through each set of points within the load range used for determination of modulus, and the slopes $d\epsilon_a / dP$ and $d\epsilon_t / dP$, of those lines are determined. The use of a least squares method of calculation will reduce errors resulting from drawing lines. Poisson's Ratio, $|\mu|$, is then calculated as follows:

$$|\mu| = (d\epsilon_t/dP)/(d\epsilon_a/dP) \tag{A3.1}$$

where:

- $d\epsilon_t$ = change in transverse strain,
- $d\epsilon_a$ = change in axial strain, and
- dP = change in applied load;

$$|\mu| = (d\epsilon_t)/(d\epsilon_a) \tag{A3.2}$$

A3.10.1.2 The errors that are introduced by drawing a straight line through the points are reduced by applying the least squares method.

A3.10.1.3 For those materials where there is no proportionality of stress to strain evident determine the ratio of $d\epsilon_t / d\epsilon_a$ when $d\epsilon_a = 0.002$ (based on axial strain range of 0.0005 to 0.0025 mm/mm) and after toe compensation has been made.

$$|\mu| = d\epsilon_t/0.002 \tag{A3.3}$$

A3.11. Report

A3.11.1 Report the following information:

- A3.11.1.1 Complete identification of the material tested, including type, source, manufacturer's code numbers, form, principal dimensions, previous history, etc.,
- A3.11.1.2 Method of preparing test specimens,
- A3.11.1.3 Type of test specimen and dimensions,
- A3.11.1.4 Conditioning procedure used,
- A3.11.1.5 Atmospheric conditions in test room,
- A3.11.1.6 Number of specimens tested,
- A3.11.1.7 Speed of testing,
- A3.11.1.8 Classification of extensometers used. A description of measuring technique and calculations employed,

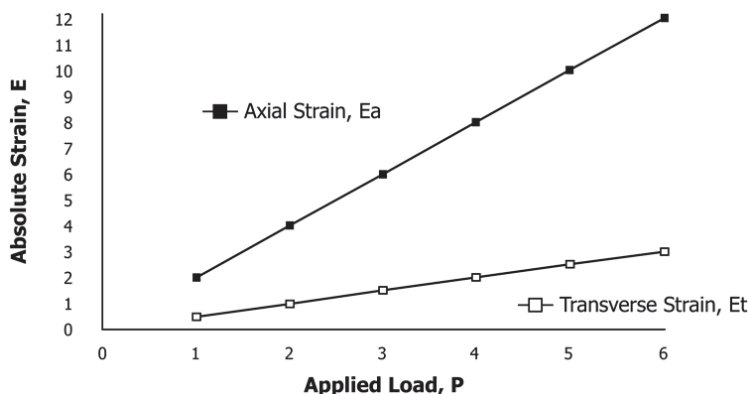


FIG. A3.1 Plot of Strains Versus Load for Determination of Poisson's Ratio

A3.11.1.9 Poisson's ratio, average value, standard deviation, and statement of whether there was proportionality within the strain range,

A3.11.1.10 Date of test, and

A3.11.1.11 Revision date of Test Method **D618**.

A3.12. Precision and Bias

A3.12.1 *Precision*—The repeatability standard deviation has been determined to be the following (see **Table A3.1**.) An attempt to develop a full precision and bias statement for this test method will be made at a later date. For this reason, data

on precision and bias cannot be given. Because this test method does not contain a round-robin based numerical precision and bias statement, it shall not be used as a referee test method in case of dispute. Anyone wishing to participate in the development of precision and bias data should contact the Chairman, Subcommittee D20.10 Mechanical Properties, ASTM International, 100 Barr Harbor, West Conshohocken, PA 19428.

A3.13 Keywords

axial strain; Poisson's ratio; transverse strain

TABLE A3.1 Poisson's Ratio Based on One Laboratory

Material	Extensometer Type	Average	V_r^A	V_R^B	r^C	R^D
PP Copolymer	2–point	0.408	0.011		0.031	
PP Copolymer	4–point	0.392	0.010		0.028	
PP Homopolymer with 20 % Glass	2–point	0.428	0.013		0.036	
PP Homopolymer with 20 % Glass	4–point	0.410	0.015		0.042	

^A S_r = within laboratory standard deviation for the indicated material. It is obtained by first pooling the with-laboratory standard deviations of the test results from all the participating laboratories:

$$S_r = \{[(S_1)^2 + (S_2)^2 + \dots + (S_n)^2]/n\}^{1/2}$$

^B S_R = between-laboratories reproducibility, expressed as standard deviation: $S_R = [S_r^2 + S_L^2]^{1/2}$

^C r = within-laboratory critical interval between two test results = $2.8 \times S_r$

^D R = between-laboratories critical interval between two test results = $2.8 \times S_R$

SUMMARY OF CHANGES

Committee D20 has identified the location of selected changes to this standard since the last issue (D638 - 10) that may impact the use of this standard. (December 15, 2014)

- | | |
|--|---|
| (1) Revised Note 1 since changes were made to ISO 527-1, and it is no longer equivalent to this standard. | (3) Made some editorial changes. |
| (2) Removed permissive language. | (4) Moved Tables 2-5 to Section 13 on Precision and Bias. |
| | (5) Revised Summary of Changes section. |

ASTM International takes no position respecting the validity of any patent rights asserted in connection with any item mentioned in this standard. Users of this standard are expressly advised that determination of the validity of any such patent rights, and the risk of infringement of such rights, are entirely their own responsibility.

This standard is subject to revision at any time by the responsible technical committee and must be reviewed every five years and if not revised, either reapproved or withdrawn. Your comments are invited either for revision of this standard or for additional standards and should be addressed to ASTM International Headquarters. Your comments will receive careful consideration at a meeting of the responsible technical committee, which you may attend. If you feel that your comments have not received a fair hearing you should make your views known to the ASTM Committee on Standards, at the address shown below.

This standard is copyrighted by ASTM International, 100 Barr Harbor Drive, PO Box C700, West Conshohocken, PA 19428-2959, United States. Individual reprints (single or multiple copies) of this standard may be obtained by contacting ASTM at the above address or at 610-832-9585 (phone), 610-832-9555 (fax), or service@astm.org (e-mail); or through the ASTM website (www.astm.org). Permission rights to photocopy the standard may also be secured from the Copyright Clearance Center, 222 Rosewood Drive, Danvers, MA 01923, Tel: (978) 646-2600; http://www.copyright.com/



Designation: D256 – 10^{ε1}

Standard Test Methods for Determining the Izod Pendulum Impact Resistance of Plastics¹

This standard is issued under the fixed designation D256; the number immediately following the designation indicates the year of original adoption or, in the case of revision, the year of last revision. A number in parentheses indicates the year of last reapproval. A superscript epsilon (ϵ) indicates an editorial change since the last revision or reapproval.

This standard has been approved for use by agencies of the U.S. Department of Defense.

^{ε1} NOTE—Editorially corrected Figure 2 in October 2015.

1. Scope*

1.1 These test methods cover the determination of the resistance of plastics to “standardized” (see [Note 1](#)) pendulum-type hammers, mounted in “standardized” machines, in breaking standard specimens with one pendulum swing (see [Note 2](#)). The standard tests for these test methods require specimens made with a milled notch (see [Note 3](#)). In Test Methods A, C, and D, the notch produces a stress concentration that increases the probability of a brittle, rather than a ductile, fracture. In Test Method E, the impact resistance is obtained by reversing the notched specimen 180° in the clamping vise. The results of all test methods are reported in terms of energy absorbed per unit of specimen width or per unit of cross-sectional area under the notch. (See [Note 4](#).)

NOTE 1—The machines with their pendulum-type hammers have been “standardized” in that they must comply with certain requirements, including a fixed height of hammer fall that results in a substantially fixed velocity of the hammer at the moment of impact. However, hammers of different initial energies (produced by varying their effective weights) are recommended for use with specimens of different impact resistance. Moreover, manufacturers of the equipment are permitted to use different lengths and constructions of pendulums with possible differences in pendulum rigidities resulting. (See [Section 5](#).) Be aware that other differences in machine design may exist. The specimens are “standardized” in that they are required to have one fixed length, one fixed depth, and one particular design of milled notch. The width of the specimens is permitted to vary between limits.

NOTE 2—Results generated using pendulums that utilize a load cell to record the impact force and thus impact energy, may not be equivalent to results that are generated using manually or digitally encoded testers that measure the energy remaining in the pendulum after impact.

NOTE 3—The notch in the Izod specimen serves to concentrate the stress, minimize plastic deformation, and direct the fracture to the part of the specimen behind the notch. Scatter in energy-to-break is thus reduced. However, because of differences in the elastic and viscoelastic properties of plastics, response to a given notch varies among materials. A measure

¹ These test methods are under the jurisdiction of ASTM Committee D20 on Plastics and are the direct responsibility of Subcommittee D20.10 on Mechanical Properties.

Current edition approved May 1, 2010. Published June 2010. Originally approved in 1926. Last previous edition approved in 2006 as D256 - 06a^{ε1}. DOI: 10.1520/D0256-10.

of a plastic’s “notch sensitivity” may be obtained with Test Method D by comparing the energies to break specimens having different radii at the base of the notch.

NOTE 4—Caution must be exercised in interpreting the results of these standard test methods. The following testing parameters may affect test results significantly:

- Method of fabrication, including but not limited to processing technology, molding conditions, mold design, and thermal treatments;
- Method of notching;
- Speed of notching tool;
- Design of notching apparatus;
- Quality of the notch;
- Time between notching and test;
- Test specimen thickness,
- Test specimen width under notch, and
- Environmental conditioning.

1.2 The values stated in SI units are to be regarded as standard. The values given in parentheses are for information only.

1.3 *This standard does not purport to address all of the safety concerns, if any, associated with its use. It is the responsibility of the user of this standard to establish appropriate safety and health practices and determine the applicability of regulatory limitations prior to use.*

NOTE 5—These test methods resemble ISO 180:1993 in regard to title only. The contents are significantly different.

2. Referenced Documents

2.1 ASTM Standards:²

- D618 Practice for Conditioning Plastics for Testing
- D883 Terminology Relating to Plastics
- D3641 Practice for Injection Molding Test Specimens of Thermoplastic Molding and Extrusion Materials
- D4066 Classification System for Nylon Injection and Extrusion Materials (PA)
- D5947 Test Methods for Physical Dimensions of Solid Plastics Specimens

² For referenced ASTM standards, visit the ASTM website, www.astm.org, or contact ASTM Customer Service at service@astm.org. For *Annual Book of ASTM Standards* volume information, refer to the standard’s Document Summary page on the ASTM website.

*A Summary of Changes section appears at the end of this standard

Copyright © ASTM International, 100 Barr Harbor Drive, PO Box C700, West Conshohocken, PA 19428-2959, United States

Copyright ASTM International
Not for Resale, 12/09/2015 21:35:33 MST

Provided by IHS under license with ASTM
Licensee=Uni of Technology Sydney/5928310001

D6110 Test Method for Determining the Charpy Impact Resistance of Notched Specimens of Plastics

E691 Practice for Conducting an Interlaboratory Study to Determine the Precision of a Test Method

2.2 ISO Standard:

ISO 180:1993 Plastics—Determination of Izod Impact Strength of Rigid Materials³

3. Terminology

3.1 *Definitions*—For definitions related to plastics see Terminology D883.

3.2 *Definitions of Terms Specific to This Standard:*

3.2.1 *cantilever*—a projecting beam clamped at only one end.

3.2.2 *notch sensitivity*—a measure of the variation of impact energy as a function of notch radius.

4. Types of Tests

4.1 Four similar methods are presented in these test methods. (See Note 6.) All test methods use the same testing machine and specimen dimensions. There is no known means for correlating the results from the different test methods.

NOTE 6—Previous versions of this test method contained Test Method B for Charpy. It has been removed from this test method and has been published as D6110.

4.1.1 In Test Method A, the specimen is held as a vertical cantilever beam and is broken by a single swing of the pendulum. The line of initial contact is at a fixed distance from the specimen clamp and from the centerline of the notch and on the same face as the notch.

4.1.2 Test Method C is similar to Test Method A, except for the addition of a procedure for determining the energy expended in tossing a portion of the specimen. The value reported is called the “estimated net Izod impact resistance.” Test Method C is preferred over Test Method A for materials that have an Izod impact resistance of less than 27 J/m (0.5 ft-lbf/in.) under notch. (See Appendix X4 for optional units.) The differences between Test Methods A and C become unimportant for materials that have an Izod impact resistance higher than this value.

4.1.3 Test Method D provides a measure of the notch sensitivity of a material. The stress-concentration at the notch increases with decreasing notch radius.

4.1.3.1 For a given system, greater stress concentration results in higher localized rates-of-strain. Since the effect of strain-rate on energy-to-break varies among materials, a measure of this effect may be obtained by testing specimens with different notch radii. In the Izod-type test it has been demonstrated that the function, energy-to-break versus notch radius, is reasonably linear from a radius of 0.03 to 2.5 mm (0.001 to 0.100 in.), provided that all specimens have the same type of break. (See 5.8 and 22.1.)

4.1.3.2 For the purpose of this test, the slope, *b* (see 22.1), of the line between radii of 0.25 and 1.0 mm (0.010 and 0.040

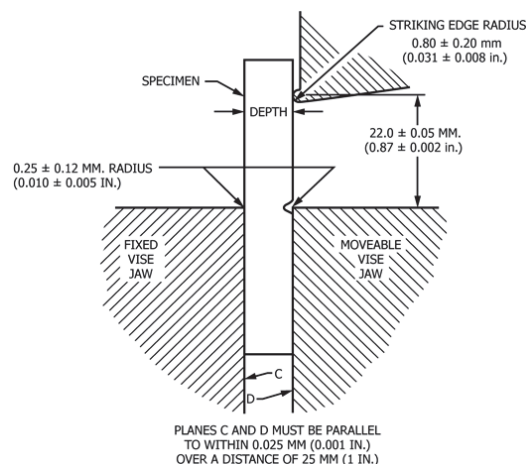


FIG. 1 Relationship of Vise, Specimen, and Striking Edge to Each Other for Izod Test Methods A and C

in.) is used, unless tests with the 1.0-mm radius give “non-break” results. In that case, 0.25 and 0.50-mm (0.010 and 0.020-in.) radii may be used. The effect of notch radius on the impact energy to break a specimen under the conditions of this test is measured by the value *b*. Materials with low values of *b*, whether high or low energy-to-break with the standard notch, are relatively insensitive to differences in notch radius; while the energy-to-break materials with high values of *b* is highly dependent on notch radius. The parameter *b* cannot be used in design calculations but may serve as a guide to the designer and in selection of materials.

4.2 Test Method E is similar to Test Method A, except that the specimen is reversed in the vise of the machine 180° to the usual striking position, such that the striker of the apparatus impacts the specimen on the face opposite the notch. (See Fig. 1, Fig. 2.) Test Method E is used to give an indication of the unnotched impact resistance of plastics; however, results obtained by the reversed notch method may not always agree with those obtained on a completely unnotched specimen. (See 28.1.)^{4,5}

5. Significance and Use

5.1 Before proceeding with these test methods, reference should be made to the specification of the material being tested. Any test specimen preparation, conditioning, dimensions, and testing parameters covered in the materials specification shall take precedence over those mentioned in these test methods. If there is no material specification, then the default conditions apply.

⁴ Supporting data giving results of the interlaboratory tests are available from ASTM Headquarters. Request RR:D20-1021.

⁵ Supporting data giving results of the interlaboratory tests are available from ASTM Headquarters. Request RR:D20-1026.

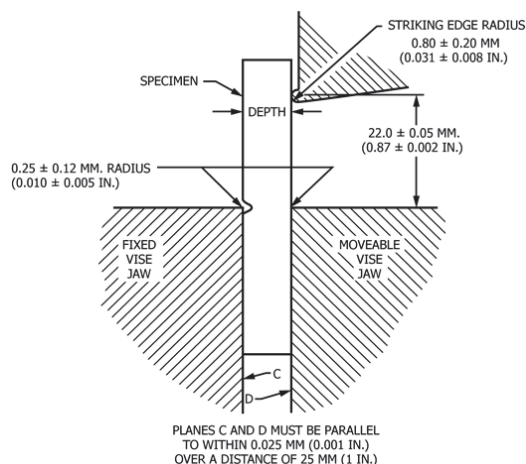


FIG. 2 Relationship of Vise, Specimen, and Striking Edge to Each Other for Test Method E

5.2 The pendulum impact test indicates the energy to break standard test specimens of specified size under stipulated parameters of specimen mounting, notching, and pendulum velocity-at-impact.

5.3 The energy lost by the pendulum during the breakage of the specimen is the sum of the following:

- 5.3.1 Energy to initiate fracture of the specimen;
- 5.3.2 Energy to propagate the fracture across the specimen;
- 5.3.3 Energy to throw the free end (or ends) of the broken specimen (“toss correction”);
- 5.3.4 Energy to bend the specimen;
- 5.3.5 Energy to produce vibration in the pendulum arm;
- 5.3.6 Energy to produce vibration or horizontal movement of the machine frame or base;
- 5.3.7 Energy to overcome friction in the pendulum bearing and in the indicating mechanism, and to overcome windage (pendulum air drag);
- 5.3.8 Energy to indent or deform plastically the specimen at the line of impact; and
- 5.3.9 Energy to overcome the friction caused by the rubbing of the striker (or other part of the pendulum) over the face of the bent specimen.

5.4 For relatively brittle materials, for which fracture propagation energy is small in comparison with the fracture initiation energy, the indicated impact energy absorbed is, for all practical purposes, the sum of factors 5.3.1 and 5.3.3. The toss correction (see 5.3.3) may represent a very large fraction of the total energy absorbed when testing relatively dense and brittle materials. Test Method C shall be used for materials that have an Izod impact resistance of less than 27 J/m (0.5 ft-lbf/in.). (See Appendix X4 for optional units.) The toss correction obtained in Test Method C is only an approximation of the toss error, since the rotational and rectilinear velocities may not be the same during the re-toss of the specimen as for the original

toss, and because stored stresses in the specimen may have been released as kinetic energy during the specimen fracture.

5.5 For tough, ductile, fiber filled, or cloth-laminated materials, the fracture propagation energy (see 5.3.2) may be large compared to the fracture initiation energy (see 5.3.1). When testing these materials, factors (see 5.3.2, 5.3.5, and 5.3.9) can become quite significant, even when the specimen is accurately machined and positioned and the machine is in good condition with adequate capacity. (See Note 7.) Bending (see 5.3.4) and indentation losses (see 5.3.8) may be appreciable when testing soft materials.

NOTE 7—Although the frame and base of the machine should be sufficiently rigid and massive to handle the energies of tough specimens without motion or excessive vibration, the design must ensure that the center of percussion be at the center of strike. Locating the striker precisely at the center of percussion reduces vibration of the pendulum arm when used with brittle specimens. However, some losses due to pendulum arm vibration, the amount varying with the design of the pendulum, will occur with tough specimens, even when the striker is properly positioned.

5.6 In a well-designed machine of sufficient rigidity and mass, the losses due to factors 5.3.6 and 5.3.7 should be very small. Vibrational losses (see 5.3.6) can be quite large when wide specimens of tough materials are tested in machines of insufficient mass, not securely fastened to a heavy base.

5.7 With some materials, a critical width of specimen may be found below which specimens will appear ductile, as evidenced by considerable drawing or necking down in the region behind the notch and by a relatively high-energy absorption, and above which they will appear brittle as evidenced by little or no drawing down or necking and by a relatively low-energy absorption. Since these methods permit a variation in the width of the specimens, and since the width dictates, for many materials, whether a brittle, low-energy break or a ductile, high energy break will occur, it is necessary that the width be stated in the specification covering that material and that the width be reported along with the impact resistance. In view of the preceding, one should not make comparisons between data from specimens having widths that differ by more than a few mils.

5.8 The type of failure for each specimen shall be recorded as one of the four categories listed as follows:

- C = Complete Break—A break where the specimen separates into two or more pieces.
- H = Hinge Break—An incomplete break, such that one part of the specimen cannot support itself above the horizontal when the other part is held vertically (less than 90° included angle).
- P = Partial Break—An incomplete break that does not meet the definition for a hinge break but has fractured at least 90 % of the distance between the vertex of the notch and the opposite side.
- NB = Non-Break—An incomplete break where the fracture extends less than 90 % of the distance between the vertex of the notch and the opposite side.

For tough materials, the pendulum may not have the energy necessary to complete the breaking of the extreme fibers and toss the broken piece or pieces. Results obtained from “non-break” specimens shall be considered a departure from standard and shall not be reported as a standard result. Impact

resistance cannot be directly compared for any two materials that experience different types of failure as defined in the test method by this code. Averages reported must likewise be derived from specimens contained within a single failure category. This letter code shall suffix the reported impact identifying the types of failure associated with the reported value. If more than one type of failure is observed for a sample material, then the report will indicate the average impact resistance for each type of failure, followed by the percent of the specimens failing in that manner and suffixed by the letter code.

5.9 The value of the impact methods lies mainly in the areas of quality control and materials specification. If two groups of specimens of supposedly the same material show significantly different energy absorptions, types of breaks, critical widths, or critical temperatures, it may be assumed that they were made of different materials or were exposed to different processing or conditioning environments. The fact that a material shows twice the energy absorption of another under these conditions of test does not indicate that this same relationship will exist under another set of test conditions. The order of toughness may even be reversed under different testing conditions.

NOTE 8—A documented discrepancy exists between manual and digital impact testers, primarily with thermoset materials, including phenolics, having an impact value of less than 54 J/m (1 ft-lb/in.). Comparing data on the same material, tested on both manual and digital impact testers, may show the data from the digital tester to be significantly lower than data from a manual tester. In such cases a correlation study may be necessary to properly define the true relationship between the instruments.

TEST METHOD A—CANTILEVER BEAM TEST

6. Apparatus

6.1 The machine shall consist of a massive base on which is mounted a vise for holding the specimen and to which is connected, through a rigid frame and bearings, a pendulum-type hammer. (See 6.2.) The machine must also have a pendulum holding and releasing mechanism and a mechanism for indicating the breaking energy of the specimen.

6.2 A jig for positioning the specimen in the vise and graphs or tables to aid in the calculation of the correction for friction and windage also should be included. One type of machine is shown in Fig. 3. One design of specimen-positioning jig is illustrated in Fig. 4. Detailed requirements are given in subsequent paragraphs. General test methods for checking and calibrating the machine are given in Appendix X2. Additional instructions for adjusting a particular machine should be supplied by the manufacturer.

6.3 The pendulum shall consist of a single or multi-membered arm with a bearing on one end and a head, containing the striker, on the other. The arm must be sufficiently rigid to maintain the proper clearances and geometric relationships between the machine parts and the specimen and to minimize vibrational energy losses that are always included in the measured impact resistance. Both simple and compound pendulum designs may comply with this test method.

6.4 The striker of the pendulum shall be hardened steel and shall be a cylindrical surface having a radius of curvature of 0.80 ± 0.20 mm (0.031 ± 0.008 in.) with its axis horizontal

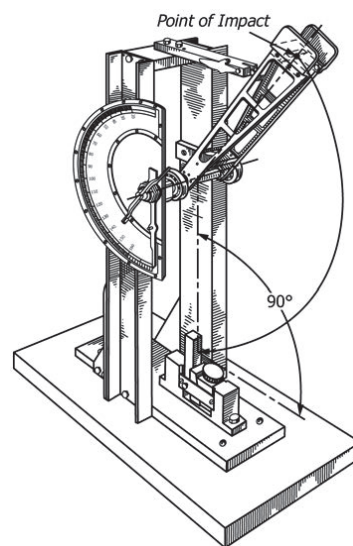


FIG. 3 Cantilever Beam (Izod-Type) Impact Machine



FIG. 4 Jig for Positioning Specimen for Clamping

and perpendicular to the plane of swing of the pendulum. The line of contact of the striker shall be located at the center of percussion of the pendulum within ±2.54 mm (±0.100 in.) (See Note 9.) Those portions of the pendulum adjacent to the cylindrical striking edge shall be recessed or inclined at a suitable angle so that there will be no chance for other than this cylindrical surface coming in contact with the specimen during the break.

NOTE 9—The distance from the axis of support to the center of percussion may be determined experimentally from the period of small

amplitude oscillations of the pendulum by means of the following equation:

$$L = (g/4\pi^2)p^2$$

where:

- L = distance from the axis of support to the center of percussion, m or (ft),
- g = local gravitational acceleration (known to an accuracy of one part in one thousand), m/s² or (ft/s²),
- π = 3.1416 ($4\pi^2 = 39.48$), and
- p = period, s, of a single complete swing (to and fro) determined by averaging at least 20 consecutive and uninterrupted swings. The angle of swing shall be less than 5° each side of center.

6.5 The position of the pendulum holding and releasing mechanism shall be such that the vertical height of fall of the striker shall be 610 ± 2 mm (24.0 ± 0.1 in.). This will produce a velocity of the striker at the moment of impact of approximately 3.5 m (11.4 ft)/s. (See [Note 10](#).) The mechanism shall be so constructed and operated that it will release the pendulum without imparting acceleration or vibration to it.

NOTE 10—

$$V = (2gh)^{0.5}$$

where:

- V = velocity of the striker at the moment of impact (m/s),
- g = local gravitational acceleration (m/s²), and
- h = vertical height of fall of the striker (m).

This assumes no windage or friction.

6.6 The effective length of the pendulum shall be between 0.33 and 0.40 m (12.8 and 16.0 in.) so that the required elevation of the striker may be obtained by raising the pendulum to an angle between 60 and 30° above the horizontal.

6.7 The machine shall be provided with a basic pendulum capable of delivering an energy of 2.7 ± 0.14 J (2.00 ± 0.10 ft-lbf). This pendulum shall be used with all specimens that extract less than 85 % of this energy. Heavier pendulums shall be provided for specimens that require more energy to break. These may be separate interchangeable pendulums or one basic pendulum to which extra pairs of equal calibrated weights may be rigidly attached to opposite sides of the pendulum. It is imperative that the extra weights shall not significantly change the position of the center of percussion or the free-hanging rest point of the pendulum (that would consequently take the machine outside of the allowable calibration tolerances). A range of pendulums having energies from 2.7 to 21.7 J (2 to 16 ft-lbf) has been found to be sufficient for use with most plastic specimens and may be used with most machines. A series of pendulums such that each has twice the energy of the next will be found convenient. Each pendulum shall have an energy within ± 0.5 % of its nominal capacity.

6.8 A vise shall be provided for clamping the specimen rigidly in position so that the long axis of the specimen is vertical and at right angles to the top plane of the vise. (See [Fig. 1](#).) This top plane shall bisect the angle of the notch with a tolerance of 0.12 mm (0.005 in.). Correct positioning of the specimen is generally done with a jig furnished with the machine. The top edges of the fixed and moveable jaws shall have a radius of 0.25 ± 0.12 mm (0.010 ± 0.005 in.). For specimens whose thickness approaches the lower limiting

value of 3.00 mm (0.118 in.), means shall be provided to prevent the lower half of the specimen from moving during the clamping or testing operations (see [Fig. 4](#) and [Note 11](#).)

NOTE 11—Some plastics are sensitive to clamping pressure; therefore, cooperating laboratories should agree upon some means of standardizing the clamping force. One method is using a torque wrench on the screw of the specimen vise. If the faces of the vise or specimen are not flat and parallel, a greater sensitivity to clamping pressure may be evident. See the calibration procedure in [Appendix X2](#) for adjustment and correction instructions for faulty instruments.

6.9 When the pendulum is free hanging, the striking surface shall come within 0.2 % of scale of touching the front face of a standard specimen. During an actual swing this element shall make initial contact with the specimen on a line 22.00 ± 0.05 mm (0.87 ± 0.002 in.) above the top surface of the vise.

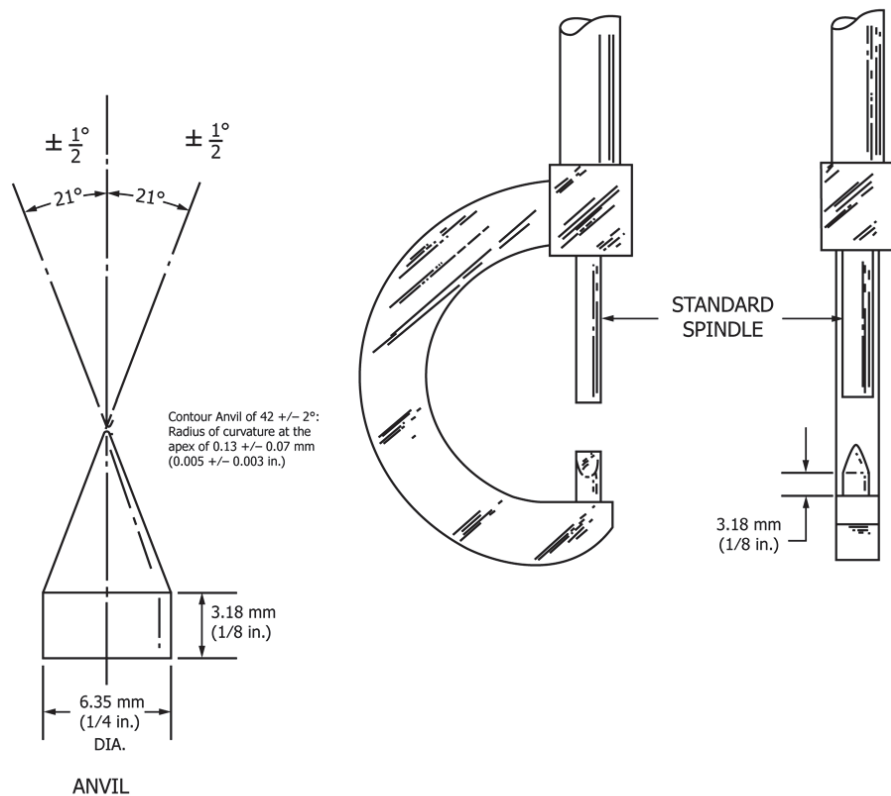
6.10 Means shall be provided for determining the energy expended by the pendulum in breaking the specimen. This is accomplished using either a pointer and dial mechanism or an electronic system consisting of a digital indicator and sensor (typically an encoder or resolver). In either case, the indicated breaking energy is determined by detecting the height of rise of the pendulum beyond the point of impact in terms of energy removed from that specific pendulum. Since the indicated energy must be corrected for pendulum-bearing friction, pointer friction, pointer inertia, and pendulum windage, instructions for making these corrections are included in [10.3](#) and [Annex A1](#) and [Annex A2](#). If the electronic display does not automatically correct for windage and friction, it shall be incumbent for the operator to determine the energy loss manually. (See [Note 12](#).)

NOTE 12—Many digital indicating systems automatically correct for windage and friction. The equipment manufacturer may be consulted for details concerning how this is performed, or if it is necessary to determine the means for manually calculating the energy loss due to windage and friction.

6.11 The vise, pendulum, and frame shall be sufficiently rigid to maintain correct alignment of the hammer and specimen, both at the moment of impact and during the propagation of the fracture, and to minimize energy losses due to vibration. The base shall be sufficiently massive that the impact will not cause it to move. The machine shall be so designed, constructed, and maintained that energy losses due to pendulum air drag (windage), friction in the pendulum bearings, and friction and inertia in the indicating mechanism are held to a minimum.

6.12 A check of the calibration of an impact machine is difficult to make under dynamic conditions. The basic parameters are normally checked under static conditions; if the machine passes the static tests, then it is assumed to be accurate. The calibration procedure in [Appendix X2](#) should be used to establish the accuracy of the equipment. However, for some machine designs it might be necessary to change the recommended method of obtaining the required calibration measurements. Other methods of performing the required checks may be substituted, provided that they can be shown to result in an equivalent accuracy. [Appendix X1](#) also describes a dynamic test for checking certain features of the machine and specimen.

IZOD



SCALE: 4:1

- NOTE 1—These views not to scale.
- NOTE 2—Micrometer to be satin-chrome finished with friction thimble.
- NOTE 3—Special anvil for micrometer caliper 0 to 25.4 mm range (50.8 mm frame) (0 to 1 in. range (2-in. frame)).
- NOTE 4—Anvil to be oriented with respect to frame as shown.
- NOTE 5—Anvil and spindle to have hardened surfaces.
- NOTE 6—Range: 0 to 25.4 mm (0 to 1 in. in thousandths of an inch).
- NOTE 7—Adjustment must be at zero when spindle and anvil are in contact.

FIG. 5 Early (ca. 1970) Version of a Notch-Depth Micrometer

6.13 *Micrometers*—Apparatus for measurement of the width of the specimen shall comply with the requirements of Test Methods D5947. Apparatus for the measurement of the depth of plastic material remaining in the specimen under the notch shall comply with requirements of Test Methods D5947, provided however that the one anvil or presser foot shall be a tapered blade conforming to the dimensions given in Fig. 5. The opposing anvil or presser foot shall be flat and conforming to Test Methods D5947.

7. Test Specimens

7.1 The test specimens shall conform to the dimensions and geometry of Fig. 6, except as modified in accordance with 7.2, 7.3, 7.4, and 7.5. To ensure the correct contour and conditions of the specified notch, all specimens shall be notched as directed in Section 8.

7.1.1 Studies have shown that, for some materials, the location of the notch on the specimen and the length of the impacted end may have a slight effect on the measured impact

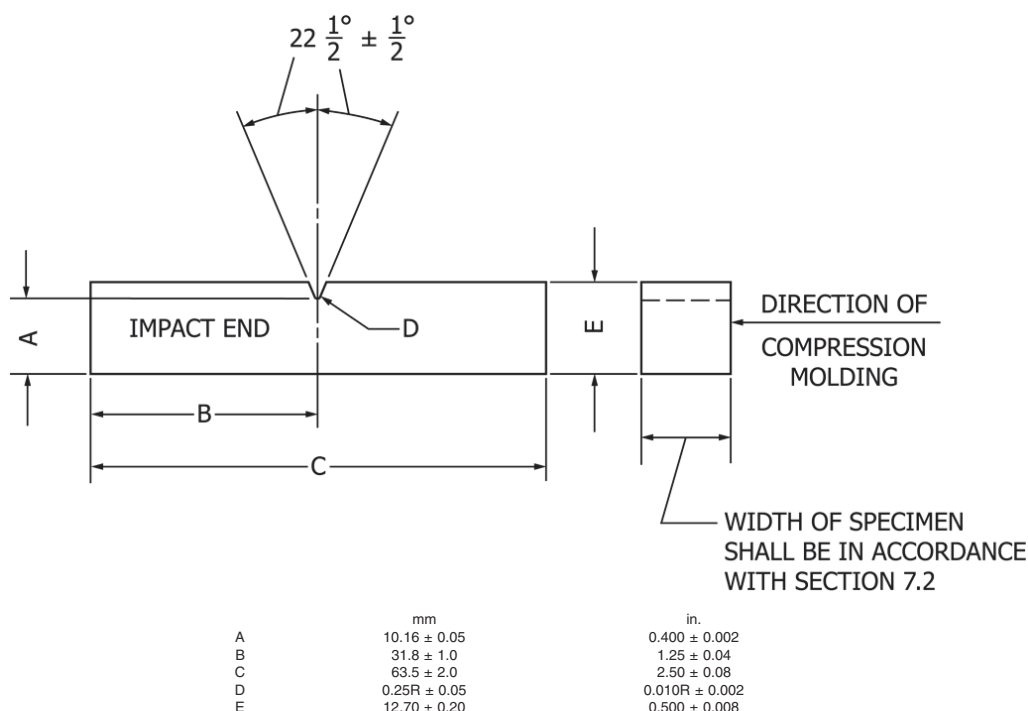


FIG. 6 Dimensions of Izod-Type Test Specimen

resistance. Therefore, unless otherwise specified, care must be taken to ensure that the specimen conforms to the dimensions shown in Fig. 6 and that it is positioned as shown in Fig. 1 or Fig. 2.

7.2 Molded specimens shall have a width between 3.0 and 12.7 mm (0.118 and 0.500 in.). Use the specimen width as specified in the material specification or as agreed upon between the supplier and the customer. All specimens having one dimension less than 12.7 mm (0.500 in.) shall have the notch cut on the shorter side. Otherwise, all compression-molded specimens shall be notched on the side parallel to the direction of application of molding pressure. (See Fig. 6.)

NOTE 13—While subsection 7.5 requires perpendicular pairs of plane parallel surfaces, the common practice has been to accept the non-parallel drafted surfaces formed when directly injection molding specimens for Izod testing. Users must be aware that employing a trapezoidal section rather than a rectangular section may lead to data shifts and scatter. Unequal stress, created by clamping in the fracture region and dynamic twisting, caused by uneven striking of the specimen are prone to occur when the faces of the specimen are not parallel. Interlaboratory comparisons must clearly spell out the specimen preparation conditions.

7.2.1 Extreme care must be used in handling specimens less than 6.35 mm (0.250 in.) wide. Such specimens must be accurately positioned and supported to prevent twist or lateral buckling during the test. Some materials, furthermore, are very sensitive to clamping pressure (see Note 11).

7.2.2 A critical investigation of the mechanics of impact testing has shown that tests made upon specimens under 6.35 mm (0.250 in.) wide absorb more energy due to crushing, bending, and twisting than do wider specimens. Therefore, specimens 6.35 mm (0.250 in.) or over in width are recommended. The responsibility for determining the minimum specimen width shall be the investigator's, with due reference to the specification for that material.

7.2.3 Material specification should be consulted for preferred molding conditions. The type of mold and molding machine used and the flow behavior in the mold cavity will influence the impact resistance obtained. A specimen taken from one end of a molded plaque may give different results than a specimen taken from the other end. Cooperating laboratories should therefore agree on standard molds conforming to the material specification. Practice D3641 can be used as a guide for general molding tolerances, but refer to the material specification for specific molding conditions.

7.2.4 The impact resistance of a plastic material may be different if the notch is perpendicular to, rather than parallel to, the direction of molding. The same is true for specimens cut with or across the grain of an anisotropic sheet or plate.

7.3 For sheet materials, the specimens shall be cut from the sheet in both the lengthwise and crosswise directions unless otherwise specified. The width of the specimen shall be the

thickness of the sheet if the sheet thickness is between 3.0 and 12.7 mm (0.118 and 0.500 in.). Sheet material thicker than 12.7 mm shall be machined down to 12.7 mm. Specimens with a 12.7-mm square cross section may be tested either edgewise or flatwise as cut from the sheet. When specimens are tested flatwise, the notch shall be made on the machined surface if the specimen is machined on one face only. When the specimen is cut from a thick sheet, notation shall be made of the portion of the thickness of the sheet from which the specimen was cut, for example, center, top, or bottom surface.

7.4 The practice of cementing, bolting, clamping, or otherwise combining specimens of substandard width to form a composite test specimen is not recommended and should be avoided since test results may be seriously affected by interface effects or effects of solvents and cements on energy absorption of composite test specimens, or both. However, if Izod test data on such thin materials are required when no other means of preparing specimens are available, and if possible sources of error are recognized and acceptable, the following technique of preparing composites may be utilized.

7.4.1 The test specimen shall be a composite of individual thin specimens totaling 6.35 to 12.7 mm (0.250 to 0.500 in.) in width. Individual members of the composite shall be accurately aligned with each other and clamped, bolted, or cemented together. The composite shall be machined to proper dimensions and then notched. In all such cases the use of composite specimens shall be noted in the report of test results.

7.4.2 Care must be taken to select a solvent or adhesive that will not affect the impact resistance of the material under test. If solvents or solvent-containing adhesives are employed, a conditioning procedure shall be established to ensure complete removal of the solvent prior to test.

7.5 Each specimen shall be free of twist (see Note 14) and shall have mutually perpendicular pairs of plane parallel surfaces and free from scratches, pits, and sink marks. The specimens shall be checked for compliance with these requirements by visual observation against straightedges, squares, and flat plates, and by measuring with micrometer calipers. Any specimen showing observable or measurable departure from one or more of these requirements shall be rejected or machined to the proper size and shape before testing.

NOTE 14—A specimen that has a slight twist to its notched face of 0.05 mm (0.002 in.) at the point of contact with the pendulum striking edge will be likely to have a characteristic fracture surface with considerable greater fracture area than for a normal break. In this case the energy to break and toss the broken section may be considerably larger (20 to 30 %) than for a normal break. A tapered specimen may require more energy to bend it in the vise before fracture.

8. Notching Test Specimens

8.1 Notching shall be done on a milling machine, engine lathe, or other suitable machine tool. Both the feed speed and the cutter speed shall be constant throughout the notching operation (see Note 15). Provision for cooling the specimen with either a liquid or gas coolant is recommended. A single-tooth cutter shall be used for notching the specimen, unless notches of an equivalent quality can be produced with a multi-tooth cutter. Single-tooth cutters are preferred because of

the ease of grinding the cutter to the specimen contour and because of the smoother cut on the specimen. The cutting edge shall be carefully ground and honed to ensure sharpness and freedom from nicks and burrs. Tools with no rake and a work relief angle of 15 to 20° have been found satisfactory.

NOTE 15—For some thermoplastics, cutter speeds from 53 to 150 m/min (175 to 490 ft/min) at a feed speed of 89 to 160 mm/min (3.5 to 6.3 in./min) without a water coolant or the same cutter speeds at a feed speed of from 36 to 160 mm/min (1.4 to 6.3 in./min) with water coolant produced suitable notches.

8.2 Specimens may be notched separately or in a group. However, in either case an unnotched backup or “dummy bar” shall be placed behind the last specimen in the sample holder to prevent distortion and chipping by the cutter as it exits from the last test specimen.

8.3 The profile of the cutting tooth or teeth shall be such as to produce a notch of the contour and depth in the test specimen as specified in Fig. 6 (see Note 16). The included angle of the notch shall be $45 \pm 1^\circ$ with a radius of curvature at the apex of 0.25 ± 0.05 mm (0.010 ± 0.002 in.). The plane bisecting the notch angle shall be perpendicular to the face of the test specimen within 2°.

NOTE 16—There is evidence that notches in materials of widely varying physical dimensions may differ in contour even when using the same cutter.

8.4 The depth of the plastic material remaining in the specimen under the notch shall be 10.16 ± 0.05 mm (0.400 ± 0.002 in.). This dimension shall be measured with apparatus in accordance with 6.13. The tapered blade will be fitted to the notch. The specimen will be approximately vertical between the anvils. For specimens with a draft angle, position edge of the non-cavity (wider edge) surface centered on the micrometer's flat circular anvil.

8.5 Cutter speed and feed speed should be chosen appropriate for the material being tested since the quality of the notch may be adversely affected by thermal deformations and stresses induced during the cutting operation if proper conditions are not selected.⁶ The notching parameters used shall not alter the physical state of the material such as by raising the temperature of a thermoplastic above its glass transition temperature. In general, high cutter speeds, slow feed rates, and lack of coolant induce more thermal damage than a slow cutter speed, fast feed speed, and the use of a coolant. Too high a feed speed/cutter speed ratio, however, may cause impacting and cracking of the specimen. The range of cutter speed/feed ratios possible to produce acceptable notches can be extended by the use of a suitable coolant. (See Note 17.) In the case of new types of plastics, it is necessary to study the effect of variations in the notching conditions. (See Note 18.)

NOTE 17—Water or compressed gas is a suitable coolant for many plastics.

NOTE 18—Embedded thermocouples, or another temperature measuring device, can be used to determine the temperature rise in the material near the apex of the notch during machining. Thermal stresses induced during the notching operation can be observed in transparent materials by

⁶ Supporting data are available from ASTM Headquarters. Request RR:D20-1066.

viewing the specimen at low magnification between crossed polars in monochromatic light.

8.6 A notching operation notches one or more specimens plus the “dummy bar” at a single pass through the notcher. The specimen notch produced by each cutter will be examined after every 500 notching operations or less frequently if experience shows this to be acceptable. The notch in the specimen, made of the material to be tested, shall be inspected and verified. One procedure for the inspection and verification of the notch is presented in **Appendix X1**. Each type of material being notched must be inspected and verified at that time. If the angle or radius does not fall within the specified limits for materials of satisfactory machining characteristics, then the cutter shall be replaced with a newly sharpened and honed one. (See **Note 19**.)

NOTE 19—A carbide-tipped or industrial diamond-tipped notching cutter is recommended for longer service life.

9. Conditioning

9.1 *Conditioning*—Condition the test specimens at $23 \pm 2^\circ\text{C}$ ($73 \pm 3.6^\circ\text{F}$) and $50 \pm 10\%$ relative humidity for not less than 40 h after notching and prior to testing in accordance with Procedure A of Practice **D618**, unless it can be documented (between supplier and customer) that a shorter conditioning time is sufficient for a given material to reach equilibrium of impact resistance.

9.1.1 Note that for some hygroscopic materials, such as nylons, the material specifications (for example, Specification **D4066**) call for testing “dry as-molded specimens.” Such requirements take precedence over the above routine preconditioning to 50 % relative humidity and require sealing the specimens in water vapor-impermeable containers as soon as molded and not removing them until ready for testing.

9.2 *Test Conditions*—Conduct tests in the standard laboratory atmosphere of $23 \pm 2^\circ\text{C}$ ($73 \pm 3.6^\circ\text{F}$) and $50 \pm 10\%$ relative humidity, unless otherwise specified in the material specification or by customer requirements. In cases of disagreement, the tolerances shall be $\pm 1^\circ\text{C}$ ($\pm 1.8^\circ\text{F}$) and $\pm 5\%$ relative humidity.

10. Procedure

10.1 At least five and preferably ten or more individual determinations of impact resistance must be made on each sample to be tested under the conditions prescribed in Section 9. Each group shall consist of specimens with the same nominal width ($\pm 0.13\text{ mm}$ ($\pm 0.005\text{ in.}$)). In the case of specimens cut from sheets that are suspected of being anisotropic, prepare and test specimens from each principal direction (lengthwise and crosswise to the direction of anisotropy).

10.2 Estimate the breaking energy for the specimen and select a pendulum of suitable energy. Use the lightest standard pendulum that is expected to break each specimen in the group with a loss of not more than 85 % of its energy (see **Note 20**). Check the machine with the proper pendulum in place for conformity with the requirements of Section 6 before starting the tests. (See **Appendix X1**.)

NOTE 20—Ideally, an impact test would be conducted at a constant test velocity. In a pendulum-type test, the velocity decreases as the fracture progresses. For specimens that have an impact energy approaching the capacity of the pendulum there is insufficient energy to complete the break and toss. By avoiding the higher 15 % scale energy readings, the velocity of the pendulum will not be reduced below 1.3 m/s (4.4 ft/s). On the other hand, the use of too heavy a pendulum would reduce the sensitivity of the reading.

10.3 If the machine is equipped with a mechanical pointer and dial, perform the following operations before testing the specimens. If the machine is equipped with a digital indicating system, follow the manufacturer’s instructions to correct for windage and friction. If excessive friction is indicated, the machine shall be adjusted before starting a test.

10.3.1 With the indicating pointer in its normal starting position but without a specimen in the vise, release the pendulum from its normal starting position and note the position the pointer attains after the swing as one reading of Factor *A*.

10.3.2 Without resetting the pointer, raise the pendulum and release again. The pointer should move up the scale an additional amount. Repeat (10.3.2) until a swing causes no additional movement of the pointer and note the final reading as one reading of Factor *B* (see **Note 21**).

10.3.3 Repeat the preceding two operations several times and calculate and record the average *A* and *B* readings.

NOTE 21—Factor *B* is an indication of the energy lost by the pendulum to friction in the pendulum bearings and to windage. The difference *A* – *B* is an indication of the energy lost to friction and inertia in the indicating mechanism. However, the actual corrections will be smaller than these factors, since in an actual test the energy absorbed by the specimen prevents the pendulum from making a full swing. Therefore, the indicated breaking energy of the specimen must be included in the calculation of the machine correction before determining the breaking energy of the specimen (see 10.8). The *A* and *B* values also provide an indication of the condition of the machine.

10.3.4 If excessive friction is indicated, the machine shall be adjusted before starting a test.

10.4 Check the specimens for conformity with the requirements of Sections 7, 8, and 10.1.

10.5 Measure and record the width of each specimen after notching to the nearest 0.025 mm (0.001 in.). Measure the width in one location adjacent to the notch centered about the anticipated fracture plane.

10.6 Measure and record the depth of material remaining in the specimen under the notch of each specimen to the nearest 0.025 mm (0.001 in.). The tapered blade will be fitted to the notch. The specimen will be approximately vertical between the anvils. For specimens with a draft angle, position edge of the non-cavity (wider edge) surface centered on the micrometer’s flat circular anvil.

10.7 Position the specimen precisely (see 6.7) so that it is rigidly, but not too tightly (see **Note 11**), clamped in the vise. Pay special attention to ensure that the “impacted end” of the specimen as shown and dimensioned in **Fig. 6** is the end projecting above the vise. Release the pendulum and record the indicated breaking energy of the specimen together with a description of the appearance of the broken specimen (see failure categories in 5.8).

10.8 Subtract the windage and friction correction from the indicated breaking energy of the specimen, unless determined automatically by the indicating system (that is, digital display or computer). If a mechanical dial and pointer is employed, use the *A* and *B* factors and the appropriate tables or the graph described in [Annex A1](#) and [Annex A2](#) to determine the correction. For those digital systems that do not automatically compensate for windage and friction, follow the manufacturer's procedure for performing this correction.

10.8.1 In other words, either manually or automatically, the windage and friction correction value is subtracted from the uncorrected, indicated breaking energy to obtain the new breaking energy. Compare the net value so found with the energy requirement of the hammer specified in [10.2](#). If a hammer of improper energy was used, discard the result and make additional tests on new specimens with the proper hammer. (See [Annex A1](#) and [Annex A2](#).)

10.9 Divide the net value found in [10.8](#) by the measured width of the particular specimen to obtain the impact resistance under the notch in J/m (ft-lbf/in.). If the optional units of kJ/m² (ft-lbf/in.²) are used, divide the net value found in [10.8](#) by the measured width and depth under the notch of the particular specimen to obtain the impact strength. The term, "depth under the notch," is graphically represented by Dimension A in [Fig. 6](#). Consequently, the cross-sectional area (width times depth under the notch) will need to be reported. (See [Appendix X4](#).)

10.10 Calculate the average Izod impact resistance of the group of specimens. However, only values of specimens having the same nominal width and type of break may be averaged. Values obtained from specimens that did not break in the manner specified in [5.8](#) shall not be included in the average. Also calculate the standard deviation of the group of values.

11. Report

11.1 Report the following information:

11.1.1 The test method used (Test Method A, C, D, or E),

11.1.2 Complete identification of the material tested, including type source, manufacturer's code number, and previous history,

11.1.3 A statement of how the specimens were prepared, the testing conditions used, the number of hours the specimens were conditioned after notching, and for sheet materials, the direction of testing with respect to anisotropy, if any,

11.1.4 The capacity of the pendulum in joules, or foot pound-force, or inch pound-force,

11.1.5 The width and depth under the notch of each specimen tested,

11.1.6 The total number of specimens tested per sample of material,

11.1.7 The type of failure (see [5.8](#)),

11.1.8 The impact resistance must be reported in J/m (ft-lbf/in.); the optional units of kJ/m² (ft-lbf/in.²) may also be required (see [10.9](#)),

11.1.9 The number of those specimens that resulted in failures which conforms to each of the requirement categories in [5.8](#),

11.1.10 The average impact resistance and standard deviation (in J/m (ft-lbf/in.)) for those specimens in each failure

category, except non-break as presented in [5.8](#). Optional units (kJ/m² (ft-lbf/in.²)) may also need to be reported (see [Appendix X4](#)), and

11.1.11 The percent of specimens failing in each category suffixed by the corresponding letter code from [5.8](#).

TEST METHOD C—CANTILEVER BEAM TEST FOR MATERIALS OF LESS THAN 27 J/m (0.5 ft-lbf/in.)

12. Apparatus

12.1 The apparatus shall be the same as specified in [Section 6](#).

13. Test Specimens

13.1 The test specimens shall be the same as specified in [Section 7](#).

14. Notching Test Specimens

14.1 Notching test specimens shall be the same as specified in [Section 8](#).

15. Conditioning

15.1 Specimen conditioning and test environment shall be in accordance with [Section 9](#).

16. Procedure

16.1 The procedure shall be the same as in [Section 10](#) with the addition of a procedure for estimating the energy to toss the broken specimen part.

16.1.1 Make an estimate of the magnitude of the energy to toss each different type of material and each different specimen size (width). This is done by repositioning the free end of the broken specimen on the clamped portion and striking it a second time with the pendulum released in such a way as to impart to the specimen approximately the same velocity it had attained during the test. This is done by releasing the pendulum from a height corresponding to that to which it rose following the breakage of the test specimen. The energy to toss is then considered to be the difference between the reading previously described and the free swing reading obtained from this height. A reproducible method of starting the pendulum from the proper height must be devised.

17. Report

17.1 Report the following information:

17.1.1 Same as [11.1.1](#),

17.1.2 Same as [11.1.2](#),

17.1.3 Same as [11.1.3](#),

17.1.4 Same as [11.1.4](#),

17.1.5 Same as [11.1.5](#),

17.1.6 Same as [11.1.6](#),

17.1.7 The average reversed notch impact resistance, J/m (ft-lbf/in.) (see [5.8](#) for failure categories),

17.1.8 Same as [11.1.8](#),

17.1.9 Same as [11.1.9](#),

17.1.10 Same as [11.1.10](#), and

17.1.11 Same as [11.1.11](#).

17.1.12 The estimated toss correction, expressed in terms of joule (J) or foot pound-force (ft-lbf).

17.1.13 The difference between the Izod impact energy and the toss correction energy is the net Izod energy. This value is divided by the specimen width (at the base of notch) to obtain the net Izod impact resistance for the report.

TEST METHOD D—NOTCH RADIUS SENSITIVITY TEST

18. Apparatus

18.1 The apparatus shall be the same as specified in Section 6.

19. Test Specimens

19.1 The test specimens shall be the same as specified in Section 7. All specimens must be of the same nominal width, preferably 6.35-mm (0.25-in.).

20. Notching Test Specimens

20.1 Notching shall be done as specified in Section 8 and Fig. 6, except those ten specimens shall be notched with a radius of 0.25 mm (0.010 in.) and ten specimens with a radius of 1.0 mm (0.040 in.).

21. Conditioning

21.1 Specimen conditioning and test environment shall be in accordance with Section 9.

22. Procedure

22.1 Proceed in accordance with Section 10, testing ten specimens of each notch radius.

22.2 The average impact resistance of each group shall be calculated, except that within each group the type of break must be homogeneously C, H, C and H, or P.

22.3 If the specimens with the 0.25-mm (0.010-in.) radius notch do not break, the test is not applicable.

22.4 If any of ten specimens tested with the 1.0-mm (0.040-in.) radius notch fail as in category NB, non-break, the notch sensitivity procedure cannot be used without obtaining additional data. A new set of specimens should be prepared from the same sample, using a 0.50-mm (0.020-in.) notch radius and the procedure of 22.1 and 22.2 repeated.

23. Calculation

23.1 Calculate the slope of the line connecting the values for impact resistance for 0.25 and 1.0-mm notch radii or (0.010 and 0.040-in. notch radii) by the equation presented as follows. (If a 0.500-mm (0.020-in.) notch radius is substituted, adjust the calculation accordingly.)

$$b = (E_2 - E_1)/(R_2 - R_1)$$

where:

E_2 = average impact resistance for the larger notch, J/m of notch,

E_1 = average impact resistance for the smaller notch, J/m of notch,

R_2 = radius of the larger notch, mm, and
 R_1 = radius of the smaller notch, mm.

Example:

$$\begin{aligned} E_{1.0} &= 330.95 \text{ J/m}; E_{0.25} = 138.78 \text{ J/m} \\ b &= (330.95 - 138.78 \text{ J/m}) / (1.00 - 0.25 \text{ mm}) \\ b &= 192.17 \text{ J/m} / 0.75 \text{ mm} = 256.23 \text{ J/m} \\ &\text{of notch per mm of radius} \end{aligned}$$

24. Report

24.1 Report the following information:

24.1.1 Same as 11.1.1,

24.1.2 Same as 11.1.2,

24.1.3 Same as 11.1.3,

24.1.4 Same as 11.1.4,

24.1.5 Same as 11.1.5,

24.1.6 Same as 11.1.6,

24.1.7 The average reversed notch impact resistance, in J/m (ft-lbf/in.) (see 5.8 for failure categories),

24.1.8 Same as 11.1.8,

24.1.9 Same as 11.1.9,

24.1.10 Same as 11.1.10, and

24.1.11 Same as 11.1.11.

24.1.12 Report the average value of b with its units, and the average Izod impact resistance for a 0.25-mm (0.010-in.) notch.

TEST METHOD E—CANTILEVER BEAM REVERSED NOTCH TEST

25. Apparatus

25.1 The apparatus shall be the same as specified in Section 6.

26. Test Specimens

26.1 The test specimen shall be the same as specified in Section 7.

27. Notching Test Specimens

27.1 Notch the test specimens in accordance with Section 8.

28. Conditioning

28.1 Specimen conditioning and test environment shall be in accordance with Section 9.

29. Procedure

29.1 Proceed in accordance with Section 10, except clamp the specimen so that the striker impacts it on the face opposite the notch, hence subjecting the notch to compressive rather than tensile stresses during impact (see Fig. 2 and Note 22, Note 23, and Note 24).

NOTE 22—The reversed notch test employs a standard 0.25-mm (0.010-in.) notch specimen to provide an indication of unnotched impact resistance. Use of the reversed notch test obviates the need for machining unnotched specimens to the required 10.2 ± 0.05 -mm (0.400 ± 0.002 -in.) depth before testing and provides the same convenience of specimen mounting as the standard notch tests (Test Methods A and C).

NOTE 23—Results obtained by the reversed notch test may not always agree with those obtained on unnotched bars that have been machined to the 10.2-mm (0.400-in.) depth requirement. For some materials, the

TABLE 1 Precision Data, Test Method A—Notched Izod

NOTE 1—Values in ft-lbf/in. of width (J/m of width).

NOTE 2—See Footnote 10.

Material	Average	S_r^A	S_R^B	I_r^C	I_R^D	Number of Laboratories
Phenolic	0.57 (30.4)	0.024 (1.3)	0.076 (4.1)	0.06 (3.2)	0.21 (11.2)	19
Acetal	1.45 (77.4)	0.075 (4.0)	0.604 (32.3)	0.21 (11.2)	1.70 (90.8)	9
Reinforced nylon	1.98 (105.7)	0.083 (4.4)	0.245 (13.1)	0.23 (12.3)	0.69 (36.8)	15
Polypropylene	2.66 (142.0)	0.154 (8.2)	0.573 (30.6)	0.43 (23.0)	1.62 (86.5)	24
ABS	10.80 (576.7)	0.136 (7.3)	0.585 (31.2)	0.38 (20.3)	1.65 (88.1)	25
Polycarbonate	16.40 (875.8)	0.295 (15.8)	1.056 (56.4)	0.83 (44.3)	2.98 (159.1)	25

^A S_r = within-laboratory standard deviation of the average.

^B S_R = between-laboratories standard deviation of the average.

^C I_r = 2.83 S_r .

^D I_R = 2.83 S_R .

effects arising from the difference in the clamped masses of the two specimen types during test, and those attributable to a possible difference in toss energies ascribed to the broken ends of the respective specimens, may contribute significantly to a disparity in test results.

NOTE 24—Where materials are suspected of anisotropy, due to molding or other fabricating influences, notch reversed notch specimens on the face opposite to that used for the standard Izod test; that is, present the same face to the impact blow.

30. Report

30.1 Report the following information:

30.1.1 Same as 11.1.1,

30.1.2 Same as 11.1.2,

30.1.3 Same as 11.1.3,

30.1.4 Same as 11.1.4,

30.1.5 Same as 11.1.5,

30.1.6 Same as 11.1.6,

30.1.7 The average reversed notch impact resistance, J/m (ft-lbf/in.) (see 5.8 for failure categories),

30.1.8 Same as 11.1.8,

30.1.9 Same as 11.1.9,

30.1.10 Same as 11.1.10, and

30.1.11 Same as 11.1.11.

31. Precision and Bias

31.1 Table 1 and Table 2 are based on a round robin in accordance with Practice E691. For each material, all the test bars were prepared at one source, except for notching. Each participating laboratory notched the bars that they tested. Table 1 and Table 2 are presented on the basis of a test result being the average for five specimens. In the round robin each laboratory tested, on average, nine specimens of each material.

31.2 Table 3 is based on a round robin⁵ involving five materials tested by seven laboratories. For each material, all the samples were prepared at one source, and the individual specimens were all notched at the same laboratory. Table 3 is presented on the basis of a test result being the average for five specimens. In the round robin, each laboratory tested ten specimens of each material.

31.3 *Concept of I_r and I_R* —If S_r and S_R have been calculated from a large enough body of data, and for test results that were averages from testing five specimens. (**Warning**—The following explanations of I_r and I_R (see 31.3 – 31.3.3) are only intended to present a meaningful way of considering the precision of this test method. The data in Tables 1-3 should not be rigorously applied to acceptance or rejection of material, as those data are specific to the round robin and may not be representative of other lots, conditions, materials, or laboratories. Users of this test method should apply the principles outlined in Practice E691 to generate data specific to their laboratory and materials, or between specific laboratories. The principles of 31.3 – 31.3.3 would then be valid for such data.)

31.3.1 *Repeatability, I_r (Comparing Two Test Results for the Same Material, Obtained by the Same Operator Using the Same Equipment on the Same Day)*—The two test results should be judged not equivalent if they differ by more than the I_r value for that material.

31.3.2 *Reproducibility, I_R (Comparing Two Test Results for the Same Material, Obtained by Different Operators Using Different Equipment on Different Days)*—The two test results should be judged not equivalent if they differ by more than the I_R value for that material.

31.3.3 Any judgment in accordance with 31.3.1 and 31.3.2 would have an approximate 95 % (0.95) probability of being correct.

31.4 *Bias*—There is no recognized standards by which to estimate bias of these test methods.

NOTE 25—Numerous changes have occurred since the collection of the original round-robin data in 1973. Consequently, a new task group has been formed to evaluate a precision and bias statement for the latest revision of these test methods.

32. Keywords

32.1 impact resistance; Izod impact; notch sensitivity; notched specimen; reverse notch impact

TABLE 2 Precision Data, Test Method C—Notched Izod

NOTE 1—Values in ft-lbf/in. of width (J/m of width).

NOTE 2—See Footnote 10.

Material	Average	S_r^A	S_R^B	I_r^C	I_R^D	Number of Laboratories
Phenolic	0.45 (24.0)	0.038 (2.0)	0.129 (6.9)	0.10 (5.3)	0.36 (19.2)	15

^A S_r = within-laboratory standard deviation of the average.

^B S_R = between-laboratories standard deviation of the average.

^C I_r = 2.83 S_r .

^D I_R = 2.83 S_R .

TABLE 3 Precision Data, Test Method E—Reversed Notch Izod

NOTE 1—Values in ft-lbf/in. of width (J/m of width).

NOTE 2—See Footnote 8.

Material	Average	S_r^A	S_R^B	I_r^C	I_R^D
Acrylic sheet, unmodified	3.02 (161.3)	0.243 (13.0)	0.525 (28.0)	0.68 (36.3)	0.71 (37.9)
Premix molding compounds laminate	6.11 (326.3)	0.767 (41.0)	0.786 (42.0)	2.17 (115.9)	2.22 (118.5)
acrylic, injection molded	10.33 (551.6)	0.878 (46.9)	1.276 (68.1)	2.49 (133.0)	3.61 (192.8)
compound (SMC) laminate	11.00 (587.4)	0.719 (38.4)	0.785 (41.9)	2.03 (108.4)	2.22 (118.5)
Preformed mat laminate	19.43 (1037.6)	0.960 (51.3)	1.618 (86.4)	2.72 (145.2)	4.58 (244.6)

^A S_r = within-laboratory standard deviation of the average.

^B S_R = between-laboratories standard deviation of the average.

^C I_r = 2.83 S_r .

^D I_R = 2.83 S_R .

ANNEXES

(Mandatory Information)

A1. INSTRUCTIONS FOR THE CONSTRUCTION OF A WINDAGE AND FRICTION CORRECTION CHART

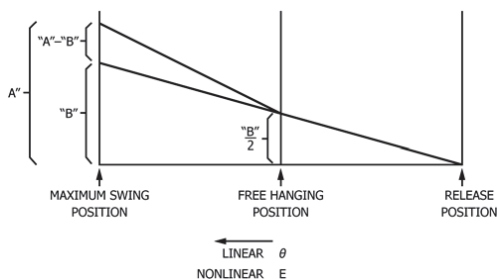


FIG. A1.1 Method of Construction of a Windage and Friction Correction Chart

A1.1 The construction and use of the chart herein described is based upon the assumption that the friction and windage losses are proportional to the angle through which these loss torques are applied to the pendulum. Fig. A1.1 shows the assumed energy loss versus the angle of the pendulum position during the pendulum swing. The correction chart to be described is principally the left half of Fig. A1.1. The windage and friction correction charts should be available from commercial testing machine manufacturers. The energy losses designated as A and B are described in 10.3.

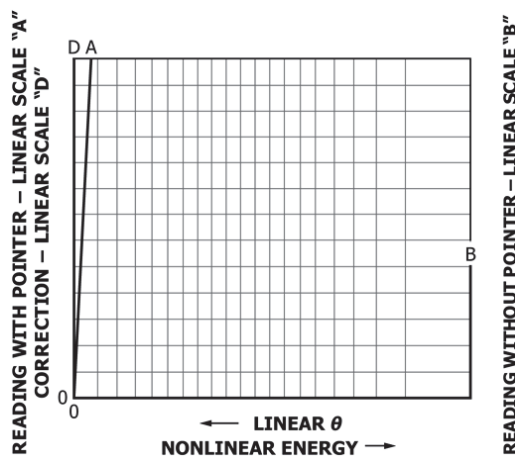


FIG. A1.2 Sample Windage and Friction Correction Chart

A1.2 Start the construction of the correction chart (see Fig. A1.2) by laying off to some convenient linear scale on the abscissa of a graph the angle of pendulum position for the

portion of the swing beyond the free hanging position. For convenience, place the free hanging reference point on the right end of the abscissa with the angular displacement increasing linearly to the left. The abscissa is referred to as Scale C. Although angular displacement is the quantity to be represented linearly on the abscissa, this displacement is more conveniently expressed in terms of indicated energy read from the machine dial. This yields a nonlinear Scale C with indicated pendulum energy increasing to the right.

A1.3 On the right-hand ordinate lay off a linear Scale B starting with zero at the bottom and stopping at the maximum expected pendulum friction and windage value at the top.

A1.4 On the left ordinate construct a linear Scale D ranging from zero at the bottom to 1.2 times the maximum ordinate value appearing on Scale B, but make the scale twice the scale used in the construction of Scale B.

A1.5 Adjoining Scale D draw a curve OA that is the focus of points whose coordinates have equal values of energy correction on Scale D and indicated energy on Scale C. This curve is referred to as Scale A and utilizes the same divisions and numbering system as the adjoining Scale D.

A1.6 Instructions for Using Chart:

A1.6.1 Locate and mark on Scale A the reading A obtained from the free swing of the pendulum with the pointer repositioned in the free hanging or maximum indicated energy position on the dial.

A1.6.2 Locate and mark on Scale B the reading B obtained after several free swings with the pointer pushed up close to the zero indicated energy position of the dial by the pendulum in accordance with instructions in 10.3.

A1.6.3 Connect the two points thus obtained by a straight line.

A1.6.4 From the indicated impact energy on Scale C project up to the constructed line and across to the left to obtain the correction for windage and friction from Scale D.

A1.6.5 Subtract this correction from the indicated impact reading to obtain the energy delivered to the specimen.

A2. PROCEDURE FOR THE CALCULATION OF WINDAGE AND FRICTION CORRECTION

A2.1 The procedure for the calculation of the windage and friction correction in this annex is based on the equations developed by derivation in Appendix X3. This procedure can be used as a substitute for the graphical procedure described in Annex A1 and is applicable to small electronic calculator and computer analysis.

A2.2 Calculate L , the distance from the axis of support to the center of percussion as indicated in 6.3. (It is assumed here that the center of percussion is approximately the same as the center of gravity.)

A2.3 Measure the maximum height, h_M , of the center of percussion (center of gravity) of the pendulum at the start of the test as indicated in X2.16.

A2.4 Measure and record the energy correction, E_A , for windage of the pendulum plus friction in the dial, as determined with the first swing of the pendulum with no specimen in the testing device. This correction must be read on the energy scale, E_M , appropriate for the pendulum used.

A2.5 Without resetting the position of the indicator obtained in A2.4, measure the energy correction, E_B , for pendulum windage after two additional releases of the pendulum with no specimen in the testing device.

A2.6 Calculate β_{\max} as follows:

$$\beta_{\max} = \cos^{-1} \{1 - [(h_M/L)(1 - E_A/E_M)]\}$$

where:

- E_A = energy correction for windage of pendulum plus friction in dial, J (ft-lbf),
- E_M = full-scale reading for pendulum used, J (ft-lbf),
- L = distance from fulcrum to center of gravity of pendulum, m (ft),
- h_M = maximum height of center of gravity of pendulum at start of test, m (ft), and
- β_{\max} = maximum angle pendulum will travel with one swing of the pendulum.

A2.7 Measure specimen breaking energy, E_s , J (ft-lbf).

A2.8 Calculate β for specimen measurement E_s as:

$$\beta = \cos^{-1} \{1 - [(h_M/L)(1 - E_s/E_M)]\}$$

where:

- β = angle pendulum travels for a given specimen, and
- E_s = dial reading breaking energy for a specimen, J (ft-lbf).

A2.9 Calculate total correction energy, E_{TC} , as:

$$E_{TC} = (E_A - (E_B/2))(\beta/\beta_{\max}) + (E_s/2)$$

where:

- E_{TC} = total correction energy for the breaking energy, E_s , of a specimen, J (ft-lbf), and

D256 – 10^{e1}

E_B = energy correction for windage of the pendulum, J (ft·lbf).

where:

I_s = impact resistance of specimen, J/m (ft·lbf/in.) of width, and

t = width of specimen or width of notch, m (in.).

A2.10 Calculate the impact resistance using the following formula:

$$I_s = (E_s - E_{TC})/t$$

APPENDIXES

(Nonmandatory Information)

X1. PROCEDURE FOR THE INSPECTION AND VERIFICATION OF NOTCH

X1.1 The purpose of this procedure is to describe the microscopic method to be used for determining the radius and angle of the notch. These measurements could also be made using a comparator if available.

NOTE X1.1—The notch shall have a radius of 0.25 ± 0.05 mm (0.010 \pm 0.002 in.) and an angle of $45 \pm 1^\circ$.

X1.2 Apparatus:

X1.2.1 *Optical Device* with minimum magnification of 60 \times , Filar glass scale and camera attachment.

X1.2.2 *Transparent Template*, (will be developed in this procedure).

X1.2.3 *Ruler*.

X1.2.4 *Compass*.

X1.2.5 *Plastic 45°–45°–90° Drafting Set Squares (Triangles)*.

X1.3 A transparent template must be developed for each magnification and for each microscope used. It is preferable that each laboratory standardize on one microscope and one magnification. It is not necessary for each laboratory to use the same magnification because each microscope and camera combination has somewhat different blowup ratios.

X1.3.1 Set the magnification of the optical device at a suitable magnification with a minimum magnification of 60 \times .

X1.3.2 Place the Filar glass slide on the microscope platform. Focus the microscope so the most distinct image of the Filar scale is visible.

X1.3.3 Take a photograph of the Filar scale (see Fig. X1.1).

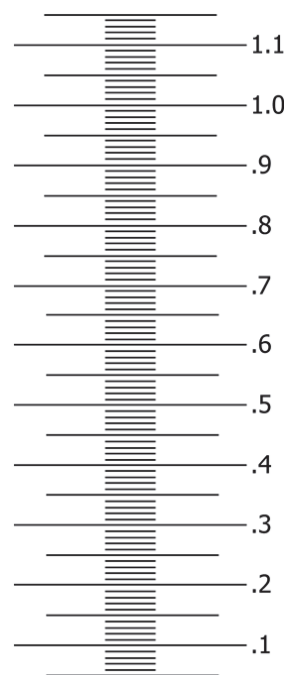
X1.3.4 Create a template similar to that shown in Fig. X1.2.

X1.3.4.1 Find the approximate center of the piece of paper.

X1.3.4.2 Draw a set of perpendicular coordinates through the center point.

X1.3.4.3 Draw a family of concentric circles that are spaced according to the dimensions of the Filar scale.

X1.3.4.4 This is accomplished by first setting a mechanical compass at a distance of 0.1 mm (0.004 in.) as referenced by the magnified photograph of the Filar eyepiece. Subsequent circles shall be spaced 0.02 mm apart (0.001 in.), as rings with the outer ring being 0.4 mm (0.016 in.) from the center.

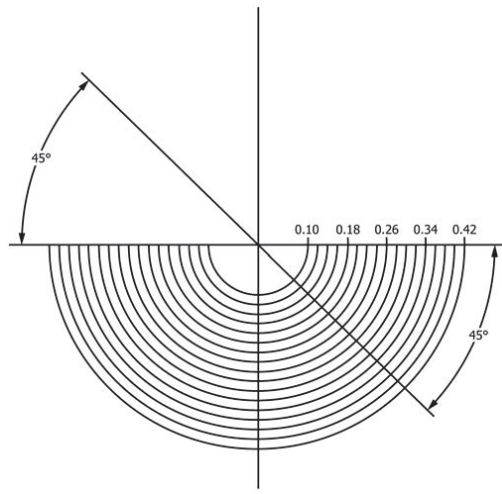


NOTE 1—100 \times reference.
NOTE 2—0.1 mm major scale; 0.01 mm minor scale.

FIG. X1.1 Filar Scale

X1.3.5 Photocopy the paper with the concentric circles to make a transparent template of the concentric circles.

X1.3.6 Construct Fig. X1.3 by taking a second piece of paper and find its approximate center and mark this point. Draw one line through this center point. Label this line zero degree (0°). Draw a second line perpendicular to the first line through this center point. Label this line “90°.” From the center draw a line that is 44 degrees relative to the “0°.” Label the line “44°.” Draw another line at 46°. Label the line “46°.”



NOTE 1—Magnification = 100x.
FIG. X1.2 Example of Transparent Template for Determining Radius of Notch

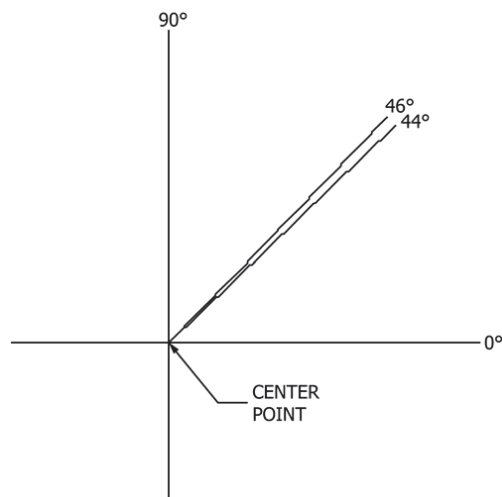


FIG. X1.3 Example of Transparent Template for Determining Angle of Notch

X1.4 Place a microscope glass slide on the microscope platform. Place the notched specimen on top of the slide. Focus the microscope. Move the specimen around using the platform adjusting knobs until the specimen's notch is centered and near the bottom of the viewing area. Take a picture of the notch.

X1.4.1 *Determination of Notching Radius* (see Fig. X1.4):

X1.4.1.1 Place the picture on a sheet of paper. Position the picture so that bottom of the notch in the picture faces

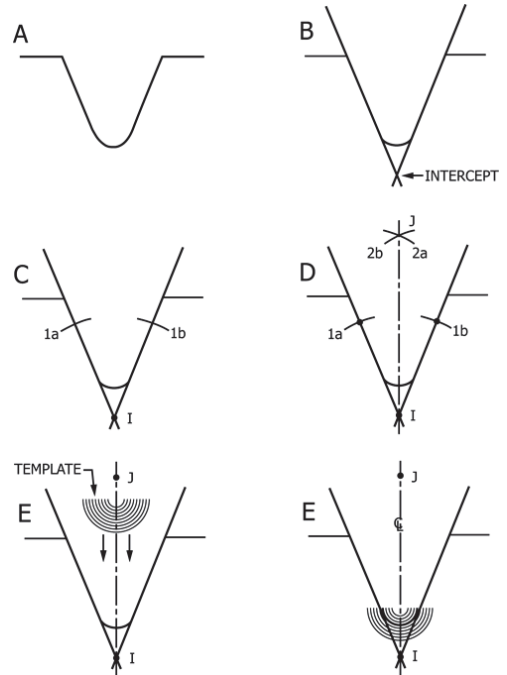


FIG. X1.4 Determination of Notching Radius

downwards and is about 64 mm (2.5 in.) from the bottom of the paper. Tape the picture down to the paper.

X1.4.1.2 Draw two lines along the sides of the notch projecting down to a point where they intersect below Notch Point I (see Fig. X1.4).

X1.4.1.3 Open the compass to about 51 mm (2 in.). Using Point I as a reference, draw two arcs intersecting both sides of the notch (see Fig. X1.4). These intersections are called 1a and 1b.

X1.4.1.4 Close the compass to about 38 mm (1.5 in.). Using Point 1a as the reference point draw an arc (2a) above the notch, draw a second arc (2b) that intersects with arc 2a at Point J. Draw a line between I and J. This establishes the centerline of the notch (see Fig. X1.4).

X1.4.1.5 Place the transparent template on top of the picture and align the center of the concentric circles with the drawn centerline of the notch (see Fig. X1.4).

X1.4.1.6 Slide the template down the centerline of the notch until one concentric circle touches both sides of the notch. Record the radius of the notch and compare it against the ASTM limits of 0.2 to 0.3 mm (0.008 to 0.012 in.).

X1.4.1.7 Examine the notch to ensure that there are no flat spots along the measured radius.

X1.4.2 *Determination of Notch Angle:*

X1.4.2.1 Place transparent template for determining notch angle (see Fig. X1.3) on top of the photograph attached to the sheet of paper. Rotate the picture so that the notch tip is pointed

towards you. Position the center point of the template on top of Point I established in 0° axis of the template with the right side straight portion of the notch. Check the left side straight portion of the notch to ensure that this portion falls between the 44 and 46° degree lines. If not, replace the blade.

X1.5 A picture of a notch shall be taken at least every 500 notches or if a control sample gives a value outside its three-sigma limits for that test.

X1.6 If the notch in the control specimen is not within the requirements, a picture of the notching blade should be taken

and analyzed by the same procedure used for the specimen notch. If the notching blade does not meet ASTM requirements or shows damage, it should be replaced with a new blade which has been checked for proper dimensions.

X1.7 It is possible that the notching cutter may have the correct dimensions but does not cut the correct notch in the specimen. If that occurs it will be necessary to evaluate other conditions (cutter and feed speeds) to obtain the correct notch dimension for that material.

X2. CALIBRATION OF PENDULUM-TYPE HAMMER IMPACT MACHINES FOR USE WITH PLASTIC SPECIMENS

X2.1 This calibration procedure applies specifically to the Izod impact machine. However, much of this procedure can be applied to the Charpy impact machine as well.

X2.2 Locate the impact machine on a sturdy base. It shall not “walk” on the base and the base shall not vibrate appreciably. Loss of energy from vibrations will give high readings. It is recommended that the impact tester be bolted to a base having a mass of at least 23 kg if it is used at capacities higher than 2.7 J (2 ft-lbf).

X2.3 Check the level of the machine in both directions in the plane of the base with spirit levels mounted in the base, by a machinist’s level if a satisfactory reference surface is available, or with a plumb bob. The machine should be made level to within $\tan^{-1} 0.001$ in the plane of swing and to within $\tan^{-1} 0.002$ in the plane perpendicular to the swing.

X2.4 With a straightedge and a feeler gauge or a depth gauge, check the height of the movable vise jaw relative to the fixed vise jaw. It must match the height of the fixed vise jaw within 0.08 mm (0.003 in.).

X2.5 Contact the machine manufacturer for a procedure to ensure the striker radius is in tolerance (0.80 ± 0.20 mm) (see 6.3).

X2.6 Check the transverse location of the center of the pendulum striking edge that shall be within 0.40 mm (0.016 in.) of the center of the vise. Readjust the shaft bearings or relocate the vise, or straighten the pendulum shaft as necessary to attain the proper relationship between the two centers.

X2.7 Check the pendulum arm for straightness within 1.2 mm (0.05 in.) with a straightedge or by sighting down the shaft. Allowing the pendulum to slam against the catch sometimes bends the arm especially when high-capacity weights are on the pendulum.

X2.8 Insert vertically and center with a locating jig and clamp in the vise a notched machined metal bar 12.7-mm (0.500-in.) square, having opposite sides parallel within 0.025 mm (0.001 in.) and a length of 60 mm (2.4 in.). Check the bar for vertical alignment within $\tan^{-1} 0.005$ in both directions

with a small machinist’s level. Shim up the vise, if necessary, to correct for errors in the plane of pendulum swing, using care to preserve solid support for the vise. For errors in the plane perpendicular to the plane of pendulum swing, machine the inside face of the clamp-type locating jig for correct alignment if this type of jig is used. If a blade-type jig is used, use shims or grind the base of the vise to bring the top surface level.

X2.9 Insert and clamp the bar described in X2.8 in a vertical position in the center of the vise so that the notch in the bar is slightly below the top edge of the vise. Place a thin film of oil on the striking edge of the pendulum with an oiled tissue and let the striking edge rest gently against the bar. The striking edge should make contact across the entire width of the bar. If only partial contact is made, examine the vise and pendulum for the cause. If the cause is apparent, make the appropriate correction. If no cause is apparent, remove the striker and shim up or grind its back face to realign the striking edge with the surface of the bar.

X2.10 Check the oil line on the face of the bar for horizontal setting of striking edge within $\tan^{-1} 0.002$ with a machinist’s square.

X2.11 Without taking the bar of X2.8 from the vise of the machine, scratch a thin line at the top edge of the vise on the face opposite the striking face of the bar. Remove the bar from the vise and transfer this line to the striking face, using a machinist’s square. The distance from the striking oil line to the top edge of the vise should be 22 ± 0.05 mm (0.87 ± 0.002 in.). Correct with shims or grinding, as necessary, at the bottom of the vise.

X2.12 When the pendulum is hanging free in its lowest position, the energy reading must be within 0.2 % of full scale.

X2.13 Insert the bar of X2.8 into the vise and clamp it tightly in a vertical position. When the striking edge is held in contact with the bar, the energy reading must be within 0.2 % of full scale.

X2.14 Swing the pendulum to a horizontal position and support it by the striking edge in this position with a vertical bar. Allow the other end of this bar to rest at the center of a load

pan on a balanced scale. Subtract the weight of the bar from the total weight to find the effective weight of the pendulum. The effective pendulum weight should be within 0.4 % of the required weight for that pendulum capacity. If weight must be added or removed, take care to balance the added or removed weight without affecting the center of percussion relative to the striking edge. It is not advisable to add weight to the opposite side of the bearing axis from the striking edge to decrease the effective weight of the pendulum since the distributed mass can lead to large energy losses from vibration of the pendulum.

X2.15 Calculate the effective length of the pendulum arm, or the distance to the center of percussion from the axis of rotation, by the procedure in **Note 9**. The effective length must be within the tolerance stated in **6.6**.

X2.16 Measure the vertical distance of fall of the pendulum striking edge from its latched height to its lowest point. This distance should be 610 ± 2.0 mm (24 ± 0.1 in.). This measurement may be made by blocking up a level on the top of the vise and measuring the vertical distance from the striking edge to the bottom of the level (top of vise) and subtracting 22.0 mm (0.9 in.). The vertical falling distance may be adjusted by varying the position of the pendulum latch.

X2.17 Notch a standard specimen on one side, parallel to the molding pressure, at 32 mm (1.25 in.) from one end. The depth of the plastic material remaining in the specimen under the notch shall be 10.16 ± 0.05 mm (0.400 ± 0.002 in.). Use a jig to position the specimen correctly in the vise. When the specimen is clamped in place, the center of the notch should be within 0.12 mm (0.005 in.) of being in line with the top of the fixed surface of the vise and the specimen should be centered midway within 0.40 mm (0.016 in.) between the sides of the clamping faces. The notched face should be the striking face of the specimen for the Izod test. Under no circumstances during the breaking of the specimen should the top of the specimen touch the pendulum except at the striking edge.

X2.18 If a clamping-type locating jig is used, examine the clamping screw in the locating jig. If the thread has a loose fit the specimen may not be correctly positioned and may tend to creep as the screw is tightened. A burred or bent point on the screw may also have the same effect.

X2.19 If a pointer and dial mechanism is used to indicate the energy, the pointer friction should be adjusted so that the pointer will just maintain its position anywhere on the scale. The striking pin of the pointer should be securely fastened to the pointer. Friction washers with glazed surfaces should be replaced with new washers. Friction washers should be on either side of the pointer collar. A heavy metal washer should back the last friction washer installed. Pressure on this metal washer is produced by a thin-bent, spring washer and locknuts. If the spring washer is placed next to the fiber friction washer the pointer will tend to vibrate during impact.

X2.20 The free-swing reading of the pendulum (without specimen) from the latched height should be less than 2.5 % of

pendulum capacity on the first swing. If the reading is higher than this, then the friction in the indicating mechanism is excessive or the bearings are dirty. To clean the bearings, dip them in grease solvent and spin-dry in an air jet. Clean the bearings until they spin freely, or replace them. Oil very lightly with instrument oil before replacing. A reproducible method of starting the pendulum from the proper height must be devised.

X2.21 The shaft about which the pendulum rotates shall have no detectable radial play (less than 0.05 mm (0.002 in.)). An endplay of 0.25 mm (0.010 in.) is permissible when a 9.8-N (2.2-lbf) axial force is applied in alternate directions.

X2.22 The clamping faces of the vise should be parallel in the horizontal and vertical directions within 0.025 mm (0.001 in.). Inserting the machined square metal bar of **X2.7** into the vise in a vertical position and clamping until the jaws begin to bind may check parallelism. Any freedom between the metal bar and the clamping surfaces of the jaws of the vise must not exceed the specified tolerance.

X2.23 The top edges of the fixed and moveable jaws of the vise shall have a radius of 0.25 ± 0.12 mm (0.010 ± 0.005 in.). Depending upon whether Test Method A, C, D, or E is used, a stress concentration may be produced as the specimen breaks. Consequently, the top edge of the fixed and moveable jaw needs to be carefully examined.

X2.24 If a brittle unfilled or granular-filled plastic bar such as a general-purpose wood-flour-filled phenolic material is available, notch and break a set of bars in accordance with these test methods. Examine the surface of the break of each bar in the vise. If the break is flat and smooth across the top surface of the vise, the condition of the machine is excellent. Considerable information regarding the condition of an impact machine can be obtained by examining the broken sections of specimens. No weights should be added to the pendulum for the preceding tests.

X2.25 The machine should not be used to indicate more than 85 % of the energy capacity of the pendulum. Extra weight added to the pendulum will increase available energy of the machine. This weight must be added so as to maintain the center of percussion within the tolerance stated in **6.4**. Correct effective weight for any range can be calculated as follows:

$$W = E_p/h$$

where:

- W = effective pendulum weight, N (lbf) (see **X2.14**),
- E_p = potential or available energy of the machine, J (ft-lbf), and
- h = vertical distance of fall of the pendulum striking edge, m (ft) (see **X2.16**).

Each 4.5 N (1 lbf) of added effective weight increases the capacity of the machine by 2.7 J (2 ft-lbf).

NOTE X2.1—If the pendulum is designed for use with add-on weight, it is recommended that it be obtained through the equipment manufacturer.

X3. DERIVATION OF PENDULUM IMPACT CORRECTION EQUATIONS

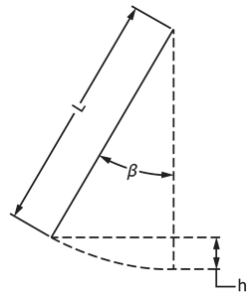


FIG. X3.1 Swing of Pendulum from Its Rest Position

X3.1 From right triangle distances in Fig. X3.1:

$$L - h = L \cos \beta \quad (X3.1)$$

X3.2 But the potential energy gain of pendulum E_p is:

$$E_p = h W_p g \quad (X3.2)$$

X3.3 Combining Eq X3.1 and Eq X3.2 gives the following:

$$L - E_p / W_p g = L \cos \beta \quad (X3.3)$$

X3.4 The maximum energy of the pendulum is the potential energy at the start of the test, E_M , or

$$E_M = h_M W_p g \quad (X3.4)$$

X3.5 The potential energy gained by the pendulum, E_p , is related to the absorption of energy of a specimen, E_s , by the following equation:

$$E_M - E_s = E_p \quad (X3.5)$$

X3.6 Combining Eq X3.3-X3.5 gives the following:

$$(E_M - E_s) / E_M = L / h_M (1 - \cos \beta) \quad (X3.6)$$

X3.7 Solving Eq X3.6 for β gives the following:

$$\beta = \cos^{-1} \{ 1 - [(h_M / L)(1 - E_s / E_M)] \} \quad (X3.7)$$

X3.8 From Fig. X3.2, the total energy correction E_{TC} is given as:

$$E_{TC} = m\beta + b \quad (X3.8)$$

X3.9 But at the zero point of the pendulum potential energy:

$$E_p / 2 = m(0) + b \quad (X3.9)$$

or:

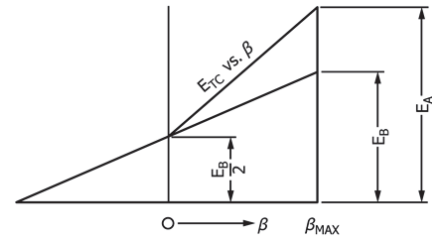


FIG. X3.2 Total Energy Correction for Pendulum Windage and Dial Friction as a Function of Pendulum Position

$$b = E_p / 2 \quad (X3.10)$$

X3.10 The energy correction, E_A , on the first swing of the pendulum occurs at the maximum angle, β_{max} . Substituting in Eq X3.8 gives the following:

$$E_A = m\beta_{max} + (E_p / 2) \quad (X3.11)$$

X3.11 Combining Eq X3.8 and Eq X3.11 gives the following:

$$E_{TC} = (E_A - (E_p / 2))(\beta / \beta_{max}) + (E_p / 2) \quad (X3.12)$$

X3.12 Nomenclature:

- b = intercept of total correction energy straight line,
- E_A = energy correction, including both pendulum windage plus dial friction, J,
- E_B = energy correction for pendulum windage only, J,
- E_M = maximum energy of the pendulum (at the start of test), J,
- E_p = potential energy gain of pendulum from the pendulum rest position, J,
- E_s = uncorrected breaking energy of specimen, J,
- E_{TC} = total energy correction for a given breaking energy, E_s , J,
- g = acceleration of gravity, m/s^2 ,
- h = distance center of gravity of pendulum rises vertically from the rest position of the pendulum, m,
- h_M = maximum height of the center of gravity of the pendulum, m,
- m = slope of total correction energy straight line,
- L = distance from fulcrum to center of gravity of pendulum, m,
- W_p = weight of pendulum, as determined in X2.14, kg, and
- β = angle of pendulum position from the pendulum rest position.

X4. UNIT CONVERSIONS

X4.1 Joules per metre (J/m) cannot be converted directly into kJ/m². Note that the optional units of kJ/m² (ft·lb/in.²) may also be required; therefore, the cross-sectional area under the notch must be reported.

X4.2.2 Example 2:

1 ft·lb/1550 in. ²	= 1.356 J/m ²
1 ft·lb/in. ²	= (1550)(1.356) J/m ²
1 ft·lb/in. ²	= 2101 J/m ²
1 ft·lb/in. ²	= 2.1 kJ/m ²

X4.2 The following examples are approximations:

X4.2.1 Example 1:

1 ft·lb/39.37 in.	= 1.356 J/m
1 ft·lb/in.	= (39.37)(1.356) J/m
1 ft·lb/in.	= 53.4 J/m
1 ft·lb/in.	= 0.0534 kJ/m

SUMMARY OF CHANGES

Committee D20 has identified the location of selected changes to this standard since the last issue, D256 - 06a^{e1}, that may impact the use of this standard. (May 1, 2010)

(1) Revised **Note 6** and **Note 16**.

(2) Revised **Section 9**.

ASTM International takes no position respecting the validity of any patent rights asserted in connection with any item mentioned in this standard. Users of this standard are expressly advised that determination of the validity of any such patent rights, and the risk of infringement of such rights, are entirely their own responsibility.

This standard is subject to revision at any time by the responsible technical committee and must be reviewed every five years and if not revised, either reapproved or withdrawn. Your comments are invited either for revision of this standard or for additional standards and should be addressed to ASTM International Headquarters. Your comments will receive careful consideration at a meeting of the responsible technical committee, which you may attend. If you feel that your comments have not received a fair hearing you should make your views known to the ASTM Committee on Standards, at the address shown below.

This standard is copyrighted by ASTM International, 100 Barr Harbor Drive, PO Box C700, West Conshohocken, PA 19428-2959, United States. Individual reprints (single or multiple copies) of this standard may be obtained by contacting ASTM at the above address or at 610-832-9585 (phone), 610-832-9555 (fax), or service@astm.org (e-mail); or through the ASTM website (www.astm.org). Permission rights to photocopy the standard may also be secured from the Copyright Clearance Center, 222 Rosewood Drive, Danvers, MA 01923, Tel: (978) 646-2600; http://www.copyright.com/

No reproduction or secondary distribution permitted without the prior written permission of ASTM International.



Designation: D790 – 15^{e2}

Standard Test Methods for Flexural Properties of Unreinforced and Reinforced Plastics and Electrical Insulating Materials¹

This standard is issued under the fixed designation D790; the number immediately following the designation indicates the year of original adoption or, in the case of revision, the year of last revision. A number in parentheses indicates the year of last reapproval. A superscript epsilon (ϵ) indicates an editorial change since the last revision or reapproval.

This standard has been approved for use by agencies of the U.S. Department of Defense.

ϵ^1 NOTE—Editorially corrected 4.3 in January 2016.

ϵ^2 NOTE—Editorial corrections were made in February 2016.

1. Scope*

1.1 These test methods are used to determine the flexural properties of unreinforced and reinforced plastics, including high modulus composites and electrical insulating materials utilizing a three-point loading system to apply a load to a simply supported beam (specimen). The method is generally applicable to both rigid and semi-rigid materials, but flexural strength cannot be determined for those materials that do not break or yield in the outer surface of the test specimen within the 5.0 % strain limit.

1.2 Test specimens of rectangular cross section are injection molded or, cut from molded or extruded sheets or plates, or cut from molded or extruded shapes. Specimens must be solid and uniformly rectangular. The specimen rests on two supports and is loaded by means of a loading nose midway between the supports.

1.3 Measure deflection in one of two ways; using crosshead position or a deflectometer. Please note that studies have shown that deflection data obtained with a deflectometer will differ from data obtained using crosshead position. The method of deflection measurement shall be reported.

NOTE 1—Requirements for quality control in production environments are usually met by measuring deflection using crosshead position. However, more accurate measurement may be obtained by using an deflection indicator such as a deflectometer.

NOTE 2—Materials that do not rupture by the maximum strain allowed under this test method may be more suited to a 4-point bend test. The basic difference between the two test methods is in the location of the maximum bending moment and maximum axial fiber stresses. The maximum axial fiber stresses occur on a line under the loading nose in 3-point bending and over the area between the loading noses in 4-point bending. A four-point loading system method can be found in Test Method D6272.

¹ These test methods are under the jurisdiction of ASTM Committee D20 on Plastics and are the direct responsibility of Subcommittee D20.10 on Mechanical Properties.

Current edition approved Dec. 1, 2015. Published January 2016. Originally approved in 1970. Last previous edition approved in 2010 as D790 – 10. DOI: 10.1520/D0790-15E02.

1.4 The values stated in SI units are to be regarded as the standard. The values provided in parentheses are for information only.

1.5 *The text of this standard references notes and footnotes that provide explanatory material. These notes and footnotes (excluding those in tables and figures) shall not be considered as requirements of the standard.*

1.6 *This standard does not purport to address all of the safety concerns, if any, associated with its use. It is the responsibility of the user of this standard to establish appropriate safety and health practices and determine the applicability of regulatory limitations prior to use.*

NOTE 3—This standard and ISO 178 address the same subject matter, but differ in technical content.

2. Referenced Documents

2.1 ASTM Standards:²

D618 Practice for Conditioning Plastics for Testing

D638 Test Method for Tensile Properties of Plastics

D883 Terminology Relating to Plastics

D4000 Classification System for Specifying Plastic Materials

D4101 Specification for Polypropylene Injection and Extrusion Materials

D5947 Test Methods for Physical Dimensions of Solid Plastics Specimens

D6272 Test Method for Flexural Properties of Unreinforced and Reinforced Plastics and Electrical Insulating Materials by Four-Point Bending

E4 Practices for Force Verification of Testing Machines

E691 Practice for Conducting an Interlaboratory Study to Determine the Precision of a Test Method

E2309 Practices for Verification of Displacement Measuring

² For referenced ASTM standards, visit the ASTM website, www.astm.org, or contact ASTM Customer Service at service@astm.org. For *Annual Book of ASTM Standards* volume information, refer to the standard's Document Summary page on the ASTM website.

*A Summary of Changes section appears at the end of this standard

Copyright © ASTM International, 100 Barr Harbor Drive, PO Box C700, West Conshohocken, PA 19428-2959, United States

Copyright ASTM International
Provided by IHS under license with ASTM
No reproduction or networking permitted without license from IHS

Licensee—Uni of Technology Sydney/5928310001, User—Lie, Stefan
Not for Resale, 12/15/2016 17:16:00 MST

Systems and Devices Used in Material Testing Machines

2.2 ISO Standard:³

ISO 178 Plastics—Determination of Flexural Properties

3. Terminology

3.1 *Definitions*—Definitions of terms applying to these test methods appear in Terminology D883 and Annex A2 of Test Method D638.

4. Summary of Test Method

4.1 A test specimen of rectangular cross section rests on two supports in a flat-wise position and is loaded by means of a loading nose located midway between the supports. Unless testing certain laminated materials (see 7 for guidance), a support span-to-depth (of specimen) ratio 16:1 shall be used. The specimen is deflected until rupture occurs in the outer surface of the test specimen or until a maximum strain (see 5.1.6) of 5.0 % is reached, whichever occurs first.

4.2 *Procedure A* is designed principally for materials that break at comparatively small deflections and it shall be used for measurement of flexural properties, particularly flexural modulus, unless the material specification states otherwise. Procedure A employs a strain rate of 0.01 mm/mm/min (0.01 in./in./min) and is the preferred procedure for this test method.

4.3 *Procedure B* is designed principally for those materials that do not break or yield in the outer surface of the test specimen within the 5.0 % strain limit when Procedure A conditions are used. Procedure B employs a strain rate of 0.10 mm/mm/min (0.10 in./in./min).

4.4 Type I tests utilize crosshead position for deflection measurement.

4.5 Type II tests utilize an instrument (deflectometer) for deflection measurement.

4.6 The procedure used and test type shall be reported

NOTE 4—Comparative tests may be run in accordance with either procedure, provided that the procedure is found satisfactory for the material being tested. Tangent modulus data obtained by Procedure A tends to exhibit lower standard deviations than comparable results obtained by means of Procedure B.

5. Significance and Use

5.1 Flexural properties as determined by this test method are especially useful for quality control and specification purposes. They include:

5.1.1 *Flexural Stress (σ_f)*—When a homogeneous elastic material is tested in flexure as a simple beam supported at two points and loaded at the midpoint, the maximum stress in the outer surface of the test specimen occurs at the midpoint. Flexural stress is calculated for any point on the load-deflection curve using equation (Eq 3) in Section 12 (see Notes 5 and 6).

NOTE 5—Eq 3 applies strictly to materials for which stress is linearly proportional to strain up to the point of rupture and for which the strains are small. Since this is not always the case, a slight error will be introduced if Eq 3 is used to calculate stress for materials that are not true

Hookean materials. The equation is valid for obtaining comparison data and for specification purposes, but only up to a maximum fiber strain of 5 % in the outer surface of the test specimen for specimens tested by the procedures described herein.

NOTE 6—When testing highly orthotropic laminates, the maximum stress may not always occur in the outer surface of the test specimen.⁴ Laminated beam theory must be applied to determine the maximum tensile stress at failure. If Eq 3 is used to calculate stress, it will yield an apparent strength based on homogeneous beam theory. This apparent strength is highly dependent on the ply-stacking sequence of highly orthotropic laminates.

5.1.2 *Flexural Stress for Beams Tested at Large Support Spans (σ_f)*—If support span-to-depth ratios greater than 16 to 1 are used such that deflections in excess of 10 % of the support span occur, the stress in the outer surface of the specimen for a simple beam is reasonably approximated using equation (Eq 4) in 12.3 (see Note 7).

NOTE 7—When large support span-to-depth ratios are used, significant end forces are developed at the support noses which will affect the moment in a simple supported beam. Eq 4 includes additional terms that are an approximate correction factor for the influence of these end forces in large support span-to-depth ratio beams where relatively large deflections exist.

5.1.3 *Flexural Strength (σ_{FM})*—Maximum flexural stress sustained by the test specimen (see Note 6) during a bending test. It is calculated according to Eq 3 or Eq 4. Some materials that do not break at strains of up to 5 % give a load deflection curve that shows a point at which the load does not increase with an increase in strain, that is, a yield point (Fig. 1, Curve b), *Y*. The flexural strength is calculated for these materials by letting *P* (in Eq 3 or Eq 4) equal this point, *Y*.

5.1.4 *Flexural Offset Yield Strength*—Offset yield strength is the stress at which the stress-strain curve deviates by a given strain (offset) from the tangent to the initial straight line portion of the stress-strain curve. The value of the offset must be given whenever this property is calculated.

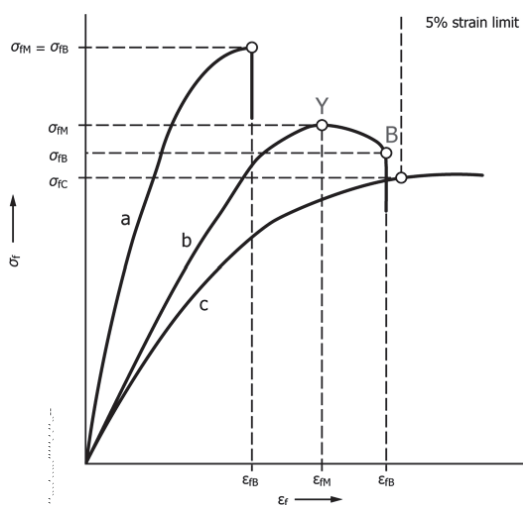
NOTE 8—Flexural Offset Yield Strength may differ from flexural strength defined in 5.1.3. Both methods of calculation are described in the annex to Test Method D638.

5.1.5 *Flexural Stress at Break (σ_{FB})*—Flexural stress at break of the test specimen during a bending test. It is calculated according to Eq 3 or Eq 4. Some materials give a load deflection curve that shows a break point, *B*, without a yield point (Fig. 1, Curve a) in which case $\sigma_{FB} = \sigma_{FM}$. Other materials give a yield deflection curve with both a yield and a break point, *B* (Fig. 1, Curve b). The flexural stress at break is calculated for these materials by letting *P* (in Eq 3 or Eq 4) equal this point, *B*.

5.1.6 *Stress at a Given Strain*—The stress in the outer surface of a test specimen at a given strain is calculated in accordance with Eq 3 or Eq 4 by letting *P* equal the load read from the load-deflection curve at the deflection corresponding to the desired strain (for highly orthotropic laminates, see Note 6).

⁴ For a discussion of these effects, see Zweben, C., Smith, W. S., and Wardle, M. W., "Test Methods for Fiber Tensile Strength, Composite Flexural Modulus and Properties of Fabric-Reinforced Laminates," *Composite Materials: Testing and Design (Fifth Conference)*, ASTM STP 674, 1979, pp. 228–262.

³ Available from American National Standards Institute (ANSI), 25 W. 43rd St., 4th Floor, New York, NY 10036, <http://www.ansi.org>.



NOTE 1—Curve a: Specimen that breaks before yielding.
 Curve b: Specimen that yields and then breaks before the 5 % strain limit.
 Curve c: Specimen that neither yields nor breaks before the 5 % strain limit.

FIG. 1 Typical Curves of Flexural Stress (σ_f) Versus Flexural Strain (ϵ_f)

5.1.7 *Flexural Strain, ϵ_f* —Nominal fractional change in the length of an element of the outer surface of the test specimen at midspan, where the maximum strain occurs. Flexural strain is calculated for any deflection using Eq 5 in 12.4.

5.1.8 *Modulus of Elasticity:*

5.1.8.1 *Tangent Modulus of Elasticity*—The tangent modulus of elasticity, often called the “modulus of elasticity,” is the ratio, within the elastic limit, of stress to corresponding strain. It is calculated by drawing a tangent to the steepest initial straight-line portion of the load-deflection curve and using Eq 6 in 12.5.1 (for highly anisotropic composites, see Note 15).

NOTE 9—Shear deflections can seriously reduce the apparent modulus of highly anisotropic composites when they are tested at low span-to-depth ratios.⁴ For this reason, a span-to-depth ratio of 60 to 1 is recommended for flexural modulus determinations on these composites. Flexural strength should be determined on a separate set of replicate specimens at a lower span-to-depth ratio that induces tensile failure in the outer fibers of the beam along its lower face. Since the flexural modulus of highly anisotropic laminates is a critical function of ply-stacking sequence, it will not necessarily correlate with tensile modulus, which is not stacking-sequence dependent.

5.1.8.2 *Secant Modulus*—The secant modulus is the ratio of stress to corresponding strain at any selected point on the stress-strain curve, that is, the slope of the straight line that joins the origin and a selected point on the actual stress-strain curve. It shall be expressed in megapascals (pounds per square inch). The selected point is chosen at a pre-specified stress or strain in accordance with the appropriate material specification or by customer contract. It is calculated in accordance with Eq 6 by letting m equal the slope of the secant to the load-

deflection curve. The chosen stress or strain point used for the determination of the secant shall be reported.

5.1.8.3 *Chord Modulus (E_f)*—The chord modulus is calculated from two discrete points on the load deflection curve. The selected points are to be chosen at two pre-specified stress or strain points in accordance with the appropriate material specification or by customer contract. The chosen stress or strain points used for the determination of the chord modulus shall be reported. Calculate the chord modulus, E_f using Eq 7 in 12.5.2.

5.2 Experience has shown that flexural properties vary with specimen depth, temperature, atmospheric conditions, and strain rate as specified in Procedures A and B.

5.3 Before proceeding with these test methods, refer to the ASTM specification of the material being tested. Any test specimen preparation, conditioning, dimensions, or testing parameters, or combination thereof, covered in the ASTM material specification shall take precedence over those mentioned in these test methods. Table 1 in Classification System D4000 lists the ASTM material specifications that currently exist for plastics.

6. Apparatus

6.1 *Testing Machine*—A testing machine capable of being operated at constant rates of crosshead motion over the range indicated and comprised of the following:

6.1.1 *Load Frame*—The stiffness of the testing machine shall be such that the total elastic deformation of the system does not exceed 1 % of the total deflection of the test specimen during testing, or appropriate corrections shall be made.

6.1.1.1 *Fixed Member*—A fixed or essentially stationary member holding the specimen supports;

6.1.1.2 *Movable Member*—A movable member carrying the loading nose.

6.1.2 *Loading Noses and Supports*—The loading nose and supports shall have cylindrical surfaces.

6.1.2.1 The radii of the loading nose and supports shall be 5.0 ± 0.1 mm (0.197 ± 0.004 in.) unless otherwise specified in an ASTM material specification or as agreed upon between interested parties.

6.1.2.2 *Other Radii for Loading Noses and Supports*—Alternative loading noses and supports are permitted to be used in order to avoid excessive indentation or failure due to stress concentration directly under the loading nose or if required by an ASTM material specification. If alternative loading nose and support radii are used, the dimensions of the loading nose and supports shall be clearly identified in the test report and reference shall be made to any applicable specifications.

(1) Alternative supports shall have a minimum radius of 3.2 mm ($1/8$ in.) When testing specimens 3.2 mm or greater in depth, the radius of the loading nose and supports are permitted to be up to 1.6 times the specimen depth.

(2) The arc of the loading nose in contact with the specimen shall be sufficiently large to prevent contact of the specimen with the sides of the nose. Alternative loading noses shall be sufficiently large to prevent contact of the specimen with the sides of the nose. The maximum radius of the loading nose shall be no more than four times the specimen depth.

6.1.3 *Drive Mechanism*—A drive mechanism for imparting to the movable member a uniform, controlled velocity with respect to the stationary member, with this velocity to be regulated as specified in Procedure A or B.

6.1.4 *Load Indicator*—A suitable load-indicating mechanism capable of showing the total load applied to specimen when in position on the flex fixture. This mechanism shall be essentially free of inertia lag at the specified rate of testing and shall indicate the load with an accuracy of $\pm 1\%$ of the indicated value, or better. The accuracy of the testing machine shall be verified in accordance with Practices E4.

6.1.5 *Deflection Measuring Device*—The deflection measuring device used shall be selected from the following two choices:

6.1.5.1 *Type I—Crosshead Position Indicating System*—A suitable deflection indicating mechanism capable of showing the amount of change in crosshead movement. This mechanism shall be essentially free of inertial lag at the specified rate of testing and shall indicate the crosshead movement. The crosshead position indicating system shall be verified in accordance with Practice E2309 and minimally meets the requirements of a Class D system.

6.1.5.2 *Type II—Deflection Indicator (Deflectometer)*—A suitable instrument for more accurately determining the deflection of the specimen distance between two designated points. This instrument shall be essentially free of inertia at the specified speed of testing. The deflection indicator system shall be verified in accordance with Practice E2309 and minimally meets the requirements of a Class B system.

NOTE 10—It is desirable, but not essential, that this instrument automatically record this distance, or any change in it, as a function of the load on the test specimen or of the elapsed time from the start of the test, or both. If only the latter is obtained, it has been found useful to also record load-time data.

6.2 *Micrometers*—Apparatus for measuring the width and thickness of the test specimen shall comply with the requirements of Test Method D5947.

7. Test Specimens

7.1 Test specimens that are cut from sheets, plates, or molded or extruded shapes, or molded to the desired finished dimensions are acceptable. The actual dimensions used shall be measured in accordance with Test Methods D5947. The depth of the specimen shall be defined as the thickness of the material. The depth shall not exceed the width (see Note 11). The crosssection of the specimens shall be rectangular with opposite sides flat and parallel (± 0.2 mm) and adjacent sides perpendicular along the full length of the specimen.

7.2 Whenever possible, the original surface of the sheet shall be unaltered. However, where testing machine limitations make it impossible to follow the above criterion on the unaltered sheet, one or both surfaces shall be machined to provide the desired dimensions, and the location of the specimens with reference to the total depth shall be noted. Consequently, any specifications for flexural properties on thicker sheets must state whether the original surfaces are to be retained or not. When only one surface was machined, it must be stated whether the machined surface was on the tension or

compression side of the beam. Any necessary polishing of specimens shall be done only in the lengthwise direction of the specimen.

NOTE 11—The value obtained on specimens with machined surfaces may differ from those obtained on specimens with original surfaces.

7.3 *Sheet Materials (Except Laminated Thermosetting Materials and Certain Materials Used for Electrical Insulation, Including Vulcanized Fiber and Glass Bonded Mica)*:

7.3.1 *Materials 1.6 mm (1/16 in.) or Greater in Thickness*—Specimen width shall not exceed one fourth of the support span for specimens greater than 3.2 mm (1/8 in.) in depth. Specimens 3.2 mm or less in depth shall be 12.7 mm (1/2 in.) in width. The specimen shall be long enough to allow for overhanging on each end of at least 10% of the support span, but in no case less than 6.4 mm (1/4 in.) on each end. Overhang shall be sufficient to prevent the specimen from slipping through the supports. A support span of 16 ± 1 times the depth of the specimen is used for these specimens.

7.3.2 *Materials Less than 1.6 mm (1/16 in.) in Thickness*—The specimen shall be 50.8 mm (2 in.) long by 12.7 mm (1/2 in.) wide, tested flatwise on a 25.4-mm (1-in.) support span.

NOTE 12—Use of the formulas for simple beams cited in these test methods for calculating results presumes that beam width is small in comparison with the support span. Therefore, the formulas do not apply rigorously to these dimensions.

NOTE 13—Where machine sensitivity is such that specimens of these dimensions cannot be measured, wider specimens or shorter support spans, or both, may be used, provided the support span-to-depth ratio is at least 14 to 1. All dimensions must be stated in the report (see also Note 12).

7.4 *Laminated Thermosetting Materials and Sheet and Plate Materials Used for Electrical Insulation, Including Vulcanized Fiber and Glass-Bonded Mica*—For paper-base and fabric-base grades over 25.4 mm (1 in.) in nominal thickness, the specimens shall be machined on both surfaces to a depth of 25.4 mm. For glass-base and nylon-base grades, specimens over 12.7 mm (0.5 in.) in nominal depth shall be machined on both surfaces to a depth of 12.7 mm. The support span-to-depth ratio shall be chosen such that failures occur in the outer fibers of the specimens, due only to the bending moment. As a general rule, support span-to-specimen depth ratios of 16:1 are satisfactory when the ratio of the tensile strength to shear strength is less than 8 to 1, but the support span-to-depth ratio must be increased for composite laminates having relatively low shear strength in the plane of the laminate and relatively high tensile strength parallel to the support span (32:1 or 40:1 are recommended). When laminated materials exhibit low compressive strength perpendicular to the laminations, they shall be loaded with a large radius loading nose (up to four times the specimen depth to prevent premature damage to the outer fibers).

7.5 *Molding Materials (Thermoplastics and Thermosets)*—The preferred specimen dimensions for molding materials is 12.7 mm (0.5 in.) wide, 3.2 mm (0.125 in.) thick, and 127 mm (5.0 in.) long. They are tested flatwise on the support span, resulting in a support span-to-depth ratio of 16:1 (tolerance ± 1). Thicker specimens are to be avoided if they exhibit significant sink marks or bubbles when molded.

7.6 High-Strength Reinforced Composites, Including Highly Orthotropic Laminates—The span-to-depth ratio shall be chosen such that failure occurs in the outer fibers of the specimens and is due only to the bending moment. As a general rule, support span-to-depth ratios of 16:1 are satisfactory when the ratio of the tensile strength to shear strength is less than 8 to 1, but the support span-to-depth ratio must be increased for composite laminates having relatively low shear strength in the plane of the laminate and relatively high tensile strength parallel to the support span (32:1 or 40:1 are recommended). For some highly anisotropic composites, shear deformation can significantly influence modulus measurements, even at span-to-depth ratios as high as 40:1. Hence, for these materials, an increase in the span-to-depth ratio to 60:1 is recommended to eliminate shear effects when modulus data are required, it should also be noted that the flexural modulus of highly anisotropic laminates is a strong function of ply-stacking sequence and will not necessarily correlate with tensile modulus, which is not stacking-sequence dependent.

8. Number of Test Specimens

8.1 Test at least five specimens for each sample in the case of isotropic materials or molded specimens.

8.2 For each sample of anisotropic material in sheet form, test at least five specimens cut in the desired direction. For the purposes of this test, “lengthwise” designates the principal axis of anisotropy and shall be interpreted to mean the direction of the sheet known to be stronger in flexure. “Crosswise” indicates the sheet direction known to be the weaker in flexure and shall be at 90° to the lengthwise direction. The direction of test, whether it be lengthwise, crosswise, or some angle relative to these shall be noted in the report.

9. Conditioning

9.1 **Conditioning**—Condition the test specimens in accordance with Procedure A of Practice **D618** unless otherwise specified by contract or the relevant ASTM material specification. Conditioning time is specified as a minimum. Temperature and humidity tolerances shall be in accordance with Section 7 of Practice **D618** unless specified differently by contract or material specification.

9.2 **Test Conditions**—Conduct the tests at the same temperature and humidity used for conditioning with tolerances in accordance with Section 7 of Practice **D618** unless otherwise specified by contract or the relevant ASTM material specification.

10. Procedure

10.1 Procedure A:

10.1.1 Use an untested specimen for each measurement. Measure the width and depth of the specimen to the nearest 0.03 mm (0.001 in.) at the center of the support span. For specimens less than 2.54 mm (0.100 in.) in depth, measure the depth to the nearest 0.003 mm (0.0005 in.). These measurements shall be made in accordance with Test Methods **D5947**.

10.1.2 Determine the support span to be used as described in Section 7 and set the support span to within 1 % of the determined value.

10.1.3 For flexural fixtures that have continuously adjustable spans, measure the span accurately to the nearest 0.1 mm (0.004 in.) for spans less than 63 mm (2.5 in.) and to the nearest 0.3 mm (0.012 in.) for spans greater than or equal to 63 mm (2.5 in.). Use the actual measured span for all calculations. For flexural fixtures that have fixed machined span positions, verify the span distance the same as for adjustable spans at each machined position. This distance becomes the span for that position and is used for calculations applicable to all subsequent tests conducted at that position. See **Annex A2** for information on the determination of and setting of the span.

10.1.4 Calculate the rate of crosshead motion as follows and set the machine for the rate of crosshead motion as calculated by **Eq 1**:

$$R = ZL^2/6d \quad (1)$$

where:

R = rate of crosshead motion, mm (in.)/min,

L = support span, mm (in.),

d = depth of beam, mm (in.), and

Z = rate of straining of the outer fiber, mm/mm/min (in./in./min). Z shall be equal to 0.01.

In no case shall the actual crosshead rate differ from that calculated using **Eq 1**, by more than ± 10 %.

10.1.5 Align the loading nose and supports so that the axes of the cylindrical surfaces are parallel and the loading nose is midway between the supports. Center the specimen on the supports, with the long axis of the specimen perpendicular to the loading nose and supports. The loading nose should be close to, but not in contact with the specimen (see **Note 14**).

NOTE 14—The parallelism of the apparatus may be checked by means of a plate with parallel grooves into which the loading nose and supports will fit when properly aligned (see **A2.3**).

10.1.6 Apply the load to the specimen at the specified crosshead rate, and record simultaneous load-deflection data.

10.1.7 Measure deflection either by measurement of the motion of the loading nose relative to the supports (crosshead position) (Type I) or by a deflection indicator (deflectometer) under the specimen in contact with it at the center of the support span, the gauge being mounted stationary relative to the specimen supports (Type II). Load-deflection curves are used to determine the flexural strength, chord or secant modulus or the tangent modulus of elasticity, and the total work as measured by the area under the load-deflection curve. Perform the necessary toe compensation (see **Annex A1**) to correct for seating and indentation of the specimen and deflections in the machine.

10.1.8 Terminate the test when the maximum strain in the outer surface of the test specimen has reached 0.05 mm/mm (in./in.) or at break if break occurs prior to reaching the maximum strain (**Notes 15 and 16**). The deflection at which this strain will occur is calculated by letting r equal 0.05 mm/mm (in./in.) in **Eq 2**:

$$D = rL^2/6d \quad (2)$$

where:

D = midspan deflection, mm (in.),

r = strain, mm/mm (in./in.),

L = support span, mm (in.), and
 d = depth of beam, mm (in.).

NOTE 15—For some materials that do not yield or break within the 5 % strain limit when tested by Procedure A, the increased strain rate allowed by Procedure B (see 10.2) may induce the specimen to yield or break, or both, within the required 5 % strain limit.

NOTE 16—Beyond 5 % strain, this test method is not applicable. Some other mechanical property might be more relevant to characterize materials that neither yield nor break by either Procedure A or Procedure B within the 5 % strain limit (for example, Test Method D638 may be considered).

10.2 Procedure B:

10.2.1 Use an untested specimen for each measurement.

10.2.2 Test conditions shall be identical to those described in 10.1, except that the rate of straining of the outer surface of the test specimen shall be 0.10 mm/mm (in./in.)/min.

10.2.3 If no break has occurred in the specimen by the time the maximum strain in the outer surface of the test specimen has reached 0.05 mm/mm (in./in.), discontinue the test (see Note 16).

11. Retests

11.1 Values for properties at rupture shall not be calculated for any specimen that breaks at some obvious, fortuitous flaw, unless such flaws constitute a variable being studied. Retests shall be made for any specimen on which values are not calculated.

12. Calculation

12.1 Toe compensation shall be made in accordance with Annex A1 unless it can be shown that the toe region of the curve is not due to the take-up of slack, seating of the specimen, or other artifact, but rather is an authentic material response.

12.2 Flexural Stress (σ_f):

$$\sigma_f = 3PL/2bd^2 \quad (3)$$

where:

σ = stress in the outer fibers at midpoint, MPa (psi),
 P = load at a given point on the load-deflection curve, N (lbf),

L = support span, mm (in.),
 b = width of beam tested, mm (in.), and
 d = depth of beam tested, mm (in.).

NOTE 17—Eq 3 is not valid if the specimen slips excessively between the supports.

12.3 Flexural Stress for Beams Tested at Large Support Spans (σ_f):

$$\sigma_f = (3PL/2bd^2)[1 + 6(D/L)^2 - 4(d/L)(D/L)] \quad (4)$$

where:

σ_f , P , L , b , and d = the same as for Eq 3, and
 D = deflection of the centerline of the specimen at the middle of the support span, mm (in.).

NOTE 18—When large support span-to-depth ratios are used, significant end forces are developed at the support noses, which will affect the moment in a simple supported beam. Eq 4 includes additional terms that are an approximate correction factor for the influence of these end forces in large support span-to-depth ratio beams where relatively large deflections exist.

12.4 Flexural Strain, ϵ_f —Nominal fractional change in the length of an element of the outer surface of the test specimen at midspan, where the maximum strain occurs. It may be calculated for any deflection using Eq 5:

$$\epsilon_f = 6Dd/L^2 \quad (5)$$

where:

ϵ_f = strain in the outer surface, mm/mm (in./in.),
 D = maximum deflection of the center of the beam, mm (in.),

L = support span, mm (in.), and
 d = depth, mm (in.) of beam tested.

12.5 Modulus of Elasticity:

12.5.1 Tangent Modulus of Elasticity:

$$E_B = L^3m/4bd^3 \quad (6)$$

where:

E_B = modulus of elasticity in bending, MPa (psi),

L = support span, mm (in.),

b = width of beam tested, mm (in.),

d = depth of beam tested, mm (in.), and

m = slope of the tangent to the initial straight-line portion of the load-deflection curve, N/mm (lbf/in.) of deflection.

12.5.2 Chord Modulus (E_f)—

$$E_f = (\sigma_{f2} - \sigma_{f1})/(\epsilon_{f2} - \epsilon_{f1}) \quad (7)$$

where:

σ_{f2} and σ_{f1} = the flexural stresses, calculated from Eq 3 or Eq 4 and measured at the predefined points on the load deflection curve, and ϵ_{f2} and

ϵ_{f1} = the flexural strain values, calculated from Eq 5 and measured at the predetermined points on the load deflection curve.

12.6 Arithmetic Mean—For each series of tests, the arithmetic mean of all values obtained shall be calculated to three significant figures and reported as the “average value” for the particular property in question.

12.7 Standard Deviation—The standard deviation (estimated) shall be calculated as follows and be reported to two significant figures:

$$s = \sqrt{(\sum X^2 - n\bar{X}^2)/(n - 1)} \quad (8)$$

where:

s = estimated standard deviation,

X = value of single observation,

n = number of observations, and

\bar{X} = arithmetic mean of the set of observations.

13. Report

13.1 Report the following information:

13.1.1 Complete identification of the material tested, including type, source, manufacturer’s code number, form, principal dimensions, and previous history (for laminated materials, ply-stacking sequence shall be reported),

13.1.2 Method of specimen preparation,

13.1.3 Direction of cutting and loading specimens, when appropriate,

- 13.1.4 Conditioning procedure,
- 13.1.5 Depth and width of specimen,
- 13.1.6 Reference to this international standard, the Procedure used (A or B), and type test performed (I or II), for example D790-AI
- 13.1.7 Support span length,
- 13.1.8 Support span-to-depth ratio if different than 16:1,
- 13.1.9 Radius of supports and loading noses, if different than 5 mm. When support and/or loading nose radii other than 5 mm are used, the results shall be identified as being generated by a modified version of this test method and the referring specification referenced as to the geometry used.
- 13.1.10 Rate of crosshead motion,
- 13.1.11 Flexural strain at any given stress, average value and standard deviation,
- 13.1.12 If a specimen is rejected, reason(s) for rejection,
- 13.1.13 Tangent, secant, or chord modulus in bending, average value, standard deviation, and the strain level(s) used if secant or chord modulus,
- 13.1.14 Flexural strength (if desired), average value, and standard deviation,
- 13.1.15 Stress at any given strain up to and including 5 % (if desired), with strain used, average value, and standard deviation,
- 13.1.16 Flexural stress at break (if desired), average value, and standard deviation,
- 13.1.17 Type of behavior, whether yielding or rupture, or both, or other observations, occurring within the 5 % strain limit, and
- 13.1.18 Date of specific version of test used.

14. Precision and Bias

14.1 Tables 1 and 2 are based on a round-robin test conducted in 1984, in accordance with Practice E691, involving six materials tested by six laboratories using Procedure A. For each material, all the specimens were prepared at one

TABLE 1 Flexural Strength

Material	Mean, 10 ³ psi	Values Expressed in Units of % of 10 ³ psi			
		V _r ^A	V _R ^B	r ^C	R ^D
ABS	9.99	1.59	6.05	4.44	17.2
DAP thermoset	14.3	6.58	6.58	18.6	18.6
Cast acrylic	16.3	1.67	11.3	4.73	32.0
GR polyester	19.5	1.43	2.14	4.05	6.08
GR polycarbonate	21.0	5.16	6.05	14.6	17.1
SMC	26.0	4.76	7.19	13.5	20.4

^A V_r = within-laboratory coefficient of variation for the indicated material. It is obtained by first pooling the within-laboratory standard deviations of the test results from all of the participating laboratories: $S_r = \sqrt{[(s_1)^2 + (s_2)^2 + \dots + (s_n)^2]/n}$ then V_r = (S_r divided by the overall average for the material) × 100.
^B V_R = between-laboratory reproducibility, expressed as the coefficient of variation: $S_R = (S_r^2 + S_L^2)^{1/2}$ where S_L is the standard deviation of laboratory means. Then: V_R = (S_R divided by the overall average for the material) × 100.
^C r = within-laboratory critical interval between two test results = 2.8 × V_r.
^D R = between-laboratory critical interval between two test results = 2.8 × V_R.

TABLE 2 Flexural Modulus

Material	Mean, 10 ³ psi	Values Expressed in units of % of 10 ³ psi			
		V _r ^A	V _R ^B	r ^C	R ^D
ABS	338	4.79	7.69	13.6	21.8
DAP thermoset	485	2.89	7.18	8.15	20.4
Cast acrylic	810	13.7	16.1	38.8	45.4
GR polyester	816	3.49	4.20	9.91	11.9
GR polycarbonate	1790	5.52	5.52	15.6	15.6
SMC	1950	10.9	13.8	30.8	39.1

^A V_r = within-laboratory coefficient of variation for the indicated material. It is obtained by first pooling the within-laboratory standard deviations of the test results from all of the participating laboratories: $S_r = \sqrt{[(s_1)^2 + (s_2)^2 + \dots + (s_n)^2]/n}$ then V_r = (S_r divided by the overall average for the material) × 100.
^B V_R = between-laboratory reproducibility, expressed as the coefficient of variation: $S_R = (S_r^2 + S_L^2)^{1/2}$ where S_L is the standard deviation of laboratory means. Then: V_R = (S_R divided by the overall average for the material) × 100.
^C r = within-laboratory critical interval between two test results = 2.8 × V_r.
^D R = between-laboratory critical interval between two test results = 2.8 × V_R.

source. Each “test result” was the average of five individual determinations. Each laboratory obtained two test results for each material.

NOTE 19—**Caution:** The following explanations of r and R (14.2 – 14.2.3) are intended only to present a meaningful way of considering the approximate precision of these test methods. The data given in Tables 1 and 2 should not be applied rigorously to the acceptance or rejection of materials, as those data are specific to the round robin and may not be representative of other lots, conditions, materials, or laboratories. Users of these test methods should apply the principles outlined in Practice E691 to generate data specific to their laboratory and materials, or between specific laboratories. The principles of 14.2 – 14.2.3 would then be valid for such data.

14.2 Concept of “r” and “R” in Tables 1 and 2—If S_r and S_R have been calculated from a large enough body of data, and for test results that were averages from testing five specimens for each test result, then:

14.2.1 Repeatability—Two test results obtained within one laboratory shall be judged not equivalent if they differ by more than the r value for that material. r is the interval representing the critical difference between two test results for the same material, obtained by the same operator using the same equipment on the same day in the same laboratory.

14.2.2 Reproducibility—Two test results obtained by different laboratories shall be judged not equivalent if they differ by more than the R value for that material. R is the interval representing the critical difference between two test results for the same material, obtained by different operators using different equipment in different laboratories.

14.2.3 The judgments in 14.2.1 and 14.2.2 will have an approximately 95 % (0.95) probability of being correct.

14.3 Bias—Make no statement about the bias of these test methods, as there is no standard reference material or reference test method that is applicable.

15. Keywords

- 15.1 flexural properties; plastics; stiffness; strength

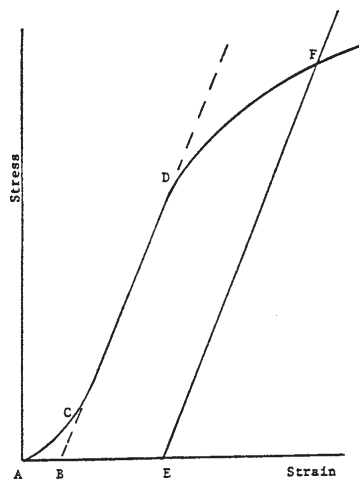
A1. TOE COMPENSATION

A1.1 In a typical stress-strain curve (see Fig. A1.1) there is a toe region, AC, that does not represent a property of the material. It is an artifact caused by a takeup of slack and alignment or seating of the specimen. In order to obtain correct values of such parameters as modulus, strain, and offset yield point, this artifact must be compensated for to give the corrected zero point on the strain or extension axis.

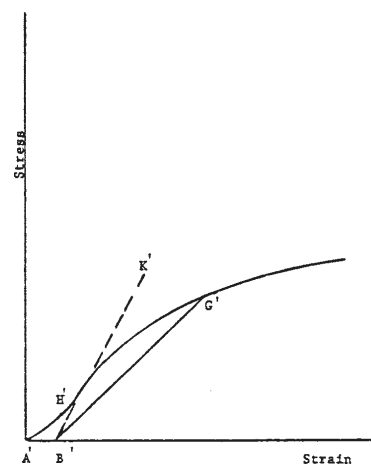
A1.2 In the case of a material exhibiting a region of Hookean (linear) behavior (see Fig. A1.1), a continuation of the linear (CD) region of the curve is constructed through the zero-stress axis. This intersection (B) is the corrected zero-strain point from which all extensions or strains must be measured, including the yield offset (BE), if applicable. The

elastic modulus can be determined by dividing the stress at any point along the Line CD (or its extension) by the strain at the same point (measured from Point B, defined as zero-strain).

A1.3 In the case of a material that does not exhibit any linear region (see Fig. A1.2), the same kind of toe correction of the zero-strain point can be made by constructing a tangent to the maximum slope at the inflection Point H'. This is extended to intersect the strain axis at Point B', the corrected zero-strain point. Using Point B' as zero strain, the stress at any point (G') on the curve can be divided by the strain at that point to obtain a secant modulus (slope of Line B'G'). For those materials with no linear region, any attempt to use the tangent through the inflection point as a basis for determination of an offset yield point may result in unacceptable error.



NOTE 1—Some chart recorders plot the mirror image of this graph.
FIG. A1.1 Material with Hookean Region



NOTE 1—Some chart recorders plot the mirror image of this graph.
FIG. A1.2 Material with No Hookean Region

A2. MEASURING AND SETTING SPAN

A2.1 For flexural fixtures that have adjustable spans, it is important that the span between the supports is maintained constant or the actual measured span is used in the calculation of stress, modulus, and strain, and the loading nose or noses are positioned and aligned properly with respect to the supports. Some simple steps as follows can improve the repeatability of your results when using these adjustable span fixtures.

A2.2 Measurement of Span:

A2.2.1 This technique is needed to ensure that the correct span, not an estimated span, is used in the calculation of results.

A2.2.2 Scribe a permanent line or mark at the exact center of the support where the specimen makes complete contact. The type of mark depends on whether the supports are fixed or rotatable (see Figs. A2.1 and A2.2).

A2.2.3 Using a vernier caliper with pointed tips that is readable to at least 0.1 mm (0.004 in.), measure the distance between the supports, and use this measurement of span in the calculations.

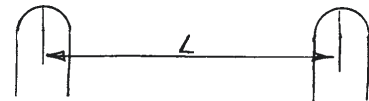


FIG. A2.1 Markings on Fixed Specimen Supports

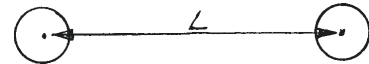


FIG. A2.2 Markings on Rotatable Specimen Supports

A2.3 *Setting the Span and Alignment of Loading Nose(s)*—To ensure a consistent day-to-day setup of the span and ensure the alignment and proper positioning of the loading nose, simple jigs should be manufactured for each of the standard setups used. An example of a jig found to be useful is shown in Fig. A2.3.

ASTM D790 - 15e2

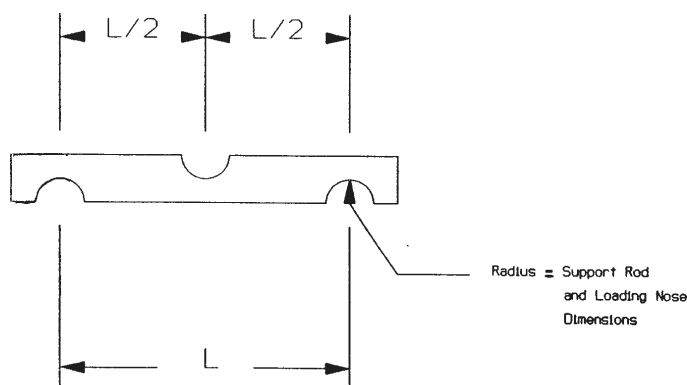


FIG. A2.3 Fixture Used to Set Loading Nose and Support Spacing and Alignment

APPENDIX

(Nonmandatory Information)

X1. DEVELOPMENT OF A FLEXURAL MACHINE COMPLIANCE CORRECTION

X1.1 Introduction

X1.1.1 Universal Testing instrument drive systems always exhibit a certain level of compliance that is characterized by a variance between the reported crosshead displacement and the displacement actually imparted to the specimen. This variance is a function of load frame stiffness, drive system wind-up, load cell compliance and fixture compliance. To accurately measure the flexural modulus of a material, this compliance should be measured and empirically subtracted from test data. Flexural modulus results without the corrections are lower than if the correction is applied. The greater the stiffness of the material the more influence the system compliance has on results.

X1.1.2 It is not necessary to make the machine compliance correction when a deflectometer/extensometer is used to measure the actual deflection occurring in the specimen as it is deflected.

X1.2 Terminology

X1.2.1 *Compliance*—The displacement difference between test machine drive system displacement values and actual specimen displacement

X1.2.2 *Compliance Correction*—An analytical method of modifying test instrument displacement values to eliminate the amount of that measurement attributed to test instrument compliance.

X1.3 Apparatus

X1.3.1 Universal Testing machine

X1.3.2 Load cell

X1.3.3 Flexure fixture including loading nose and specimen supports

X1.3.4 Computer Software to make corrections to the displacements

X1.3.5 Steel bar, with smoothed surfaces and a calculated flexural stiffness of more than 100 times greater than the test material. The length should be at least 13 mm greater than the support span. The width shall match the width of the test specimen and the thickness shall be that required to achieve or exceed the target stiffness.

X1.4 Safety Precautions

X1.4.1 The universal testing machine should stop the machine crosshead movement when the load reaches 90 % of load cell capacity, to prevent damage to the load cell.

X1.4.2 The compliance curve determination should be made at a speed no higher than 2 mm/min. Because the load builds up rapidly since the steel bar does not deflect, it is quite easy to exceed the load cell capacity.

X1.5 Procedure

NOTE X1.1—A new compliance correction curve should be established each time there is a change made to the setup of the test machine, such as, load cell changed or reinstallation of the flexure fixture on the machine. If the test machine is dedicated to flexural testing, and there are no changes to the setup, it is not necessary to re-calculate the compliance curve.

NOTE X1.2—On those machines with computer software that automatically make this compliance correction; refer to the software manual to determine how this correction should be made.

X1.5.1 The procedure to determine compliance follows:

X1.5.1.1 Configure the test system to match the actual test configuration.

X1.5.1.2 Place the steel bar in the test fixture, duplicating the position of a specimen during actual testing.

X1.5.1.3 Set the crosshead speed to 2 mm/min. or less and start the crosshead moving in the test direction recording crosshead displacement and the corresponding load values.

X1.5.1.4 Increase load to a point exceeding the highest load expected during specimen testing. Stop the crosshead and return to the pre-test location.

X1.5.1.5 The recorded load-deflection curve, starting when the loading nose contacts the steel bar to the time that the highest load expected is defined as test system compliance.

X1.5.2 Procedure to apply compliance correction is as follows:

X1.5.2.1 Run the flexural test method on the material at the crosshead required for the measurement.

X1.5.2.2 It is preferable that computer software be used to make the displacement corrections, but if it is not available compliance corrections can be made manually in the following manner. Determine the range of displacement (D) on the load versus displacement curve for the material, over which the modulus is to be calculated. For Young's Modulus that would be steepest region of the curve below the proportional limit. For Secant and Chord Moduli that would be at specified level of strain or specified levels of strain, respectively. Draw two vertical lines up from the displacement axis for the two chosen displacements (D1, D2) to the load versus displacement curve for the material. In some cases one of these points maybe at zero displacement after the toe compensation correction is made. Draw two horizontal lines from these points on the load displacement curve to the Load (P) axis. Determine the loads (L1, L2).

X1.5.2.3 Using the Compliance Correction load displacement curve for the steel bar, mark off L1 and L2 on the Load (P) axis. From these two points draw horizontal lines across till they contact the load versus displacement curve for the steel bar. From these two points on the load deflection curve draw two vertical lines downwards to the displacement axis. These two points on the displacement axis determine the corrections (c1, c2) that need to be made to the displacements measurements for the test material.

X1.5.2.4 Subtract the corrections (c1, c2) from the measured displacements (D1, D2), so that a true measures of test specimen deflection (D1-c1, D2-c2) are obtained.

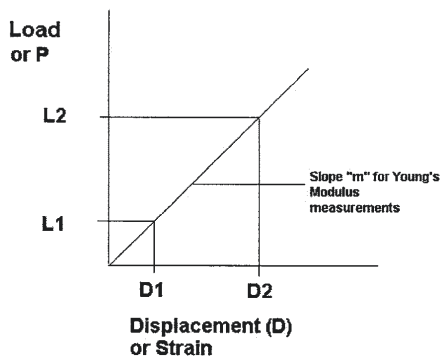


FIG. X1.1 Example of Modulus Curve for a Material

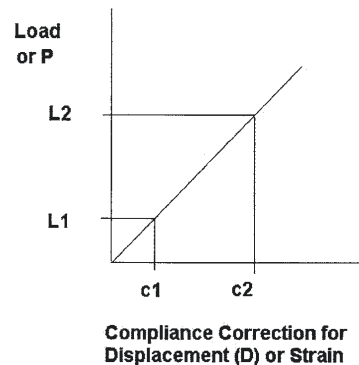


FIG. X1.2 Compliance Curve for Steel Bar

X1.6 Calculations

X1.6.1 Calculation of Chord Modulus

X1.6.1.1 Calculate the stresses (σ_1 , σ_2) for load points L1 and L2 from Fig. X1.1 using the equation in 12.2, Eq 3.

X1.6.1.2 Calculate the strains (ϵ_1 , ϵ_2) for displacements D1-c1 and D2-c2 from Fig. X1.3 using the equation in 12.4, Eq 5.

X1.6.1.3 Calculate the flexural chord modulus in accordance with 12.5.2, Eq 7.

X1.6.2 Calculation of Secant Modulus

X1.6.2.1 Calculation of the Secant Modulus at any strain along the curve would be the same as conducting a chord modulus measurement, except that $\sigma_1 = 0$, $L_1 = 0$, and $D_1 - c_1 = 0$.

X1.6.3 Calculation of Young's Modulus

X1.6.3.1 Determine the steepest slope "m" along the curve, below the proportional limit, using the selected loads L1 and L2 from Fig. X1.1 and the displacements D1-c1 and D2-c2 from Fig. X1.3.

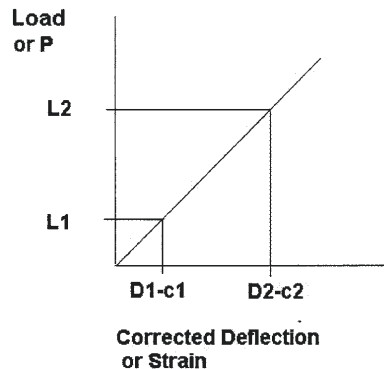


FIG. X1.3 Example of the Material Curve Corrected for the Compliance Corrected Displacement or Strain

X1.6.3.2 Calculate the Young's modulus in accordance with 12.5.1, Eq 6.

SUMMARY OF CHANGES

Committee D20 has identified the location of selected changes to this standard since the last issue (D790 - 10) that may impact the use of this standard. (December 1, 2015)

(1) Significantly modified the format of the standard from the previous edition. (2) Reporting requirements have been changed.

ASTM International takes no position respecting the validity of any patent rights asserted in connection with any item mentioned in this standard. Users of this standard are expressly advised that determination of the validity of any such patent rights, and the risk of infringement of such rights, are entirely their own responsibility.

This standard is subject to revision at any time by the responsible technical committee and must be reviewed every five years and if not revised, either reapproved or withdrawn. Your comments are invited either for revision of this standard or for additional standards and should be addressed to ASTM International Headquarters. Your comments will receive careful consideration at a meeting of the responsible technical committee, which you may attend. If you feel that your comments have not received a fair hearing you should make your views known to the ASTM Committee on Standards, at the address shown below.

This standard is copyrighted by ASTM International, 100 Barr Harbor Drive, PO Box C700, West Conshohocken, PA 19428-2959, United States. Individual reprints (single or multiple copies) of this standard may be obtained by contacting ASTM at the above address or at 610-832-9585 (phone), 610-832-9555 (fax), or service@astm.org (e-mail); or through the ASTM website (www.astm.org). Permission rights to photocopy the standard may also be secured from the Copyright Clearance Center, 222 Rosewood Drive, Danvers, MA 01923, Tel: (978) 646-2600; <http://www.copyright.com/>

Bibliography

- Ahn, D., Kim, H. & Lee, S. 2007, 'Fabrication direction optimization to minimize post-machining in layered manufacturing', *International Journal of Machine Tools and Manufacture*, vol. 47, no. 3, pp. 593-606.
- Ahn, D., Kweon, J.-H., Kwon, S., Song, J. & Lee, S. 2009, 'Representation of surface roughness in fused deposition modeling', *Journal of Materials Processing Technology*, vol. 209, no. 15, pp. 5593-600.
- Ahn, S.-H., Montero, M., Odell, D., Roundy, S. & Wright, P.K. 2002, 'Anisotropic material properties of fused deposition modeling ABS', *Rapid Prototyping Journal*, vol. 8, no. 4, pp. 248-57.
- Ajoku, U., Saleh, N., Hopkinson, N., Hague, R. & Erasenthiran, P. 2006, 'Investigating mechanical anisotropy and end-of-vector effect in laser-sintered nylon parts', *Proceedings of the Institution of Mechanical Engineers, Part B: Journal of Engineering Manufacture*, vol. 220, no. 7, pp. 1077-86.
- Alifui-Segbaya, F., Varma, S., Lieschke, G.J. & George, R. 2017, 'Biocompatibility of photopolymers in 3d printing', *3D Printing and Additive Manufacturing*, vol. 4, no. 4, pp. 185-91.
- ASTM 2009a, *Committee F42 on Additive Manufacturing Technologies*, ASTM International, Conshohocken, PA, USA.
- ASTM 2009b, *Subcommittee F42.01 on Test Methods*, ASTM International, Conshohocken, PA, USA.
- ASTM 2010, *ASTM D256 – 10, Standard Test Methods for Determining the Izod Pendulum Impact Resistance of Plastics*, ASTM International, Conshohocken, PA, USA.
- ASTM 2013a, *ASTM D618 – 13, Standard Practice for Conditioning Plastics for Testing*, ASTM International, Conshohocken, PA, USA.
- ASTM 2013b, *ISO/ASTM 52921:2013, Standard Terminology for Additive Manufacturing - Coordinate Systems and Test Methodologies*, ASTM International, Conshohocken, PA, USA.
- ASTM 2014, *ASTM D638 – 14, Standard Test Method for Tensile Properties of Plastics*, ASTM International, Conshohocken, PA, USA.
- ASTM 2015a, *ASTM D790 – 15, Standard Test Methods for Flexural Properties of Unreinforced and Reinforced Plastics and Electrical Insulating Materials*, ASTM International, Conshohocken, PA, USA.
- ASTM 2015b, *ISO/ASTM 52900:2015, Standard Terminology for Additive Manufacturing - General Principles - Terminology*, ASTM International, Conshohocken, PA, USA.

- ASTM 2017, *ISO/ASTM 52910:2017, Standard Guidelines for Design for Additive Manufacturing*, ASTM International, Conshohocken, PA, USA.
- Ball, R. & Overhill, H. 2012, *DesignDirect: How to Start Your Own Micro Brand*, PTeC.
- Barclift, M.W. & Williams, C.B. 2012, 'Examining variability in the mechanical properties of parts manufactured via polyjet direct 3D printing', *International Solid Freeform Fabrication Symposium*, pp. 6-8.
- Bibby, P. 2010, 'Bridge workers fear cancer cluster', *Sydney Morning Herald*, October 14, viewed 12 September 2011, <https://www.smh.com.au/national/nsw/bridge-workers-fear-cancer-cluster-20101014-16l7c.html>
- Bodein, Y., Rose, B., & Caillaud, E. 2013, 'A roadmap for parametric CAD efficiency in the automotive industry', *Computer-Aided Design*, 45 (10), 1198-1214.
- Bongers, A., Smith, S., Donker, V. & Pickrell, M. 2014, 'Interactive Rehabilitation Tiles', *Tangible, Conference on Embedded and Embodied Interaction (TEI)*.
- Bongers, A.J., Smith, S., Donker, V., Pickrell, M., Hall, R. & Lie, S. 2014, 'Interactive Infrastructures: physical rehabilitation modules for pervasive healthcare technology', in *Pervasive Health*, Springer, London, pp. 229-254.
- Boschetto, A., Giordano, V. & Veniali, F. 2013, '3D roughness profile model in fused deposition modelling', *Rapid Prototyping Journal*, vol. 19, no. 4, pp. 240-52.
- Bourell, D.L., Watt, T.J., Leigh, D.K. & Fulcher, B. 2014, 'Performance limitations In polymer laser sintering', *Physics Procedia*, vol. 56, pp. 147-56.
- Byun, H.-S. & Lee, K.H., 2006, 'Determination of the optimal build direction for different rapid prototyping processes using multi-criterion decision making', *Robotics and Computer-Integrated Manufacturing*, vol. 22, no. 1, pp. 69-80.
- Cambridge English Dictionary, 2019, viewed 1 July 2019, <https://dictionary.cambridge.org/dictionary/english/scenario>
- Campbell, R.I., Hague, R.J., Sener, B. & Wormald, P.W. 2003, 'The potential for the bespoke industrial designer', *The Design Journal*, vol. 6, no. 3, pp. 24-34.
- Campbell, R.I., Martorelli, M. & Lee, H.S. 2002, 'Surface roughness visualisation for rapid prototyping models', *Computer-Aided Design*, vol. 34, no. 10, pp. 717-25.

- Caulfield, B., McHugh, P. & Lohfeld, S. 2007, 'Dependence of mechanical properties of polyamide components on build parameters in the SLS process', *Journal of Materials Processing Technology*, vol. 182, no. 1, pp. 477-88.
- Cazón, A., Morer, P. & Matey, L. 2014, 'PolyJet technology for product prototyping: Tensile strength and surface roughness properties', *Proceedings of the Institution of Mechanical Engineers, Part B: Journal of Engineering Manufacture*, vol. 228, no. 12, pp. 1664-75.
- Chu, C., Graf, G. & Rosen, D.W. 2008, 'Design for additive manufacturing of Cellular structures', *Computer-Aided Design and Applications*, vol. 5, no. 5, pp. 686-96.
- Chung Wang, C., Lin, T.W. & Hu, S.S. 2007, 'Optimizing the rapid prototyping process by integrating the Taguchi method with the Gray relational analysis', *Rapid Prototyping Journal*, vol. 13, no. 5, pp. 304-15.
- Cross, N. 2006, *Designerly ways of knowing*, Springer, London.
- Davis, J.R. 2004, *Tensile testing*, 2nd edn, ASM international, Materials Park, Ohio, USA.
- Diegel, O., Kristav, P., Motte, D. & Kianian, B. 2016, 'Additive manufacturing and its effect on sustainable design', *Handbook of sustainability in additive manufacturing*, Springer, Singapore, pp. 73-99.
- Edgar, R. 2016, 'Why 3D printing may be the answer for small companies with big ideas', *Sydney Morning Herald*, June 6, viewed 2 July 2020, <https://www.smh.com.au/entertainment/art-and-design/why-3d-printing-may-be-the-answer-for-small-companies-with-big-ideas-20170605-gwkwq1.html>
- Eckhart. (2018, August 14). *Improving life on the line*. https://www.eckhartusa.com/blog_posts/eckhart-is-leading-industry-4-0-with-additive-manufacturing-solutions/
- E-NABLE (2019, July 2), *Enabling the Future*, <http://enablingthefuture.org>
- Gerdeen, J.C. & Rorrer, R.A.L. 2012, *Engineering Design with Polymers and Composites*, 2nd edn., Taylor & Francis, Boca Raton, Florida.
- Gibson, I., Rosen, D.W. & Stucker, B. 2010, *Additive Manufacturing Technologies*, Springer, Boston, Massachusetts.
- Gibson, I. & Shi, D. 1997, 'Material properties and fabrication parameters in selective laser sintering process', *Rapid Prototyping Journal*, vol. 3, no. 4, pp. 129-36.
- Gibson, J.J. 1977, 'The theory of affordances', in R. Shaw & J. Bransford (eds), *Perceiving, acting, and knowing: Toward an ecological psychology*, Lawrence Erlbaum Associates, Hillsdale, New Jersey, pp. 67-82.

- Gillespie, L.R.K. 2017, *Design for Advanced Manufacturing: Technologies, and Processes*, McGraw-Hill Education.
- Guan, H.W., Savalani, M.M., Gibson, I. & Diegel, O. 2015, 'Influence of fill gap on Flexura I strength of parts fabricated by curved layer fused deposition modeling', *Procedia Technology*, vol. 20, pp. 243-8.
- Guessasma, S., Zhang, W., Zhu, J., Belhabib, S. & Nouri, H. 2015, 'Challenges of additive manufacturing technologies from an optimisation perspective', *International Journal for Simulation and Multidisciplinary Design Optimization*, vol. 6, p. A9.
- Hague, R., Mansour, S. & Saleh, N. 2003, 'Design opportunities with rapid manufacturing', *Assembly Automation*, vol. 23, no. 4, pp. 346-56.
- Hopkinson, N. & Dickens, P. 2001, 'Rapid prototyping for direct manufacture', *Rapid Prototyping Journal*, vol. 7, no. 4, pp. 197-202.
- Kęsy, A. & Kotliński, J. 2010, 'Mechanical properties of parts produced by using polymer jetting technology', *Archives of Civil and Mechanical Engineering*, vol. 10, no. 3, pp. 37-50.
- Kim, G.D. & Oh, Y.T. 2008, 'A benchmark study on rapid prototyping processes and machines: Quantitative comparisons of mechanical properties, accuracy, roughness, speed, and material cost', *Proceedings of the Institution of Mechanical Engineers, Part B: Journal of Engineering Manufacture*, vol. 222, no. 2, pp. 201-15.
- Kotlinski, J. 2014, 'Mechanical properties of commercial rapid prototyping materials', *Rapid Prototyping Journal*, vol. 20, no. 6, pp. 499-510.
- Kumar, V. 2012, *101 design methods: A structured approach for driving innovation in your organization*, John Wiley & Sons.
- Leutenecker-Twelsiek, B., Klahn, C. & Meboldt, M. 2016, 'Considering part orientation in design for additive manufacturing', *Procedia CIRP*, vol. 50, pp. 408-13.
- Levy, G.N., Schindel, R. & Kruth, J.P. 2003, 'Rapid manufacturing and rapid tooling with layer manufacturing (lm) technologies, state of the art and future perspectives', *CIRP Annals - Manufacturing Technology*, vol. 52, no. 2, pp. 589-609.
- Lie, S. 2012, 'A cooperative design approach to the design of interactive devices for small, specialized user groups', MEng by research thesis, University of Technology Sydney, Sydney.
- Lie, S., Liu, D. & Bongers, B. 2012, 'A cooperative approach to the design of an Operator Control Unit for a semi-autonomous grit-blasting robot', paper presented to the *Australasian Conference on Robotics and Automation*, Wellington, New Zealand.

- Liu, D., Dissanayake, G., Manamperi, P.B., Brooks, P.A., Fang, G., Paul, G., Webb, S., Kirchner, N., Chotiprayanakul, P., Kwok, N.M. & Ren, T.R. 2008, 'A Robotic System for Steel Bridge Maintenance: Research Challenges and System Design', paper presented to the *Australasian Conference on Robotics and Automation*, Canberra, Australia.
- Loy, J. 2015, 'The future for design education: preparing the design workforce for additive manufacturing', *International Journal of Rapid Manufacturing*, vol. 5, no. 2, pp. 199-212.
- Loy, J., Canning, S. & Haskell, N. 2016, '3D Printing Sociocultural Sustainability', *Handbook of Sustainability in Additive Manufacturing*, Springer, pp. 51-72.
- Ludden, G.D.S. & van Rompay, T.J.L. 2015, 'How does it feel? Exploring touch on different levels of product experience', *Journal of Engineering Design*, vol. 26, no. 4-6, pp. 157-68.
- Masood, S.H., Rattanawong, W. & Lovenitti, P. 2003, 'A generic algorithm for a best part orientation system for complex parts in rapid prototyping', *Journal of Materials Processing Technology*, vol. 139, no. 1-3, pp. 110-6.
- Milton, A. & Rodgers, P. 2013, *Research methods for product design*, Laurence King publishing.
- Mohamed, O.A., Masood, S.H. & Bhowmik, J.L. 2015, 'Optimization of fused deposition modeling process parameters: A review of current research and future prospects', *Advances in Manufacturing*, vol. 3, no. 1, pp. 42-53.
- Monzón, M., Ortega, Z., Martínez, A. & Ortega, F. 2015, 'Standardization in additive manufacturing: activities carried out by international organizations and projects', *The International Journal of Advanced Manufacturing Technology*, vol. 76, no. 5-8, pp. 1111-21.
- Moroni, G., Syam, W.P. & Petrò, S. 2015, 'Functionality-based part orientation for additive manufacturing', *Procedia CIRP*, vol. 36, pp. 217-22.
- Mueller, J., Shea, K. & Daraio, C. 2015, 'Mechanical properties of parts fabricated with inkjet 3D printing through efficient experimental design', *Materials & Design*, vol. 86, pp. 902-12.
- Muratovski, G. 2015, *Research for designers: A guide to methods and practice*, Sage.
- Murtezaoglu, Y., Plakhotnik, D., Stautner, M., Vaneker, T. & van Houten, F.J. 2018, 'Geometry-Based Process Planning for Multi-Axis Support-Free Additive Manufacturing', *Procedia CIRP*, vol. 78, pp. 73-8.
- Norman, D.A. 2004, *Emotional design: Why we love (or hate) everyday things*, Basic Books, New York.
- Norman, D.A. 2010, *Living with complexity*, MIT Press.

- Oropallo, W. & Piegl, L.A. 2016, 'Ten challenges in 3D printing', *Engineering With Computers*, vol. 32, no. 1, pp. 135-48.
- Pandey, P.M., Venkata Reddy, N.V. & Dhande, S.G. 2007, 'Part deposition orientation studies in layered manufacturing', *Journal of Materials Processing Technology*, vol. 185, no. 1, pp. 125-31.
- Paul, G., Webb, S., Liu, D. & Dissanayake, G. 2010, 'A Robotic System for Steel Bridge Maintenance: Field Testing', paper presented to the *Australasian Conference on Robotics and Automation*, Brisbane, Australia.
- Phatak, A.M. & Pande, S.S. 2012, 'Optimum part orientation in rapid prototyping using genetic algorithm', *Journal of Manufacturing Systems*, vol. 31, no. 4, pp. 395-402.
- Pilipović, A., Raos, P. & Šercer, M. 2009, 'Experimental analysis of properties of materials for rapid prototyping', *The International Journal of Advanced Manufacturing Technology*, vol. 40, no. 1-2, pp. 105-15.
- Rae, J.B. 1967, *The American Automobile: A Brief History*, University of Chicago Press, Chicago.
- Rael, R. & San Fratello, V. 2018, *Printing Architecture: Innovative Recipes for 3D Printing*, Princeton Architectural Press, New York.
- Rayegani, F. & Onwubolu, G. 2014, 'Fused deposition modelling (FDM) process parameter prediction and optimization using group method for data handling (GMDH) and differential evolution (DE)', *International Journal of Advanced Manufacturing Technology*, vol. 73.
- Schmid, M., Kleijnen, R., Vetterli, M. & Wegener, K. 2017, 'Influence of the origin of polyamide 12 Powder on the laser sintering process and laser sintered parts', *Applied Sciences*, vol. 7, no. 5, p. 462.
- Seepersad, C.C. 2017, 'Design for powder bed fusion of polymer parts', in L.R.K. Gillespie (ed.), *Design for Advanced Manufacturing: Technologies, and Processes*, McGraw-Hill Education, pp. 139 - 46.
- Sembach, K.J., Leuthäuser, G. & Gössel, P. 1991, *Twentieth-century Furniture Design*, Taschen, Koln, Germany.
- Sennett, R. 2009, *The Craftsman*, Penguin Books Limited.
- Singamneni, S., Diegel, O., Huang, B., Gibson, I. & Chowdhury, R. 2010, 'Curved-layer fused deposition modelling', *Journal for New Generation Sciences*, vol. 8, no. 2, pp. 95-107.
- Sparke, P. 1992, *An Introduction to Design and Culture in the Twentieth Century*, 3rd edn., Routledge, London.
- Stansbury, J.W. & Idacavage, M.J. 2016, '3D printing with polymers: Challenges among expanding options and opportunities', *Dental Materials*, vol. 32, no. 1, pp. 54-64.

- Starr, T.L., Gornet, T.J. & Usher, J.S. 2011, 'The effect of process conditions on mechanical properties of laser-sintered nylon', *Rapid Prototyping Journal*, vol. 17, no. 6, pp. 418-23.
- Sterling, B. 2005, *Shaping Things*, MIT Press, Massachusetts.
- Thompson, M.K., Moroni, G., Vaneker, T., Fadel, G., Campbell, R.I., Gibson, I., Bernard, A., Schulz, J., Graf, P. & Ahuja, B. 2016, 'Design for additive manufacturing: trends, opportunities, considerations, and constraints', *CIRP Annals-Manufacturing Technology*, vol. 65, no. 2, pp. 737-60.
- Thrimurthulu, K., Pandey, P.M. & Venkata Reddy, N. 2004, 'Optimum part deposition orientation in fused deposition modeling', *International Journal of Machine Tools and Manufacture*, vol. 44, no. 6, pp. 585-94.
- Verma, A. & Rai, R. 2014, 'Computational geometric solutions for efficient Additive manufacturing process planning', *ASME Paper No. DETC2014-34067*.
- Walden, R. & Dorst, K. 2013, 'The integration of design parameters and the establishment of constraint and priority for innovation', paper presented at *DesignEd Asia Conference 2013: Delimitation-Creating with Constraints*, The Hong Kong Polytechnic University.
- Wendel, B., Rietzel, D., Kühnlein, F., Feulner, R., Hülder, G. & Schmachtenberg, E. 2008, 'Additive processing of polymers', *Macromolecular materials and engineering*, vol. 293, no. 10, pp. 799-809.
- Whelan, A. 2012, *Polymer Technology Dictionary*, Springer, Netherlands.
- Williams, C.B. & Meisel, N.A. 2017, 'Designing for material jetting additive processes', in L.R.K. Gillespie (ed.), *Design for Advanced Manufacturing: Technologies, and Processes*, McGraw-Hill Education, [place of publication], pp. 127 - 37.
- Wilson, F.R. 1998, *The Hand: How Its Use Shapes the Brain, Language, and Human Culture*, Pantheon Books.
- Wohlers, T. 2016, *Wohlers report 2016*, Wohlers Associates, Inc.
- Yang, S. & Zhao, Y. 2015, 'Additive manufacturing-enabled design theory and methodology: a critical review', *International Journal of Advanced Manufacturing Technology*, vol. 80.
- Zaragoza-Siqueiros, J. & Medellín-Castillo, H.I. 2014, 'Design for Rapid Prototyping, Manufacturing and Tooling: Guidelines', *Proceedings of the ASME 2014 International Mechanical Engineering Congress and Exposition*.
- Zhang, Y., Bernard, A., Gupta, R.K. & Harik, R. 2014, 'Evaluating the design for additive manufacturing: a process planning perspective', *Procedia CIRP*, vol. 21, pp. 144-50.

Zhang, Y., Bernard, A., Harik, R. & Karunakaran, K. 2017, 'Build orientation optimization for multi-part production in additive manufacturing', *Journal of Intelligent Manufacturing*, vol. 28, no. 6, pp. 1393-407.

Ziemian, C., Sharma, M. & Ziemian, S. 2012, 'Anisotropic mechanical properties of ABS parts fabricated by fused deposition modelling', *Mechanical engineering*, InTech.